Rapid Fabrication Methods for Sheet Metal Forming Dies

by

Daniel Francis Walczyk

M.S., Mechanical Engineering
Rensselaer Polytechnic Institute, 1991

B.S., Mechanical Engineering
Syracuse University, 1986

Submitted to the Department of Mechanical Engineering
in Partial Fulfillment of the Requirements for the Degree of

Doctor of Philosophy

at the

Massachusetts Institute of Technology

February 1996

Signature of Author . . . . . .
Department of Mechanical Engineering
February 15, 1996

Certified by . . . . . .
David E. Hardt
Professor of Mechanical Engineering
Thesis Supervisor

Accepted by . . . . . .
Ain A. Sonin
Chairman, Department Committee on Graduate Students

v. 1

ARCHIVES

Rapid Fabrication Methods for Sheet Metal Forming Dies

by

Daniel F. Walczyk

Submitted to the Department of Mechanical Engineering in February of 1996, in Partial Fulfillment of the Requirements for the Degree of Doctor of Philosophy.

ABSTRACT

The main goal of this research is to significantly advance the state-of-the-art in rapid fabrication methods for sheet metal forming dies. Rapid fabrication methods are directed towards flexible manufacturing systems that incorporate closed-loop process control principles in tooling development. After reviewing the sheet forming processes currently used in industry, it becomes evident that the most expensive and time-consuming part of tooling development is fabricating the rigid die(s). Out of all the known rigid die fabrication methods, three rapid, low-cost methods are chosen for investigation and comparison including CNC-machining a solid billet of material (standard), assembling and clamping an array of laminations, and configuring and clamping a discrete die with close-packed elements.

The current state-of-the-art for each fabrication method is first benchmarked and then improved upon if needed. A matched set of steel CNC-machined dies for forming a benchmark part shape are fabricating using high-speed machining techniques. Because of inherent problems with the laminated die construction currently used in industry, a new lamination-based die fabrication method has been developed that involves stacking and securing a vertically-oriented array of Profiled-Edge Laminations (PEL) whose top edges form a segmented forming surface. The PEL die method facilitates easier and faster handling, securing, and recontouring of die laminations compared to the current method. New apparatus concepts for quickly fabricating PEL dies are presented and the optimal techniques for cutting die lamination's top edge are identified. A matched-set of steel PEL dies for forming the benchmark part are also constructed. Regarding discrete forming dies, techniques for clamping the matrix of die elements into a rigid tool are surveyed and structural behavior theories of the clamped element matrix are proposed and experimentally verified. Furthermore, new techniques and mechanisms for setting the die shape are presented. A matched-die set of discrete dies are fabricated for forming the benchmark part shape.

Objective comparisons between each of the three fabrication methods are made as part of a study involving stamping experiments of the benchmark part shape. Cost and lead-time are the main criteria used in the study. Based on the conclusions reached, recommendations for future work on the PEL die and discrete die fabrications method are suggested.

Thesis Supervisor: David Hardt
Title: Professor of Mechanical Engineering

Dedication

This thesis is dedicated to the memory of my father

Robert S. Walczyk, Sr.
(1928 - 1994)

a man of great intelligence and wit
who inspired me to strive for excellence
in all of life's endeavors.

Acknowledgments

During my four years at MIT, many people have helped me either directly or indirectly with the research work presented in this thesis document.

Most importantly, I would like to thank my thesis advisor, Professor David E. Hardt, for his skillful guidance of my thesis work and for the sound career advice. He has also unwittingly served as an excellent role model for my future academic career. I would also like to thank the other members of my thesis committee: Professor Alexander Slocum for his innovative ideas and practical suggestions that helped to focus the scope of my thesis, and Professor Mary Boyce for suggestions that helped me develop a more disciplined approach to research and technical writing.

Many thanks go out to my good friends at MIT including Upendra Ummethala and Mohsen Mosleh for their useful comments on many of my research ideas; Apostolos Karafillis for his expert analytical support; Fred Coté for teaching me how to machine; Gerry Wentworth for answering all of my unusual manufacturing questions; Andrew Parris for providing me with useful information on sheet metal forming; and Jorgé Arinez for helping to keep me awake during many of those long nights spent machining parts and running experiments.

I would also like to acknowledge Eugenia Bulawa Walczyk, my mother, whose loving support helped motivate me to finish; and Dr. Jeffrey Walczyk, my brother, who helped persuade me to pursue both a Ph.D. and a career in academia.

Finally, I would like to thank Ms. Ann M. Seman—my best friend, confidant, and wife—who helped me in immeasurable ways during the final push to finish this thesis.

This work was supported solely by the National Science Foundation Grant No. DDM-9202362.

Table of Contents

List of Figures

List of Tables

Chapter 1 - Introduction

1.1 THE PROBLEMS WITH SHEET METAL FORMING

As manufacturing companies around the globe adopt "lean production" techniques to stay competitive in the world economy, there is an effort afoot in the sheet metal forming sector of industry to reduce the lead time and investment costs of tooling development [Womack,1991]. For the sake of clarity, sheet metal is defined as any piece of uniform thickness metal less than 6.4 mm thick characterized by a high ratio of surface area to thickness [Semiatin,1993]. Such an effort to reduce lead-time and cost is sorely needed because the development of dies used to form sheet metal parts is extremely time-consuming and expensive for industry. The following examples support this point:

> In the auto industry, construction of forming dies for sheet metal is the longest lead time element of any new major vehicle program [Walker,1993]. A new major vehicle program typically requires stamping dies for around 100 sheet metal parts. In one particular instance, a major U.S. die builder designed and fabricated 11 prototype (kirksite) and production (cast iron) die sets made for stamping the left and right quarter panels of a mid-size car. The die sets, which will stamp about 1.5 million panels during their lifetime, cost the customer $3,200,000 and took over 60 weeks to complete [Wagner,1995].
>
> For a particular U.S. aerospace company, a Richlite die (paper laminates impregnated with phenolic resins) used for stretch forming aircraft body panels costs $19,000 and takes 90 hours to fabricate (including tool design effort) on average [Nardiello,1995]. Since each F-14 fighter aircraft manufactured by this company has about 300 stretch-formed fuselage skins, the total cost of stretch forming tooling used for only about 750 planes was over $5,000,000.
>
> The leading air conditioning equipment manufacturer in the world uses a set of four stamping dies (draw, trim, flange, and side pierce) to stamp a 0.55 m x 0.44 m x 0.3 m draw base pan for a residential air-conditioning unit. These dies, which will stamp 1,000,000 panels during their lifetime, took 14 weeks to design and fabricate (over 50% of time due to internal delays) at a cost of $150,000 [Dastidar,1995].

The high cost and long lead-times of die development can be blamed on the traditional trial and error procedure used by skilled die builders to obtain the correct tooling shape and forming conditions which will yield the desired part shape [Siekerk,1986]. To understand

how this current approach developed, we need to look at the historical development of sheet metal forming technology and practices.

1.2 ORIGIN OF THE PROBLEMS

For thousands of years, sheet metal forming was been practiced by skilled artisans like the metalworkers of the ancient Greek and Egyptian cultures who hand-hammered cooking implements out of copper and bronze. Roman soldiers and medieval knights used hand-shaped metal plates for portions of their military dress. Ornamental sheet metal implements were created by the skilled gold and bronze workers of old Italy and Spain. Early artisans individually formed each sheet metal part using a hammer, mandrel, and some basic forms or dies [Wilson,1980]. Repeated forming of the same sheet metal part using dies didn't become a common manufacturing method until the 19th century [Smith,1896]. During this period, there were many new sheet metal forming processes invented (e.g. drawing, curling, blanking), for which special tooling was contrived. The tooling was used on any of a wide array of hand-operated and powered presses. Furthermore, the introduction of continuous strip mills in the 1920's and 1930's helped pave the way for pressforming of large panels. Such advances in tooling and equipment technology allowed cheap and uniform production of much of the everyday hardware (cooking utensils, typewriters, etc.) created during the industrial revolution. Since then, the forming of sheet metal had become a popular manufacturing method for creating net shape parts economically and efficiently.

As previously mentioned, arriving at the correct tooling shape and forming conditions for forming sheet metal parts on a mass scale - the most expensive and time-consuming activity in the tooling development - has historically been a trial and error procedure based on the skill and experience of die builders. This heuristic approach was seen as the only way to handle the springback in the deformed sheet metal; warping of the part shape from cutting operations like punching, slotting, lancing and trimming; heat treatment of the metal; non-linear mechanical properties of the material; and the complexities of the tribological conditions during forming. In addition, forming conditions which cause tearing and buckling of the sheet metal have to be avoided [Hosford,1983].

Circa 1960, the approach to sheet metal part and tooling development was still more of an art than a science [Bezier,1990]. For example, with the automotive companies, stylists designed the shape of a car through a sketch or small mock-up. Body designers would then express the shape by it's cross-sections which were used by Plasterers and Patternmakers to create the plaster master model of the sheet metal part shape. This hand-

crafted model would then be used by the tool designers and builders as the template for creating the forming dies. Eventually the die cavities were machined into a casting or billet by tracing out the plaster templates, i.e. copy milling. The trouble with copy milling dies with plaster templates is that part dimensional tolerances of more than 1.5 mm outside the product specifications are common [O'Connor, 1994]. Furthermore, these templates are expensive. In the die tryout, die engineers and builders would typically begin with tooling that slightly overdraws the sheet metal blank to account for springback. The procedures used to converge to the correct tooling conditions included adjusting the shape of the forming surface by adding (e.g. welding on) and removing (e.g. grinding away) material; varying the binder force with draw beads or by changing the binder pressure; and varying friction between the die and the blank by changing the finish of the die surface and/or changing the lubrication. Recent progress in tooling development which is discussed in the next section has significantly shortened the time and expense of this procedure by reducing the design time and the number of forming iterations needed to converge to the correct die shape.

1.3 THE CURRENT STATE OF TOOLING DEVELOPMENT

Until World War II, only modest improvements were made in sheet metal forming technology, mainly in the area of equipment. Since then, extensive research and developmental effort has been expended on gaining a better understanding of the forming process, predicting the dynamic behavior of the deforming sheet, and optimizing the production techniques used to form sheet metal parts [Hosford,1983]. The main goal of this research has simply been to reduce the cost and lead-time of tooling development. With the advent of practical computers in the late 1960's, significant progress has been made in Computer-Aided Design (CAD) software used for the design of 3-D sheet metal parts and forming surfaces; accurate simulation of the forming process using Finite-element Analysis (FEA) software; algorithms for generating the NC code needed to automatically machine the forming dies used in Computer-Aided Manufacturing (CAM) software; CNC-based part trimming; and computer-based digitization of the part geometry after a forming trial.

The vast majority of industries that make sheet metal parts, especially automotive and aircraft, are embracing the new computer hardware and software, and analysis tools which can be used for rapid and inexpensive tooling development [Nakagawa,1994]. In fact, the new tooling development system that has emerged begins with sheet metal parts that are designed on a computer using any number of commercially-available CAD

packages like CATIA™, AutoCAD™, and ProEngineer™. A designer creates the shape of a part with mathematically-defined 3-D surfaces like spheres and planes which are defined with Cartesian coordinates (analytic surfaces). For more complex 3-D part surfaces, a designer will first create a wire-frame model of the surface with geometry-defining boundaries or edges. This wire-frame model is an assembly of closed trilateral or quadrilateral boundaries which share common edges as shown in figure 1.1. To create the complete 'composite' part surfaces (i.e. surface that resembles a quilt), each closed boundary is then meshed in, as is also shown in figure 1.1 (sculpted surface), using a surface patch of parametric form $r = r(u,v)$ where the function is single-valued in u and v. Parametric surfaces that are often used in CAD software include Bezier, B-Spline, NURBS, or Coons patches [Faux,1979]. Both analytic and sculpted CAD surfaces allow a designer to view the sheet metal part from different viewpoints and even incorporate light sources and shading. Since the CAD models of the sheet metal part and forming tools are essentially exact, the subjectivity of the 3-D coordinate data, in contrast with the older non-computer based method, is eliminated. The CAD surface database can be used for aerodynamic analyses (e.g. Computational Fluid Dynamics programs) of sheet metal body skins as is done in the automotive and aerospace industries. Design changes or corrections are then easily incorporated into the CAD models of each part because it's all done electronically.

Once the sheet metal part is designed, the one or more operations required to transform the sheet metal blank into the desired part, including both die shape and forming conditions (binder design, lubrication, etc.), can be accurately simulated using FEA. See [Honecker,1989] and [DaRe,1994], for example. Powerful FEA codes such as ABAQUS™ Explicit and DYNA-3D™ are used for this purpose. With FEA, both the die shape and various process variables can be changed "off-line" in a more sophisticated trial and error correction procedure. Since the forming simulation doesn't model the system exactly, there are always some modifications that must made to the initial die shape and process parameters (prescribed by the simulation results) but not nearly as much as with older die development methods.

Along with the developments in design and analysis software, computer technology has helped to reduce the time needed to fabricate the tooling used in sheet metal forming. As compared to traditional methods of fabrication [Anonymous,1968], both soft (e.g. kirksite, epoxy) or hard tooling (e.g. cast iron, tool steel) used for die tryout and parts production are rapidly machined to the correct shape using NC code generated by a CAM software package (e.g. Mastercam™, Cimatron™) based on a spatial representation (e.g.

CAD model or 3-D coordinates from scanning) of the required die surface. Stamped sheet metal parts that require blanking, perimeter trimming, or cut-out operations normally require the development of special dies. Trimming and cutting of stamped sheet metal parts with multi-axis CNC laser and AWJ cutters has eliminated the need for these types of dies in many forming situations [Connolly,1994]. As part of the developmental process, a contact-type Coordinate Measuring Machine (CMM) is used to quickly measure the geometry of a stamped part. Accurate measurements of various part features are compared with the CAD part shape and the difference between the actual and CAD shapes (i.e. shape error) is used by die makers and engineers to determine how to correctly change the die shape and forming conditions. This trial-and-error procedure is repeated until the stamped parts are consistently within specifications. Unfortunately, modifications to the die shape are still performed manually. This "current" tooling development system is illustrated in figure 1.2.

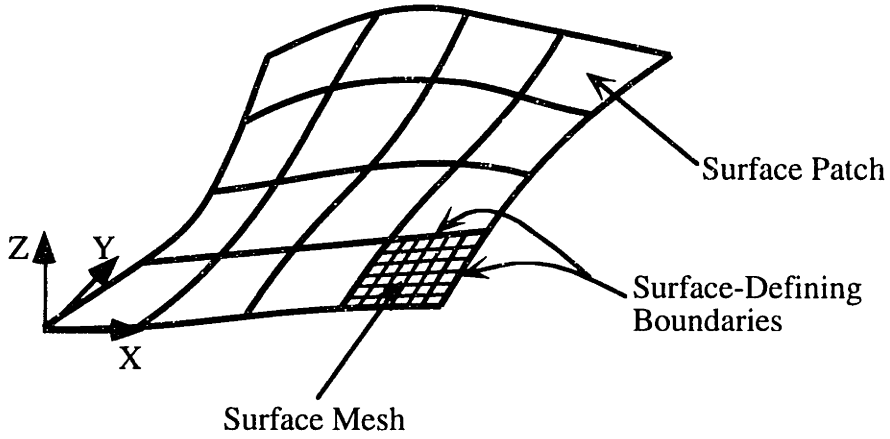

Figure 1.1 - Surface-defining boundaries of a CAD surface model with a meshed-in surface patch.

1.4 THE FUTURE OF TOOLING DEVELOPMENT

"Although the rationalization of the design and manufacturing processes has helped reduce the manufacturing time substantially, the time needed to correct the die after trial forming has yet to be shortened" [Nakagawa,1994]. This represents about 40% of the total die development time. The application of closed loop process control to sheet metal die development is an alternative approach to tooling design which has the potential to dramatically reduce the time needed to correct or adjust the die shape. As illustrated in figure 1.3, closed-loop process control naturally incorporates the newest software tools, hardware, and die fabrication methods. Webb and Hardt have developed a closed-loop approach that treats the complex material deformation of the forming process as a system

identification problem where the tooling-part transformation is developed as a spatial frequency domain transfer function [Webb,1991;Hardt,1982]. It has been shown experimentally [Ousterhout,1991] and through FEA simulations [Karafillis,1992] that such a transfer function can be used to implement closed-loop process control of 3-dimensional sheet metal forming via rapid die redesign. Karafillis has also shown how the correct tooling shape and binder design can be found with FEA-based inverse springback calculations [Karafillis,1992 and 1994]. Process control of this sort takes the place of the time consuming trial-and-error procedure.

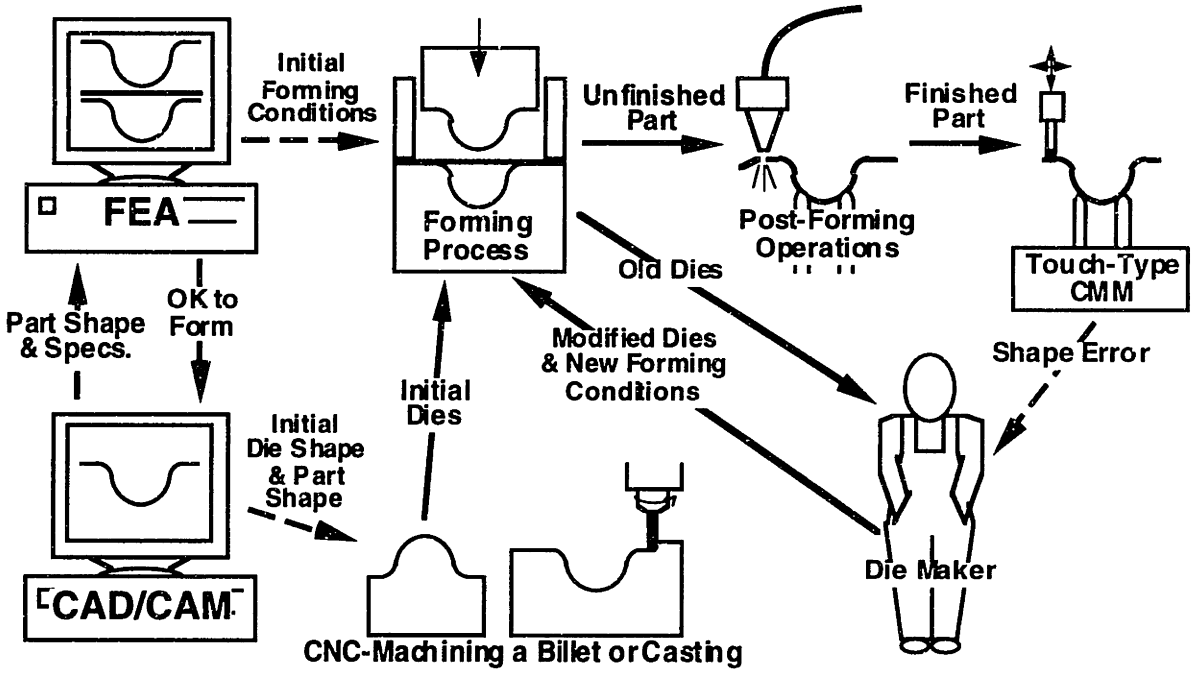

Figure 1.2 - "Current" development system for sheet metal forming tools.

As shown in figure 1.3, a concurrent part shape and forming process development system which utilizes tooling development algorithms and closed-loop simulations will be used initially to design a theoretically correct die shape and forming conditions. Eventually the concurrent design of sheet metal parts and the associated tooling may be done completely off-line in a visually-based virtual reality environment [Chiangi,1994]. Closed-loop process control applied to a physical prototyping system will be used to fine-tune the process (i.e. automatically sense and account for deviations from the CAD part shape). Specifically, the finished part shape will be measured in a parallel fashion using some sort of non-contact surface scanning system [Karlin,1995]. Required shape modifications of the die forming surfaces will be based on a closed-loop shape control algorithm thereby obviating the subjectivity of experienced tool makers and tooling engineers.

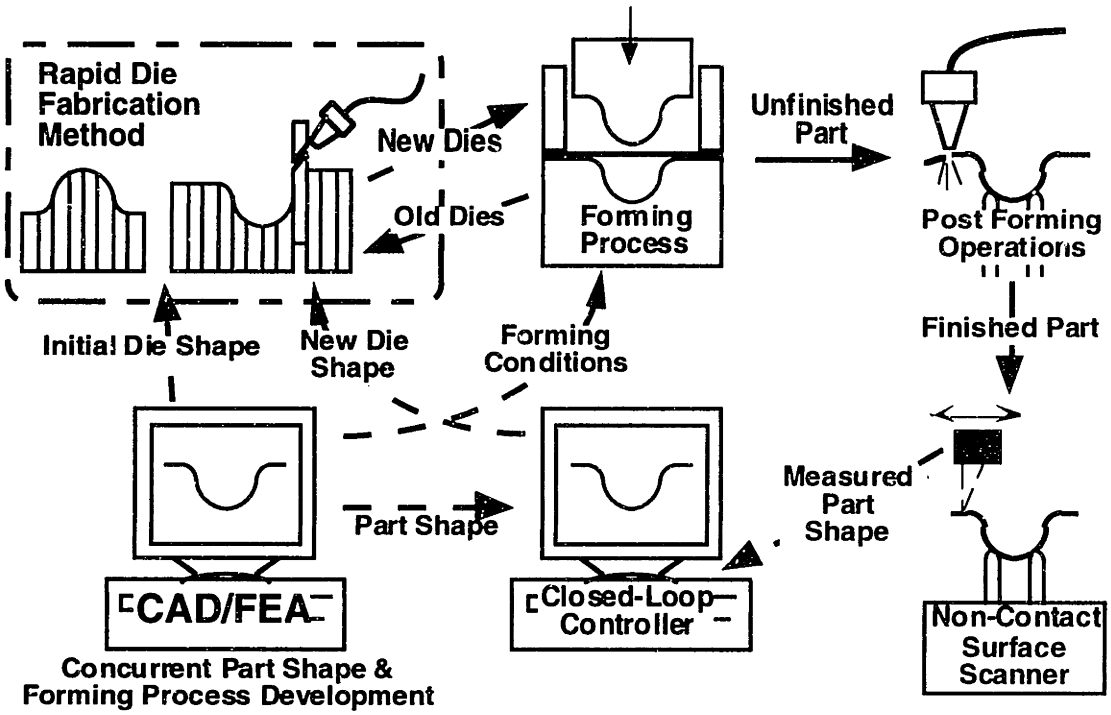

Figure 1.3 - Future tooling development system that incorporates closed-loop shape control.

With either the conventional trial-and-error procedure or the recently developed closed-loop procedure, the high cost and long lead-times associated with die development still persist although significantly less for the latter case [Ousterhout,1991]. As computer-based die design algorithms and FEA-based simulations become quicker and more accurate, the fabrication and modification method used for the die development process plays a greater role than ever in reducing these factors. For these reasons, the die fabrication/modification method used in a modern die development program should ideally be both rapid and low-cost.

1.5 FABRICATION METHODS FOR RAPID DIE DEVELOPMENT

The remainder of this thesis focuses on identifying existing methods and developing new fabrication methods for sheet metal forming dies that are both rapid and low-cost. The chosen methods are earmarked for use in flexible or "agile" manufacturing systems such as the closed-loop control system developed by Hardt et al. [Hardt,1982; Webb,1991; Ousterhout,1991; Karafillis,1992]. Consequently, the thesis is organized as follows:

Chapter 2 begins by reviewing the state-of-the-art on all sheet metal forming processes. This review shows how the most important issue in tooling

development for all the commercially-viable forming processes is the need for one or two rigid dies. This observation further focuses the scope of this thesis to rigid die fabrication methods only. Three rigid die fabrication methods identified as rapid and low-cost include CNC-machining a solid billet (standard), a new way of assembling and clamping an array of laminations, and configuring and clamping a close-packed matrix of discrete elements. The reasons for choosing to study and develop these three methods are then discussed. Finally, a benchmark part shape for forming out of sheet metal is designed. This part is formed using dies fabricated using each of the 3 candidate fabrication methods as part of a comparative study.

Chapter 3 further reviews the state-of-the-art in CNC-machining of die surfaces, and describes the detailed fabrication of a matched set of solid dies that are CNC-machined from solid steel billets.

Chapter 4 introduces the new laminated die method (i.e. Profiled-Edge Lamination or PEL die) and discusses various aspects of the method in detail; describes new apparatus concepts for fabricating such dies; identifies the optimal method(s) for making profiled beveled cuts into PEL laminations; and finally describes the construction of a matched set of steel PEL dies.

Chapter 5 further reviews the state-of-the-art in close-packed discrete element dies; describes new developments in setting and clamping an array of discrete elements; and describes the detailed design, construction, and setting of a matched set of high-resolution steel discrete dies.

Chapter 6 describes an experimentally-based comparative study of the 3 candidate fabrication methods; the successes and failures of forming sheet metal parts with each of the die sets; and then makes comparisons between each of the fabrication methods based on cost, lead-time, flexibility and accuracy issues.

Chapter 7 formalizes the conclusions of the comparative study, summarizes how the state-of-the-art in laminated and discrete die design has been advanced by this thesis work, and makes recommendations for future research in these areas. Also in this chapter; a new fabrication method is introduced which is a hybrid between CNC-machining a continuous die and assembling an array of PELs; and the detailed design and construction of one such die is presented. It will be called the CNC-Machined Lamination (CML) die method.

Besides addressing the immediate need for rapid and low-cost fabrication methods for sheet metal tooling development, this thesis also addresses the fundamental issues of developing new equipment for new manufacturing processes that are introduced. In this case, the new manufacturing processes for which equipment needs to be developed are the PEL die, discrete die, and CML die fabrication methods. From the comparative study described in chapter 6 and the discussion in chapter 7, all three of these die fabrication methods are shown to have certain advantages over the industry's standard of CNC-machining a solid billet. The advantages of these new methods will undoubtedly make their implementation attractive to companies that have to deal with in-house or outside-vendor tooling development. Without the availability of the necessary equipment, a

manufacturing company is usually unwilling to commit the resources necessary to develop the machinery and so they eventually lose interest. Academic researchers in the U.S. are beginning to realize the lost commercial opportunities from not following through with equipment development of new manufacturing technologies. To address these opportunities, many universities have created laboratories and technology centers (e.g. Manufacturing Institute at MIT) that work closely with industrial partners to only focus on process machinery development. In this spirit, this thesis also investigates many of the machinery issues associated with the PEL die, discrete die, and CML die methods in an attempt to help "jump start" their commercialization.

Chapter 2 - Background

The main goal of this chapter is to show the rationality behind choosing the three candidate fabrication methods for detailed study. This is accomplished by first providing background material on all the commercially-viable processes for forming sheet metal parts. After a detailed investigation of these processes, we see that the most important issue in modern tooling development is actually in the rapid and low-cost fabrication of rigid dies. What follows is a brief investigation of all the existing methods of rigid die fabrication. What we find is that only three methods fit the rapid and low-cost criteria. Moreover, these chosen methods are conducive to the newly-emerging tooling development system for sheet metal parts presented in section 1.4. Finally, the design and analysis of the benchmark shape used to compare the candidate fabrication methods is described.

2.1 SHEET METAL FORMING PROCESSES

There are many different processes currently used by manufacturers for forming parts from sheet metal. In a recent survey by the Fabricators & Manufacturers Association, International [FMA,1994], the member companies—most based in the U.S.—were asked among other things to indicate which sheet metal forming processes they use in the manufacture of their products. Out of the 1439 member companies listed, a breakdown of the forming processes they use and their relative usage among all the members is listed in table 2.1. The cold forming category encompasses all processes where strain hardening in the plastically deformed sheet metal is present due to conditions of low strain rate and temperature during forming. The category of hot forming then encompasses all processes where strain hardening is avoided because of higher forming temperatures. Two very common forming process which were not separate categories in the survey are matched-die forming used extensively in the auto industry and stretch-forming used extensively by the aircraft industry [Williams,1977]. Other less common forming processes which were also excluded from the survey include hydromechanical forming used extensively by the Toyota Motor Corp. [Nakamura,1994], creep forming, androforming, and drop hammer forming. Two new processes that are currently being developed but have yet to be used

commercially include forming with Sacrificial tooling and Laserforming. While using any of the forming processes mentioned in table 2.1 or the above mentioned ones, the formability of the sheet metal can be enhanced by forming in it's superplastic condition due to heating (superplastic forming) or by applying ultrasonic energy in the form of high-frequency vibrations (ultrasonic-activated forming) [Wick,1984].

Table 2.1 - Sheet Metal Forming Processes used in Industry

Sheet Metal Forming Process	Number of Companies	Percentage of Total Membership
Cold Forming and Bending	393	27
Roll Forming	198	13.8
Drawing	155	10.8
Roll Bending	129	9.0
Deep Drawing	93	6.5
Hot Forming and Bending	52	3.6
Hydroforming and Rubber Pad Forming	38	2.6
Conventional Spinning	36	2.5
Peen Forming	6	0.4
Electrohydraulic Forming	4	0.3
Electromagnetic (magnetic-pulse)	3	0.2
Ultrasonic-Activated Forming	2	0.1
Explosive Forming	1	0.1

Each of the aforementioned processes will be briefly discussed to point out what the major issues are in tooling development that contribute to the high cost and long lead-times. Since we are interested in processes which are suitable for creating 3-dimensional sheet metal parts of arbitrary shape, roll forming and roll bending will be excluded in this discussion. Roll bending is used to induce only simple curvature in sheet metal (i.e. cylindrical shells) and roll forming is used to produce long components of various 2-dimensional cross-sections.

2.1.1 Dual Die Processes

All the processes described in this section require the fabrication of two rigid dies which impart their shape into the sheet metal blank. To avoid wrinkling and tearing in the metal during forming, a blankholder is used to restrain the movement of workpiece.

2.1.1.1 Matched-Die Forming

In matched-die forming, a male die (called a punch) and a matching female die (simply called a die) are used to form arbitrary 3-D shapes in sheet metal. The punch and die are not perfectly matched because they must account for the sheet metal thickness during forming. As shown in figure 2.1, many different types of sheet metal parts are formed with this process including most auto body panels.

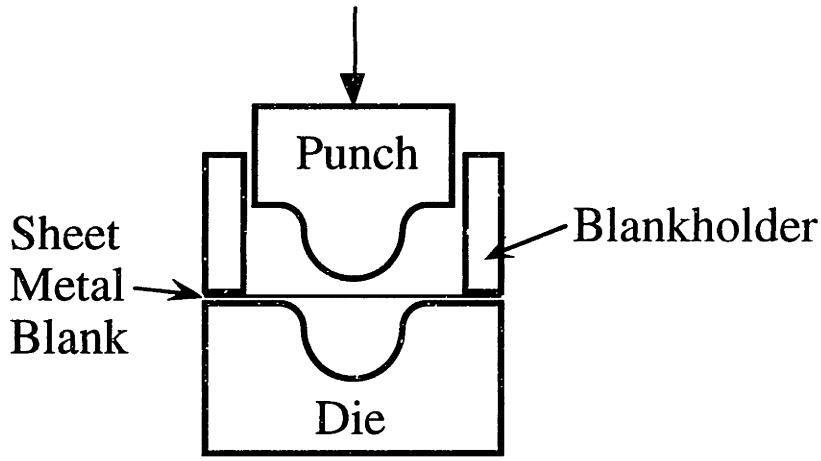

Figure 2.1 - Matched-set of forming dies.

These die sets are typically mounted in a machine tool known as a press which has a stationary bed and a ram that moves at right angles to the bed surface with a linear motion. This type of press is known as single-acting. A variety of forming presses are currently used in industry including:

- mechanical presses which use a slider-crank or knucklejoint mechanism to give a limited stroke,
- screw presses that derive their energy from a flywheel attached to the screw and are not stroke limited,
- hydraulic presses that have a constant low speed and allow the force to be controlled during the forming operation, and
- gravity-drop hammer presses that derives the energy required for forming from a falling ram.

2.1.1.2 Drawing/Deep Drawing

Drawing refers to the process for producing a cup-like sheet metal part from a flat blank. This process is performed by pressing the metal blank that is firmly held between two blankholding surfaces into a die with a punch. The die and punch may or may not have the same shape as the formed part. If the depth of the formed cup is equal to or more than the radius of the cup, the process is known as deep drawing. Deep drawn parts are typically formed with a double-acting press which is equipped with an inner ram (known as the slide) and an outer ram (known as the blankholder). An axisymmetric part that's being deep drawn in a double-acting press is shown in figure 2.2.

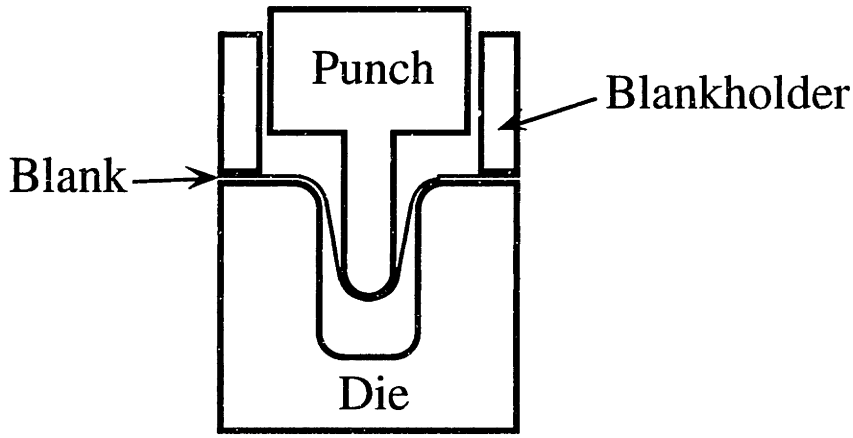

Figure 2.2 - Axisymmetric part formed with a set of deep draw dies.

2.1.2 Single Die Processes

Each of the processes described in this section requires the fabrication of only one shape-defining rigid die which imparts the part shape into the sheet metal blank through various means. A blankholder may or may not be used in each of these processes.

2.1.2.1 Forming with Flexible Tooling

Forming processes involving flexible tooling require only one shape-defining rigid die and a flexible member which replaces the redundant second rigid die of matched tooling sets. The first type of flexible tooling was developed back in 1935 at the Douglas Aircraft Co. It is known as the Guerin rubber-pad process named after the engineer that developed it but is commonly referred to as rubberforming [Schubert,1966]. As shown in figure 2.3, the sheet metal part is formed by first placing a metal blank and a draw ring between a lower rigid male or female die and an upper pad of rubber, usually urethane, which should

have a thickness about three times the maximum draw height. As the rubber die descends, the rubber deforms and pushes the metal over or into the rigid die. This process is used extensively in the aircraft industry, particularly in making parts with shallow flanges. Another method, the marform process, is identical to rubber forming except that the blankholder pressure is automatically regulated through a pressure-control valve.

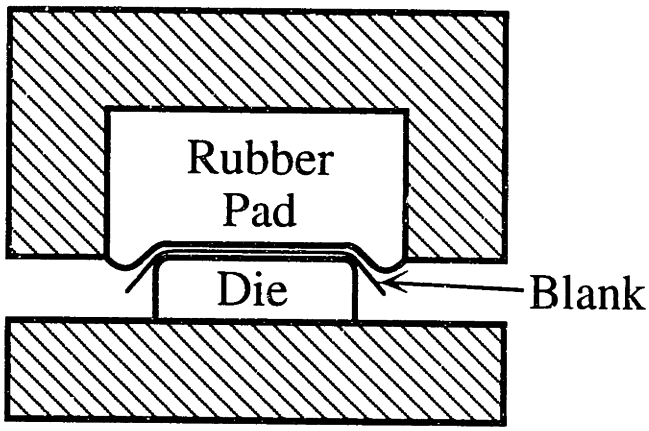

Figure 2.3 - Schematic of the rubber forming process

The Verson-Wheelon process is similar to rubberforming except that the rubber pad is forced around the lower rigid die by an inflatable rubber bag. The bag is inflated with high pressure hydraulic fluid. Since the forming pressures are about 4 to 5 times that of the rubberforming process, deeper and more complex part shapes can be formed. Hydroforming is similar to the Verson-Wheelon process in that the die consists of a flexible rubber diaphragm backed by high pressure fluid [Nilsson,1989]. The main difference is that a hydroforming press doesn't use an inflatable bag and a thick rubber die. As hydraulic fluid is pumped into the void behind the diaphragm, it expands over the rigid die and forces the metal blank to take on the desired shape as shown in figure 2.4. The first hydroforming machine was developed in the 1950's by the Cincinnati Milling Machine Co. Both methods allow trimming and piercing operations to take place during forming. Furthermore, the fluid pressure can be controlled during the entire forming cycle.

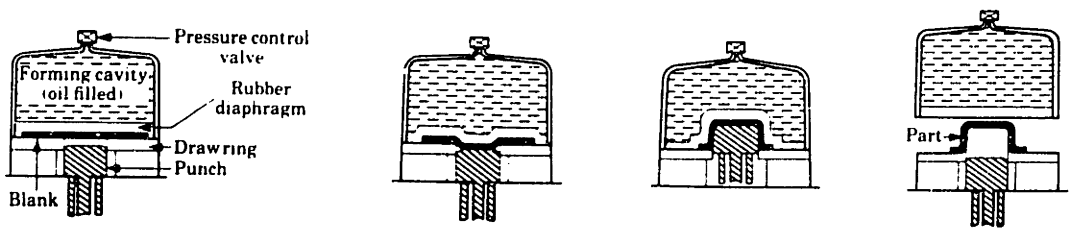

Figure 2.4 - Schematic of the hydroforming process [Kalpakjian,1984]

Hydromechanical drawing, also known as liquid-pressure press forming, is a newly developed method of flexible forming which combines features of both rubberforming and hydroforming. [Nakamura,1994] has helped apply it to the mass production of auto body panels. The method involves binding the sheet metal blank around it's entire periphery and suspending it over a tank of hydraulic fluid as seen in figure 2.5. As a rigid male die draws the blank downward, the fluid pressure generated on the opposite side of the blank pushes the sheet metal into the rigid die. However, trimming and piercing operations cannot be performed with this method since the high fluid pressure would be lost immediately.

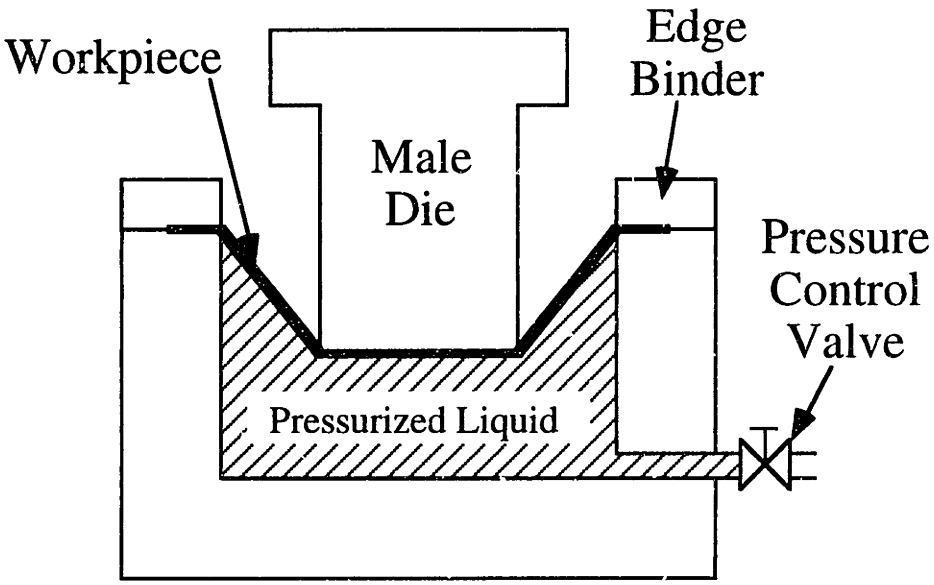

Figure 2.5 - Schematic of the hydromechanical forming process.

2.1.2.2 Spinning

Spinning is a process which is used form axially symmetric sheet metal parts over a mandrel with the use of rigid tools or rollers. A circular sheet metal blank is attached to the mandrel by an outer diameter clamping ring or a small centrally-located clamping disk. There are two main types of spinning which are conventional spinning and shear forming. As seen in figure 2.6a, a conventional spinning operation forms the blank over the mandrel through a sequence of passes using either manually or hydraulically-actuated tool. Shear forming is a rotary-point extrusion process which involves an axial-radial pass of a roller tool as shown in figure 2.6b.

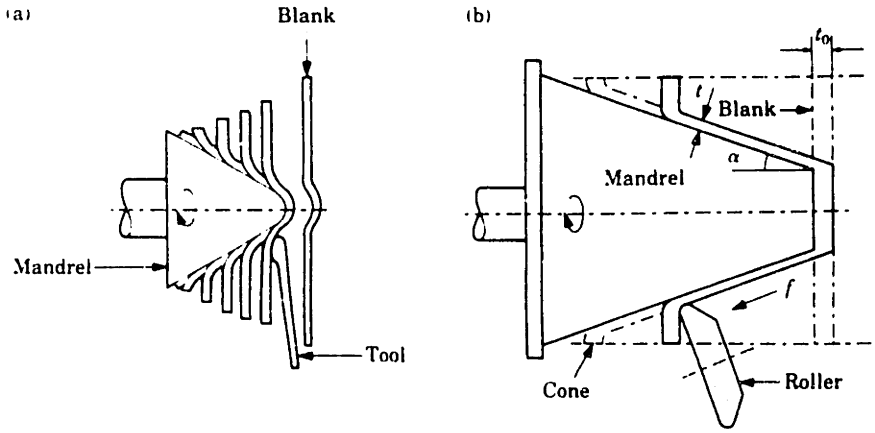

Figure 2.6 - Schematics of a) Conventional spinning and b) shear forming [Kalpakjian,1984]

2.1.2.3 Stretch Forming

The stretch forming process is used to form sheet metal parts by clamping the blank at its edges and then stretching it over a single die [see Williams,1977]. The tension or stretch applied to the material causes permanent or plastic strains to occur in varying degree across the cross section of the sheet metal thereby minimizing the springback in the part. Two methods that are currently used to induce stretching in the material are tranditional stretch forming (figure 2.7) where the die moves into the clamped sheet, and stretch-wrap forming where the sheet is first yielded and then wrapped over the die. Stretch forming can handle doubly-curved parts but it's limited to convex shapes that have gradual contours and no sharp bends.

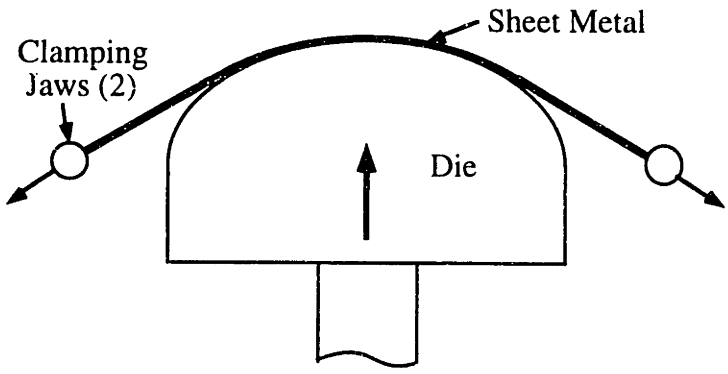

Figure 2.7 -Schematic of stretch forming.

2.1.2.4 Peen Forming

Peen forming is a process whereby curvatures of a die are imparted in sheet metal by shot peening the non-die side surface of the sheet. The shot peened surface of the sheet metal is subjected to compressive stresses which tends to expand this layer. The material layer expansion causes the sheet to develop a curvature until it eventually contacts the rigid die beneath. The residual compressive stresses in the metal improve the fatigue strength of the material. Like stretch forming, this process is used extensively by the aircraft industry for forming aircraft wing skins.

2.1.2.5 Creep Forming

A good example of hot working sheet metal is with a process know as creep forming. When heat is applied to a metal blank draped over a convex die for a sufficient period of time, metallurgical creep causes relaxation of the induced elastic stresses to such a level that plastic deformation of the sheet is achieved. Thus, the sheet metal takes on the shape of the die. This process is used almost exclusively by the aircraft industry to form aircraft body panels [Wick,1984].

2.1.2.6 High-Energy-Rate Forming (HERF)

Forming processes that are categorized as HERF use chemical, electrical, and magnetic sources of energy to achieve high power (i.e. energy rate) for forming [Davies,1970]. In explosive forming an explosive charge is detonated in a tank of transmitting fluid (usually water) above a sheet metal blank which is clamped to a forming die. The resulting pressure wave forces the sheet metal into the die by it's own kinetic energy. Electro-hydraulic forming is similar to explosive forming except that the shock wave is created by the rapid discharge of electricity across two electrodes that are immersed in water and connected together by a thin initiating wire. A rapid discharge of electrical current is also the energy source for electromagnetic (magnetic-pulse) forming. With this process, the rapid electrical discharge through a magnetic coil produces a strong magnetic field. This strong magnetic field induces eddy currents in the neighboring sheet metal which in turn creates it's own magnetic field. The interaction of these two opposing magnetic fields generates high repelling forces on the sheet metal which forces the metal into the rigid die.

2.1.3 Die-Less Processes

Each process described in this section requires no rigid dies to impart the desired shape into the sheet metal. Androforming is currently a commercially-viable process while flexible stretch forming, forming with sacrificial tooling and laserforming are still in the developmental stage.

2.1.3.1 Androforming

The androforming process is used to form sheet metal parts with compound curvatures without the need for rigid dies [Wick,1984]. The shape of the part is established by pulling the sheet material with a set of conformable gripping jaws through three stages of dynamically-controlled forming elements. The first stage consists of a pair of straight forming dies. The second and third stages consist of adjustable contour dies which are programmable. The final shape of the formed sheet metal part is determined by adjusting the positions of the three stages with respect to each other. Typical androformed parts are the panel sections that form large satellite dishes.

2.1.3.2 Flexible Stretchforming

Instead of using a fixed die for stretchforming (see section 2.1.2.3), a sheet metal part can also be progressively stretchformed with freely positionable tool sets (ram and die). [Eckart,1993] has created such a forming press whose tool sets are under CNC control.

2.1.3.3 Forming with Sacrificial Tooling

Sacrificial tooling is typically made of a polymer foam or any high compressive strength material which collapses (reducing in volume) when subjected to a specific surface pressure. [Appleton,1984] has used a two part foam, made by cementing hollow glass microspheres with a binder, as a sacrificial backing material for a single spherical programmable roller working from one side of the sheet metal. As shown in figure 2.8, the desired part shape is generated progressively by repeated passes of the working roller incrementing the roller at each pass. During this process, the sacrificial backing material permanently collapses on the opposite side of the sheet metal.

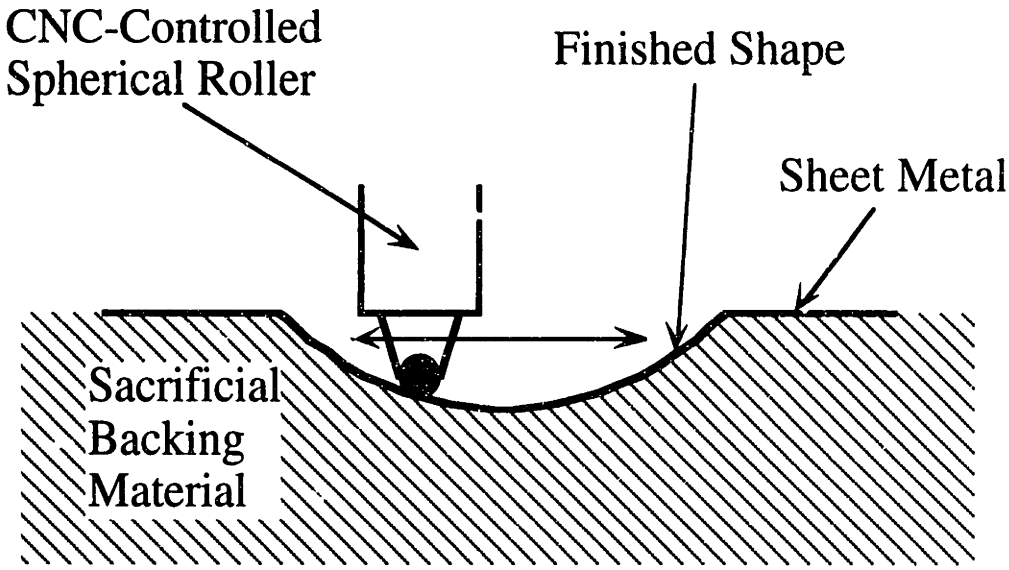

Figure 2.8 - Schematic of sacrificial tooling for sheet metal forming

2.1.3.4 Laser Forming

Laser forming is a brand new process for shaping sheet metal into usable parts. This process involves heating the sheet metal blank along a straight line with a laser beam (e.g. CO_2) directed normal to the surface and cooling the heated line with a jet stream of cold gas or misted water that follows the beam [Vaccari,1994]. Heating is controlled to create a plasticized zone that only partially penetrates the sheet thickness, causing the sheet to bend away from the beam. Intense cooling severely contracts the heated region, causing the sheet metal to bend toward the beam at a greater angle than it is bent away at. The net effect is that there is a permanent bend that propagates through the workpiece in a wavelike fashion. Even thought the process is very slow with scanning speeds on the order of 0.5 meters/sec, it may prove useful for prototype work and small batch runs of parts.

2.1.4 The Dominant Lead-Time and Cost Factor in Tooling Development

With the exception of die-less forming processes which constitute a negligible portion of all sheet metal part production, the real time and expense of tooling development for all the aforementioned forming processes comes from having to create at least one rigid die. Every process listed in sections 2.1.1 and 2.1.2 requires at least one rigid die for imparting the correct shape onto the sheet metal blank. Therefore, the next section of this

chapter focuses on the current methods of fabricating rigid dies used for sheet metal forming.

2.2 METHODS FOR FABRICATING RIGID DIES

From an extensive survey of the available literature on rigid die fabrication methods, the rigid die constructions currently used in industry can be categorized as either Continuous (including die inserts), an Array of Laminations, and a Matrix of Discrete Elements (discrete die). Dies of a continuous construction constitute the vast majority of prototype and production tooling currently used in industry. However, dies of a laminated and discrete (reconfigurable) construction are slowly gaining acceptance because of their applicability to flexible manufacturing systems as will be shown later in this thesis.

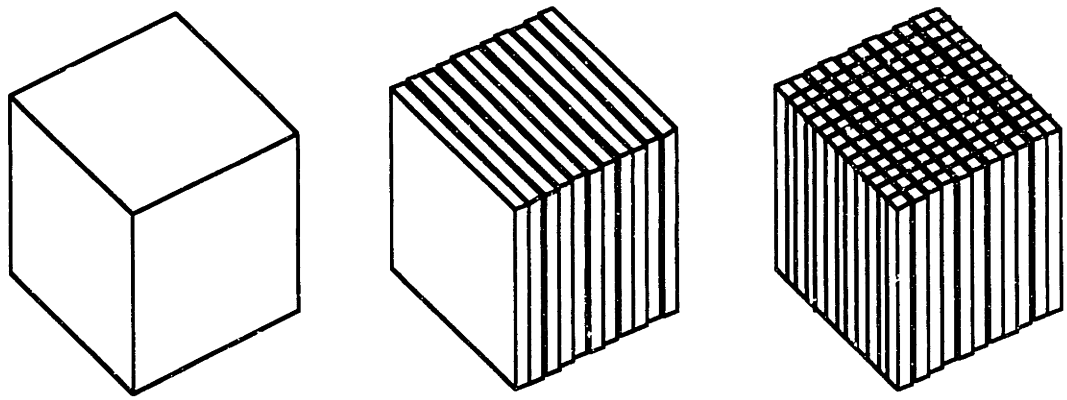

a) Continuous [monolithic] b) Laminated c) Discrete

Figure 2.9 - Construction methods for rigid dies used in sheet metal forming

2.2.1 Continuous Die Construction

Many methods are used to fabricate continuous dies (see figure 2.9a) including CNC-machining and/or Electro-Discharge Machining (EDM) a billet of die material, and casting it in a mold. Eventually rapid tool making processes (e.g. selective laser sintering) will also be used.

The materials used for continuous sheet metal forming dies are usually selected on the basis of providing adequate die life at minimum cost. Wear—produced by abrasion and/or adhesion (galling)—determines the useful performance of a die. The total wear is primarily affected by the length of the part production run and the severity of the forming

operation (e.g. relative amount of sliding between the die and workpiece, contact pressures, frictional coefficient, and propensity for galling).

Forming dies for steel and aluminum parts that are subject to severe forming conditions are primarily made of tool steel, alloy steel (for aluminum only) and carbide. For dies requiring significantly high wear life when forming with lubrication (e.g. car body panels), tool steels such as D3, D4, A7, D7, M2 and M4 are recommended. When application of a lubricant is difficult as is the case with automatically fed high-production presses, die materials that are highly resistant to galling such as aluminum bronze, D2 steel, and carbide must be used. Aluminum bronzes are used for dies in applications where the best surface finish is required for stainless steel or carbon steel parts. For high temperature forming, A2 and D2 tool steels are used because these materials are more temper-resistant, i.e. able to withstand the effects of higher temperatures. For dies subjected to severe impact in service, shock resistant steels such as S1 and S5 should be used. The ultimate tool material in terms of resistance to galling, wear, and the detrimental effects of high temperatures is cemented carbide. However, it's cost is high and machining it is difficult (usually requiring EDM). For long runs (e.g. over 1 million parts), cemented carbides have proven to be the most economical die material.

Dies for steel and aluminum parts that are subject to milder forming conditions (e.g. shorter production runs, lower contact stresses) can be made from a wider range of materials. Such conditions exist in matched-die forming where the lower die typically lasts 10 times longer than the punch made of the same die material due to lower wear (i.e. workpiece sliding over the die surface). Another example is restriking dies that are subject to milder forming conditions when compared with the primary dies of a transfer line. For mild forming conditions, dies made of carburized hot-rolled steel, gray cast iron with hardened surfaces or hardened alloy steel produce parts of equal quality to those formed with dies made of other tool steels. For low production runs of steel parts then alloy steel, mild steel or zinc alloy dies are recommended. For low production runs of aluminum parts, epoxy-metal, polyester-metal, zinc alloy or mild steel dies are recommended [Semiatin,1988].

2.2.1.1 CNC-Machining

The most common method for fabricating sheet metal dies is CNC (computer numerical control) machining a solid billet of material. Prior to the development of CNC-machining, the die shape was machined into a billet of die material by copy milling from a master model. Numerical control of machine tools for diemaking began in the early 1960's

primarily with the automakers [Anonymous,1968]. Full-size models of the car body panels were either used as templates for copy-milling of the dies or their surfaces were digitized with scanners (early CMM's) to create the necessary NC database. The NC code was then used to run a 3-axis CNC milling machine with a ball endmill. CAD/CAM software, which allows die surfaces to be designed and then tooling paths generated using the computer, wasn't developed until the late 1970's [Chan,1980].

Currently, CNC milling centers with 3 to 5 axes of motion are used to machine complex 3-D die surfaces and CNC lathes are used to machine axisymmetric draw and spinning dies. The tooling (or cutter) paths needed to accurately rough-out and finish machine the forming die CAD surface are first defined, and then simulated in a CAM software package. When the die designer is satisfied with the simulations, the NC code needed to control the CNC machine is created. First the approximate die shape is created by a series of roughing cuts. Roughing cuts are ceased when a minimum value of metal removal is reached. The near-net die shape is then created with a series of finishing cuts (i.e. parallel machining passes with an endmill that a close together). The roughing and finishing cuts used to machine complex 3-D die surfaces typically take a long time and leave the surface scalloped. For an auto body panel die, a typical accuracy for the machining passes of a 13 mm end mill is 0.75 mm spacing between passes [Mayes,1993]. While the size of the scallops can be minimized by programming a finer step-over distance between adjacent cutter paths (small pitch cutting), this has the effect of significantly increasing the time required to machine the surface. The roughness of the scalloped surface can be minimized or even avoided by using flat bottom radiused endmills mounted in a 5-axis milling center which can keep the tool normal to the die surface. A grinding and polishing operation is always needed to remove the scallops before the machined die can be used to stamp sheet metal parts.

2.2.1.2 Casting

Continuous metal dies for sheet metal forming are often cast to near-net or net shape. Usually cast iron or cast steel is used for dies which are used to either form thick sheet metal stampings or large numbers of parts. Kirksite (zinc-based alloy) and fusible alloy (Wood's metal, type metal, 50% Zn/ 50% Sn, bismuth-based alloys) dies are typically used for prototypes or small batch runs of sheet metal parts. The main difficulties in making cast metal dies is their tendency to shrink as the dies cool down from the casting temperature as the die cures. In addition, their rough "as cast" forming surfaces usually require finishing cuts, grinding, and polishing. For a matched set of cast dies, oftentimes

one die is completely polished and then used as the electrode for electro-discharge machining (discussed in next section) the forming surface of the matching die.

Molds for the cast dies are made of sand (usually with a clay, thermosetting resin, or sodium silicate binder), plaster of Paris (gypsum), or a slurry of refractory ceramics which is formed around a model (investment casting) [Kalpakjian,1984]. Plaster and ceramic molds offer more precise castings because of the low mold shrinkage rate and the better dimensional accuracy they offer over sand castings. In an attempt to lessen the effect of mold expansion as the molten metal is poured in, [James,1967] was granted a patent for a sheet metal forming die consisting of brazed steel shot which has the same coefficient of thermal expansion as it's ceramic mold.

An alternative to dies made of a single material (e.g. steel) are cast composite dies which consist of a hard wear surface and a suitable backing material. The backing material is typically cast iron, steel, kirksite, concrete, or filled epoxy resin. The facing options are ceramics, metal-spray, filled epoxy resin, and Teflon [Langdon,1993]. As with all cast dies, a mold for the die is required. Numerous patents for composite dies have been issued including a laminated stretch form die [Querreiro,1971], cast resin die with fiberglass reinforcement at the surface [Kalis,1963; Miura,1992], and a cast resin die with a urethane forming face [Krowl,1985].

To make the model for a cast-die mold or to create a backing form for a composite die, there are numerous conventional and rapid prototyping technologies which can be used. On the conventional side, a builder constructs a model by assembling simple geometric shapes together, by conventional or CNC machining of a soft material (e.g. wax, plastic), foam for lost-foam casting, or with molding clay (e.g. for car body panels). New layer manufacturing processes which can create accurate die models are stereolithography (SLA), selective laser sintering (SLS), three-dimensional printing (3DP), and laminated object manufacturing (LOM). Stereolithography involves building up a model layer by layer with a UV laser that selectively solidifies a photosensitive liquid resin [Hull,1986]. An SLA mold has been used to cast a cement-based composite material as a rigid sheet metal forming die used in a hydroforming process [Berger,1993]. SLS models are created in a similar fashion to SLA but instead of a photosensitive resin, a deposited layer of polycarbonate, nylon, or wax is selectively sintered by a high-powered CO_2 laser [Deckard,1989]. The 3DP process creates models by repetitively spreading a layer of powder and selectively joining the powder within the layer by ink-jet printing of a binder material [Sachs,1993]. Either the model or the actual ceramic casting mold can be created with 3D printing [Sachs,1992]. A model made of paper or polyester can be created with an LOM which repetitively cuts thin sheet material into cross-sections of the CAD model with

a CO_2 laser and then stacks and bonds the laminations on top of each other [Feygin,1991]. Kruth discusses other developing rapid prototyping processes which will be able to produce mold models [Kruth,1991]. Finally, using a clamped matrix of individual elements has been proposed as a variable configuration die for casting sheet metal forming dies [Todoroki,1993].

An interesting method for creating a set of matched sheet metal dies from an existing sheet metal part sample is called Dualforming. The process involves the use of fusible alloy tooling which is cast by the Dualform press itself [Anonymous,1989]. Since fusible metal alloy is bismuth-based, it experiences very low shrinkage as the material cools as opposed to the significant shrinkage experienced by cast kirksite and steel dies [Morrison,1992]. For example, MCP System Incorporated's METSPEC 136 alloy has a low melting point of 58°C which means that the temperature drop after cooling is around 40°C. This amounts to a very low 1 mm/meter of shrinkage. A perforated sheet metal part is submerged in a bath of molten fusible alloy after which an upper platen with anchor mountings is lowered into the newly created pool just above the part. The entire bath is then cooled down to allow the fusible alloy to solidify and then the upper platen raises to separate the tooling. Finally, the perforated part is separated from the new bottom die. An existing 3-dimensional model can also be used to create a die set. The matched set of tooling can then be used to stamp sheet metal prototype parts or small batch runs of parts.

2.2.1.3 Electro-Discharge Machining

In industry, the process of electro-discharge machining a sheet metal forming die with a ram-type EDM machine is known as "die-sinking". This process is based on the erosion of metal by spark discharges between two electrodes (tool and the workpiece) that are immersed in a dielectric fluid bath (e.g. mineral oil). The term "die-sinking" refers to the tool sinking into the workpiece to form a cavity. EDM electrodes are made of brass, copper, copper-tungsten, or graphite. The workpiece can be any electrically-conductive metal (e.g. tool steel, cast iron) but it's rate of erosion during EDM must be much greater than that of the electrode for the sake of dimensional accuracy. Because of their hardness, carbide dies are almost exclusively machined with EDM. The surface finish of the electrically-eroded surface is similar to that obtained by investment casting so that only a polishing operation is usually necessary [Kalpakjian,1984].

Electrodes for EDM are created in much the same way as the models for cast die molds. Conventional methods include CNC machining the copper or graphite electrode. In an attempt to avoid the time spent machining an electrode, researchers have tried to use

rapid prototyping technologies in the fabrication process. Jensen has plated a rapid prototyped (RP) model with copper to act as the electrode [Jensen,1992] while Gupta and Jensen et al. has both used an RP model to produce a casting mold for a copper electrode [Gupta,1993; Jensen,1993]. An interesting German invention by Haas uses a copper-plated male die as an electrode to completely EDM the female die thus creating the die set [Haas,1976].

2.2.1.4 Layer Manufacturing

As an alternative to traditional machining methods, layer manufacturing methods can be used to directly create sheet metal forming dies is Rapid Tool Making (RTM). Such methods as 3D printing, SLS or SLA may soon be used to build up dies layer-by-layer with a cured polymer or bonded layers of metal powder. For instance, 3-D Systems, Inc. uses an epoxy-based liquid resin (SL5170) in their SLA process that has similar mechanical properties in it's post-cured condition to those of cast rigid epoxy (Bisphenol A) already used for forming dies. Using the 3DP process, [Michaels,1992] has created a metal injection mold out of 316L stainless steel powder. This mold was then used to injection mold a polypropylene part. Currently, no one has directly created a sheet metal forming die using layer manufacturing methods but research activity in this area is headed in that direction [Hilton,1995].

2.2.2 Laminated Die Construction

The concept of making intricate parts (e.g. transformer core, door lock assembly, gear) by assembling contoured laminations is a well-established manufacturing technique [Berry,1966]. Only recently, however, has this fabrication method been used to make sheet metal forming dies like that shown in figure 2.9b. One of the first methods for automatically generating an array of contoured laminations used in a die was developed by [DiMatteo,1976]. Basically, a model of a 3-D surface is rotated about an axis while a contour follower, which is connected to a transducer, is used to run a lamination cutter. The contour follower is moved to different cross-sections of the surface and the resulting cut laminations are assembled into the 3-D surface. [Kunieda,1984] successfully created a sheet metal forming die (Kunieda Die) made of horizontally-oriented laminations by slicing up a CAD model of the 3-D forming surface and using the resulting data to CNC laser-cut the required contours out of sheet material. The contoured laminations were secured to one another by a combination of cementing with adhesives, clamping with bolts, and laser-

welding the edges. [Nakagawa,1985] formed a solid tool out of stacked laminations by diffusion-bonding the laser-cut laminations together. Since the lamination edges were cut normal to the surface and not beveled, the forming surface of the resulting dies had a stepped profile and thus needed to be CNC-machined with finishing cuts, ground, and polished in order to achieve the necessary smoothness. In industry, this stepped profile is sometimes smoothed out by filling in the steps with epoxy [Dastidar,1995].

[Weaver,1991] was granted a patent for a laminated tooling (Weaver Die) with the contours machined into each lamination using beveled edges and not just normal cuts. This change in the art obviates a smoothing operation and only requires a grinding and polishing operation. The smoothing operation also becomes unnecessary as the laminations get very thin and the resulting steps between laminations are negligible. For instance, LOM can create a forming die for low force forming that has nearly smooth surfaces since laminations are as thin as 0.05 mm. The biggest limitation with current LOM paper/adhesive models is that they have low compressive strength (26 MPa). This is one-fifth the compressive strength of the cast epoxy (140 MPa) that is used in forming dies.

2.2.3 Discrete Element Die Construction

There are two types of discrete die constructions; a matrix of separated elements and a matrix of packed elements. As is evident from the previous discussion, continuous and laminated dies are both permanent tools. However, discrete dies can either be a reconfigurable or a permanent tool.

2.2.3.1 Matrix of Separated Elements

The idea of a reconfigurable discrete die with separated elements (see figure 2.10) used for forming sheet metal is not new. As long ago as 1923, a patent was granted for a 2-dimensional forming device for automobile leaf springs which consists of two opposed sets of individually adjustable elements [Williams,1923]. The adjustments were performed manually. The elements are uniformly spaced apart to form a single row and their ends have pivoting work-engaging heads to contact the leaf spring. Corresponding elements in the opposing dies are in alignment. [Walters,1943] took this same idea and expanded it to 3-dimensions by adding multiple rows for the purpose of shaping sheet metal in an opposed press arrangement. As with the 2-D version, each element was manually set to the

necessary height. A flexible lining between the forming ends of the elements and the sheet metal workpiece was also added.

Since the late 1960's, The Boeing Company has expended significant R&D effort in the area of reconfigurable tooling. Boeing was interested in using a discrete die for stretch-forming airplane skins that have relatively large radii of curvature and rather small rates of change in these radii (low spatial frequency content). In fact, Boeing's interest can be traced back to 1968 when they sponsored [Wolak,1973] at the University of Washington to perform a preliminary study of an infinitely variable surface generator (discrete die) to be used as a stretch-forming die. The die used in the study consisted of a 16 by 23 matrix of manually-set threaded elements which were separated from one another. The idea of using the die for stretch-forming was eventually abandoned "due to the lack of desired rigidity of the constituent elements of the conceived adjustable dies." Instead they used it as an infinitely variable mold for casting a continuous sheet metal forming die made of green rigidax.

[Pinson,1980] and The Boeing Company were granted a patent for a 3-D discrete die press similar to the design of [Walters,1943] except that the each element is automatically set with individual computer-controlled servo actuators. The patent drawing for this matched-die discrete element press is shown in figure 2.11. At present, Boeing is not using this type of discrete die for sheet metal forming probably for the same reasons as [Wolak,1973]. However, these devices are used in industry (including Boeing) as reconfigurable fixturing devices for such things as composite airplane parts during a periphery trim operation with a water jet cutter [West,1994]. Companies like CNA Manufacturing Systems (Redmont, WA) and Manca, Inc. (Westwood, N.J.) presently manufacture and sell these types of universal holding fixtures.

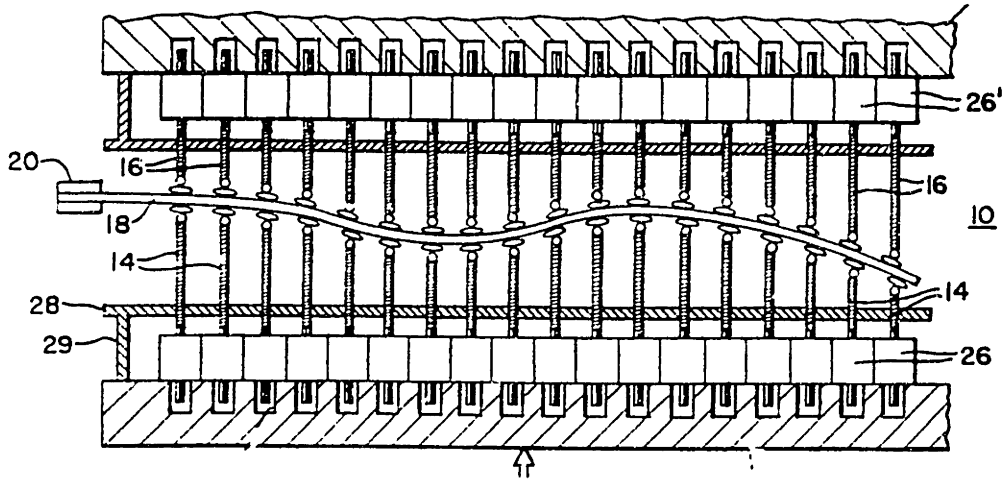

Figure 2.10 - Discrete die with separated elements [Pinson,1980]

For discrete dies with separated elements, each element is completely separated from it's neighboring elements by a set spacing to allow for individual positioning and to avoid unwanted interactions between elements. This arrangement is fine for low forming force applications but as the force increases due to deeper part draws or thicker sheet materials used, the threat of element buckling and bending increases.

2.2.3.2 Matrix of Close-Packed Elements

In order to withstand higher forming loads, elements must be packed closely together (i.e. with no spaces in between) into a matrix so that adjacent pins can support each other as shown in figure 2.9b. As long ago as 1931, [Hess,1931] was granted a patent for a set of discrete dies with close-packed elements used to stamp shoe forms out of sheet metal. With this invention, a person's foot is depressed into the matrix of spring-loaded equal-length square elements and the matrix is locked to retain the impression. The upper matrix of elements is then forced into the lower die to transfer the shape and also locked.

If a permanent die using close-packed elements is desired, square die elements can be cut to a specified length, assembled together in the right order, and clamped around the perimeter to make a forming die, as was proposed by [Hicks,1961]. Using a matrix of square or hexagonal elements which are joined together (e.g. brazing) to form a solid forming die has also been patented [Wakefield,1943; Whiteacre,1971, respectively].

To make a discrete die into a flexible manufacturing tool for sheet metal parts like Hess's invention, it should be automatically reconfigurable (i.e. rams or pins are computer-actuated). The previously-mentioned 3D Boeing press [Pinson,1980] is easily automated because the distance between elements allows room for their individual drive mechanisms. However, when elements are close-packed together in a matrix, individual actuation of each pin becomes very difficult. [Nakajima,1969] created an automatically reconfigurable discrete die (vertically-oriented) which used a positioning stylus mounted to the headstock of an NC milling machine to position the matrix of round elements. After the element positions were set, the entire element matrix was clamped from one side to form a rigid tool and a sheet of rubber was placed between the discrete forming surface and the sheet metal blank to avoid part dimpling. The main problems with Nakajima's die design are:

1) the tendency for a pushed element to drag adjacent elements along thereby upsetting previously set elements and
2) the non-uniform distribution of locking force within the matrix.

To begin addressing the setting and clamping problems that Nakajima experienced, [Hardt,1980] designed a servo-controlled apparatus for setting a 3D discrete die made of square elements. The setting apparatus essentially used a form of mechanical multiplexing. In addition, further sheet metal forming experiments were performed to test the shape fidelity and clamping characteristics of various element shapes (square, round) and interpolator (material layer between die and blank) combinations [Hardt,1981]. A matrix of square elements was found to be the most easily clamped of all pin shapes. A new discrete die press designed and built by Hardt et al. [Hardt,1985; Robinson,1987; Knapke,1988; Gusterhout,1991] at MIT between 1985 and 1991 consists of two 45 by 48 matrices of equal length 6.4 mm square elements. This machine automatically sets the dies to the correct forming shape, clamps them into a rigid tool, and serves as a hydraulic forming press. The die elements and press are oriented horizontally and each vertical row of elements (defined as perpendicular to the direction of load) is separated from other rows by sheet metal spacers which are rigidly attached to the discrete die outer frame. Separating the element rows allow an automatic profiling mechanism to impress the correct profile on each row separately. This design also helps transmit the forming force applied to the clamped element matrix to the frame better than friction alone. After the discrete dies are clamped, their forming surfaces are covered with a thin layer of low-softening temperature thermoplastic (e.g. ethylene vinyl acetate), called an interpolator, in order to avoid dimpling of the workpiece. This thermoplastic interpolator is premolded to the spherical ends of the each die element prior to forming.

Inspired by the work of Hardt et al. and Nakajima, [Finckenstein,1991] developed a vertically-oriented machine that automatically sets a discrete die consisting of a 33 by 33 matrix of close-packed 6 mm square elements. Using a 4-axis servomechanism, the machine individually positions threaded rods which are arranged in a similar 33 by 33 matrix. This matrix of threaded rods, similar to the [Wolak,1973] infinitely variable surface generator, is then used to impart the desired die shape onto the discrete die. Specifically, the die elements of the discrete die, which is placed above the matrix of threaded rods, are allowed to fall onto the rod ends thereby acquiring the desired shape. The elements of the discrete die are subsequently clamped in both the X and Y directions to create a rigid tool. In contrast to the aforementioned MIT discrete die press, only the setting function (and not the forming) is accomplished with this machine. The configured discrete die is removed from this setting machine for use in either a hydroforming or stretch-forming press. An elastomeric interpolator is placed between the discrete die and the workpiece prior to forming.

Another element setting method for discrete has been proposed by [Todoroki,1993] which involves two industrial robots. An element placing robots picks elements from an element storing container and places them one-by-one on a flat horizontal base until all the elements in a row are positioned correctly. A pin handling robot then clamps the correctly configured row of elements and places it in the discrete die frame. Once all the element rows have been placed, the element matrix is clamped with a rigid frame.

2.3 RAPID, LOW-COST FABRICATION METHODS FOR DIES

Which of the die fabrication methods discussed in the previous section can be considered both rapid and low-cost? One key aspect of such a method is to eliminate as many intermediate processing steps as possible, especially the need for a model of the intended forming surface. In other words, it is better to create the rigid forming die directly from the computer model without having to first create a model of mold. This is the main criteria used in choosing particular fabrication methods for investigation in this thesis work. In the remainder of this section, we focus on the specific fabrication methods chosen for investigation.

CONTINUOUS DIES: Of the continuous die fabrication methods, CNC-machining a solid billet, the industry standard, is chosen for investigation. Although casting and EDM are frequently used methods, they are generally more expensive and time-consuming than CNC machining. More importantly, a cast die requires a model and a mold during fabrication and an EDM die needs an inverse shaped electrode. A die made directly by layer manufacturing methods appears to be a promising method but currently the machinery is very expensive ($200K-800K), the build times are relatively long (>10 hours) compared to CNC-machining, the sizes are limited, and the material properties are only sufficient for low forming force applications [Aubin,1994].

LAMINATED DIES: As shown by [Kunieda,1984], laminated forming dies can be created directly from a computer model of the intended forming surface. Because machining of laminations used in a laminated die is only done in 2-dimensions, such dies potentially have advantages over CNC-machining a solid billet in terms of fabrication time and die shape flexibility. For these reasons, laminated forming dies are also chosen for investigation. However, the current method of stacking

contoured laminations will not be considered for the same reasons why it has not been embraced by industry.

The current method—stacking and bonding contoured-laminations that are oriented in a horizontal plane like the previously-mentioned Kunieda and Weaver dies—has not proliferated in industry as a rapid tooling method because of certain inherent difficulties in the process. Because of their inherent non-uniformity, handling the contoured-laminations and assuring their correct registration in the array is a difficult operation to automate. In fact, these operations are often performed manually which adds significantly to the fabrication time of the die [Dastidar,1995]. Securing laminations to one another is also difficult because all clamping must be internal to the die structure. Holes must be strategically machined in each lamination to allow clamping bolts or rivets to hold the entire array together. These fasteners must also be recessed so as to not become an impression on the formed sheet metal part. If an adhesive is used to bond the laminations (e.g. epoxy, heat-curable nylon), it normally must be applied to the lamination just prior to placement on the array which complicates the handling. Laser welding the lamination edges together requires an additional processing step roughly equal in expense and time to the contouring operation is required. Processing time is also significantly increased when laminations are brazed or soldered together. Companies like Ford Motor Co. have had disappointing results with brazed lamination dies intended for prototype work [White,1993].

Since the tooling development process for a flexible manufacturing system requires rapid die redesign during the forming iterations, contour lamination dies are simply not well-suited for this purpose. Separation of the die laminations which are riveted, glued, welded, brazed, soldered, or diffusion-bonded together for recontouring the forming shape is either impossible or impractical so that the entire die must be remachined using a CNC machining center (like a continuous die). If the die is only bolted together, the problem of handling and remachining a large number of loose laminations with no established reference edges still remains.

For these reasons, a new lamination-based method, called the Profiled-Edge Lamination or simply PEL method, has been developed as an alternative candidate. The PEL die method improves upon all of the shortcomings associated with stacking and bonding contoured laminations. The details of this method are discussed in chapter 4.

DISCRETE ELEMENT DIES: As shown by [Ousterhout,1991], a reconfigurable discrete die can be used as a rigid tool for sheet metal forming. Furthermore, it's shape can be set directly from a CAD model of the die surface. Because of it's reconfigurable and universal nature (i.e. relative positions of elements can be continuously varied), a discrete die has the potential to be more rapid and low cost than CNC-machining. Even considering the ease with which the die shape can be set, a discrete die consisting of separated elements is not chosen because this configuration cannot withstand the forming pressures encountered with most sheet metal forming processes. For this reason, a discrete die with closed-packed elements is chosen as a candidate method.

In summary, the following fabrication methods have been chosen as candidates for further investigation and eventual comparison with one another in terms of a flexible manufacturing system's die development scheme:

- CNC-machining a solid billet
- assembling and clamping an array of profiled-edge laminations and
- configuring and clamping a discrete die with close-packed elements.

The resulting tools will simply be referred to as a CNC-machined die, a PEL die, and a discrete die, respectively.

2.4 DESIGN OF A BENCHMARK PART

A shallow pan roughly 7x7 cm square by 2 cm deep with 4 different wall angles (45°,52°,60°, and 68°) and a central reverse curvature section serves as the benchmark part for comparing the candidate fabrication methods. [The benchmark part is described in this chapter because it's referred to in all of the subsequent 5 chapters of this thesis.] The part is stamped out of 0.64 mm thick DQAK (Draw Quality Aluminum Killed) steel and the inner radii of all bends is 3.2 cm. An engineering drawing of the benchmark part is shown in figure 2.11. *Dimensions on the drawing are in inches but we will refer to metric dimensions for the rest of this thesis.* Using AutoCAD™, this part was designed as a wireframe model and then meshed-in with NURBS surface patches as shown in figure 2.12. The CAD geometry was then transferred to the ABAQUS™ FEA program (explicit analysis used) via a custom-written conversion program. An FEA model of a matched-die forming arrangement with a 15x15 cm square blank shape was used to verify that the desired part was formable. Tensile tests performed on this steel established the yield strength, ultimate tensile strength, and elongation strain to be 178 MPa, 412 MPa, and

27%, respectively, which were used in the forming simulations. A constant binder force was evenly distributed around the perimeter of the blank. The total time to design and verify the part, and to develop engineering drawings (refer to figure 2.11) was 4 man-days, i.e. 2 days for designing and 2 days for FEA analysis.

Both the FEA analysis and the material testing performed proved to be quite useful [Karafillis,1994]. For example, the part draw height and the binder force had to be decreased from the 2.54 to 1.91 cm and 150 to 67 kN, respectively, because the FEA simulation predicted tearing in the punch tip radii, especially in the corners, with the original forming conditions. Furthermore, the blank had to be trimmed in the corners (2.5 cm chamfers) in order to minimize the draw-in resistance in these areas and minimize the tearing problem. As shown in an FEA plot of the sheet metal thickness distribution (figure 2.13), the simulation identified that the angled walls of the 1.91 cm high part are being formed in almost a pure plane-stretching condition leading to a small height springback. It also predicted high compressive straining (thickening) in the part flange near each corner of the pan which is indicative of impending buckling.

By design, many different forming modes are incorporated into the benchmark part. Cup drawing occurs in each of the corners. Plane strain stretching occurs in the angled walls of the pan section while biaxial stretching occurs in the centrally-located reverse curvature section. Bending and straightening are occurring in the upper and lower corners of the pan. In this forming mode, metal is pulled from a flange, bent over a die radius, and then restraightened.

The shape and forming conditions of this benchmark part were chosen particularly to highlight the advantages and disadvantages of each different type of die construction. The plane-stretching that occurs in the angled walls causes highly localized forming pressures at the upper and lower bends of the dies. For the PEL dies, this situation is a good test of how an unbonded lamination construction resists delamination, i.e. lateral forming forces bending the plates. For the discrete dies, the high forming pressures tests the ability of a surface interpolator to prevent die elements from dimpling the part surface. Furthermore, the high forming forces are directly transmitted to the die elements possibly causing them to slip. Forming with high forces is good test of how well the element clamping scheme works (i.e. effective distribution and eventual transmission of forming forces to die frame).

With all of these different forming modes occurring, the benchmark part is a challenge to form with any type of die including conventional tooling (i.e. CNC-machined die). It is asymmetrical with four different wall angles and corner conditions (X-Y plane radii) since the ends of the angled walls are blended with parametric surface patches. The

sheet metal tends to buckle in the flange near the corners and tends to tear in the upper part of the corners, both which are considered material failures. It really can be considered a borderline part in the sense that it has a propensity for some sort of part failure (tearing, buckling) if the friction and/or binder force is too high or tool low. These forming characteristics are an important test of how well the unconventional die constructions (i.e. PEL and discrete dies) compare with standard CNC-machined die in a realistic forming situation.

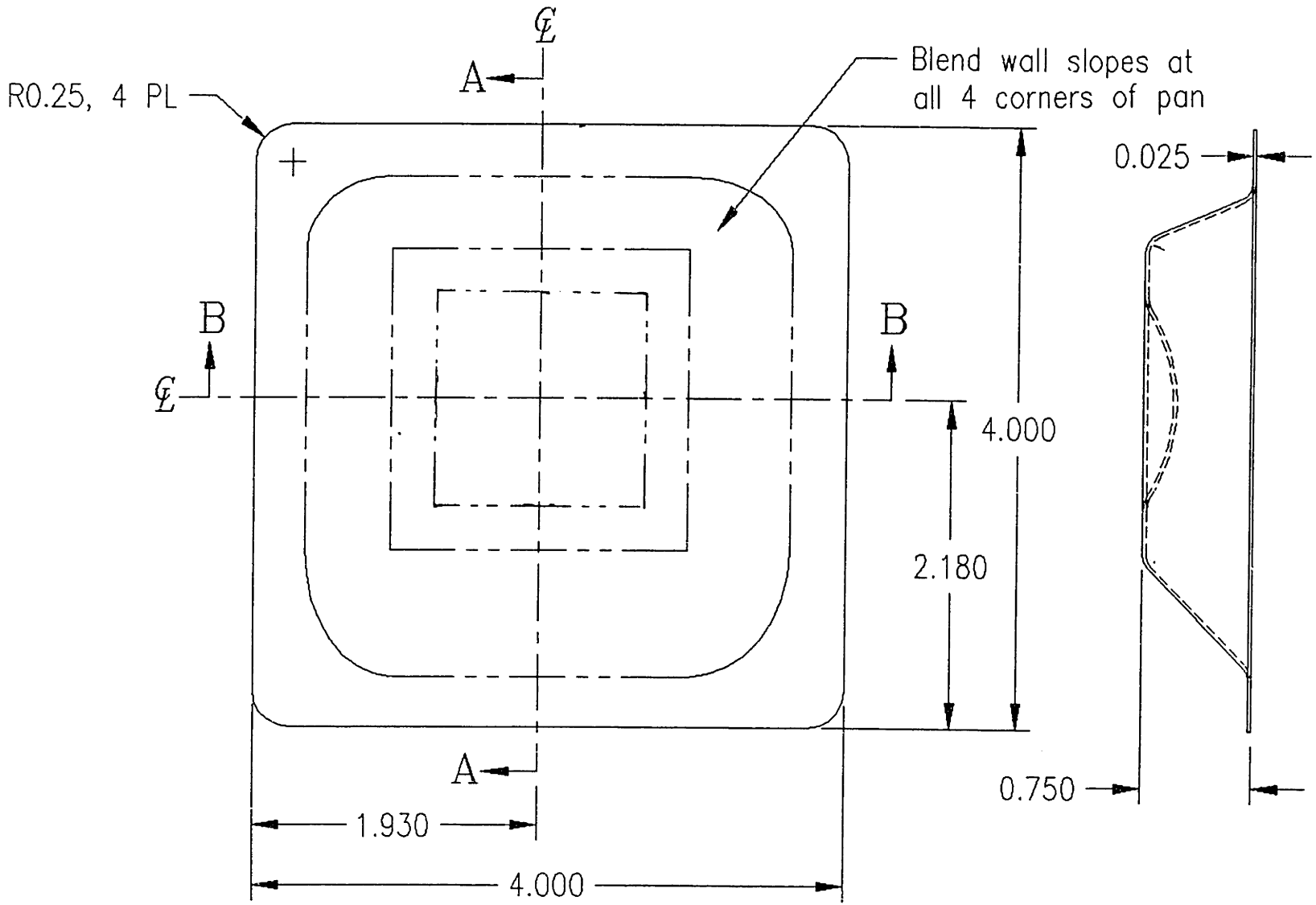

NOTES:
1. Unless otherwise specified, inside radius of all bends to be 0.125 in.
2. For dimensions and section views, see sheet 2.
3. All dimensions are in inches.

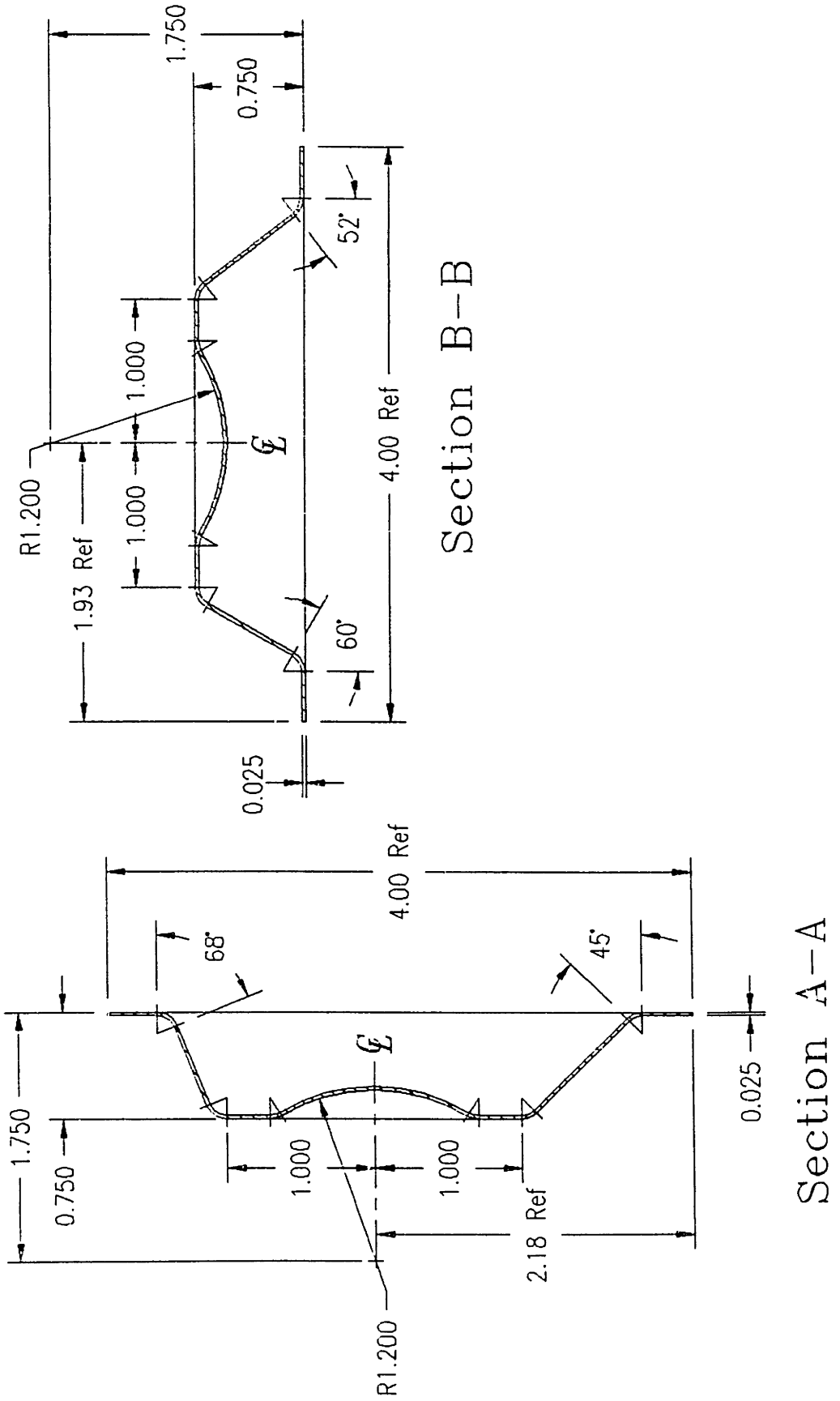

Figure 2.11 - Engineering drawing of benchmark part.

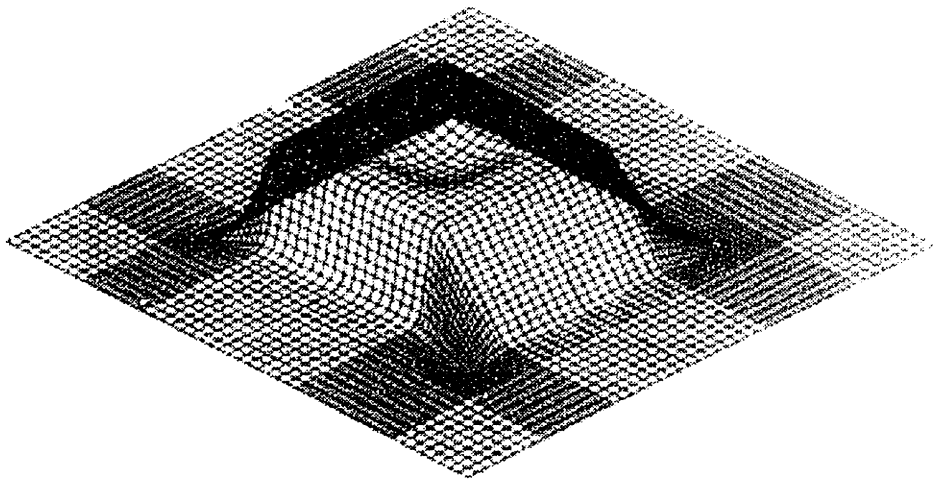

Figure 2.12 - Meshed-in CAD surface model of the benchmark part

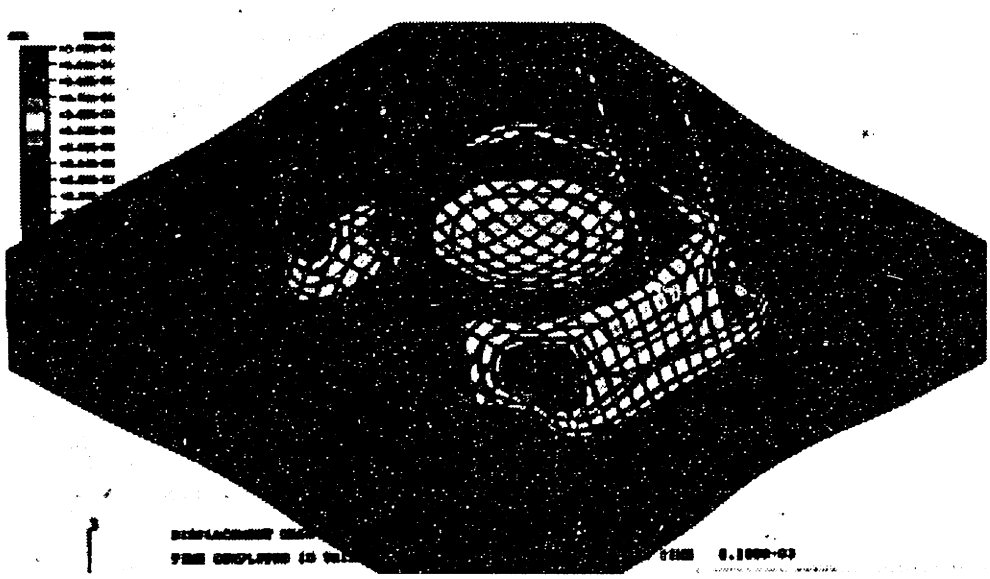

Figure 2.13 - FEA thickness distribution plot of the formed benchmark part.

Chapter 3 - CNC-Machined Forming Dies

CNC-machining is arguably the most common method used by diemakers to either completely fabricating dies out of a solid billet or bring cast dies to near-net shape before a finishing operation. It will also serve as the fabrication method that the two non-standard methods chosen for investigation, i.e. assembling a lamination array and configuring a discrete die, will be compared with. In this chapter:

- the state-of-the-art in CNC-machining of die surfaces is reviewed
- mathematical equations that will help predict surface finish, machining time, and the amount of post-grinding necessary for different combinations of machine and cutting tool are discussed
- the construction of a matched set of CNC-machined sheet metal forming dies is presented
- and the general procedure for designing and fabricating a CNC-machined die is outlined.

The matched-set of dies fabricated for the case study are 10.2 cm. square and made out of 11L17 steel. A 3-axis CNC machining center was used to make the roughing and finishing cuts in the die surfaces. Finishing cuts with a ball endmill left a scalloped surface which had to be ground-out with a hand-held die grinder. The die surfaces had to be polished to make them suitable for forming sheet metal parts. The forming dies and a benchmark part stamped from steel sheet using these dies are shown in figures 3.1a and 3.1b, respectively.

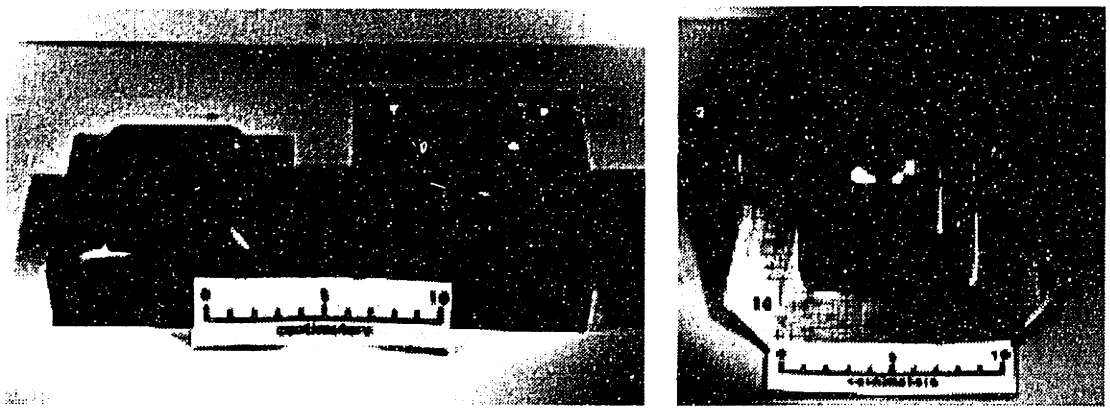

Figure 3.1 - a) Matched set of CNC-machined dies for stamping
b) benchmark part stamped out of steel sheet using these dies.

3.1 CNC MACHINERY AND MACHINING METHODS

Based on the CAD surface model of a die (see figure 1.1), a CAM software package is used to generate the tooling path NC instructions (tool position and sometimes tool orientation) used by a multi-axis CNC machining center to accurately machine the desired surface. A number of tooling paths must be defined by the CAM software. For rough cutting the cutter spacing is based on the maximum metal removal without exceeding the power of the machine or it's stability. However, for finishing cuts, the spacing represents a compromise between excessive scallop height and long machining times.

Considering only the die surface, the three main objectives of the tool path generation algorithm and CNC-machining method used are to:

1) get as close to near net shape as possible thereby minimizing the need for extensive post-grinding and finishing the die surface

2) accomplish this task as rapidly as possible and

3) at the lowest overall cost [Lange,1985].

These objectives are achieved by the right combination of CAM software (i.e. tool path generation algorithm used), machining center, cutting tool, and machining method.

In general, CNC machining centers used for machining forming dies combine servo-driven multiple axes of motion (including translation and rotation) with a rotating tool spindle. A cutting tool mounted in the rotating spindle removes the unwanted material from the die billet in order to create the die surface. Typical cutting tools used for machining include a conventional endmill, ball endmill, and a toroidal cutter or radiused endmill. The maximum size die that can be handled by the machining center, i.e. volume of space accessible by the cutting tool, is defined by the travel length of each translation axis (X, Y, Z). The orientation of the cutting tool is either fixed or can be dynamically changed when one or two rotational axes (known as A and B in the machine tool industry) are added. Translational and rotational motion of the machine is controlled by a high-speed CNC controller.

3.1.1 Three-Axis Machining with an Endmill

A three-axis machining center that removes material with an endmill is one of the most common combinations of machine and cutting tool used by industrial firms to fabricate dies. This type of machining center has three orthogonal translational axes of motion in the X, Y, and Z directions and depending on the machine design, either the workpiece or the spindle may be moved. The spindle is typically mounted horizontally or vertically. A machine which only moves the workpiece and has a vertically-oriented spindle is shown in figure 3.2. Prior to the finishing cut with a ball endmill, a large diameter endmill (ball or straight) is used to rough cut the majority of the unwanted die material away. Large volumes of material can be roughed out most efficiently using strong, rigid roughing endmills that are capable of withstanding high removal rates. If more than one roughing pass is needed, the depth of cut for each additional pass cannot exceed the capacity (e.g. flute length, strength) of the endmill. After the roughing cut, the 3-axis machine makes the finishing cuts with a rotating ball or conventional endmill using either a zig-zag, reciprocal, or contouring type motion. Die surfaces with small radii of curvature and rapid changes in geometry can only be machined by long thin endmills. This leads to low material removal rates and high machining times. The final finish pass (if more than one is needed) leaves the die surface *near-net-shape* with a scalloped surface that must be ground and polished. Many algorithms for generating roughing and finishing tool paths have been devised that incorporate direct gouge elimination and tool path step-over distance adjustment [Huang,1994; Kuragano,1992].

Conventional straight endmills are occasionally used to machine the forming surface of mildly-curved sheet metal forming dies. If a straight endmill is used for surface-machining, inclined portions of the die surface will have a stair step profile as shown in figure 3.3a. The scallop height **h** of a planar machined surface is given by

$$h = \delta \cdot \sin\alpha \cdot \cos\alpha. \qquad (3.1)$$

where: δ = a constant step over distance along the surface
α = angle of surface inclination.

The height estimated by equation 3.1 is based on the assumption that the surface being machined is either flat or gently-curving. The surface roughness average $\mathbf{R_a}$ is the arithmetic average of the absolute values of the measured profile height deviations taken within the sampling length and measured from the graphical centerline. As an estimate,

$R_a \approx h/4$ [ANSI B46.1-1985]. The amount of material per unit of die surface area V_r that must be removed during the post-grinding operation is estimated by dividing the cross-sectional area of the scallop A_{cs} by δ to get

$$V_r = \frac{A_{cs}}{\delta} = \frac{\delta \cdot h}{2 \cdot \delta} = \frac{\delta}{2} \cdot \sin\alpha \cdot \cos\alpha \qquad (3.2).$$

Equation 3.2 and the other equations presented in section 3.1 that estimate V_r will not include the volume of material left behind subsequent cutter rotations (i.e. wake material) since it is usually much less than the scallops between adjacent cutting passes. It is reasonable to assume that the time required for post-grinding is proportional to the amount of material that must be removed V_r. However, equation 3.2 does not include the additional problem of having to remove the deep machining marks left by the 90° cutting edge of the tool.

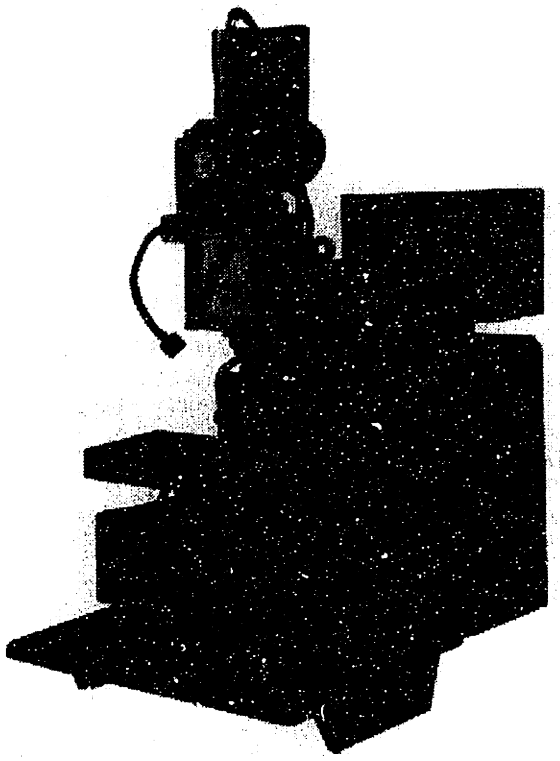

Figure 3.2 - Three-axis CNC machining center

A better cutting tool to use in this situation is a ball endmill which leaves a scalloped surface that is much easier to ground on inclined surfaces and around fine surface details. The entire die will have a scalloped surface like that shown in figure 3.3b. Making the same assumptions as before, the scallop height is given by

$$h = \frac{1}{2} \cdot \left[D - \sqrt{D^2 - \delta^2} \right] \qquad (3.3)$$

where: D = diameter of the ball endmill.

[Choi,1988] deals with scallop height estimation for 3-axis machining of curved surfaces with a ball endmill. The amount of material per unit of die surface area that must be removed is

$$V_r = \frac{D}{2} - \frac{1}{4}\sqrt{D^2 - \delta^2} - \frac{D^2}{4\delta}\sin^{-1}\frac{\delta}{D} \qquad (3.4).$$

Finishing of a die surface machined with a ball endmill is easier than the previous case because there is less material to remove. For example, if we use the typical machining passes for the 45° surface of an auto body die [Mayes,1993] with D=13 mm and δ=0.75 mm, the scallop height and removal volume for both endmill types is given in table 3.1. In this case, a ball endmill leaves significantly less material to be removed than a conventional endmill.

Table 3.1 - Scallop height and material removal for 3-axis machining

	h (mm)	V_r (mm^3 / mm^2)
Ball Endmill	0.011	0.0036
Conventional Endmill	0.375	0.188

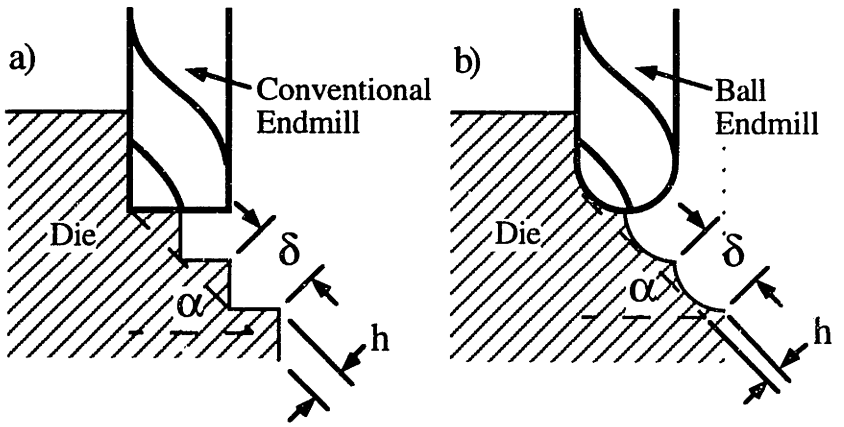

Figure 3.3 - Machined surface profiles for a) conventional endmill and b) ball endmill

One problem with using a ball endmill in a 3-axis machining center is that the material smears at and near the tool center. The reasons for this is that the tool's center has

inadequate cutting edges combined with a low cutting velocity [Schey,1987]. As a result, the scalloped die surface has a poor surface finish and the tool life is reduced.

3.1.2 Four-Axis Machining with a Ball Endmill

The poor surface finish from machining with a ball endmill in a 3-axis machining center can be improved by adding a rotational axis about the x or y axes, commonly referred to as the A and B axes, respectively [Zeni,1995]. Specifically, a three-axis machine can be retrofitted with a tilting table thereby becoming a four-axis machining center with a reduced work volume. The reason for the significant machining improvement is that the ball endmill can be set to an angle ϕ relative to the normal vector at the point of tool contact with the material. Ip and Loftus have developed a machining strategy to generate tool paths and workpiece orientations which tends to minimize the scallop height and improve the surface finish compared to 3-axis ball endmilling [Ip,1993]. As shown in figure 3.4a, more of the outer cutting edge of the ball endmill and less of the tool center is in contact with workpiece. As a result, the effective maximum cutting diameter is no longer D_3 as with 3-axis cutting (see figure 3.4b) but rather it's now D_4. In this case the scallop height and volume of material per unit of die surface area that must be removed by the post-grinding operation can estimated by equations 3.3 and 3.4, respectively.

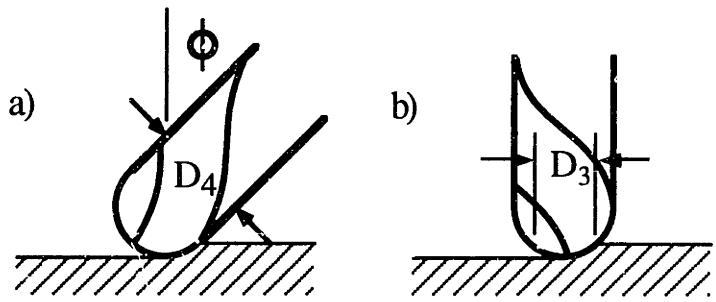

Figure 3.4 - Machining with an a) inclined ball endmill and b) vertically-oriented endmill

Besides improving the machined surface finish, ball endmill cutting with a 4-axis machine will also affect the maximum allowable machining feedrate $\mathbf{f}_m$ which then changes the fabrication time. This effect will be shown by first looking at the standard formula for calculating milling feedrates

$$f_m = f_t \cdot n_t \cdot N = \frac{f_t \cdot n_t \cdot V_c}{\pi \cdot D_e} \qquad (3.5)$$

where: f_t = maximum allowable feedrate in mm/endmill tooth for the material
n_t = number of teeth on the endmill
N = spindle speed in rotations/sec.
V_c = maximum cutting speed allowed for the material
D_e = effective cutting diameter of the endmill [Oberg,1988].

By going from 3-axis to 4-axis machining, the only variable that changes in this equation is D_e. By increasing D_e, the maximum allowable feedrate tends to reduce. The die builder can counteract this effect by increasing the number of cutter teeth in contact which will increase the feedrate. Since the integer change in n_t (e.g. 1 to 2) will probably have a greater effect than the smaller change in D_e (e.g. 10 mm to 13 mm), the net effect is to increase f_m.

3.1.3 Five-Axis Machining with a Radiused Endmill

Five-axis machining combines three-orthogonal translational axes of motion with two rotational axes (A and B) which allows the cutting tool to be arbitrarily oriented in space. As seen in figure 3.5, two examples of A and B axes configurations for a machining center are a twin-tilt spindle and a tilting rotary table. The tilting rotary table can be placed on the workpiece bed of a 3-axis machine to convert it to a 5-axis type. Since the cutting tool can now be oriented, then contour machining with a conventional endmill, as illustrated in figure 3.6, is possible. Contour machining implies that the endmill axis of rotation v'-v' will coincide or nearly coincide with the instantaneous normal vector v-v to the die surface. Although a ball endmill can be used, most advocates of five-axis machining recommend using a radiused endmill at some arbitrary fixed angle to the surface normal vector as shown in figure 3.7 [Zeni,1995]. The reason for this recommendation is because the machined surface left by a tilted, radiused endmill has hardly any machining scallops (as will be shown later in this section). Different algorithms used for generating 5-axis tool paths and cutter orientations reduce the machining time by adjustment of the tools trajectory [Marciniak, 1987], optimize the cutter path location [Choi,1993], and reduce the tooling accessibility problem [Elber,1994].

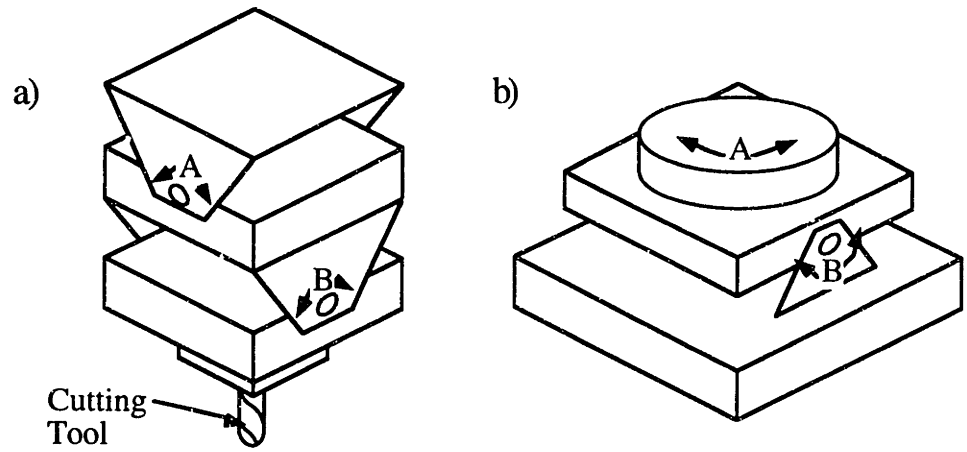

Figure 3.5 - Five-axis machining centers with a) twin-tilting spindle and b) tilting rotary table

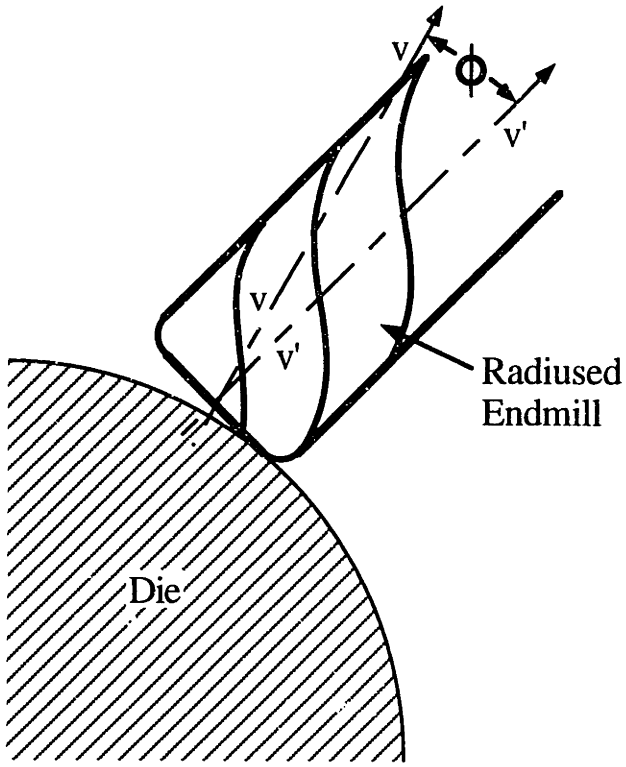

Figure 3.6 - Five-axis contour machining

Five-axis contour machining offers several advantages over other types of machining techniques. The slightly angled endmill prevents smearing of the machined surface and dramatically reduces the amount for a post-grinding needed. Referring to figure 3.7, the effective cutting radius $\mathbf{R}_e$ of the tool is

$$R_e = \frac{D - 2 \cdot r}{2} + r \cdot \sin\phi \qquad (3.6)$$

where: D = endmill diameter
r = edge radius of endmill
ϕ = inclination angle of the endmill.

The profile of the scallop cut will be an ellipse with a major and minor axes of R_e and $R_e\sin\phi$, respectively. The equation for this ellipse in an X-Y plane centered at $(0,R_e\sin\phi)$ is

$$\frac{x^2}{R_e^2}+\frac{(y-R_e\sin\phi)^2}{R_e\sin\phi}=1 \qquad (3.7)$$

By rearranging equation 3.7 and solving for **y**, the scallop height **h** of a planar machined surface is

$$h=\left[\frac{D}{2}+r\cdot(\sin\phi-1)\right]\cdot\sin\phi\cdot\left[1-\sqrt{\frac{(\delta/2)^2}{\left[\frac{D}{2}+r\cdot(\sin\phi-1)\right]^2}}\right]. \qquad (3.8)$$

where: δ = step over distance.

The amount of material per unit of die surface area $\mathbf{V_r}$ can be determined by considering the area integral $\mathbf{A_{cs}}$ between the intended die surface (x axis) and the elliptical scallop cut. Therefore, the removal volume is

$$V_r=\frac{A_{cs}}{\delta}=\frac{2}{\delta}\cdot\int_0^{\frac{\delta}{2}}f(x)\cdot dx=\frac{2}{\delta}\int_0^{\frac{\delta}{2}}R_e\sin\phi\cdot\left(1-\sqrt{1-\frac{x^2}{R_e}}\right)dx. \qquad (3.9)$$

When the integral in equ. 3.9 is evaluated, the final expression is

$$V_r=R_e\sin\phi-\frac{\sin\phi}{2}\cdot\sqrt{R_e^2-\frac{\delta^2}{4}}-\frac{R_e^2\sin\phi}{\delta}\cdot\sin^{-1}\left(\frac{\delta}{2\cdot R_e}\right) \qquad (3.10)$$

As an illustrative example of the differences between 3 and 5-axis machining, let us again use the typical machining passes for the flat surface of an auto body die [Mayes,1993] with D=13 mm and δ=0.75 mm. The scallop height and material removal volume left by a radiused endmill with r=1.5mm and ϕ=5° and a ball endmill is given in table 3.2. In this example there is an order of magnitude difference in both h and V_r between 5-axis contour machining and 3-axis ball endmill machining. [Zeni,1995] has shown with a CAM simulation that the machining time for a outer die used for an auto body hood decreased from 15 hours to 5.2 hours by using 5-axis instead of 3-axis machining. Five-axis contour machining with a radiused endmill is ideal for large, gently sloping surfaces like those in

auto body panels. However, a ball endmill must be used to cut corners, grooves, and fine details in a forming die.

Table 3.1 - Scallop height and material removal of 5-axis versus 3-axis machining

	h (mm)	V_r (mm^3 / mm^2)
Radiused Endmill	0.0012	0.0004
Ball Endmill	0.011	0.0036

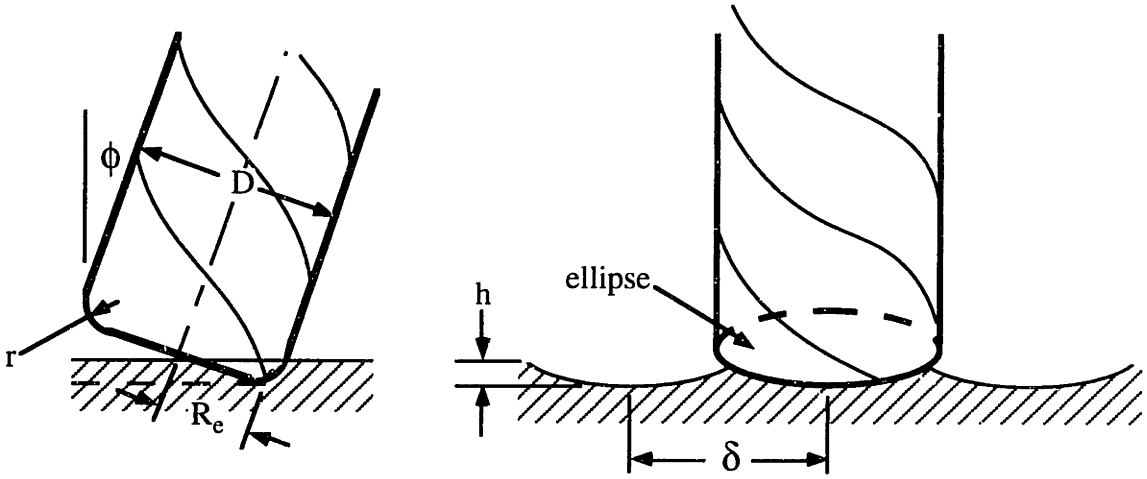

Figure 3.7 - Schematic of a radiused endmill with it's rotational axis tilted.

3.1.4 High Speed Machining with High Strength Tools [Nakagawa,1994]

There are other machining techniques and cutting tool compositions which decrease the machining time and virtually eliminate the post-grinding operation. Harder tool materials (Carbide, sintered Cubic-Boron-Nitride - CBN, Ceramic Metal - CERMET, sintered diamond, and titanium nitride coating) can be run at higher machining rates. The milling center spindle speeds can be increased to 8000 rpm with these harder materials whereas before it was only about 2000 to 4000 rpm. Even higher speeds will be considered because high speed machining centers are capable of achieving up to 30,000 rpm. Nakagawa et al. has shown that high speed milling with these high strength tools can be used to shorten machining time and to perform finish cutting with a very small step over distance δ. This method of machining leaves a very smooth surface, shortens the finishing time, and greatly increases the dimensional accuracy of the die. Besides

shortened machining time, high speed machining has been shown to reduce the number of cutting tools necessary for surface machining; reduces the heat effects of machining because heat leaves with the chips instead of localizing in the cut interface; and lowers the cutting forces on the spindle and workpiece which increases machining accuracy [Noaker,1995].

3.2 EFFECT OF DIE SIZE ON MACHINING TIME

The effect that die size has on the time it takes to machine the die's forming surface needs to be considered. In the roughing operation, a large volume of material is removed from the original block of die material. According to [Oberg, 1988], the material removal rate **Q** in a machining operation is determined from the relation

$$Q = \frac{P_m \cdot E}{K_p \cdot C \cdot W} \tag{3.11}$$

where:
P_m = power at the machine's motor
E = machine tool efficiency factor
K_p = power constant which depends on the die material
C = feed factor for the power constant which also depends on the die material
W = tool wear factor which is constant for end milling.

Assuming that a constant machine power is used during machining, then all of these variables are constant for a given combination of machine, cutting tool, and die material. Therefore, Q is also constant which means that the roughing time $\mathbf{t_r}$ is simply

$$t_r = \frac{Q}{V_{die}} \tag{3.12}$$

where V_{die} = volume of material to be removed from the die.

A formula for estimating the machining time for the finishing cuts can be determined by first considering the arbitrary die surface of area $\mathbf{A_{die}}$ shown in figure 3.8. The total distance traversed by the cutting tool over the die surface is A_{die} /δ so that the machining time $\mathbf{t_{fc}}$ is then

$$t_{fc} = \frac{A_{die}}{\delta \cdot f_m}. \tag{3.13}$$

Equation 3.13 neglects the effect (i.e. increase in machining time) of fine part details (e.g. corners, recesses) on t_{fc}. The machining time can be estimated more accurately with a CAM software simulation.

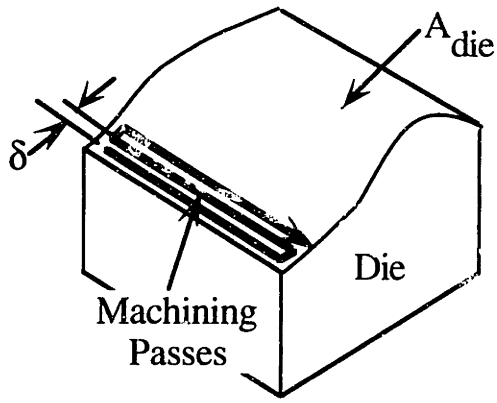

Figure 3.8 - Finish cuts on a die surface.

3.3 COMPUTER NUMERICAL CONTROL (CNC) FOR DIEMAKING

The issues of machining accuracy and speed in diemaking are directly related to the CNC functionality of the machining center. A schematic of a CNC system is shown in figure 3.9. The instructions to machine a forming die are contained in a CNC program created using a CAM software package. A CNC program contains lines or "blocks" of various sizes which are referenced by a line number and then followed by G-code (preparatory functions) and/or M-code (miscellaneous and on/off functions) instructions. The line number in any line of the CNC program is optional. The program blocks are fed into a CNC input buffer (memory) of fixed size to await processing by the CNC controller. If programs are too long for complete downloading into the input buffer, a PC can be used to drip feed the CNC programs one block at a time to the machine. This does away with the need for a large computer buffer. The time required for the CNC controller to process one instruction block is known as the block processing time (BPT). The CNC controller passes movement commands (i.e. distance to move and speed) to the servo system at a specific time interval known as the interpolation time. Finally, the servo motor's position and velocity are read (feedback), these measurements are compared to the commanded values (error determination), and a command voltage is issued to the motor to drive the various translational and rotational axes (control). The time required for this task is known

as the servo sample and update time (SST). To avoid being a processing bottleneck and meet the Nyquist sampling criteria, the SST must be less than or equal to half of the BPT.

Rapid machining a complex die surface will stretch the limits of current CNC controllers and machines. The minimum BPT in die surface machining is calculated with the formula

$$BPT = \frac{\delta_o}{f_m} \qquad (3.14)$$

where: δ_0 = distance between defined coordinate points along a machining path. [Note that the directions for the step over distance δ and the along distance δ_0 are perpendicular to each other.] Complex die making can require instantaneous communication rates beyond 100,000 bits/second [Noaker,1995]. The maximum length of a block for 5-axis machining is 64 characters or 640 bits of information [Zeni,1995]. This requires that the BPT must be no greater than 6.4 msec to prevent a processing bottleneck. The fastest CNC's currently available have a BPT of 4 msec [Noaker,1995]. Although large input buffers are not needed for drip feeding of the instruction blocks, Zeni suggests that a minimum 5 block buffer should still be maintained. CNC controllers also have a block look-ahead capability which is important for the adjustment of machining feedrate when sudden deceleration and direction changes are performed. This capability helps prevent overshoot and gouging of the cutting tool. Advanced CNC controllers currently offer 126 block look-ahead [Noaker,1995].

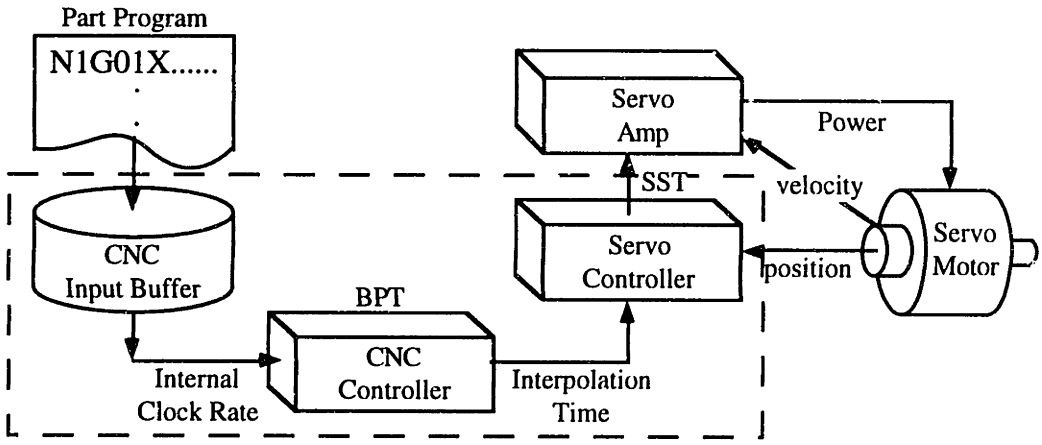

Figure 3.9 - CNC control of a machining center

3.4 GRINDING AND POLISHING OF CNC-MACHINED DIES

Grinding and polishing operations on dies are needed after the CNC finish cutting to smooth out the scallop marks left in the die surface. Otherwise, these machining marks would scratch the surface of the sheet metal blank and increase the draw-in force during forming. Grinding and polishing of die surfaces are usually manually performed by skilled workers using die grinders, grinding wheels, files, polishing stones, and various abrasives which requires considerable time. As mentioned before, the time required to manually grind a die is roughly proportional to the volume of unwanted material left over by the finish cutting operation. Equations 3.2, 3.4, and 3.10 can be used to make relative comparisons in manual grinding time between the various surface machining techniques. However, several automatic die polishing machines and various polishing end-effector designs for robots have been developed to automatically perform both the grinding and polishing operations. In grinding and polishing several auto body dies, [Hasegawa,1993] found that a robot polisher took between 23 to 36% less time than manual labor. [Lilly,1988] has effectively summarized the current state-of-the-art for automated grinding and polishing of dies.

3.5 CNC-MACHINING A MATCHED-SET OF STEEL DIES

For the comparative study, a matched-set of steel forming dies were fabricated using a 3-axis CNC machining center based on the AutoCAD™ CAD surface model of a sheet metal part. As discussed in section 2.4, a benchmark part shape was chosen for these dies. Both dies began as 10.2 cm square by 6.4 cm high steel billets from which V_{die}=100 cm^3 of material was removed during the rough cutting. To facilitate rapid machining, a leaded, free-machining steel (11L17) was chosen for these forming dies because of it's excellent machinability. A material with enhanced machinability allows contour milling of a die surface at very high feed rates which, in turn, minimizes the machining time. Furthermore, cemented carbide endmills were used for machining since such high strength cutting tools allow faster cutting speeds V_c and greater feed/tooth n_t . Specifically, A Ø12.7 mm and Ø6.4 mm 2-fluted ball endmill was used for rough and finish cutting, respectively. A Cincinatti-Milacron Model 7VC-750 3-axis machining center with an

Acramatic 850 CNC controller was used to machine the dies. The spindle motor of this machining center is power rated at 3.7 kW.

3.5.1 Computer Modeling and Simulation

The die surfaces for these continuous dies were created by offsetting the CAD surface model (zero thickness) of the benchmark part by half the material thickness in both normal directions. [Although it's usually part of the die development procedure to account for springback in the metal, the die shapes were not changed or altered from the original part shape in this case study.] The surface geometry was then transferred to a CAM software (MasterCAM) via an IGES format file. There is an infinite number of paths that the cutting tool can take to machine the die surface so a good tool path generation algorithm is needed to minimize the machining time. As is shown in figure 3.10b, a one-way milling cutter motion start at one the die corners was chosen. The contour milling paths were simulated in MasterCAM™ to check for machining problems like gouging and programming errors before any metal was cut. For larger dies like those for auto body panels, a test piece made out of plastic or wood is usually machined before committing to metal for this same purpose [Mayes,1993]. The total time required to simulate and create the CNC milling paths for the benchmark part shape was only 1 hour.

For the roughing cuts, equation 3.12 can be used to estimate the maximum possible material removal rate. From [Oberg,1988], E=0.9, K_p =0.44, C=0.96, and W=1.10 which allows a maximum Q of 160 cm^3/min based on the maximum power of the machine P_m =3.7 kW. The maximum depth of cut **d** is 2.0 cm and an arbitrary value of δ=0.25 cm was chosen. Therefore, the maximum feedrate for this case is

$$f_m = \frac{Q_{max}}{\delta \cdot d} = \frac{160}{0.25 \cdot 2.0} = 340 \text{ cm/sec.}$$

This is slightly less than the maximum feedrate of the machining center which is 380 cm/sec. We must also consider that maximum feedrate based on material considerations using equation 3.5. From [Oberg,1988], f_t =.025 cm/tooth, n_t =2, and V_c =13.000 cm/min (N=3400 rpm) which allows a maximum feedrate of only 180 cm/min. Since only one roughing pass was needed for both dies, the CAM estimate for rough cutting using a reciprocal-type motion (see fig. 3.10a) and the lower feedrate is 3.5 minutes per die.

For the finish cutting, equation 3.5 is again used to estimate the maximum feedrate. Using the same values as before except for a endmill diameter of 6.4 mm yields a maximum feedrate of 350 cm/sec. Even though the prescribed spindle speed is 6900 rpm, the machining centers maximum is only 6000 rpm. Climb cutting (i.e. cutting edge contacts widest part of chip first) is suggested for CNC-machining because it minimizes chatter and leaves a smoother machined finish [Kalpakjian,1984]. For this reason, a reciprocal type motion with an climb cutting endmill as shown in figure 3.10b was used for the simulation and the actual machining. For δ=0.05 cm and f_m =350 cm/sec, the time estimate for surface machining from the MasterCAM simulation is 15 minutes per die. If we use equation 3.13 to estimate t_{sm} using $A_{die} \approx 130$ cm^2, the value is 7.3 minutes. This large difference between the two estimates is attributable to equation 3.13 not accounting for the rapid returns of the endmill where no machining is taking place. This difference also points out that it would have been better to climb mill with a contouring type motion as shown in figure 3.10c where there are no rapid returns are necessary.

After the simulations revealed no gouging or other machining problems, the CAM software was then used to create the NC code needed by the 3-axis machining center to rough cut and finish cut the forming surfaces of the two matched dies.

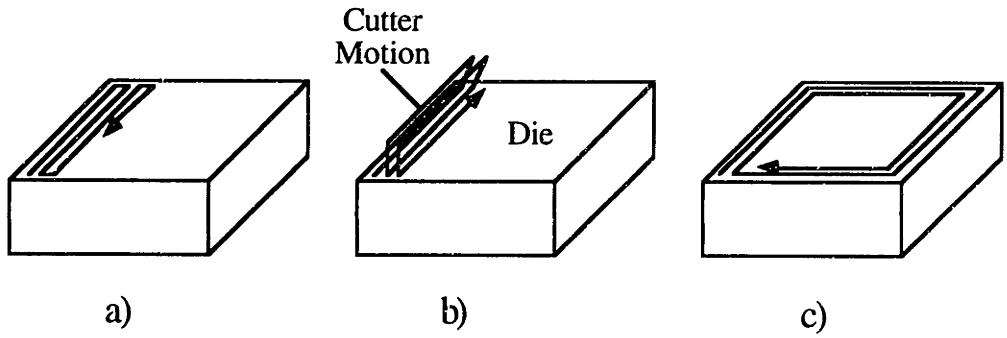

Figure 3.10 - a) Zig-zag b) one-way with rapid-return and c) contouring-type motion of an endmill

3.5.2 CNC-Machining The Dies

Before the die shape could be machined into the billet, some preparation machining was involved. The solid billets were first saw cut from 10.2 cm by 10.2 cm (4"x4") steel bar stock. One face of each billet was then machined flat to act as the die mounting surface. A threaded mounting hole was finally tapped into this machined face of the billet.

The main goal in this case study was to fabricate a set of continuous dies with the currently-available machinery in the shortest time possible. There were two problems with the machining center used to fabricate the dies that increased the machining time. The first one involved the 64 kilobyte input buffer of the CNC controller (Cincinatti-Milacron Acramatic 850). Since the size of the original roughing and surface machining NC files was 87 kilobytes and 23,000 kilobytes, respectively, these files had to be broken into a series of much smaller NC programs. Specifically, the rough cutting required 2 files and the finish cutting required 35 files. Downloading delays added 2 minutes to the per die roughing time and 1 hr. to the per die surface machining time. A drip feed feature in the machine's CNC controller would have made this time-consuming procedure unnecessary. The second problem with the machining center involved was the high BPT of it's controller. Using equation 3.14, the minimum BPT needed for roughing cutting at f_m=180 cm/sec and a δ=0.13 cm is 43 msec. Likewise, the minimum BPT for the finish cutting at f_m=350 cm/sec and a δ=0.025 cm is only 4 msec. Since the BPT of the 3-axis machining center used for this case study is 27 msec, severe bottlenecking was occurring in the data transmission for the finish cutting. In order to prevent unwanted machining marks and gouging from the stalled endmill that occurs during data downloading, the feedrate for the surface machining had to be decreased by a factor of 8 to 45 cm/sec. Because of this decreased feedrate, the actual finish cutting time increased to just over 2 hours per die. As a result of the reduced feedrates and NC program downloading delays, the total machining time for both forming dies including die preparation was 5.4 hours. The ideal and actual times required for each of the machining operations is found in table 3.2.

Table 3.2 - Times for CNC-machining operations (2 dies).

Machining Operation	Ideal Time (hrs)	Actual Time (hrs)
Die Preparation	0.5	0.5
Set Up	0.5	0.5
Rough Cutting	0.1	0.2
Finish Cutting	0.5	4.2

3.5.3 Grinding and Polishing the CNC-Machined Dies

The scalloped surface left by the surface machining operation required an extensive grinding operation. Using equations 3.3 and 3.4, the scallop height and necessary volume of material to be removed for the scalloped surface is 0.01 mm and 0.0033 mm^3/mm^2, respectively. The grinding operation performed first involved applying a blue coating to help reveal the remaining machining marks as the surface was ground flat. The surface scallops from the surface-machining were smoothed out using unitized grinding cylinders (three total) made of an A/O medium grade aluminum oxide grain. The grinding cylinder was mounted in a hand-held 25,000 RPM die grinder. The shape of the grinding cylinder was modified as needed to reach into the tight spots of the die forming surfaces. Grinding was ceased when the scallop ridges were no longer visible. After the grinding operation, a polishing compound was applied to the ground die surface with a felt polishing tip mounted in the die grinder until a finish of 0.10 μm was achieved. The finished set of CNC dies is shown in figure 3.1. Total grinding and polishing time took about 1 hour per die (2 hours total).

As observed by [Lilly,1988], grounding and polishing the dies is a significant part of the total fabrication time (up to 50%). In this case, it was 28% of the actual fabrication time and 64% of the ideal fabrication time. The time to polish these dies could have been reduced significantly if only the male and female die radius portions were polished. The die radius portions are actually the only sections of the these draw dies that see high contact pressures and friction.

3.6 GENERAL PROCEDURE FOR DESIGNING AND FABRICATING CNC-MACHINED DIES

The following discussion concludes this chapter by outlining the general procedure that is currently used for designing and fabricating CNC-machined sheet metal forming dies.

1) After considering the type of sheet metal part being formed and the expected production quantity of parts, choose an appropriate die material. The material chosen should allow for as rapid machining as is possible. [Semiatin,1988] is an excellent

reference for material selection and discussion on other design issues like binder incorporation.

2) Based on the geometry of the die surface, choose the machining method for attaining this shape. The choice is naturally constrained by the CNC machinery available for this purpose. The methods outlined in section in 3.1 are as follows:

3-Axis Machining with a Roughing Endmill is ideal for quickly removing large amounts of material.

3-Axis Machining with a Ball Endmill is ideal for small details such as grooves and small corner radii.

4-Axis Machining with a Ball Endmill is ideal for small details but it also offers an improved surface finish compared to simple 3-axis machining.

5-Axis Machining with a Radiused Endmill is ideal for gently curving surfaces. It significantly reduces the amount of time needed to grind the die surface smooth. A ball endmill can be used with the 5-axis machine for small details.

High Speed Machining Techniques should be used whenever possible.

The diameter of the roughing endmill is based on the material being machined and the capacity of the machine. However, the maximum removal rate should be the overriding objective. The diameter of the tool used for the final finish cutting should be equal to or smaller than the smallest radius of curvature of the die surface.

3) For the roughing operation, a reciprocal type motion with conventional milling, as opposed to climb milling, is used. With such large depths of cut taken in roughing, climb milling can potentially break the tool.

4) After choosing the machining method, the type of machining motion for the finish cutting operation must be selected. The fastest methods are a zigzag and contour motions. With a contour-type motion, the cutting edges of the tool circumference are used for machining resulting in good cutting conditions and smooth surface finishes.

5) Machining parameters—step-over distance δ, step-along distance δ_0, cutting feedrate $\mathbf{f}_m$, and depth of cut—that minimize the machining time, approximation error, and scallop height must be selected. There is a tradeoff between step over distance and machining time since δ must be as small as possible to minimize the grinding time and

surface approximation but not too small so that the finish cutting operation takes too long. As shown in figure 3.11, the chosen step-along distance must not cause the maximum machining error ε for the smallest radius of curvature of the die surface to exceed the maximum allowable machining error ε_{max}. In other words, $\varepsilon \leq \varepsilon_{max}$. The maximum machining error can be estimated by the relation:

$$\varepsilon = \rho - \left[\rho^2 - \left(\frac{\delta_O}{2}\right)^2\right]^{\frac{1}{2}} \qquad (3.15)$$

where: ε = maximum machining error
ρ = local radius of curvature of the CAD surface.

Finally, the maximum allowable $\mathbf{f_m}$ for the particular cutting tool and die material and the smallest possible depth of cut **h** should be chosen to minimize the machining time.

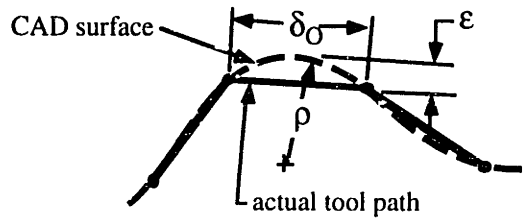

Figure 3.11 - CNC-machining error resulting from point-to-point moves.

6) Generate the NC machining instructions using a commercially-available CAM program with a robust tool path generation algorithm that checks for gouging and other machining errors.

7) The die billet should remain fixtured to the bed of the CNC machining center for the roughing, finish cutting, and automated grinding operations. Refixturing introduces unwanted machining errors into the process.

8) The geometrical accuracy of the forming die's ground surface should be checked with a CMM and then polished.

Chapter 4 - Profiled-Edge Lamination (PEL) Forming Dies

The problems with the current method of stacking and bonding a stack of horizontally-oriented contoured laminations for fabricating dies were presented in section 2.3. The main problems with this method concern the cumbersome techniques used to handle and secure laminations and to also recontour the die surface. Industry's failure to embrace the current laminated construction method can be attributed to these inherent problems. To a die maker, however, the idea of constructing dies out of a laminations which only have to be machined with narrow cuts instead of having to rough out the shape from a solid billet (e.g. by CNC-machining) is very appealing. For this reason, the author has developed a new die fabrication method which involves stacking and securing an array of vertically-oriented Profiled-Edge Laminations (PEL) whose top edges form a segmented forming surface. The PEL die construction facilitates easy handling, securing, and recontouring (if needed for shape modification) of the die laminations. In this chapter, we introduce the PEL die method and discuss various aspects of the method in detail, describe new apparatus concepts for fabricating such dies, identify the optimal method(s) for cutting PELs, describe the construction of a matched set of PEL dies, and finally outline the general procedure for designing and fabricating a PEL die.

A matched-set of PEL dies consisting of 1.47 mm thick steel laminations were fabricated for the comparitive study. The top profiled-edge of each lamination was machined with the weaving motion of a ball endmill mounted in a 3-axis CNC machining center. After assembling the laminations into a die, the resulting top surface was ground and polished using a hand-held die grinder to a smooth finish suitable for forming sheet metal parts. The two laminated forming dies and a part stamped from steel sheet using these dies is shown in figures 4.1a and 4.1b, respectively.

Figure 4.1 - a) Matched set of PEL stamping dies and b) benchmark part stamped with these dies

4.1 PROFILED-EDGE LAMINATION (PEL) METHOD

As seen in figure 4.2, a PEL die generally comprises a plurality of die lamination members, each die lamination member being substantially planar and each being disposed in a vertical plane and stacked together side-by-side in an array. The top edge of each die lamination is simultaneously profiled and beveled in such a way as to approximate a segment of the intended die surface. Specifically, this top edge is continuous in the y-direction and approximated in the x-direction. The die lamination members may be held together in a stacked array by any suitable means, but preferably with a clamping frame as shown in figure 4.3a. A common registration corner and the bottom edge of each lamination allows for easy and uniform registration in the clamping frame. One or more holes uniformly positioned in the sides of each lamination allows the whole array to be clamped so that no adhesive or other means of holding the array of die lamination members together is required. If the shape of the forming surface has to be change during the die development, the die laminations can easily be separated for remachining to update the die shape. The PEL die can be made into a solid die apart from this process by suitable means (e.g. diffusion bonding metal lamination members together) if needed or desired. Generally at least a portion of the die lamination members have a continuously changing beveled top edge. When placed together in a vertical stacked array, the top edges of the die lamination members, in the aggregate, form the top surface of the die. The advantages that a PEL array construction has over the contoured lamination stack shown in figure 4.3b is summarized in table 4.1.

Table 4.1 - Comparison of the laminated die constructions

Stack of Contoured Laminations	Array of Profiled-Edge Laminations
Difficult to automate the handling of laminations during cutting.	Laminations can slide past the profiled-edge cutting means since only top edge is cut.
Difficult to register laminations during die assembly.	Laminations are easily registered with a base plate and an edge guide.
Difficult to secure lamination stack into a rigid tool.	Lamination only needs to be clamped from the side.
Typically, laminations need to be permanently secured. Reshaping of die surface requires CNC-machining.	Unclamped laminations can be individually recut to new die shape.

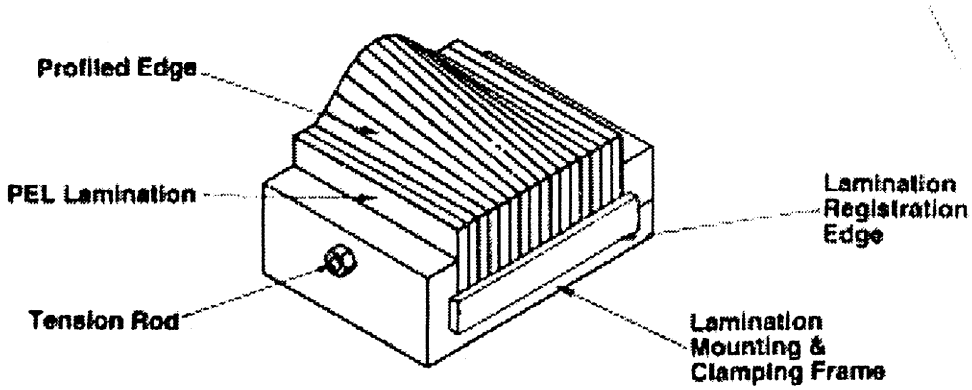

Figure 4.2 - Isometric view of an array of Profiled-Edge Laminations.

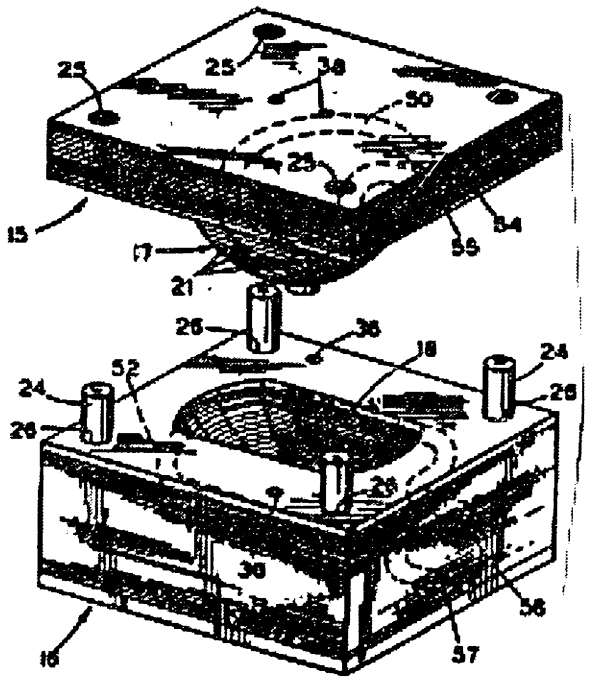

Figure 4.3 - Isometric view of a) a PEL array clamped in the die frame and b) a bonded stack of contoured laminations.

4.1.1 Extracting PEL Machining Instructions from a CAD Model

The first step in the process of creating a PEL die is to create a 3-dimensional model of the die's forming surface. This surface model may be created by a die designer using CAD software; or by a locus of surface coordinates defined by an iteration of a closed-loop control algorithm, an FEA model of the die, or a reverse engineering scan from a coordinate measuring machine (CMM). Covering the details of extracting the machining instructions for the profiled-edges of the die laminations from the die surface model is beyond the scope of this thesis. However, to illustrate the data manipulation process required, the general procedure of using a CAD surface model for this purpose will be discussed.

As shown in figure 4.4, the intersection of a 3-dimensional CAD surface model and a Y-Z cutting plane, situated at some point on the X-axis, is a 2-dimensional curve. Furthermore, if the Y-Z plane is repositioned along the X-axis by constant increments such as 1 mm, the collection of curves produced by each of the same plane/surface intersections will approximate the shape of the original 3-D surface. [Phillips,1984] and [Bobrow,1985] have developed algorithms for determining the intersection of two arbitrary surfaces

(analytic or parametric). Figure 4.5 shows how the true 3-D surface between two adjacent curves can be approximated by connecting them with a bevel. This connecting bevel constitutes the profiled-edge of each PEL die lamination. Note that the approximation of the 3-D surface gets better as the curves get closer together, i.e. as the x-increment decreases. This collection of curves serves as the machining database for creating a PEL die with the desired forming surface.

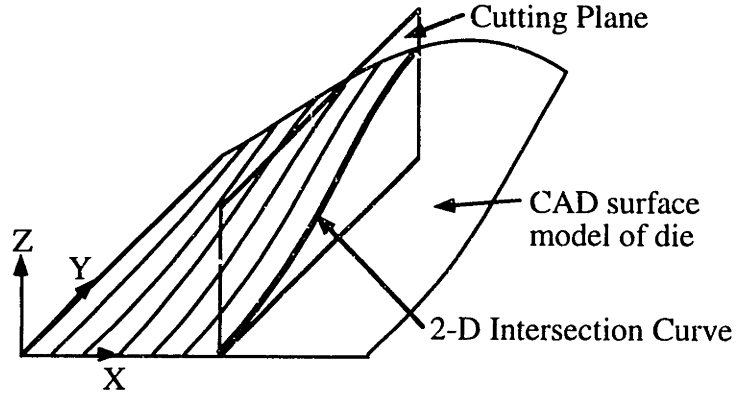

Figure 4.4 - Surface model of the die's forming surface showing intersection curves.

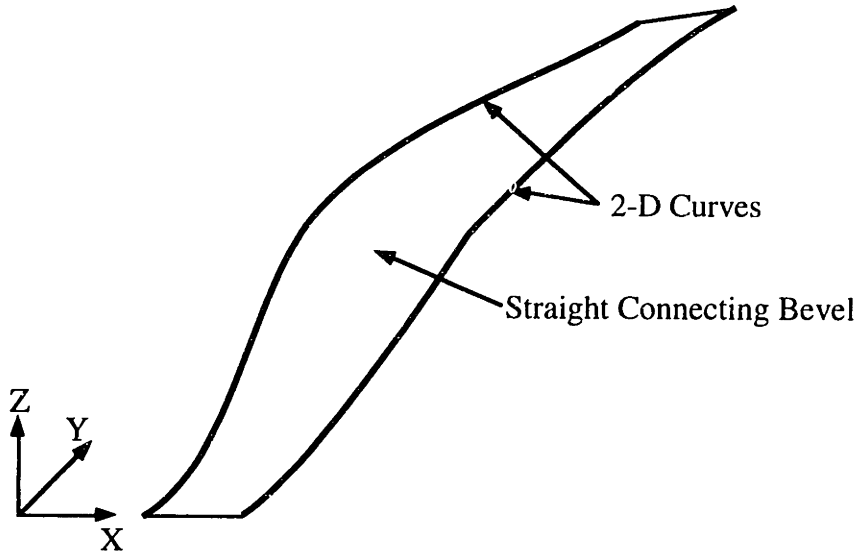

Figure 4.5 - Connecting bevel between 2 adjacent intersection curves.

Any one of several cutting methods (e.g. laser cutting, machining with an endmill, abrasive waterjet cutting, plasma-arc cutting) can be used to create the bevels into the top edges of the die laminations. These methods will be discussed in more detail in a later section of this chapter. With whatever method is used, the data needed for cutting the compound bevels is the position point $\mathbf{P}_1$ on the nearside of the lamination with

coordinates (x_1,y_1,z_1) and a unit directional vector $\bar{V} = V_1 \cdot i + V_2 \cdot j + V_3 \cdot k$ or just written as (V_1,V_2,V_3). As shown in figure 4.6, the vector components of $\bar{V}$ defined by P_1 and P_2 with coordinates (x_2,y_2,z_2) are

$$V_1 = \frac{x_2 - x_1}{|\bar{V}|} = \frac{t_L}{|\bar{V}|}, \quad V_2 = \frac{y_2 - y_1}{|\bar{V}|}, \quad \text{and} \quad V_3 = \frac{z_2 - z_1}{|\bar{V}|}. \qquad (4.1)$$

where: $$|\bar{V}| = \left[t_L^2 + (y_2 - y_1)^2 + (z_2 - z_1)^2\right]^{\frac{1}{2}}.$$

Point P_1 is easy to determine because x_1 and y_1 will be prescribed and z_1 is explicitly defined by the nearside intersection curve (see figure 4.6). Point P_2 is harder to define because there is no particular one associated with the defined point P_1. To determine P_2, an iterative procedure which minimizes the geometric error introduced by the straight bevel approximation is required. When P_2 is determined then the bevel cutting head will only require translation along the Y and Z-axes, i.e. x_p is kept constant, and rotation about the two orthogonal axes.

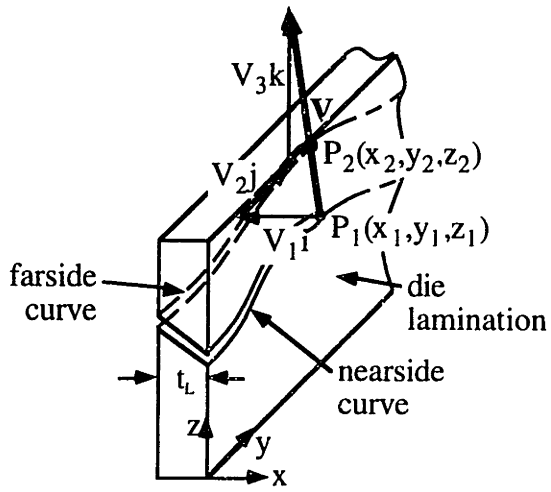

Figure 4.6 - Die lamination with beveled cut

4.1.1.1 Constraining Bevel Cutting Head to Y-Axis Rotation (Planar Beveling)

There are many forming dies used in industry for such processes as stretch-forming and rubberforming that have only mild curvatures and low draws. For these types of die shapes, reasonable die shape fidelity, i.e. small deviations of the machined shape

from the desired CAD shape, can be achieved even if the bevel cutting head is only allowed to rotate about the Y-axis. This will allow for simple planar beveling but not compound 3-D beveling like that shown in figure 4.6. A typical bevel of this type is shown in figure 4.7. The position point P_1 and orientation vector $\vec{V}$ of the bevel cutting head are defined by coordinates (x_1,y_1,z_1) and unit vectors $(V_1,0,V_3)$, respectively.

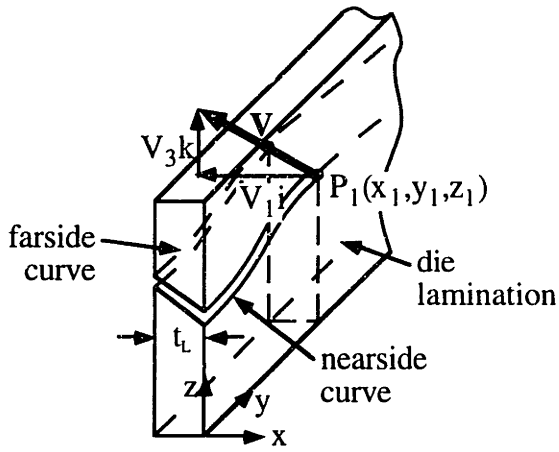

Figure 4.7 - Schematic of die lamination with a simple planar bevel.

4.1.1.2 Geometric Error Introduced by Straight Bevel Approximation

By observing the X-Z plane cross section of a die lamination in figure 4.8, it is evident that the straight bevel of the profiled edge will deviate from the desired die surface for the cutting method outlined in section 4.1.1.1. During the grinding and polishing operations on the die surface, this deviation or shape error is increased for convex cross-sectional profiles, as shown in figure 4.8a, because of material removal. For the same reason, i.e. material removal, the shape error is decreased for concave cross-sectional profiles as shown in figure 4.8b. Therefore, the extent of material removal during the smoothing operation directly affects the shape integrity of the forming die. The standard method for determining the die shape error is to directly measure the surface with a coordinate measuring machine and then compare that data with the reference CAD shape.

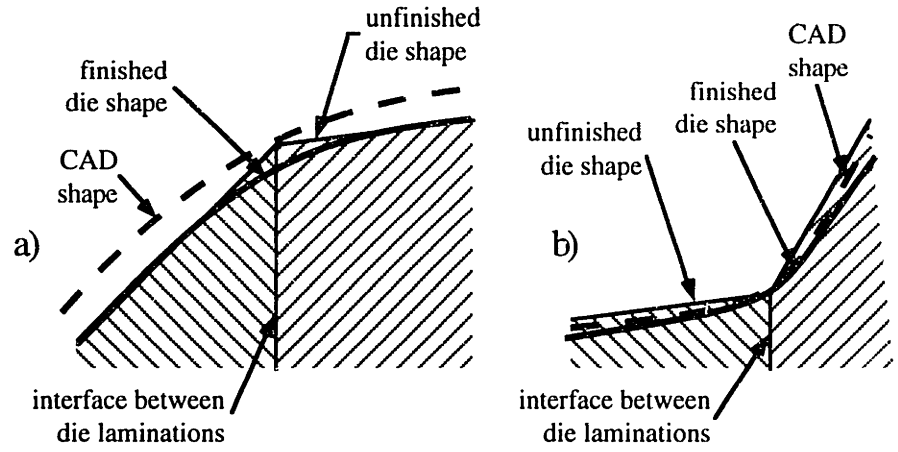

Figure 4.8 - Shape Error due to smoothing a) convex and b) concave die geometries.

Instead of having to construct a die and measure it's surface, the maximum error introduced by a particular lamination bevel can be estimated by considering the cross-sectional geometry from the CAD database as shown in figure 4.9. The actual cross-sectional curve of the die surface model can be determined using currently-available CAD software for comparison with the straight bevel. The task of extracting this curve is a cumbersome task. A simpler way to determine the maximum shape error is to estimate the die's cross-sectional curve between points (x_1,y_1) and (x_2,y_2) with a parabola. A parabola is used because it's a function that easily fits 2 coordinate points with known slopes. This parabola is defined by bevel end coordinates (x_1,z_1) and (x_2,z_2), and the corresponding instantaneous x-z slopes $\frac{\partial z_1}{\partial x_1}$, $\frac{\partial z_2}{\partial x_2}$. The coordinates and slopes are easily obtainable with certain CAD softwares [ProEngineer,1994]. The general equation of a parabola in the X-Z plane is $(x-h)^2 = 4 \cdot p \cdot (z-k)$ (4.2) if it opens upwards, i.e. $\frac{\partial z_1}{\partial x_1} < \frac{\partial z_2}{\partial x_2}$, and $(x-h)^2 = -4 \cdot p \cdot (z-k)$ (4.3) if it opens downwards, i.e. $\frac{\partial z_1}{\partial x_1} > \frac{\partial z_2}{\partial x_2}$ where p = parabola's focal length and

(h,k) = the vertex coordinates.

Fitting a parabola to the die lamination cross-section shown in figure 4.8 yields the following substitutions into equation 4.2;

$$h = x_1 - 2 \cdot p \cdot \frac{\partial z_1}{\partial x_1}; \quad k = z_1 - \frac{(x_1 - h)^2}{4 \cdot p}; \quad p = \frac{x_2 - x_1}{2 \cdot \left(\frac{\partial z_2}{\partial x_2} - \frac{\partial z_1}{\partial x_1} \right)} \tag{4.4}$$

and the following substitutions into equation 4.3;

$$h = x_1 + 2 \cdot p \cdot \frac{\partial z_1}{\partial x_1}; \quad k = z_1 + \frac{(x_1 - h)^2}{4 \cdot p}; \quad p = \frac{x_2 - x_1}{2 \cdot \left(\frac{\partial z_1}{\partial x_1} - \frac{\partial z_2}{\partial x_2} \right)}. \tag{4.5}$$

The slope **m** of the line which passes through points (x_1,y_1) and (x_2,y_2) is found by the relation

$$m = \frac{z_2 - z_1}{x_2 - x_1}. \tag{4.6}$$

The point (x_p,y_p) on the parabola with the same slope is found by setting the first derivative $\frac{\partial z}{\partial x}$ of equations 4.2 and 4.3 equal to **m**. If the parabola opens upward, then

$$x_p = h - 2 \cdot p \cdot m \text{ and } z_p = k - p \cdot m^2. \tag{4.7}$$

If the parabola opens downward, then

$$x_p = h + 2 \cdot p \cdot m \text{ and } z_p = k + p \cdot m^2. \tag{4.8}$$

To find the distance **e** between the line passing through (x_1,y_1) and (x_2,y_2) and the parallel line passing through (x_p,y_p), a line is constructed through (x_p,y_p) which is perpendicular to the other two lines, i.e. slope $= -\frac{1}{m}$. This perpendicular line intersects the (x_1,y_1) and (x_2,y_2) line at point (x_g,y_g). The values of this new intersection point are found from the equations

$$x_g = \frac{m \cdot x_1 + \frac{x_p}{m} - z_1 + z_p}{m + \frac{1}{m}} \text{ and } z_g = z_1 + m \cdot (x_g - x_1). \tag{4.9}$$

The maximum distance **e** between the parabola and the straight line representing the bevel represents is the largest error. It is calculated with the equation

$$e = \sqrt{(x_p - x_g)^2 + (z_p - z_g)^2} \tag{4.10}$$

If desired, the error can be expressed as a function of lamination thickness $\mathbf{t_L}$ so that an optimization procedure for choosing the thicknesses, interface placement, and orientation of the laminations can be implemented. The goal of the procedure would be to minimize the overall bevel approximation error.

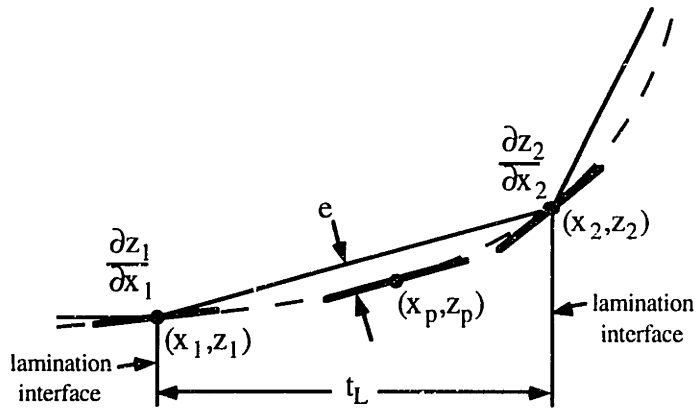

Figure 4.9 - Shape error estimation of a beveled die lamination

4.1.2 Propensity for PEL Die Delamination

If the PEL die laminations are bonded together then the composite structure becomes a continuous die. To keep the PEL die easily remachinable, the die laminations are simply clamped together with a rigid frame as shown in figure 4.3a. In a clamped configuration, individual laminations have a propensity to delaminate (i.e. separate from adjacent laminations) by elastically deforming or buckling under the high forming loads encountered. As seen in figure 4.10a, the die shape changes when a lamination(s) bends elastically resulting in dimensional changes to the parts formed. For this reason, it is important to investigate the elastic bending and buckling behavior of a clamped lamination subjected to typical forming loads.

Excessive deformation of any of the clamped die laminations beyond a certain maximum value, i.e. $\delta > \delta_{max}$, is considered a die failure. Ideally a PEL die should emulate a continuous die whose surface deformation is essentially negligible (e.g. 0.01 mm for a steel die). However, a more practical design requirement for PEL dies is to make sure that the dimensions of the formed part are within the specified tolerances. The maximum deformation value (δ_{max}) of a die lamination is explicitly determined from this requirement.

Referring to figures 4.10a and 4.10b, a group of deflected laminations (due to high forming loads) can be roughly modeled as cantilevered Euler beams in a parallel configuration. This assumes that the frictional shear forces at the interfaces between adjacent laminations are negligible. The deflection δ of a single rectangular lamination (see figure 4.10c) can be estimated using the relation

$$\delta = \frac{4 \cdot F_{bending}}{E \cdot b}\left(\frac{a}{t}\right)^3 . \qquad (4.11a)$$

where: a = lamination height
b = lamination width
t = lamination thickness
E = tensile elastic modulus of the lamination material
$F_{bending}$ = horizontal component of the laminations's total forming load.

By rearranging equation 4.11a, the spring rate $\mathbf{k_L}$ of the lamination is then

$$k_L = \frac{F_{bending}}{\delta} = \frac{b \cdot E}{4}\left(\frac{t}{a}\right)^3 . \qquad (4.11b)$$

The mode of mechanical failure of a lamination from the vertical component of the forming load $\mathbf{F_{buckling}}$ will be some form of buckling behavior. As stated by [Timeshenko,1961], " in the calculation of critical values of forces applied to the middle plane of a plate at which the flat form of equilibrium becomes unstable and the plate begins to buckle, the same methods as in the case of compressed bars can be used." Therefore, the critical buckling load $\mathbf{F_{b,critical}}$ for the lamination shown in figure 4.11a can be estimated using the Euler column buckling formula

$$F_{b,critical} = \frac{k \cdot E \cdot b \cdot t^3}{12 \cdot a^2} \qquad (4.12)$$

where: k = factor that depends on the end support conditions of lamination.

If the lamination can be modeled as a simple cantilever beam then k is 2.47. If the movement of it's upper edge is restricted horizontally then k is 20.2.

The forming forces on a lamination consist of an effective normal load $\mathbf{F_n}$ and a perpendicular frictional load $\mu \cdot F_n$ at the lamination (die) and sheet metal interface where μ is the frictional coefficient. These loads are shown in figure 4.10. The total forming load $\mathbf{F_T}$ has a magnitude of $F_n \cdot \left(1+\mu^2\right)^{\frac{1}{2}}$. As shown in figure 4.11b (vector diagram), F_T typically points inward to the die. This is a desirable situation since convex portions of the laminated die will tend to be pushed together during forming. In terms of F_T, the bending and buckling loads are $F_T \cdot \sin\left(\alpha - \tan^{-1}\mu\right)$ and $F_T \cdot \cos\left(\alpha - \tan^{-1}\mu\right)$, respectively.

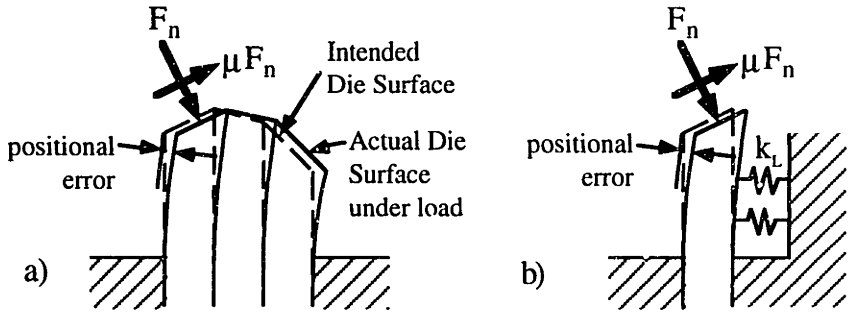

Figure 4.10 - a) Group of die laminations subjected to generic forming loads and b) modelled as cantilevered Euler beams in a parallel configuration.

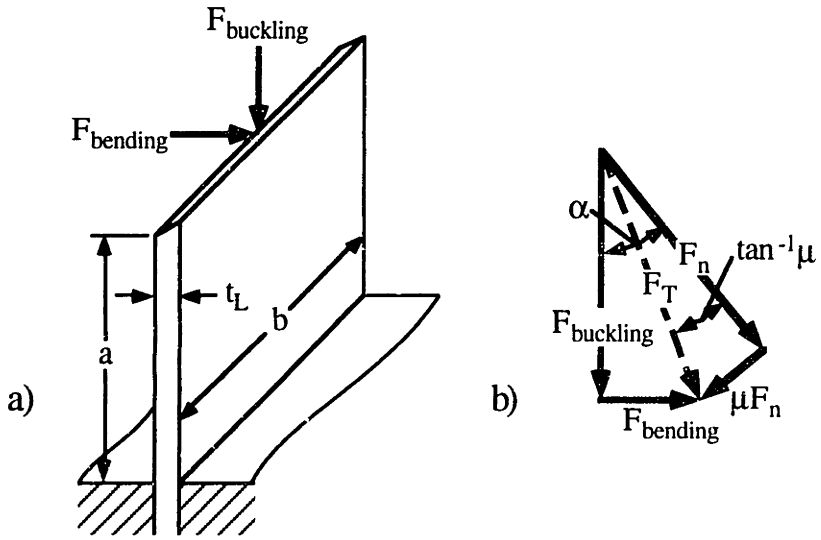

Figure 4.11 - a) Single rectangular die lamination subjected to bending & buckling loads.and b) a vector diagram of all forming loads.

As an example, the bending and buckling propensity of a single lamination from the male PEL described in the introduction of this chapter will be determined using the aforementioned analysis. The lamination chosen is located 2.8 cm in from the edge of the along the X-axis (see figure 2.12). It's profiled edge forms half of the upper bend radius for one of the benchmark part side walls. A maximum forming load of 50 kN is predicted by the FEA analysis described in section 2.4. Since the upper bend radii on the male die takes most of the total forming load, the estimated maximum normal force that this particular lamination experiences is around 6.0 kN. Additional data on the lamination is as follows:

a = 1.9 cm
b = 6.4 cm
t = 1.47 mm
E = 200 GPa

μ = 0.2 (for greased steel on steel) and
α = bevel angle = 30°.

Thus, the bending and buckling loads are 2.0 and 5.8 kN, respectively. From figure 2.12, the benchmark part dimensional tolerance is ±0.1 mm. Since this lamination is backed by 35 adjacent laminations of similar size, the estimated bending deflection using equation 4.11a is only 0.04 mm which is well below the dimensional tolerance. This simple deflection analysis doesn't even take into account the symmetrical loading on the male die which will tend to counteract the high forming load applied to this sample lamination. Finally, if we assume a worst case buckling scenario where the lamination is unsupported on it's top edge then the critical buckling load is 23 kN according to equation 4.12. This value is well above the maximum above the maximum assumed buckling load of 5.8 kN so that buckling will not be a problem

4.2 BEVEL CUTTING METHODS FOR DIE LAMINATIONS

Once the intersection curves that define the top profiled-edge bevels of each lamination are determined, the respective die lamination is ready to be processed. The machining database is used to cut new die lamination blanks or to recut existing die laminations into a new shape. Machining bevels into the die lamination edge can be accomplished by several methods. As seen in figure 4.12a, the flute-edge of a standard endmill mounted in the spindle of a 4 or 5-axis (X, Y, and Z-translation, Y and Z-rotation) CNC milling center can be used to cut bevels into a suitably-fixtured die lamination. As seen in figure 4.12b, the weaving-type motion of a ball endmill from a 3-axis (X,Y,Z translation) CNC machining center can also cut bevels. Both machining methods rely on the application of high machining forces to remove the unwanted material from the workpiece. To minimize the amount of material removed while cutting the bevel, a very narrow kerf can be cut into the die lamination using traveling wire-EDM, abrasive water-jet cutting, plasma-arc cutting, or laser cutting (both CO_2 and Nd:YAG) as seen in figure 4.12c. Each of these methods require CNC-controlled axes that move in X, Y, Z translation, and Y, Z rotation.

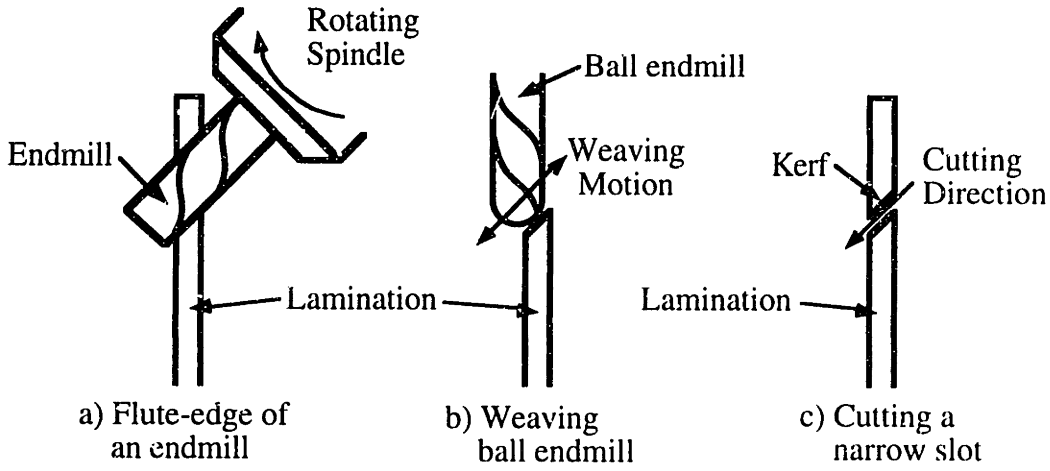

Figure 4.12 - Methods for cutting a bevel into die laminations.

The important characteristics of any bevel cutting method are the maximum achievable bevel angle, maximum cutting feedrate (speed), cut surface quality, cutting accuracy, amount of material removed, effect of material hardness on speed, tool wear, extent of metal burring, and machine cost. Quantifying the performance specifications of each of the aforementioned bevel-cutting methods is necessary so that the most suitable one(s) for machining PEL die laminations are identified. Therefore, a preliminary comparison of these cutting methods is summarized in Table 4.2. All comparisons made in this section pertain to steel which is arguably the most commonly used die material [Semiatin,1988]. The specifications listed in the table are based on the cutting of 1.47 mm thick SAE 1010 cold-drawn steel sheet. The data used to complete the table was drawn from a combination of suitable references [Oberg,1988; Kalpakjian,1992] and information solicited from various machine vendors.

The information from table 4.2 was used for a preliminary comparison of cutting methods. From this comparison, a weaving ball endmill and wire-cut EDM are immediately identified as impractical methods for cutting bevels. Cutting bevels with a weaving ball endmill is an impractical method mainly because of the short tool life, workpiece deflection, and the effect material hardness has on cutting speed. In addition to these problems, using a weaving ball endmill has the added problems of a slow feedrates and extensive edge burring. These conclusions were drawn after machining the laminations of the benchmark part PEL dies. The wire-cut EDM machine system yields a

cut of excellent quality and accuracy but the extremely slow cutting feedrate is considered unacceptable for this application.

Table 4.2 - Preliminary Comparison of Bevel Cutting Methods

	Flute-Edge of Endmill	Weaving Ball Endmill	Wire-Cut EDM	Abrasive Waterjet	Plasma-Arc	CO_2 Laser	Nd:YAG Laser
Maximum Bevel Angle	±85°	±80°	±85°	at least ±60°	at least ±60° on one edge only	±45°	±80°
Maximum Cutting Feedrate (m/min)	3.0 carbide 0.75 HSS	0.1 carbide 0.03 HSS	0.02	0.4	2.0	3.2	1.4
Surface Roughness of Cut (μm)	3.2	6.3	1.5	3.8	3.2	1.6	1.6
Cutting Accuracy (μm)	±60	±125	±2	±125	±60	±60	±60
Kerf Width (mm)	6.4 (min)	Entire upper section of laminatio n removed	0.25	0.84	1.0	0.4	0.5
Effect of Material Hardness on Maximum Feedrate	Reduction in cutting speed	Reduction in cutting speed	Negligibl e	Minimal	Minimal	Negligibl e	Negligibl e
Tool Life	1.5 hrs. (carbide) 5 hrs. (HSS)	1 hr. (HSS)	Wire is used once	125 hrs. for carbide nozzle, Abrasive used once	3 hrs. for Consum-ables	None	None
Extent of Edge Burring	Extensive at high bevel angles	Extensive at high bevel angles	None	Minimal	Extensive dross at high bevel angles	Minimal dross on farside of cut	Minimal dross on farside of cut
ApproximateM achine Cost ($)	115K	75K	130K	145K	100K	200K	200K

The bevel cutting methods that were not discounted from this preliminary study are machining with the flute-edge of an endmill, abrasive water jet cutting, plasma-arc cutting, and laser cutting. Each of these methods will be investigated in detail through a series of

bevel cutting experiments to determine how rapidly and accurately they will machine steel PEL laminations. The basis of evaluation for each beveling method will be the quality characteristics of the bevel cut that it makes. The quality characteristics are defined in figure 4.13. The lamination material used for every cutting experiment was 1.47 mm thick SAE 1010 cold drawn steel sheet.

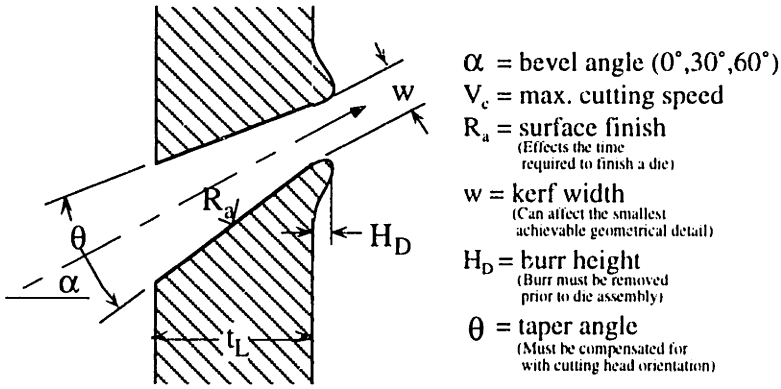

Figure 4.13 - Quality characteristics of a bevel cut.

4.2.1 Machining with the Flute-Edge of an Endmill

As seen in figure 4.14a, the profiled-edge of a die lamination can be machined using the flute-edge of an endmill mounted in 4-axis machining center for planar bevels (see figure 4.7) and a 5-axis machine for compound bevels (see figure 4.6). Cutting bevels with this method requires a significant amount of material removal (i.e. the width of the endmill) as shown in figure 4.14b. Based on the geometry of the endmill and the tilted lamination, the maximum bevel angle α that can be machined into a die lamination is

$$\alpha = \tan^{-1}\left(\frac{L_f}{t_L}\right) \qquad (4.13)$$

where: L_f = length of the cutting flute and
t_L = lamination thickness.

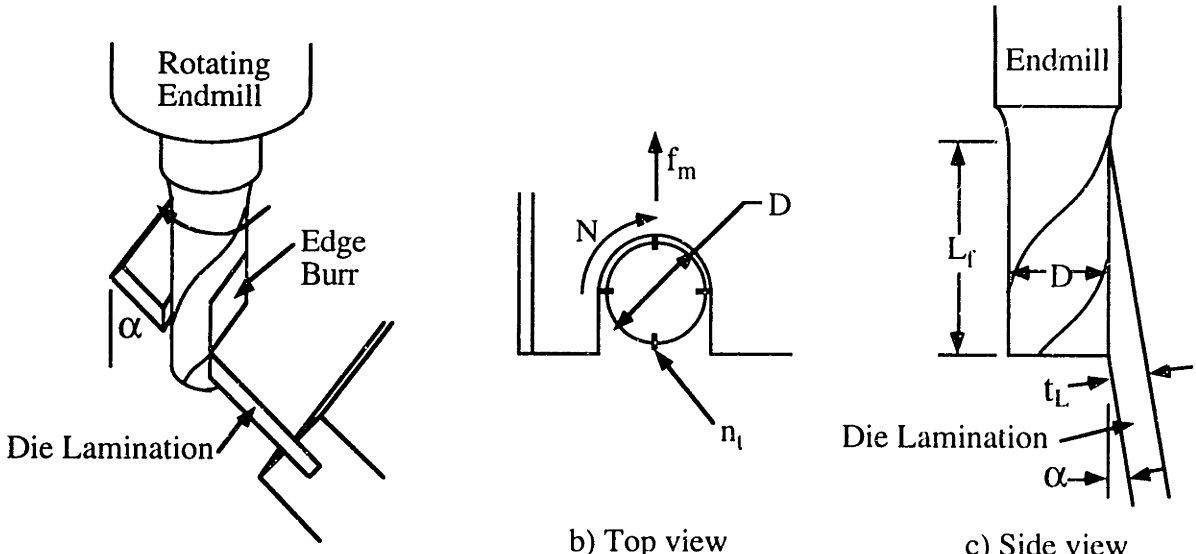

Figure 4.14 - Machining a lamination bevel with the flute-edge of an endmill.

4.2.1.1 Estimating Surface Roughness from Flute-Edge Endmilling

The roughness of the surface machined with the flute-edge of an endmill can be estimated by considering the geometry of cutting shown in figure 4.15. The position **P** of one of the endmill's cutting edges is described by the equations

$$x = \frac{D}{2} \cdot \sin 2\pi Nt + f_m \cdot t \qquad (4.14)$$

and

$$y = \frac{D}{2} \cdot (1 - \cos 2\pi Nt) \qquad (4.15)$$

where: D = endmill diameter
N = endmill rotational speed and
t = time.

The distance $\mathbf{d_e}$ that the endmill travels in the cutting direction from the position shown in figure 4.15 until the next cutting edge reaches the same y-position is $\frac{f_m}{N \cdot n_t}$. The cutting edge reaches the maximum height of the unmachined material when the endmill has travelled $d_e/2$. By substituting this distance into equation 4.14, the time it takes the cutter to move from position P to the maximum height can be determined by solving the iterative equation

$$t = \frac{1}{2 \cdot N \cdot n_t} - \frac{D}{2 \cdot f_m} \cdot \sin 2\pi N t \qquad (4.16)$$

for t. This time value is then substituted back into equation 4.15 to calculate the maximum height of the unmachined material and, hence, an estimate of the surface roughness (i.e. $R_a \approx y/4$). This model was developed to help determine the main process parameters for flute-edge endmilling.

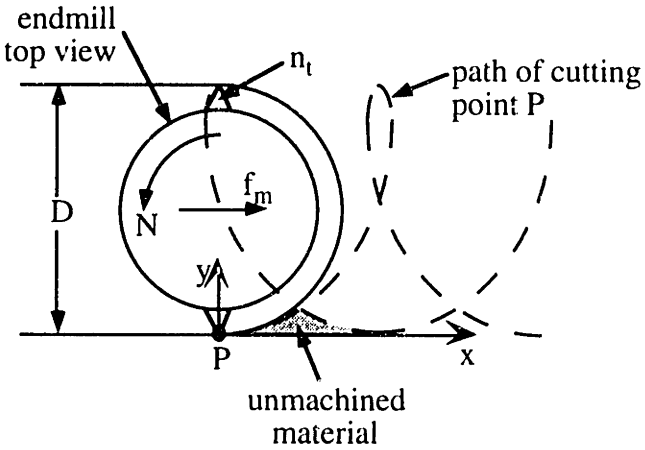

Figure 4.15 - Climb-milling of a slot with the flute-edge of an endmill.

4.2.1.2 Optimization of the Machining Parameters

For cutting with the flute-edge of an endmill, the process parameters that yield the best quality bevels in terms of surface roughness $\mathbf{R_a}$ and length of the edge burr $\mathbf{H_b}$ need to be determined. Equations 4.15 and 4.16 suggest that the feedrate f_m, spindle speed N, number of cutter teeth n_t, and the cutter diameter D will all effect the surface roughness. In addition, the presence or absence of machining coolant should have an effect. The feedrate and spindle speed are easily varied with the CNC machining center controller. The effect of changing n_t can be simulated by varying N and the cutter diameter will be dictated by the smallest radius of curvature of the die surface. All of these process parameters will also have an effect on the extent of edge burring.

The goal of this investigation is to determine the effect of each process parameter (i.e. control factor) on the surface roughness and the length of the burr as shown in figure 4.14a. One of the best experimental techniques for determining these relationships and also the optimal cutting parameters is to use Design of Experiments (DOE) [DeVor,1992]. A block diagram of the proposed experiment is shown in figure 4.16. Specifically, a full

factorial experimental design with 3 control factors at 2 distinct levels (8 experiments) was performed for 3 different signal factor levels. The signal factor in this case is the bevel angle α and the levels chosen were 0° (no bevel), 30° (mild bevel), and 60° (steep bevel). A Cincinnati-Milacron 3-axis machining center with a 6.4 mm diameter 4-fluted carbide endmill was used to machine the lamination plates. [Note: 6.4 mm is the smallest radius of curvature of the benchmark part.] Using equation 4.13, the maximum bevel angle for the endmill and lamination used for the experiments (i.e. t_L=1.47 mm and L_f=16 mm) is 85°. The control factor levels used for each particular bevel angle were determined experimentally and are listed in table 4.3. The surface roughness of a 1 mm sampling length of the machined bevel surface was measured with a profilometer. A scan of the test cut #1-0° surface is shown in figure 4.17. The experimental results for each DOE test are listed in table 4.4.

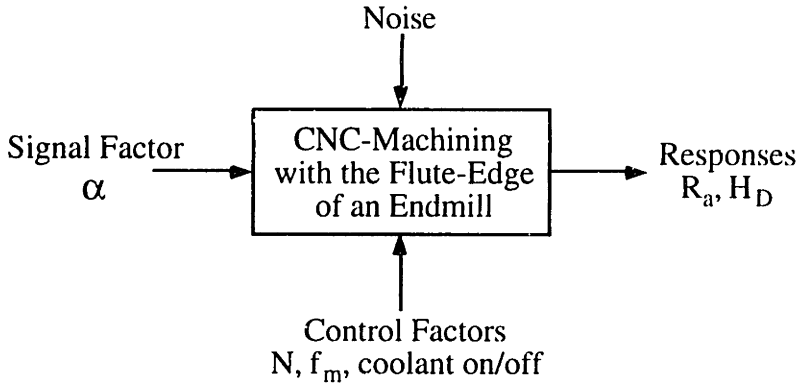

Figure 4.16 - Block diagram of the experimental design used for flute-edge endmilling.

Table 4.3 - Control factor levels used for the flute-edge endmilling experiments

α	0°		30°		60°	
Level	-1	+1	-1	+1	-1	+1
f_m (m/min)	0.152	0.305	0.152	0.305	0.102	0.203
N (rpm)	1500	3000	1500	3000	1000	2000
C (coolant state)	off	on	off	on	off	on

Because the experimental array is orthogonal, the responses can be used to calculate the main and interaction average effects of the three control factors on outputs R_a and H_D. The main and interaction effects in this case are listed in table 4.5. Details of how these effects are calculated can be found in Devor (1992). Ideally, the main and interaction

effects are used to develop a mathematical model of the process which will accurately estimate the response for a certain set of control factors. This model can also be used to pick the optimal control factors for the process.

Table 4.4 - Experimental results of the flute-edge endmilling experiments

Test	Control Factor Levels			Responses					
				0°		30°		60°	
	f_m	N	Coolant	R_a (μm)	H_D (mm)	R_a (μm)	H_D (mm)	R_a (μm)	H_D (mm)
1	-1	-1	-1	1.4	0.2	8.7	2.8	2.2	10.2
2	+1	-1	-1	1.8	3.5	14.0	3.0	6.0	5.1
3	-1	+1	-1	0.6	0.2	2.4	1.3	2.2	6.4
4	+1	+1	-1	1.2	0.1	1.5	2.5	0.8	7.4
5	-1	-1	+1	0.9	0.2	6.6	2.5	6.0	9.4
6	+1	-1	+1	15.0	0.8	5.8	2.3	2.7	10.2
7	-1	+1	+1	1.6	0.2	0.7	2.8	1.2	9.1
8	+1	+1	+1	0.7	0.1	2.3	3.3	4.4	8.9

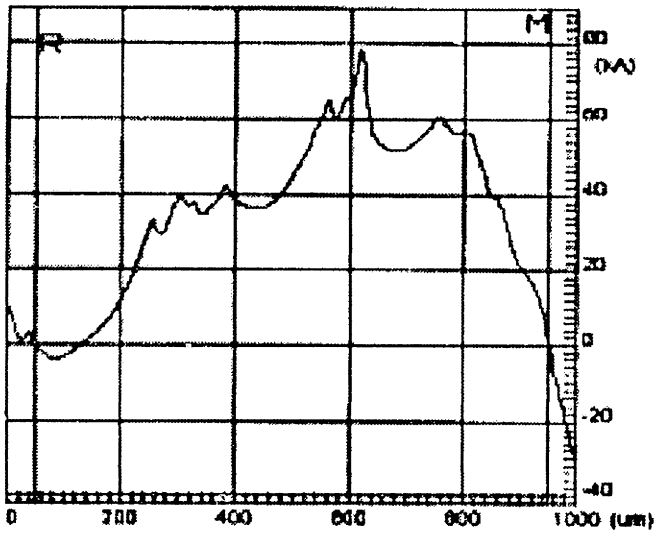

Figure 4.17 - Profilometer scan of a beveled surface machined with an endmill.

From table 4.5, it is evident that there is a high average main effect for the spindle speed N on R_a and for f_m on R_a at shallow bevel angles (i.e. 0° and 30°). The effects of f_m and N on R_a are in opposite directions, i.e. increasing f_m tends to give a rougher surface and increasing N tends to give a smoother surface. This experimentally observed trend agrees

with the geometrical model described by equations 4.15 and 4.16 for estimating the surface roughness. Using the data from test #1 listed in table 4.4, the surface roughness is calculated to be 0.006 μm. When f_m and N are individually doubled, the surface roughnesses are 0.025 μm and 0.0016 μm, respectively. These calculated values don't match the experimental values probably because of significant machining chatter that dominates the cutting process but which isn't accounted for in this simple geometric model.

Table 4.5 - Main and interaction effects of flute-edge endmilling

	α	0°		30°		60°	
	Response	R_a	H_D	R_a	H_D	R_a	H_D
Main Effects of	f_m	3.6	1.0	1.4	0.4	0.6	-0.9
	N	-3.7	-1.0	-7.0	-0.2	-2.1	-0.8
	C	3.3	-0.7	-2.8	0.3	0.8	2.2
Interactions between	N and f_m	-4.2	-1.0	-1.0	0.4	0.3	1.3
	N and C	-3.0	0.7	2.4	0.8	0.5	0.0
	f_m and C	6.1	-0.7	-1.8	-0.3	-0.6	1.1

From Table 4.4, the process parameters which yielded the best overall surface finish and smallest burr are test #'s 3 and 7. The commonality between these two tests is low feedrate and high spindle speed. The presence of coolant did not seem to have any real effect on the output responses. It does have an effect on the heat-affected zone (HAZ) of the bevel cut. For comparison purposes, the average surface roughness, burr height, and maximum feedrate for each of the bevel angles are listed in table 4.6. These averages were calculated by discarding the extreme measurements (highest and lowest) and then finding the mean of the remaining middle six measurements.

According to these experimental results, beveling the 1.47 mm thick steel laminations with an endmill's flute-edge leaves very good surface finishes but maximum feedrates are not as high as that listed in table 4.2. Slower feedrates and higher spindle speeds yield the best surface finish and the smallest burr. The maximum feedrate and spindle speed for cutting bevels is highly dependent on the material's machinability as shown in equation 3.5. Coolant should be used when cutting metal to extend the life of the tool and to minimize the HAZ of the cut. The extent of burring on the climb-milling side of the cut is extensive and it gets longer as the bevel angle increases. Due to the high

cutting forces from the large amount of material that is removed, there is also significant deflection of the lamination during machining which undoubtedly exacerbates the chattering problem and the machining inaccuracy.

Table 4.6 - Experimental results for flute-edge endmilling of bevels.

α	0°	30°	60°
Ave. R_a (μm)	1.3	4.6	3.1
Ave. H_D (mm)	0.3	2.7	8.6
Max. f_m (m/min)	0.46	0.46	0.25

4.2.2 Abrasive Water Jet (AWJ) Cutting

An abrasive water jet (AWJ) is a non-contact method for cutting bevels into die laminations. This method has been used in industry since 1982 [Tikhomirov,1992]. In AWJ cutting, water that is pressurized up to 380 kPa and then forced through a small sapphire orifice at about two and a half times the speed of sound. Garnet abrasive is then introduced into this high-speed stream of water and mixed with the water in a long carbide mixing tube. The water jet with suspended garnet particles exits the carbide tube at about the speed of sound and is then directed at the die lamination. As seen in figure 4.18, the jet drags abrasive through the material in a curved path (lag line) and the resulting centrifugal forces on the particles press them against the surface being cut. Material is abraded away from a grinding process where the forces and motions are provided by the water.

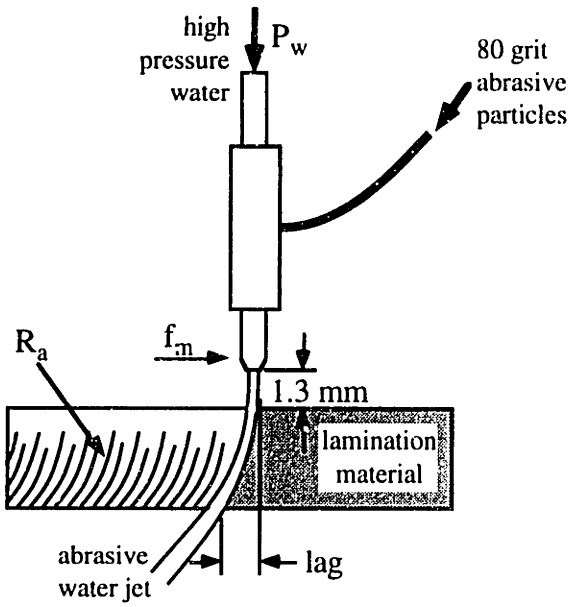

Figure 4.18 - Abrasive Water Jet Cutting

For AWJ cutting, the process parameters that yield the best quality bevels in terms of surface roughness $\mathbf{R_a}$, kerf width **w**, and height of the edge burr $\mathbf{H_D}$ (i.e. output responses) need to be determined. The control factors that are expected to affect the system responses are cutting feedrate $\mathbf{f_m}$, upstream water pressure $\mathbf{P_W}$, and size of the abrasive particles.

The goal of this investigation is to determine the effect of each control factor on the system output responses. As with the flute-edge endmilling experiments described in section 4.2.1, one of the best methods for determining these relationships and also the optimal process parameters is to use Design of Experiment (DOE) techniques. Specifically, a full factorial experimental design with 2 control factors (f_m and P_w only) at 2 distinct levels (4 experiments) was performed for 3 different signal factors α. Like the flute-edge endmilling experiments, the signal factor levers were 0°, 30°, and 60°. An OMAX JetMachining System was used for the AWJ cutting experiments. The cutting nozzle diameter and standoff distance from the lamination used for all experiments was 0.76 and 1.27 mm, respectively. The AWJ manufacturer strongly recommends that an abrasive particle of particular size be used, specifically 80 grit (i.e. 0.267 mm average particle size). Consequently, abrasive particle size was not used as a process parameter. The control factor levels used for each particular bevel angle were determined experimentally and are listed in table 4.7. As shown in a 1.0 mm scan of the test cut #2-0°

surface (figure 4.19), the surface roughness of the AWJ-cut bevel surface was measured with a profilometer. The kerf width and burr height of each experimental cut were measured with a thickness gage and dial indicator, respectively. The experimental results for each DOE test are listed in table 4.8.

The main and interaction affects for the AWJ cutting experiments are listed in table 4.9. It is difficult to generalize about what effect f_m, P_W and their interaction have R_a because the trends vary with every bevel angle. However, f_m and P_W have a significant effect on the kerf width w, but in opposite directions. Specifically, w tends to increase with higher water pressures and tends to decrease with higher feedrates. The effect that f_m and P_W. have on burr height H_D is inconclusive since there are no consistent trends in any of the main or interaction effects. One must conclude that there are really no optimal process parameters for bevel cutting with AWJ. Therefore, the author suggests a maximum feedrate and as low a pump pressure as is practical for cutting bevels.

Table 4.7 - Control factor levels used for AWJ cutting experiments

α	0°		30°		60°	
Level	-1	+1	-1	+1	-1	+1
f_m (m/min)	0.20	0.26	0.18	0.23	0.10	0.14
P_W (MPa)	210	280	210	280	210	280

Table 4.8 - Experimental results of the AWJ experiments

Test	Control Factor Levels		Responses								
			0°			30°			60°		
	f_m	P_W	R_a (µm)	w (mm)	H_D (mm)	R_a (µm)	w (mm)	H_D (mm)	R_a (µm)	w (mm)	H_D (mm)
1	-1	-1	5.0	0.64	0.06	6.5	0.64	0.14	5.1	0.83	0.04
2	-1	+1	5.1	0.68	0.06	3.4	0.68	0.08	4.9	0.86	0.04
3	+1	-1	4.7	0.56	0.07	5.4	0.58	0.14	2.9	0.76	0.06
4	+1	+1	4.4	0.61	0.06	5.0	0.64	0.04	4.2	0.73	0.08

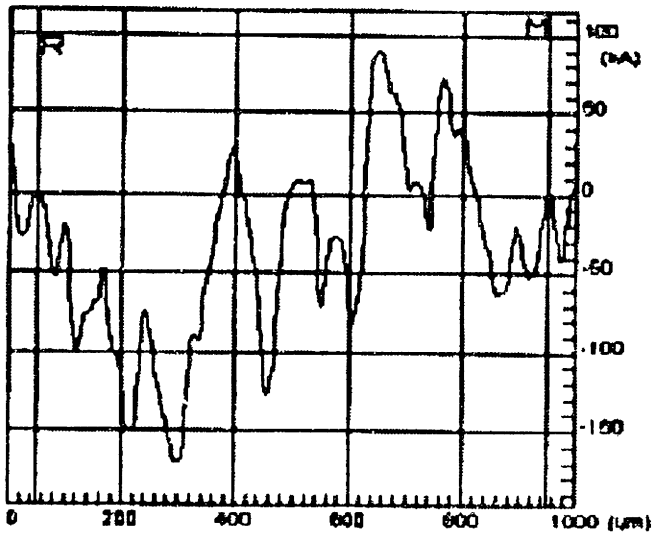

Figure 4.19 - Profilometer scan of a beveled surface cut with an AWJ.

AWJ cutting is a very good non-contact method for machining narrow cuts into die laminations. Because it is non-contact and low forces are imposed on cutting area, there is negligible deflection of the lamination during cutting. Besides a decrease in the maximum feedrate, AWJ cutting seems to have no problems cutting high bevel angles. According to [Tikhomirov,1992], the maximum feedrate for this process is highly dependent on the yield strength of the material. However, the experimentally determined f_m for same-thickness lamination material made of mild steel and much harder tool steel are very close to each other. The surface finish of the bevel cut is slightly rougher than flute-edge endmilling but much more consistent when process parameters are changed. The burr left on the far edge of the kerf is much less than CNC-machining with an endmill especially at high bevel angles. However, the kerf made with AWJ has a large taper, around 10° for all the bevel angles tested. The kerf taper angle may decrease when thicker laminations are cut and/or when the upstream water pressure P_w is increased. Average values of various quality characteristics from the AWJ experimental bevel cuts are listed in table 4.10.

Even though the cut from an abrasive waterjet introduces error in the cut because of the drag line, taper angle of the kerf, and variable kerf width; [Matsui,1991] has successfully compensated for these errors to increase the precision of the AWJ process as shown in figure 4.20. Compensation for these errors involves offsetting the centerline of the kerf by half of it's width which is a function of f_m, rotating the cutting nozzle slightly

about the direction of travel (y-axis) by half the taper angle, and tilting the cutting head backwards (about x-axis) to minimize the effect of the lag line.

Table 4.9 - Main and interaction effects of AWJ cutting

	α	0°			30°			60°		
	Response	R_a	w	H_D	R_a	w	H_D	R_a	w	H_D
Main effect of	f_m	-0.5	-0.08	0.008	0.3	-0.05	-0.02	-1.5	-0.10	0.025
	P_W	-0.1	0.05	-.003	-1.8	0.05	-0.08	0.6	0.0	0.013
f_m and P_W interaction		-0.2	0.0	0.0	1.4	0.0	-0.02	0.8	-0.03	0.008

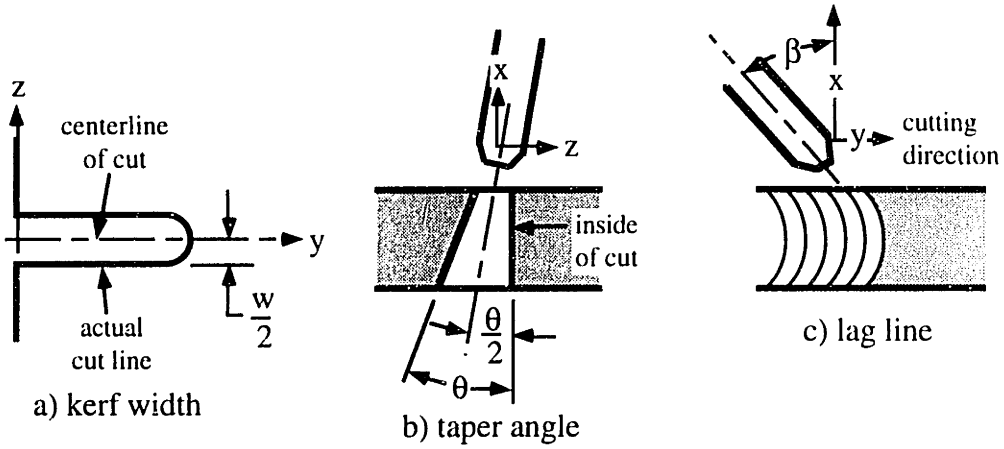

Figure 4.20 - Compensation methods for AWJ cutting error

Table 4.10 - Experimental results for AWJ bevel cutting of steel.

α	0°	30°	60°
Ave. R_a (μm)	4.8	5.1	4.3
Ave. w (mm)	0.62	0.63	0.80
Ave. H_D (mm)	0.061	0.100	0.053
effective thickness of material being cut (mm)	1.47	1.70	2.95
Max. f_m (m/min)	0.34	0.31	0.20
kerf taper	10°	11.5°	9°

4.2.3 Plasma-Arc Cutting

Using a plasma-arc is another non-contact cutting method that can be used to cut bevels into die laminations. As seen in figure 4.21, This cutting process utilizes a highly positioned nozzle orifice to constrict a very high temperature, ionized gas (plasma) so that it can be used to melt and blow away sections of electrically conductive metals. An induced vortex swirl in the plasma gas stabilizes the plasma column during cutting. Parts that wear away during operation of the plasma arc (i.e. consumibles) are the electrode, the cutting nozzle, and the shield [Colt,1995].

The system used for the bevel cutting experiments was a Hypertherm HD-1070 HyDefinition Plasma unit. The control variables in plasma-arc cutting are the plasma gas type (O_2 or Air), the plasma gas pressure P_G, the standoff distance of the cutting nozzle from the lamination H_{SD}, and the feedrate f_m. Oxygen was used as both the plasma gas and the shield gas. The DC output voltage and current from the power supply were 130 volts and 30 amps, respectively, and the torch standoff distance was kept at 1.0 mm. A series of full factorial experiments with P_G and f_m as the control factors were planned for the plasma-arc cutting.

The experiments were planned after observing the success with straight-on cuts (i.e. 0° bevel). The maximum feedrate which yielded acceptable cuts was a very rapid 3.8 m/min. The kerf width **w** and dross height were 1.1 mm and 0.15 mm, respectively. As shown in figure 4.22, the kerf from plasma-arc cutting has a quantifiable taper which is 7° in this case. When 1.5 mm thick lamination made out of hardened A2 steel plate was cut with the same control settings, the maximum feedrate and kerf width were again 3.8 m/min and 1.1 mm, respectively, but there was no dross on the back side of the kerf. This experiment demonstrates how material hardness does not adversely affect the cutting performance of a plasma-arc.

The full set of experiments was abandoned after it became apparent that a plasma-arc was not suitable for beveled cuts. Bevel cuts at angles up to 45° yielded very large tapers (>10°) in the kerf, excessive dross (H_D=0.9 mm) which was welded to the metal, and a large heat affected zone (HAZ). The large HAZ caused the cut edge of the lamination to warp slightly. The maximum bevel angle achieved was 60° but the kerf edge

closest to the cutting nozzle was consistently obliterated from an over-zealous oxidation (self-burning) of the metal during cutting.

The attractive feature of plasma-arc cutting is the allowable cutting feedrates which are typically 5 to 10 times faster than machining and water-jet cutting. Unfortunately the problems of excessive kerf taper and the tendency of kerf edge nearest to the cutting nozzle to experience self-burning make plasma-arc cutting unsuitable for cutting lamination bevels. The key to plasma-arc's successful usage in cutting bevels will be to solve the edge burning problem, minimize or even eliminate (if possible) the kerf taper, and to reduce the amount of dross. Such an effort will require more than the optimization of process parameters which is beyond the scope of this thesis.

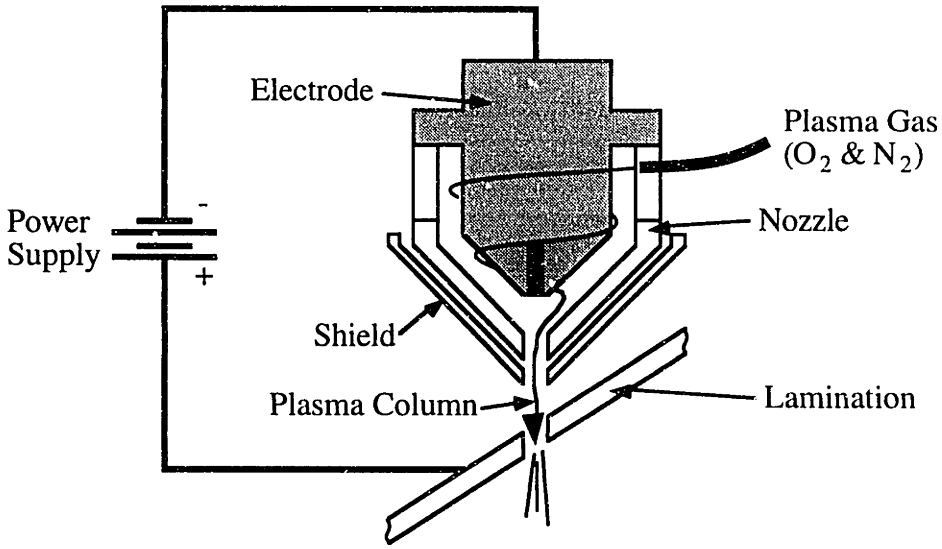

Figure 4.21 - Schematic of a plasma-arc cutting a lamination.

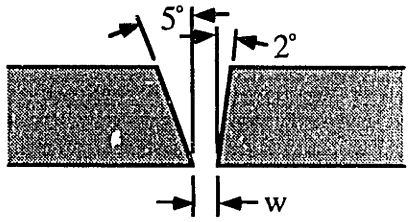

Figure 4.22 - Cross-section of a plasma-arc cut.

4.2.4 Laser Cutting

It is evident from table 4.2 that laser cutting is another promising non-contact method for machining bevels because of the rapid cutting speeds and steep bevel angles that can be achieved. The main issue to be resolved is what combination of laser type, beam temporal mode, and beam delivery system is best for cutting lamination bevels, particularly in steel. To answer this question, an experimental investigation into bevel cutting with lasers is required because literature on oblique laser cutting is scarce. To fully understand all the issues involved with laser-cutting bevels, a brief background of this machining process will be presented.

Laser cutting is machining process that can be summarized as follows:

1. A high intensity beam of infrared or near infrared light is generated by a laser. The two basic laser types used by industry for cutting are the CO_2 gas laser and the Nd:YAG solid-state laser. In the CO_2 gas laser, a gas mixture of CO_2, N_2 and He (helium) serves as the lasing medium for a stream of high energy electrons. The emitted beam is in the far infrared region with a wavelength λ of 10.6 μm. With the Nd:YAG laser, a complex crystal of Yttrium-Aluminum-Garnet ($Y_3Al_5O_{12}$) doped with Neodinium (Nd^{3+}) is optically pumped with xenon flashlamps. It's emitted beam is in the near infrared region with a wavelength of 1.06 μm.

2. The collimated laser beam is focused onto the workpiece surface by means of a converging lens. Referring to figure 4.23, the process cone angle Ø of the converging beam can be calculated using the relation

$$\phi = 2\tan^{-1}\left[\frac{D}{2F}\right] \qquad (4.17)$$

where: F = focal length of the lens
D = diameter of the collimated beam.

The **f-number** - often referred to by optical engineers - is a parameter related to the process cone angle and is defined as

$$f\text{-number} = \frac{F}{D}. \qquad (4.18)$$

A practical rule for focusing the beam is to put the focal point P someplace between the workpiece surface and 30% of the material thickness, i.e. $0.30 \times t_L$, into the workpiece [Anonymous,1991]. Actually, the laser beam does not converge down to a point but converges to a minimum "waist" instead [Chryssolouris,1991]. The theoretically minimum focused spot diameter **d** for a beam with an ideal gaussian spatial distribution is

$$d = \frac{4 \cdot \lambda \cdot F}{\pi \cdot D} \qquad (4.19)$$

and the corresponding depth of focus **b**, i.e. working range of the focused beam, is

$$b = \frac{2 \cdot \lambda}{\pi} \cdot \left(\frac{2 \cdot F}{D}\right)^2. \qquad (4.20)$$

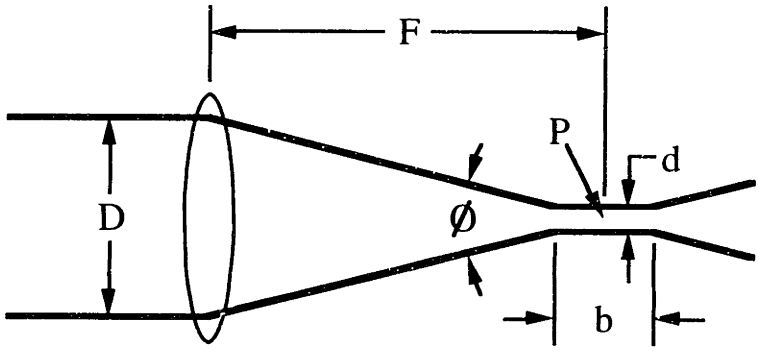

Figure 4.23 - Geometry of a collimated laser beam focused by a converging lens.

3. The focused beam heats the surface of the workpiece (sheet) and establishes a very localized melt throughout the depth of the sheet. A high beam power intensity is responsible for this localized melting. Assuming a uniform energy density of the unfocused laser beam (ideal is a gaussian distribution), the average beam power intensity **q"** (power/unit area) at the focal point P is given by

$$q'' = \frac{q_{ave}}{\pi \cdot d^2} = \frac{\text{laser power}}{\text{irradiated area}} \qquad (4.21)$$

where: q_{ave} = average power of the laser beam.

All of the laser beam energy available does not go into melting the material. As stated by [Powell,1993]; "During cutting it is often the case that the trailing edge of the cut front does not extend to the full diameter of the incident laser beam. A proportion of the available light therefore passes straight through the kerf (cut width) without interacting with the cut

front." Furthermore, some of the energy is not absorbed by the workpiece surface and cut zone during the cutting process. The reflectivity of the cut zone decreases with an increase in the surface temperature.

As shown in figure 4.24, laser beams can be emitted in a pulsed or a continuous-wave (CW) temporal mode. In the pulsed mode, a laser beam is emitted periodically. For a given beam power, pulsing allows for deeper drilling and cutting depths, smaller Heat Affected Zone (HAZ) but generally worse surface finish than the CW mode. The ease in cutting thicker materials with pulsing is due to the effect of high peak power in short pulses (i.e. high energy) which ensures efficient heating of the material. Assuming the power profile is a square wave, the energy per pulse $\mathbf{E_p}$ of a pulsed laser beam is calculated using the relation

$$E_p = \frac{q_{ave}}{f_p} \tag{4.22}$$

where: $\mathbf{f_p}$ = pulsing frequency.

The peak power of the pulse is then

$$q_{peak} = \frac{E_p}{\tau_w} = \frac{q_{ave}}{f_p \cdot \tau_w} \tag{4.23}$$

where: τ_w = pulse width.

The fraction of time that the laser pulse is "on" is known as the duty cycle **DS** which is calculated using the relation

$$DS = \frac{\tau_w}{\tau} = \tau_w \cdot f_p. \tag{4.24}$$

In the CW mode, the beam is emitted without interruption. This mode offers a better surface finish than with pulsing but a higher electrical input power is required.

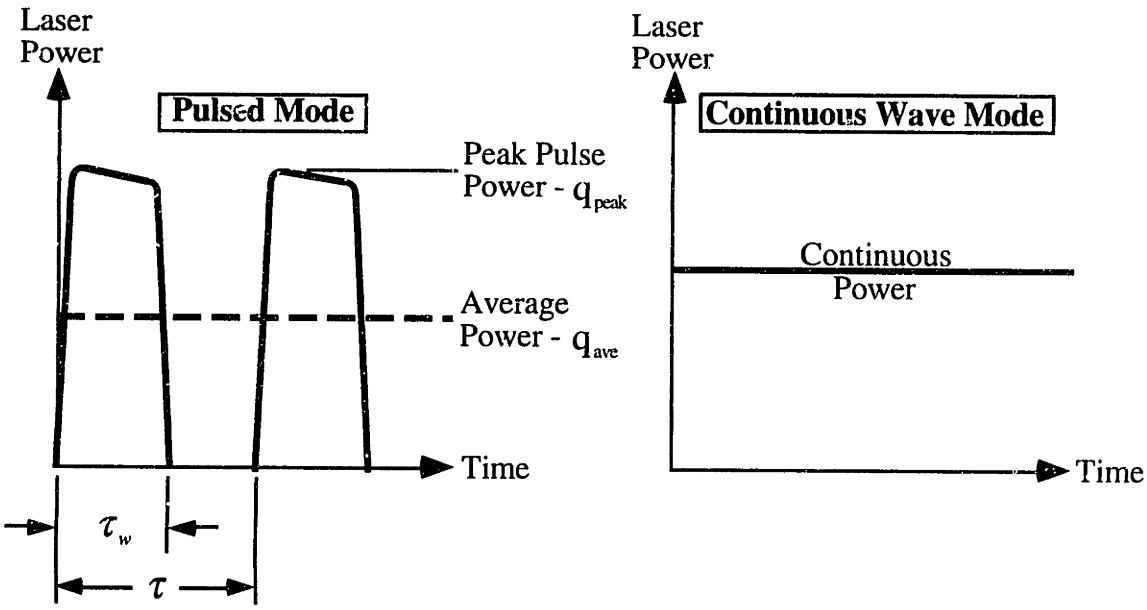

Figure 4.24 - Details of Laser Beam Temporal Modes

4. The molten material is ejected from the area by a pressurized gas jet acting coaxially with the laser beam. Figure 4.25 shows a schematic of the resulting cut zone from CW cutting. The width of the cut or kerf width **w** is denoted in this figure. When an inert gas like N_2 is used as the cutting gas, the laser beam is the sole heating source for melting the material. This technique is known as Laser Fusion Cutting. With certain workpiece materials (e.g. steel), a reactive gas (e.g. O_2) can accelerate the cutting process by doing chemical (e.g. oxidation) as well as physical (e.g. ejecting molten material) work. In fact, approximately 40% of the energy to the cut zone of steel sheet is contributed by the oxidation reaction while the remaining 60% is provided by the laser [Powell,1993]. This technique, known as Reactive Gas Cutting, uses the laser beam as a high temperature heat source to propagate the chemical reactions. It generally has higher material removal rates but poorer surface quality and kerf dimensional accuracy than laser fusion cutting [Anonymous,1991].

Near corners and detail work, the actual cutting speed of a CNC laser cutter nozzle approaches zero due to direction changes. If CW mode is used with constant laser power, the excessive overheating for fusion cutting and over-oxidation (i.e. self-burning) for reactive gas cutting has the effect of melting off or burning the sharp corners. Since

changing the laser power in-process is very difficult, a laser beam can be pulsed to reduce the amount of burning on corners and detailed work.

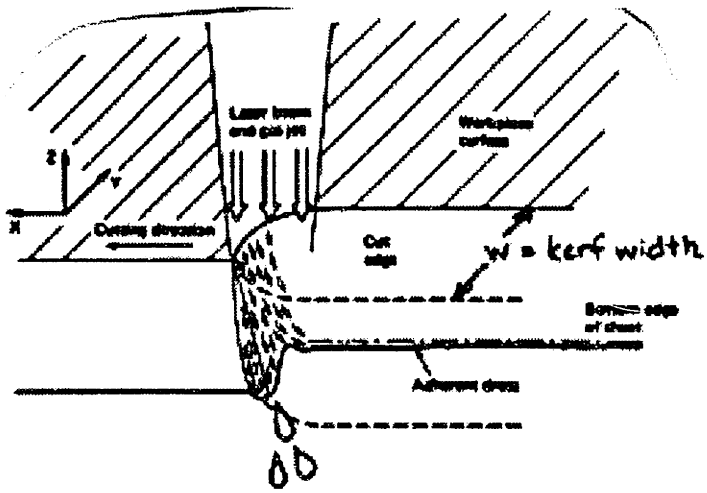

Figure 4.25 - A schematic of the cut zone when cutting in CW mode [Powell,1993].

The main idea behind pulsing is to produce striations by repeatedly drilling overlapping holes through the material. As seen in figure 4.26, surface roughness of the kerf can be controlled by varying the kerf width w, pulsing frequency f_p, and cutting speed (feedrate) f_m. From the geometry of the laser cut striations, the wavelength λ_s of the striations is

$$\lambda_s = \frac{f_m}{f_p} \qquad (4.25)$$

and their profile height **h** is

$$h = \frac{w}{2} - \frac{1}{2}\sqrt{w^2 - \lambda_s^2} \qquad (4.26)$$

This assumes that the drilled holes are circular and not elliptical. Even if this assumption is not valid, the previous formula gives a good estimate of the surface roughness. The arithmetic surface roughness average R_a of the laser cut surface is approximately h/4. The limiting cutting speed V_{max} for pulsing occurs when the drilled holes fail to overlap (see figure 4.26). Assuming perfectly circular holes, the limit to the cut speed is

$$V_{max} = w \cdot f_p. \qquad (4.27)$$

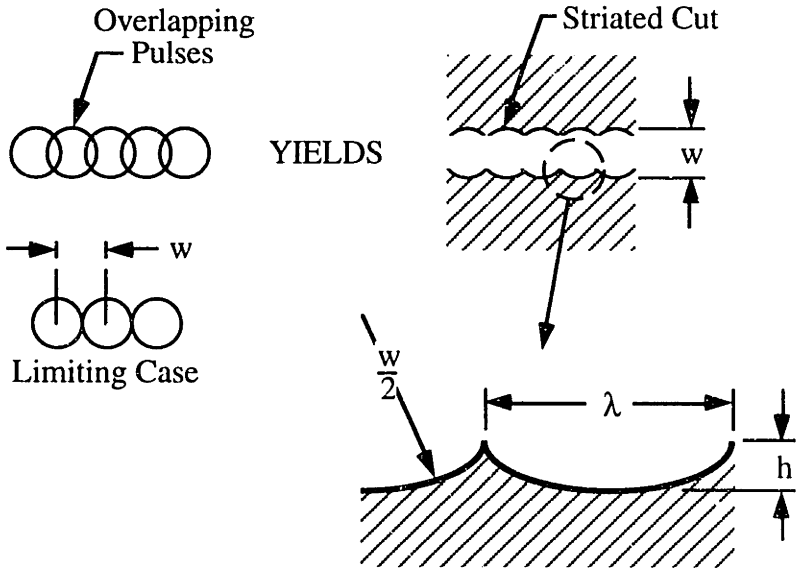

Figure 4.26 - Geometry of a Pulsed Laser Cut

Since gas assistance is so essential in laser cutting, the correct nozzle geometry and standoff distance **H** are extremely important to the efficiency of the cutting process. The nozzle geometry of a typical laser cutting head is shown in figure 4.27.

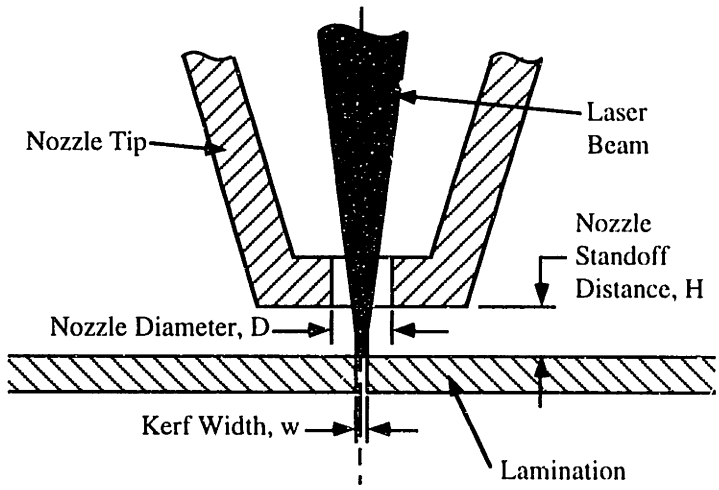

Figure 4.27 - Geometry of a laser cutting nozzle.

5. The localized area of material removal is moved across the surface of the workpiece to generate a cut. Movement is achieved by manipulation of the focused laser spot, by mechanical moving the workpiece, or by some combination of the previous two methods.

If the laser spot is moved, the beam must be delivered optically to the laser cutting head with **hard-optics**, i.e. beam steering mirrors and beam manipulating lenses, or **fiber-optics**. With hard-optic delivery, the mirrors for high power lasers are generally first surface mirrors, i.e. the reflection occurs at the top surface [Anonymous,1991]. The schematic of a typical hard-optic delivery configuration is shown in figure 4.28. Alignment of the steering mirrors is very critical in order to prevent misalignment or disturbance of the beam. Both CO_2 and Nd:YAG laser beams can be delivered with hard-optics. Compared with hard-optics, fiber-optic delivery has the advantage of simplified beam manipulation without critical alignment of steering mirrors [Bransch,1991]. The major disadvantage is that the beam quality—although not the integrity of the gaussian spatial mode—is always compromised because of beam homogenization within the fiber. A schematic of an Nd:YAG laser system with a fiber-optic delivery is shown in figure 4.29. The beam cone angles going into and out of the fiber are preserved ($\varnothing_I=\varnothing_R$). The actual focused beam diameter $\mathbf{d_f}$ is

$$d_f = \frac{C \cdot F}{F_R}. \qquad (4.28)$$

This means that the beam diameter C within the fiber is reduced to the final beam diameter d_f by the ratio of the process lens to the recollimating lens with focal length $\mathbf{F_R}$. Because most glasses have a high absorbtivity at the CO_2 wavelength and are transparent at the Nd:YAG wavelength, only Nd:YAG beams can be practically delivered with glass optical fibers.

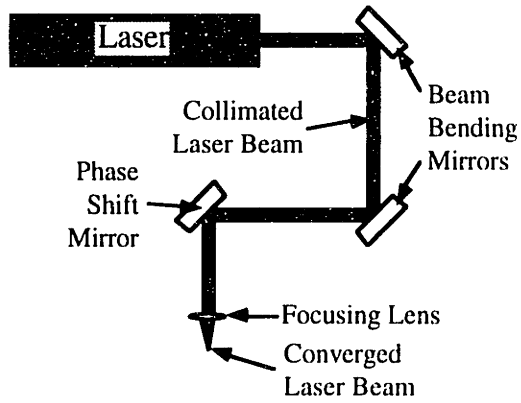

Figure 4.28 - CO_2 laser beam delivered with hard-optics.

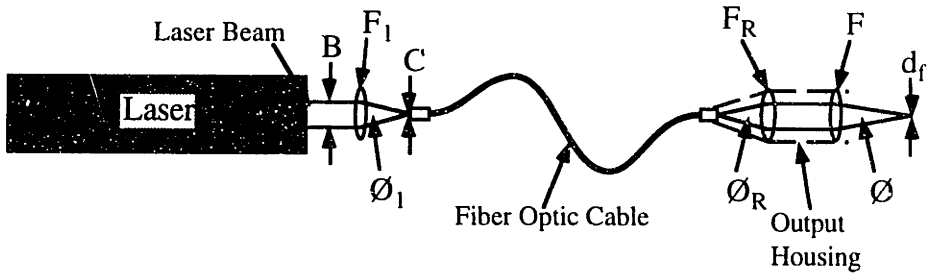

Figure 4.29 - Nd:YAG laser beam delivered with fiber-optics.

A series of experiments were performed with various laser types, cutting modes, and beam delivery configurations to quantify a laser's ability to cut bevels into lamination material. The object of these experiments was to determine the maximum bevel angles and cutting speeds achievable and not to optimize the quality of the bevel cut (e.g. surface roughness, height of the dross). Optimization of the cutting parameters is addressed after the best laser configuration is chosen.

4.2.4.1 CO_2 Laser With Fiber-Optic Beam Delivery

Fiber-optic beam delivery offers more geometric flexibility than the hard-optic delivery used for cutting bevels and profiles into PEL laminations. It also simplifies the design of a PEL die fabrication machine (discussed in a later section). Unfortunately, most glasses, including those used for fiber optic cables, have a high absorbtivity at the CO_2 laser wavelength of 10.6 μm [Powell,1993]. For this reason, fiber optic delivery for a CO_2 laser is not used and is not commercially available.

4.2.4.2 CO_2 Laser With Hard-Optic Beam Delivery

Using N_2 cutting gas (laser fusion cutting) delivered at 1000 kPa and an average power of 1.2 kW, the CO_2 laser cutter in pulsed mode (Laser Dyne Model 780 5-axis CNC Machining System with System 94 Controller and Rofin-Sinar 1700 SM laser) was able to cut 45° bevels at speeds of up to 0.76 mpm. A 16.5 mm diameter collimated laser beam was delivered with hard optics, i.e. mirrors and lenses, to a 125 mm focal length converging lens. Using equation 4.17, the process cone angle in this case is 7.5°. A table

of maximum cut rates for various angles using these aforementioned conditions is given below in table 4.11. The associated cutting parameters are also included.

Table 4.11 - Maximum cutting speeds for pulsed CO_2 laser cutter

c: (deg)	f_p (Hz)	τ_w (msec)	E_p (J/pulse)	q_{peak} (kW)	Max. Cutting Speed (mpm)	w (mm)	H_D (mm)
0	450	2	2.7	2.8	2.8	0.18	0.28
15	450	2	2.7	2.8	2.8	0.15	0.28
30	300	3	4.0	1.5	1.5	0.28	0.41
45	185	5	6.5	0.8	0.8	0.30	0.86

Cutting acceptable bevels beyond a 45° angle were not possible with this configuration. The recast material (adherent dross), as seen in figure 4.25, on the far side of all the laser cuts with bevel angles up to 45° was essentially welded to the steel test-plate. As the bevel angle increases, the amount of dross increases and the kerf width tends to decrease. The formation of this adherent dross with CO_2 laser fusion cutting requires each lamination be deburred before all the machined die laminations can be assembled into the PEL die.

Test were conducted using pure O_2 as the reactive cutting gas and average laser powers between 350 and 700 W both in pulsed and CW temporal mode. Accordingly, the laser power was decreased to see if the same cut rates as with the previous N_2 cutting tests could be matched. Table 4.12 lists the maximum cutting speed achieved for 0° bevel cuts and the corresponding process parameters. Oxygen assist gas was supplied at 310 kPa for each cut.

Table 4.12 - Maximum cutting speeds for CO_2 laser cutter using O_2 assist gas

q_{ave} (kW)	Temporal Mode	f_p (Hz)	τ_w (msec)	E_p (J/pulse)	q_{peak} (kW)	Max. Cutting Speed (mpm)	w (mm)	H_D (mm)
0.35	pulsed	500	0.5	0.7	1.4	2.5	0.23	0.30
0.35	CW	N/A	N/A	N/A	N/A	3.2	0.20	0.0
0.70	CW	N/A	N/A	N/A	N/A	5.1	0.20	0.0

Only the results of 0° bevel cuts are listed in this table because there were no acceptable cuts at bevel angles beyond 10° when oxygen was used as the assist gas. In fact, most of the cuts exhibited self-burning presumably from an excess of oxygen in the cut zone. 'Self burning' is an uncontrolled oxidation reaction caused by an excess flow of oxygen. One useful characteristic of the adherent dross (i.e. iron oxide resulting from the presence of oxygen) located on the farside of all the cuts listed in table 4.12 is that they are primarily porous and brittle. This means that most of dross can be easily flaked off without the need for a time-consuming deburring operation. Therefore, besides accelerating the cutting process, oxygen helps to minimize the post-beveling operations

[Murakawa,1987] had better success cutting bevels using a CO_2 laser and O_2 as the cutting gas. Oxygen delivered at 340 kPa was used to achieve bevel cuts up to 43° in mild sheet steel. Their experimental success is attributable to a flow of cooling water applied to the far kerf edge thereby suppressing any self-burning. The two other interesting results of this research are as follows:

1) There is a V_{min} and V_{max} (i.e. range of cutting speeds) for each particular bevel angle. The laser has insufficient energy to cut at speeds above V_{max} and experiences self-burning at speeds below V_{min}.

2) V_{min} is reduced to a negligible value when the flow of cooling water is applied.

As with the cutting tests conducted by the author, Murakawa et al. had to decrease the cutting speeds for increasing bevel angles.

4.2.4.3 Nd:YAG Laser with Fiber-Optic Beam Delivery

Because of the limited bevel angles achieved, i.e. less than 45°, with CO_2 laser cutting, the beveling performance of an Nd:YAG laser was investigated. Cutting tests were performed using a Lumonics JK701H laser (550 Watts max. average power) in pulsed temporal mode with a fiber-optic beam delivery. The laser beam is delivered to the cutting nozzle through a 1 mm dia. fiber optic cable with the cone angles (around 15°) into ($\emptyset_I$) and out of ($\emptyset_R$) the fiber optic preserved. The beam exiting the fiber optic cable is recollimated with a 160 mm focal length lens to a 40 mm diameter and then refocused on the workpiece with a 80 mm focal length lens. This gives a process cone angle of 28°. For bevel angles up to 30°, reasonable cutting speeds were measured as listed in table 4.13.

In this configuration, the laser had no trouble cutting bevels up to 30°. Narrow kerf widths and good surface finish of the cut are observed. At 40° bevels and above, however, the system is unable to make acceptable cuts. "Self-burning" of the lamination was observed, possibly from an overabundance of oxygen. When the oxygen flow was decreased when cutting at these high angles, the pulsed laser still could not make a continuous cut through the metal regardless of which process parameters where changed (e.g. pulsing frequency, pulse width, cutting speed).

Table 4.13 - Maximum cutting speeds for pulsed Nd:YAG laser cutter with fiber optic beam delivery

α (deg)	q_{ave} (kW)	Assist Gas/ Press. (kPa)	f_p (Hz)	τ_w (msec)	E_p (J/pulse)	q_{peak} (kW)	Max. Cutting Speed (mpm)	w (mm)	H_D (mm)
0	0.41	O_2@410	175	1.2	2.2	2.0	1.4	0.38	0.03
10	0.41	O_2@410	175	1.2	2.2	2.0	1.3	0.33	0.13
20	0.41	O_2@410	175	1.2	2.2	2.0	1.3	0.40	0.33
30	0.41	O_2@410	175	1.2	2.2	2.0	1.2	0.40	0.25

4.2.4.4 Nd:YAG Laser with Hard-Optic Beam Delivery

To see if even steeper bevel angles could be achieved, a Control Laser Model 480-16 Nd:YAG laser cutter with hard optic beam delivery was used for the last series of bevel-cutting experiments. The focal diameter of the beam and lens focal length were 12.7 mm and 120 mm, respectively. Acceptable cuts up to bevel angles of 70° were performed. Table 4.14 lists the maximum cut rates for bevel angles up to 70°. In figure 4.30 these values are plotted against bevel angle for the cutting of 1.47 mm steel with a low-powered laser.

A bevel of 75° to 80° probably could have been reached but the cutting angle was limited by the geometry of the beam delivery nozzle. The kerf width measured for these cuts is about double those of the CO_2 cutting experiments.

Table 4.14 - Maximum cutting speeds for low-power Nd:YAG laser cutter with hard optics

α (deg)	q_{ave} (kW)	Assist Gas/ Pressure (kPa)	f_p (Hz)	τ_w (msec)	E_p (J/pulse)	q_{peak} (kW)	Max. Cutting Speed (m/min)	w (mm)	H_D (mm)
0	0.12	O_2@900	15	1.5	7.7	5.1	0.29	0.56	0.0
10	0.12	O_2@900	15	1.5	7.7	5.1	0.29	0.53	0.15
20	0.12	O_2@900	15	1.5	7.7	5.1	0.29	0.51	0.15
30	0.12	O_2@900	15	1.5	7.7	5.1	0.23	0.53	0.03
40	0.12	O_2@900	15	1.5	7.7	5.1	0.21	0.53	0.03
50	0.12	O_2@900	15	1.5	7.7	5.1	0.18	0.56	0.03
60	0.08	O_2@900	10	1.5	7.5	5.0	0.08	0.41	0.25
70	0.08	O_2@900	5	1.5	16.4	10.9	0.02	0.60	0.0

Since an Nd:YAG laser cutter with hard optic delivery was the only configuration capable of making steep angle bevels in the steel laminations, additional cutting tests with a higher powered laser were performed to see what cutting speeds were achievable. Specifically, a Lumonics JK704 laser, with a maximum 400 watts of average output power, was used. The laser is part of a Laserdyne 5-axis model 780 CNC laser cutting system with a System 94 controller. The cutting test results for the standard lamination thickness and also thicker material are listed in table 4.15. These values are plotted against bevel angle in figure 4.30. The plot lines for 1.47 mm and 3.18 mm thick material are denoted in this figure.

The kerf widths for these test cuts are similar to those of the CO_2 cutting tests described in section 4.2.4.2. Unlike cutting with a CO_2 laser [see Murakawa,1987], there is not a lower cutting speed limit, below which self-burning will occur, for pulsed Nd:YAG laser cutting.

Table 4.15 - Maximum cutting speeds for 0.5 kW Nd:YAG laser cutter with hard optics

α (deg)	t (mm)	q_{ave} (kW)	Assist Gas/ Pressure (kPa)	f_p (Hz)	τ_w (msec)	E_p (J/pulse)	q_{peak} (kW)	Max. Cutting Speed (mpm)	w (mm)	H_D (mm)
0	1.47	0.30	Air@410	15	1.5	20	13.3	0.44	0.30	0.20
10								0.44	0.28	0.15
20								0.44	0.27	0.13
30								0.42	0.23	0.18
40								0.38	0.25	0.15
50								0.33	0.28	0.13
60								0.28	0.18	0.25
70								0.15	0.15	0.22
0	3.18	0.32	Air@410	8	1.5	39	26.0	0.20	0.23	0.25
10								0.20	0.20	0.28
20								0.19	0.23	0.28
30								0.18	0.30	0.33
40								0.15	0.28	0.25
50								0.13	0.20	0.30
60								0.08	0.18	0.41
70								0.03	0.15	2.4

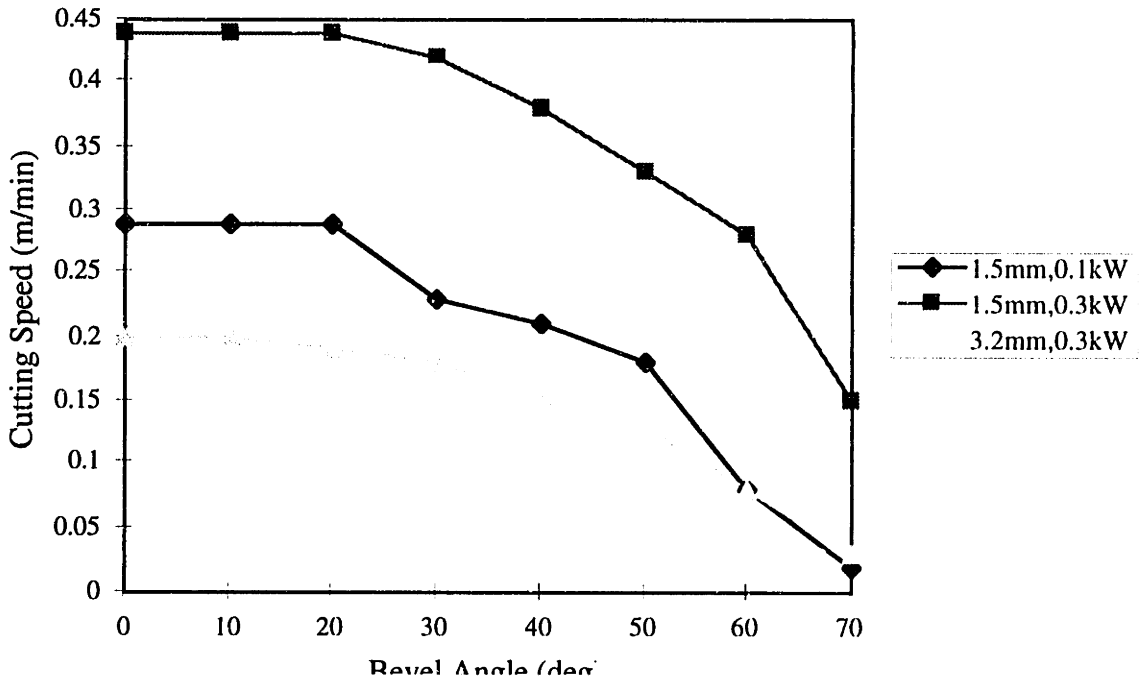

Figure 4.30 - Graph of maximum cutting speed vs. bevel angle for a pulsed Nd:YAG laser cutter.

4.2.4.5 Summary of Laser Cutting Experiments

Using the laser fusion cutting method, a pulsed CO_2 laser beam with nitrogen assist gas successfully cut bevels of up to 45° with narrow kerfs (0.18 to 0.30 mm) but with an extensive adherent dross that is hard to remove. Pulsing energies of 2.7 to 6.5 joules were used. For reactive gas cutting (i.e. oxygen assist gas), bevel angles of only 10° are achievable. However, the kerfs are narrow; the adherent dross is porous, brittle, and easily removable; and lower pulsing energies of only 0.7 joules were needed. Higher cutting speeds were achievable in the CW cutting mode.

Using an oxygen assist gas, an Nd:YAG pulsed laser beam delivered with fiber-optics could cut bevels only up to 30°. Kerf widths are also narrow (e.g. 0.33 to 0.40 mm) but the cutting dross increases with the bevel angle. Cutting speeds are slightly lower than for a CO_2 laser of similar power. Pulsing energies of 2.2 joules were used. Cutting in CW mode yielded unacceptable cuts.

When air (20% oxygen) is used as the assist gas for a pulsed Nd:YAG laser beam delivered with hard-optics, bevel cuts up to 75° were achieved. Even higher angles may be achievable. Narrow kerf cuts (i.e. 0.15 to 0.30 mm) are observed with a porous dross that remains relatively constant for all bevel angles. The lower cutting speeds are attributable to the low pulsing frequency used. Faster cutting speeds will be achievable at the low bevel angles (i.e. 0 to 40°) if higher pulsing frequencies are used (see equation 4.27). For all three sets of cutting experiments (see tables 4.14 and 4.15) that involve different lamination thicknesses and laser powers, the maximum cutting speed decreases non-linearly with increasing bevel angle because both the effective material thickness and the amount of energy absorbed by the material surface decreases.

As previously mentioned, a high laser beam power intensity at the material surface is of prime importance for cutting steep angle bevels. The limited success with the CO_2 laser beam delivered with hard optics is attributable to insufficient energy intensity at these steep angles. The energy absorbtivity of steel and other metals to CO_2 laser light is relatively low compared to Nd:YAG laser light, which contributes to this problem. From equation 4.19, the theoretical focused beam diameter is 0.102 mm in this case. The better success with Nd:YAG laser beam delivered with hard optics is attributable to the higher

absorbtivity of this shorter wavelength light by the metal and a much smaller focused spot diameter, specifically 0.008 mm and 0.013 mm for the low and high powered lasers, respectively. A small focused spot diameter yields a high energy density according to equation 4.21.

The limited beveling success of an Nd:YAG laser beam with fiber optic delivery is due to a large focused diameter and the homogenization of the laser beam within the fiber. The spot diameter of the laser beam delivered through a 1.00 mm diameter fiber is 0.5 mm as calculated with equation 4.28. Even though the focused spot diameter estimated with equation 4.19 is typically 2 to 5 times larger in reality [Powell,1993], the focused spot diameter from the hard optic delivery of an Nd:YAG laser beam is at least an order of magnitude less than the 0.5 mm spot. Furthermore, the laser beam exiting a fiber optic is homogenized as compared to the incoming beam. Homogenization lessens the exiting laser light's quality to a non-gaussian spatial distribution. This probably decreases the amount of energy absorbed by the material surface.

4.2.4.6 Optimization of Laser Cutting Parameters

The main purpose of the preceding experiments was to identify the optimal configuration of laser type, temporal mode, and beam delivery for cutting bevels into laminations. The cutting experiments also quantified both the maximum achievable bevel angle and the relationship of bevel angle to the maximum cutting speed for steel. For cutting bevels into steel sheet—the predominant material used for forming—the optimal configuration is a pulsed Nd:YAG laser with hard-optic beam delivery. However, the process parameters chosen for the cutting experiments using this configuration yielded kerfs of generally poor surface finish and geometrical accuracy. For example, the surface roughness average of the 70° bevel cut (for 1.47 mm thick material) listed in table 4.15 is about 10 to 15 μm and the cross-section of the kerf cut has the features of a laser drilled hole as shown in figure 4.31 [Chryssolouris,1991]. For Nd:YAG laser cutting to be considered a viable method for machining bevel cuts into laminations, the kerf quality must be improved over that of the previous experiments. If the kerf quality is to be improved, a rationale procedure for optimizing the process parameters like that used for the flute-edge endmilling and AWJ cutting experiments is needed.

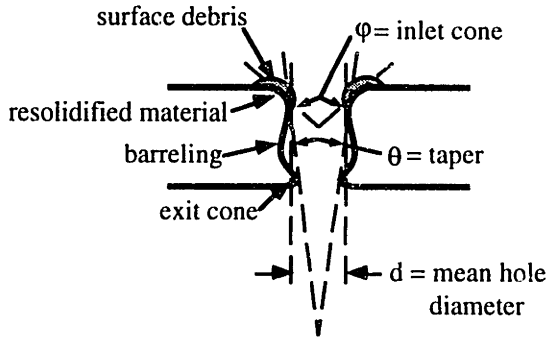

Figure 4.31 - Features of laser-drilled holes

As shown in figures 4.13 and 4.32, the easily measurable output responses that help to define the kerf quality of the laser cut bevel are the kerf width **w**, surface roughness of the kerf $\mathbf{R_a}$, the height of the burr $\mathbf{H_D}$ on the farside of the cut, and taper angle θ [DiPietro,1994]. The kerf width is measured with a thickness gage, the surface roughness with a profilometer, and the burr height with a dial indicator. A narrow kerf width is desirable so that fine details can be cut into the lamination edge instead of the minimum internal radius that's characteristic of conventional machining methods (e.g. flute-edge endmilling). A low surface roughness of the cut surface is desirable since it will decrease the grounding and polishing time of the assembled PEL die forming surface. Minimal or no dross on the farside of the kerf is desirable since any dross must be removed before the die laminations can be assembled into a complete die. This increases the overall fabrication time.

The control factors that affect these output responses are the focused spot diameter **d** which is proportional to the process lens focal length **F** by equation 4.19, pulse width τ_w, pulsing frequency $\mathbf{f_p}$, cutting speed $\mathbf{f_m}$, type of assist gas (e.g. O_2, Air, N_2), and assist gas pressure $\mathbf{P_g}$. All of these control factors are easily varied with the CNC laser cutter used for the experiments. Since almost all Nd:YAG lasers used for cutting have a tuned resonator, the output power of the laser beam is held constant to minimize the beam divergence [Chryssolouris,1991]. Therefore, the average laser output power is consistently held close to 0.25 kW in this case. Like the flute-edge endmilling and AWJ experiments, the signal factor for these bevel cutting experiments is the bevel angle α which will be 0°, 30°, and 60°.

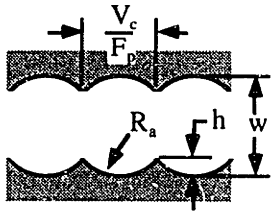

Figure 4.32 - Output responses of a pulsed laser-cut kerf (top view of a 0° bevel).

There have been numerous attempts at theoretical modeling of the laser cutting process [DiPietro,1994]. Most of these attempts have looked almost exclusively at the static state of behavior of the process. However, laser cutting is a very dynamic process that is very difficult to model accurately, especially pulsed Nd:YAG laser cutting. Therefore, empirical modeling can be used to improve upon and to understand this cutting process. In developing an empirical model, the ability to study several variables, i.e. laser cutting parameters, together but also independently observe the effect of change in each of the variables is desirable.

One method for developing empirical models for process improvement is to base it on matrix experiments using a multi-level factorial design like that of the flute-edge endmilling and AWJ cutting experiments. This experimental design allows control factor interaction effects to be determined. As is the practice with 2^k factorial design, two levels are chosen for each variable. In this case, 6 control factors with 2 redundant experiments per level, to reduce experimental error, require a 2^6 experimental matrix for a total of 64 x 2 = 128 experiments per signal factor level. Two levels of each control factor does not allow identification of any non-linear effects between the control factor and the output response and such effects were expected with laser cutting. As seen in figure 4.33, three levels are needed to capture these effects. If three levels are chosen for each control factor to capture curvature effects, a total of 1458 experiments would have to be run for each signal factor level which is economically prohibitive in this case. The main problem with a full factorial design is obviously the number of experiments that must be performed to capture all the main and interaction effects of the control factors.

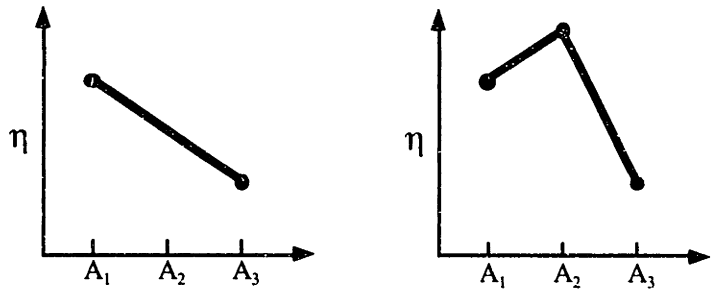

a) With 2 points we can only fit a straight line.

b) With 3 points we can identify curvature effects and, hence, peaks.

Figure 4.33 - Linear and non-linear effects of a control factor.

An alternate method for empirical modeling of the process which requires fewer experiments involves holding all but one of the control factors constant at their nominal levels and then run experiments varying this one control factor. In the case of laser bevel cutting, 6 control factors are varied at 3 different levels with 2 redundant experiments per level. We begin with 2 experiments at the nominal control factor levels. Since we need to do experiments with two alternate levels for each control factor, the 2×6×2=24 additional experiments are added to the two nominal value experiments, yielding a total of 26 for each signal factor. This is significantly less than that of a full factorial experiment. However, this 'one-factor-at-a-time' approach fails to recognize control factor interactions [DeVor,1992]. The differences between the one-factor-at-a-time and 2^k full factorial design testing arrangements for a 3 variable example, i.e. control factors X_1, X_2 and X_3, is shown in figure 4.34.

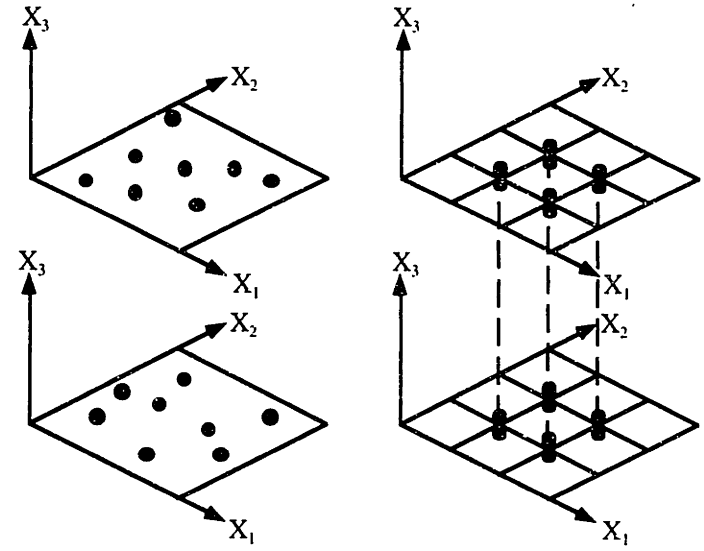

One-Factor-at-a-Time Design 2^k Full Factorial Design

Figure 4.34 - Possible test arrangements

Conducting the matrix experiment with an orthogonal array is another method which can be used to develop an empirical model. This method gives more reliable estimates of control factor effects with fewer experiments compared to the "one-factor-at-a-time" design [Phadke,1989]. An additive model is used as the empirical relationship between the output response and the control factor levels. The equation in this case is

$$\eta(A_i, B_j, C_k, D_l) = \mu + a_i + b_j + c_k + d_k + e \qquad (4.29)$$

where η is the observed output response; μ is the mean value of η for the experimental region; a_i, b_j, c_k, and d_l are the deviations from μ caused by setting control factors A, B, C, and D at level A_i; B_j, C_k, D_l, respectively; and e is the error. Interactions are considered to be errors in the additive model. The matrix experiment, followed by a verification experiment involving the optimal parameters, is a powerful tool for detecting the presence of interactions among the control factors.

For the matrix experimental design using an orthogonal array structure, the number of 2-level and 3-level factors is 1 and 5, respectively, and the interaction between $\%O_2$ and P_g will be estimated. There is an assumed interaction between $\%O_2$ and P_g since the amount of O_2 available for reactive gas cutting is a function of both of these control factors. The control factor levels used for all the experiments are listed in table 4.16. A lower concentration of oxygen had to be used at steep bevel angles (e.g. 60°) because excessive self-burning was observed with pure oxygen even at low pressures.

The number of degrees of freedom for this series of experiment is:

Overall Mean	1
One 2-level factor	1×(2-1)=1
Five 3-level factors	5× (3-1)=10
Interaction between $\%O_2$ and P_g	(2-1) × (3-1)=2
	Total = 14 d.o.f.

Therefore, we must conduct at least 14 experiments to be able to estimate the effect of each factor and the 1 interaction. Since the orthogonality of a matrix experiment is not lost by keeping one or more columns of a "standard" orthogonal array empty, a standard L_{18} orthogonal array will be used since it can handle up to 7 three-level factors and 1 two-level factor. It requires 18 experiments for orthogonality between control factors to be insured. The experimental array is shown in shown in table 4.17. With this standard array, the interaction between $\%O_2$ and P_g columns is orthogonal to all other columns so that no particular columns must be left unused. Therefore, the unused columns 7 and 8 were chosen arbitrarily.

Table 4.16 - Control factor values for laser cutting experiments.

α	0°			30°			60°		
Level	1 (low)	2 (med)	3 (high)	1	2	3	1	2	3
$\%O_2$ in assist gas (mass)	23	-	100	23	-	100	23	-	62
P_g (kPa)	140	280	410	140	210	280	140	210	280
F (cm)	7.6	12.7	20.3	7.6	12.7	20.3	7.6	12.7	20.3
f_p (Hz)	30	60	100	30	60	100	22	30	40
f_m (m/min)	0.13	0.25	0.38	0.13	0.25	0.38	0.13	0.19	0.25
τ_w (msec)	0.3	0.4	0.5	0.3	0.4	0.5	0.3	0.4	0.5

A series of matrix experiments using the L_{18} orthogonal array were performed for each signal factor, i.e. bevel angle. With 2 redundant experiments for each set of the 18 test conditions and three bevel angles, a total of 3x18x2=108 experiments will be required. Due to the long set-up time required for each process lens, all experiments with a particular focal length lens were performed at the same time. Otherwise the sequence of experiments was chosen at random. The experimental results from all the orthogonal array cutting tests are listed in table 4.18. A 1.0 mm scan of the test cut #13-0° surface measured with a profilometer is shown in figure 4.35.

Table 4.17 - L_{18} Orthogonal array used for laser cutting experiments

Test #	$\%O_2$ in assist gas	P_g	F	f_p	f_m	τ_w	unused	unused
1	1	1	1	1	1	1	1	1
2	1	1	2	2	2	2	2	2
3	1	1	3	3	3	3	3	3
4	1	2	1	1	2	2	3	3
5	1	2	2	2	3	3	1	1
6	1	2	3	3	1	1	2	2
7	1	3	1	2	1	3	2	3
8	1	3	2	3	2	1	3	1
9	1	3	3	1	3	2	1	2
10	2	1	1	3	3	2	2	1
11	2	1	2	1	1	3	3	2
12	2	1	3	2	2	1	1	3
13	2	2	1	2	3	1	3	2
14	2	2	2	3	1	2	1	3
15	2	2	3	1	2	3	2	1
16	2	3	1	3	2	3	1	2
17	2	3	2	1	3	1	2	3
18	2	3	3	2	1	2	3	1

Table 4.18 - Results of the laser cutting parameter optimization experiments

Test #	Responses η_i								
	0°			30°			60°		
	R_a (μm)	w (mm)	H_D (mm)	R_a (μm)	w (mm)	H_D (mm)	R_a (μm)	w (mm)	H_D (mm)
1	5.6	0.11	0.26	11	0.10	0.36	-	-	0.46
2	4.7	0.10	0.21	7.6	0.14	0.22	-	-	0.48
3	-	-	-	20	-	-	-	-	0.34
4	7.6	-	0.02	20	-	0.13	-	-	0.15
5	6.5	0.13	0.03	12	0.18	0.10	-	-	0.17
6	6.1	0.18	0.10	20	0.15	0.27	-	-	0.57
7	8.6	0.14	0.10	8.1	0.10	0.50	20	0.08	0.34
8	8.5	0.08	0.22	25	-	0.08	-	-	0.53
9	6.5	-	0.12	20	0.15	0.15	-	-	0.16
10	2.2	0.10	0.03	3.6	-	-	-	-	-
11	4.8	0.25	0.08	5.1	0.22	0.08	-	0.03	0.48
12	3.0	0.23	0.02	4.5	0.18	0.09	-	-	0.37
13	3.7	0.14	0.04	6.7	0.11	0.04	-	-	0.14
14	2.3	0.15	0.01	15	0.11	0.03	20	0.04	0.58
15	3.8	0.28	0.03	9.4	0.22	0.07	-	-	0.45
16	2.6	0.14	0.02	4.4	0.10	0.04	-	0.05	0.44
17	16	-	0.14	20	-	0.06	20	0.04	0.11
18	4.5	0.25	0.0	3.4	0.22	0.01	5.9	0.07	0.39

Note: A "-" entry in the table indicates that no measurement could be taken.

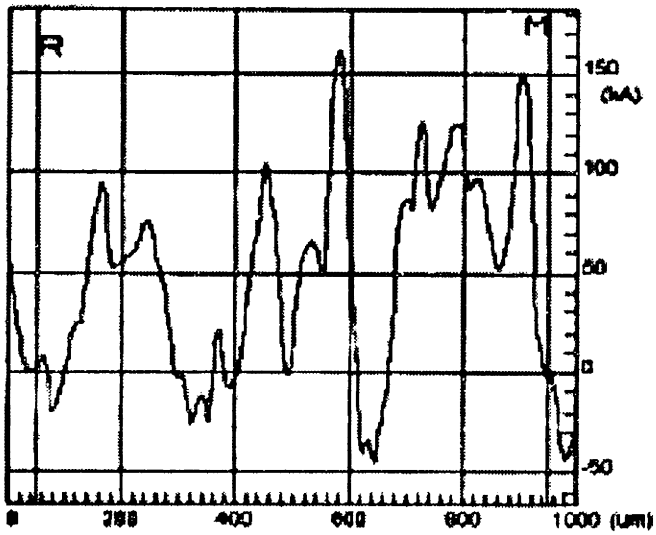

Figure 4.35 - Profilometer scan of a beveled surface cut with a pulsed Nd:YAG laser beam delivered with hard optics.

The output responses from table 4.18 can averaged over a particular control factor level to estimate the effect of that factor. For instance, the average kerf width w for the assist gas pressure P_g set at the low level (1) can be estimated with the equation

$$w_{estimate}(P_g, \text{level } 1) = \frac{w_1 + w_2 + w_3 + w_{10} + w_{11} + w_{12}}{6}. \qquad (4.30)$$

Other average output responses are calculated in a similar manner. If a single response is not available (e.g. w_3) because a measurement could not be taken (e.g. due to an incomplete cut), the average of the remaining output responses (e.g. $w_1, w_2, w_{10}, w_{11}, w_{12}$) is used as an estimate. The estimated factor effects are listed in table 4.19. To see what effect a certain factor has on the output response, the output response can be plotted against the increasing levels of the control factor. Note that there was insufficient data to calculate the R_a and w factor effects for the 60° bevel cuts.

To estimate the interaction between $\%O_2$ and P_g if there is one, the observed output responses η (e.g. R_a) are substituted into the expressions listed in table 4.20. Table 4.21 is the actual interaction table for the 0° bevel cutting experiments. By plotting the averaged output responses of P_g versus $\%O_2$, the interaction effects can be estimated. The interactions between control factors for each output response are shown in figure 4.36. From this figure it is evident that there is very little combined action of $\%O_2$ and P_g on surface roughness and kerf width. However, there is a strong combined action of these two control factors on dross height.

Table 4.19 - Factor effects for laser cutting parameter optimization experiments

	α→	0°			30°			60°
Control Factor ↓	Level ↓	R_a (μm)	w (mm)	H_D (mm)	R_a (μm)	w (mm)	H_D (mm)	H_D (mm)
$\%O_2$ in assist gas	1	6.8	0.12	0.13	16.0	0.14	0.23	0.36
	3	4.8	0.19	0.04	8.0	0.17	0.05	0.37
P_g	1	4.1	0.16	0.12	8.6	0.16	0.19	0.43
	2	5.0	0.18	0.04	13.9	0.15	0.11	0.34
	3	7.8	0.15	0.10	13.5	0.14	0.14	0.33
F	1	5.1	0.13	0.08	9.0	0.10	0.21	0.31
	2	7.1	0.14	0.12	14.1	0.16	0.10	0.39
	3	4.8	0.24	0.05	12.9	0.18	0.12	0.38
f_p	1	7.4	0.21	0.11	14.3	0.17	0.14	0.30
	2	5.2	0.17	0.07	7.1	0.16	0.16	0.32
	3	4.3	0.13	0.08	14.7	0.12	0.11	0.49
f_m	1	5.3	0.18	0.09	10.4	0.15	0.21	0.47
	2	5.0	0.17	0.09	11.8	0.16	0.11	0.40
	3	7.0	0.12	0.07	13.7	0.15	0.09	0.18
τ_w	1	7.2	0.15	0.13	14.5	0.14	0.15	0.36
	2	4.6	0.15	0.07	11.6	0.16	0.11	0.35
	3	5.3	0.19	0.05	9.8	0.16	0.16	0.37

Table 4.20 - Interaction table between $\%O_2$ and P_g.

	P_g (1)	P_g (2)	P_g (3)
$\%O_2$(1)	$\frac{\eta_1+\eta_2+\eta_3}{3}$	$\frac{\eta_4+\eta_5+\eta_6}{3}$	$\frac{\eta_7+\eta_8+\eta_9}{3}$
$\%O_2$(2)	$\frac{\eta_{10}+\eta_{11}+\eta_{12}}{3}$	$\frac{\eta_{13}+\eta_{14}+\eta_{15}}{3}$	$\frac{\eta_{16}+\eta_{17}+\eta_{18}}{3}$

Note: η_i = output response for experiment i.

Table 4.21 - Experimental $\%O_2$ and P_g interaction table for 0° bevel cuts.

Control Factor	$\%O_2$ level	P_g(1)	P_g(2)	P_g(3)
R_a (μm)	1	5.2	6.7	7.9
	3	3.3	3.3	7.7
w (mm)	1	0.11	0.16	0.11
	3	0.19	0.17	0.20
H_D (mm)	1	0.24	0.05	0.15
	3	0.04	0.03	0.05

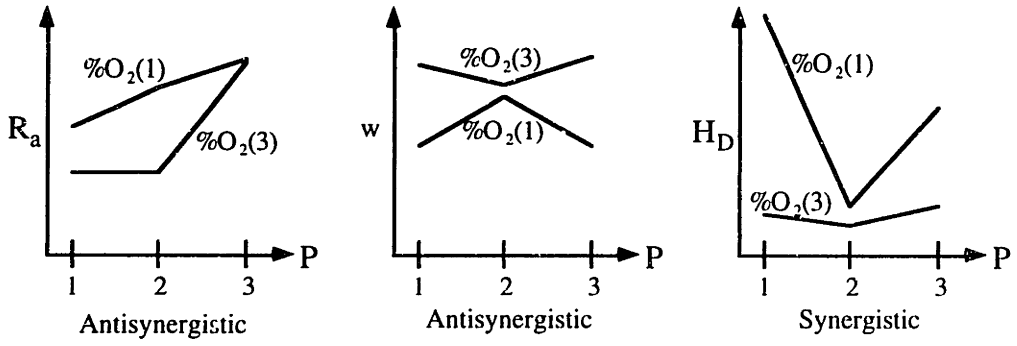

Figure 4.36 - Effect of $\%O_2$ and P_g interactions on various output responses.

4.2.4.7 Summary of Laser Cutting Parameter Optimization Experiments

In the optimization of the laser cutting parameters, the object is to minimize the surface roughness R_a. According to equations 4.25 and 4.26, R_a will decrease with higher pulsing frequency and/or lower feedrate. These equations are fairly accurate for low bevel angles. For example, the estimated surface roughness for the test #10-0° cut using these equations is 2.8 μm. The measured value is 2.2 μm. At higher bevel angles, the equations don't work as well. For example, the estimated surface roughness for the test #16-30° cut is 1.2 μm while the measured value is 4.4 μm. From table 4.19, R_a tends to decrease with higher pulsing frequency (except at higher bevel angles) and lower feedrates as predicted by equations 4.25 and 4.26. Furthermore, R_a tends to decrease with higher percentages of oxygen in the cutting gas, lower assist gas pressure P_g, and longer laser pulses τ_w. The effect of the processing lens focal length F on surface roughness is not clear from the experimental results.

The chosen process parameters can also minimize the width of the laser cut kerf. From table 4.19, the kerf width w decreases with lower concentrations of oxygen, higher pulsing frequencies, and shorter pulse widths. It also decreases with shorter processing lens focal lengths. This effect may be explained by the smaller effective focused beam diameter as predicted by equation 4.19. No significant effects on kerf width are observed from changes in assist gas pressure or cutting feedrate.

The dross height can be minimized by the proper choice of the laser cutting parameters. From table 4.19, there is a significant effect of oxygen concentration on the dross height, specifically less dross when higher concentrations are used. Less dross is

also noticed with higher cutting feedrates. The effects of assist gas pressure, processing lens focal length, laser pulsing frequency, and pulse width are either negligible or unclear.

From figure 4.35, the effect of any interactions between $\%O_2$ and P_g on the output responses can be estimated. There appears to be no significant interaction between these control factors with regards to kerf width or surface roughness. However, the increase in width with higher oxygen concentrations is evident. With regards to dross height, there appears to be a synergistic (i.e. additive) effect between the oxygen concentration and assist gas pressure.

Optimal Parameters: In the following discussion, the parameter values corresponding to the low (1), medium (2) and high (3) levels are found in table 4.16. For the smoothest surface finish, a low $\%O_2$, medium f_p, and high τ_w are recommended. For the narrowest kerf, a low $\%O_2$, high f_p, and low F are recommended. For the least amount of dross, a high $\%O_2$, medium P_g, and high f_m are recommended. Depending upon what surface qualities of the bevel cut are most important, the levels of each laser cutting parameter can be set accordingly. The test bevel cuts with the best overall kerf quality and the associated process parameters are listed in table 4.22.

Table 4.22 - Optimal control factor levels for an Nd:YAG laser cutter.

	Control Factor Levels						Output Responses		
Test #-α	$\%O_2$	P_g	F	f_p	f_m	τ_w	R_a (μm)	w (mm)	H_D (mm)
16-0°	High	High	Low	High	Med.	High	2.6	0.14	0.02
16-30°	High	High	Low	High	Med.	High	4.4	0.10	0.04
18-60°	High	High	High	Med.	Low	Med.	5.9	0.07	0.39

With optimal process parameters, lamination cutting with the same general surface finish as flute-edge endmilling and AWJ are possible but surface finish deteriorates with an increase in the bevel angle. The edge-burring due to adherent dross is comparable to AWJ but much less than endmilling. The kerf width is the smallest of all three bevel cutting methods. Although bevels up to ±80° are possible, the range of parameters that yields acceptable cuts narrows with the increase in bevel angle as is seen in table 4.18. Since there is a very small mechanical force associated with laser cutting, the fixturing required for

lamination being cut is minimal. Furthermore, the HAZ of the laser cut is very small and most of the heat-affected material is blown away during the cutting process.

4.2.5 Summary of Bevel Cutting Methods

As a final comparison of the three candidate bevel cutting methods, the beveling performance measures (i.e. cutting force, maximum f_m, maximum α, taper angle, kerf width, machining burr height, and kerf surface finish) of each method with process parameters set to their optimal levels are listed in table 5.25. The w, H_D, and R_a measurements listed in the table are for a 30° bevel. By considering the results from sections 4.2.1 (machining), 4.2.2 (AWJ) and 4.2.4 (laser), the following comparisons can be made:

- Flute-edge endmilling involves the application of a high cutting force with a cutting tool to remove the unwanted lamination material. The higher cutting forces significantly deflect the cantilevered portion of a lamination being beveled. AWJ cutting and laser cutting, i.e. non-contact cutting methods, cause negligible deflection to the lamination.
- All three cutting methods are capable of high cutting speeds but the maximum speed is highly dependent upon the material composition and hardness with flute-edge endmilling and AWJ cutting. The maximum laser cutting f_m is only dependent on laser power (i.e. proportional to q_{laser}) which means that higher cutting rates are achievable.
- The maximum bevel angle for all three methods is around ±80°.
- The kerf from AWJ cutting has a very large, consistent taper of around 10° for all bevel angles that must be compensated for during bevel cutting. Laser cutting creates only a slight kerf taper. Flute-edge endmilling leaves no appreciable kerf taper unless there is significant deflection of the lamination and cutting tool during beveling.
- The width of the kerf affects the smallest radius of curvature achievable for a PEL's profiled edge. Of the three beveling methods, laser cutting creates the narrowest kerf. The kerf from AWJ cutting is also narrow but not as much as that cut with a laser. The kerf width from endmilling is relatively large since it is the diameter of the cutting tool.
- Flute-edge endmilling leaves a very large machining burr, especially at larger bevel angles. AWJ cutting and laser cutting, on the other hand, yield much smaller machining

burrs. Laser cutting with a pure oxygen assist gas yields a porous, brittle edge burr (i.e. iron oxide) which is easily removed from the cut lamination without having to grind it off.

• Flute-edge endmilling yields the smoothest surface finish of all the methods although the finish deteriorates at higher bevel angles from more machining chatter. AWJ cutting offers the most consistent surface finish for all bevel angles. As discussed in chapter 3 for CNC-machining, a smooth surface finish helps to minimize the time required for grinding and polishing the die surface.

Table 4.23 - Comparison Table of Bevel Cutting Methods using Optimal Parameter Settings

	Cutting Method	**Flute-Edge Endmilling**	**Abrasive Water Jet Cutting**	**Nd:YAG Laser Cutting with Hard Optic Beam Delivery**
	Cutting Force	Significant (lamination bends 1-2 mm at high bevel angles)	Small (momentum transfer from abrasive)	Negligible
	Maximum f_m for 0° bevel cut (meters/min)	0.46 (affected by material hardness and composition)	0.31 (affected by material composition)	0.44 for q_{laser}=0.3 kW (max. $f_m \propto q_{laser}$ [Powell,1993])
	Maximum α	$\tan^{-1}\left(\frac{L_f}{t_L}\right) = 85°$	at least 75°	80°
	Kerf Taper Angle θ	None	+10°	-1° to -2°
30° Bevel Cut	w (mm)	6.4 (tool ∅)	0.7	0.1
	H_D (mm)	2.8	0.1	0.04 (porous edge burr)
	R_a (μm)	0.7	3.4	4.4

Based on the preceding analysis and discussion, the author ranks the suitability (best to worst) of these three bevel cutting methods for cutting steel laminations as follows:

1) Nd:YAG laser cutting because feedrate is only dependent on laser power, tool wear is non-existent, cutting force is negligible and the kerf is the narrowest of all,

2) Abrasive water jet cutting since feedrate is dependent on material hardness and the kerf taper is the largest among the three methods, and

3) Flute-edge endmilling since the cutting force, kerf width, edge burr, and feedrate's dependency on material hardness is the greatest overall.

4.3 MACHINERY FOR FABRICATING PEL DIES

As with CNC-machining a sheet metal forming die, the two most important specifications of equipment used to fabricate PEL dies are to 1) get as close to near net shape as possible thereby minimizing the need for a post-grinding or finishing operation and 2) accomplish this task as fast as possible. The key to meeting these specifications are the correct choice of a bevel cutting method, as discussed is the previous section, and the efficient handling of die laminations during the cutting. In this section, commercially-available machinery for cutting PEL die laminations will be described. In addition, two new machine design concepts are presented that can meet these specifications in a more efficient manner than commercially-available machinery.

4.3.1 Commercially-Available Multi-Axis Cutting Machines

For compound beveling of PEL die laminations, a 5-axis machining center (e.g. 3 translational & 2 rotational axes) is required to correctly position the cutting nozzle during the profiling process. There are numerous 5-axis conventional machining centers, a few laser machining centers and at least two AWJ cutting centers currently available that can be used to machine compound bevels. Conventional 5-axis CNC machining centers are discussed in greater detail in section 3.1.3 of this thesis. Using either conventional, laser and AWJ machining centers, a die lamination blank is first secured vertically to the machine's workbed and then the profiled-edge is machined. The die lamination can be handled manually or the machining center can be retrofitted with an automatic handling mechanism.

Five-axis laser machining centers are much more expensive than comparable AWJ or CNC machines. For example, a Laserdyne Model 780 BeamDirector™ 5-Axis laser machining center with a Lumonics JK704 laser currently sells for around $625K. Other laser machining centers vary in price from $500K to $700K. In contrast, a Cincinnati-Milacron Sabre-1000 CNC 3-axis vertical machining center retrofitted with a Tsudakoma TTNC-201 tilting rotary table that has a similar work volume as the Laserdyne system sells for around $120K. For $180K, a company an purchase a Jet Edge® model 55-30 AWJ cutting system that's mounted to a 5-axis, robot-controlled gantry table and has a similar

work volume as the laser system. With any of these systems, the estimated cost of a custom-built lamination handling mechanism has not been added to their overall cost.

4.3.2 Die Lamination Profiling (DLP) Machine

Both conventional CNC and laser machining centers are designed for general industrial use and not optimized for cutting die laminations in terms of speed, cost, and factory floor space required. Taking into account the high cost of commercially available equipment and the added cost of a custom-built lamination handling mechanism, a dedicated stand-alone machine for fabricating PEL dies is proposed by the author as cost-effective alternative to retrofitting currently-available 4 and 5-axis cutting machines. This specialized apparatus will be called a Die Lamination Profiling (DLP) machine. For industry to embrace the PEL die method, these machines will be required to fabricate dies in a rapid and efficient manner.

Prior to the conceptual design phase, certain general design specifications for the DLP machine embodiment were established which include:

- minimizing the number of degrees of freedom (DOF) needed to efficiently process the laminations
- maintaining the correct order to the PEL lamination array during processing; allow for different cutting methods to be used without having change the essential design of the machine (i.e. interchangability)
- simple machine adjustments to accommodate different die sizes
- eliminate the need to rotate the cutting means, if possible, and
- the need to only process one die at a time.

With regards to the last design specification, a matching set of dies could be cut simultaneously with one cutting pass, i.e. sharing a cutting line. The process parameters of the cutting means would have to be set properly adjusted so that the kerf width is equal to the necessary gap between the dies (i.e. sheet metal thickness). However, this machine capability is only suitable for the first iteration in the development process of a matched die set. Subsequent iterations on the die shape would still require individual dies of a matched set to be reprocessed separately.

Given these general design specifications, there are two different embodiments envisioned for the DLP machine. The first embodiment machines bevels into a lamination by rotating the cutting head about it's focal or center point as the lamination moves past it. This design is suitable for any type of cutting means. However, since rotation of the laser beam requires a complex set of steering mirrors and optics, eliminating the need for having to rotate the cutting head is highly desirable unless a suitable fiber-optic beam delivery system can be developed. Therefore, a second embodiment of the DLP machine cuts bevels into a lamination by rotating the lamination about the focal or center point of the cutting nozzle as the cutting nozzle moves past the lamination.

4.3.2.1 First Embodiment of DLP Machine

As shown in a numbered patent drawing, figure 4.37, the first embodiment of the DLP machine fabricates a PEL die in the following manner. The DLP machine 40 contains a loading container 42 and a receiving container 44. The side walls 46 and 48 of the loading and receiving containers 42 and 44, respectively, are adjustable to correspond to the length of the lamination blanks 50 and the "processed" profiled-edge laminations 66a. In operation, an array of die lamination blanks is placed into the loading container 42 between the loading container pusher 52 and the sliding guide 54. Each rectangular lamination blank 50 has it's bottom edge 56 and one side edge 58 machined flat and perpendicular to one another for registration purposes. Prior to a lamination blank 50 being cut to shape, the machined side edge 58 is held in contact with the fixed front wall 60 of the loading container 42 by means of the movable side wall 46.

As is best shown in figures 4.38a and 4.38b, a lamination pusher 62a attached to a conveyor belt/chain 64 contacts the perpendicular registration corner of a single lamination blank 50 and horizontally moves it past the vertically-moving and rotating cutting device 68. As is best illustrated in an isolated view in figure 4.39, the cutting head (abrasive water jet cutting head shown) which is rigidly mounted on a carriage 69, rotates about it's focal or center point by moving on a circular track 71. Other cutting means discussed in section 4.2 of this chapter (e.g. laser cutting) can also be used to machine the laminations. The carriage 69 is moved along the circular track 71 by using a friction drive or spur gear/track arrangement 70 which is driven by a servomotor 69a. The circular track 71 is rigidly

connected to a vertical track member 72 which moves in a stationary guide 73. Vertical motion of the circular track 71 and the cutting head 68 is accomplished by a spur gear/track arrangement. In this configuration, the DLP machine has three degrees of freedom, y-axis translation, z-axis translation, and y-axis rotation. These degrees of freedom only allow simple planar beveling of the laminations discussed in section 4.1.1.1.

If compound 3-D bevels are required, the carriage 73 is no longer stationary and is allowed to rotate about vertical axis z'-z' which goes through the focal or center point P of the cutting means (see figure 4.39). Rotation of the carriage 73 is afforded by an attached gear 75 which rotates about the z'-z' axis. A servomotor-driven spur gear 76 engages and rotates the driven gear 75. The combination of the cutting heads rotation about the y and z'-z' axes allows for compound beveling. In this configuration, the DLP machine has four degrees of freedom: y-axis translation, z-axis translation, y-axis rotation, and z-axis rotation.

Before the newly-cut lamination slides into the receiving container, a lamination indexer 77 which is actuated by a solenoid or an air cylinder 78 pushes the existing cut laminations ahead by one lamination thickness and then returns to its retracted position. Simultaneously, the receiving container retracting wall 53, actuated by a motor-driven leadscrew, retracts by the same amount. This combination of motions allows a newly-cut die lamination 66a to slide into the receiving container 44 with minimal resistance. A bevel corresponding to the desired 3-D die surface slice is cut into the lamination as it moves past the cutting head 68. An optional rotating grinder head 79 (CCW rotation in figure 4.35 when viewed from above) mounted vertically grinds off any machining burrs or dross left on the edge of the beveled cut opposite the cutting means. When the sliding die lamination 66 and pusher 62a clear the loading container 42, the loading container pusher 52, which is actuated by a motor-driven leadscrew, indexes forward one lamination thickness in order to push the next die lamination blank against the sliding guide 54. Finally, the pusher 62a stops moving when the newly-cut die lamination 66 is completely within the receiving container 44. At this point, the next pusher 62b attached to the conveyor belt/chain 64 is positioned to begin sliding another die lamination blank 50 out of the loading container 42. Since each lamination is handled in a similar fashion, the ordering of the die laminations within the die is accomplished by the apparatus itself. Either blank or previously cut die laminations can be machined by this apparatus. The entire operation of the DLP machine

including the receiving container pusher 52, the die lamination conveyor belt/chain 64, the circular track servomotor 76 for the cutting device, the vertical actuator for the cutting head and circular tracks, the rotational actuator for the cutting head and circular tracks, cutting device control settings (e.g. speed, power), lamination indexer actuator 75, and receiving container retractor 53 will be controlled by a single high-speed computer.

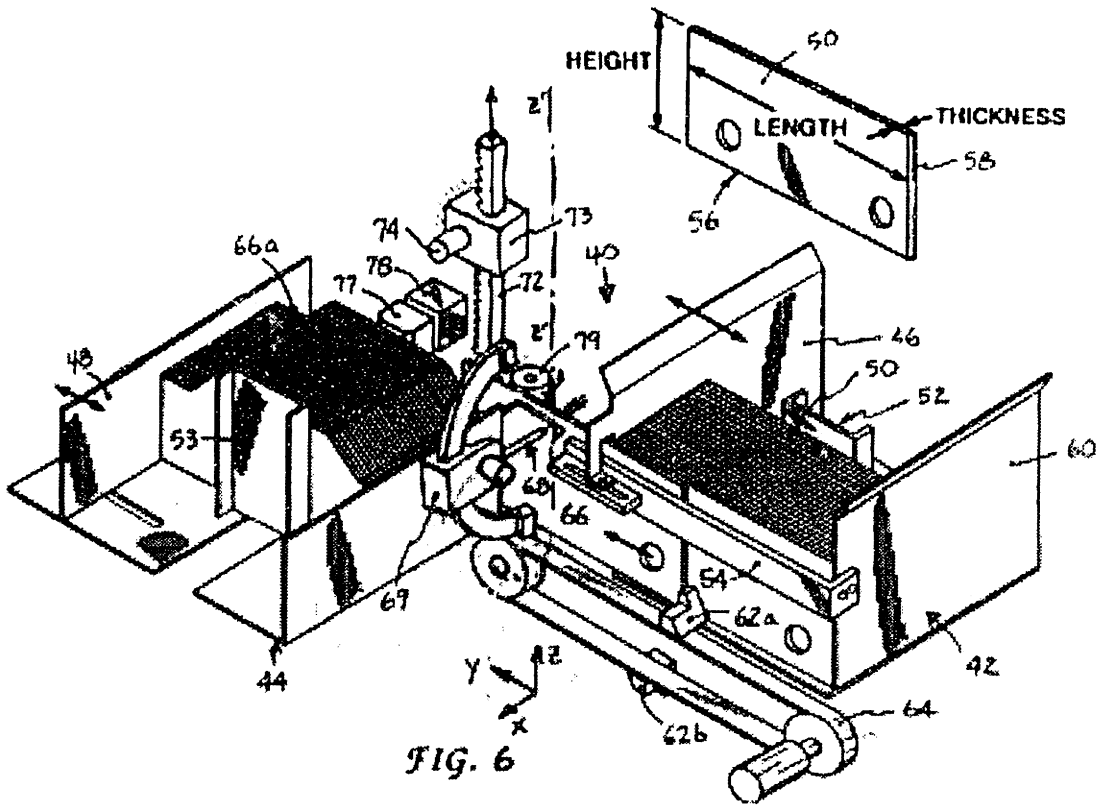

FIG. 6

Figure 4.37 - Isometric view of the DLP machine's first design embodiment.

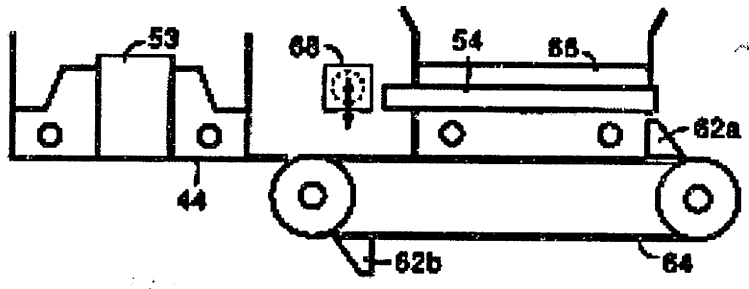

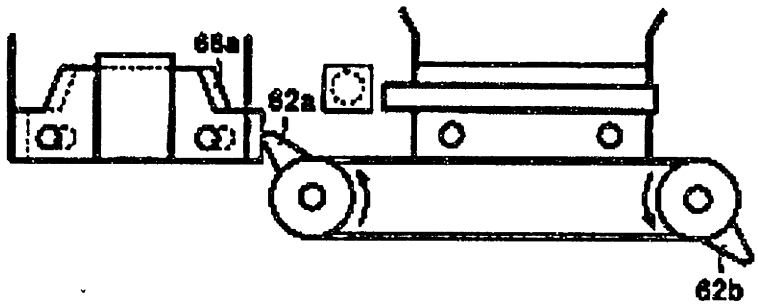

Figure 4.38 - Schematic of sliding laminations in the first DLP machine embodiment

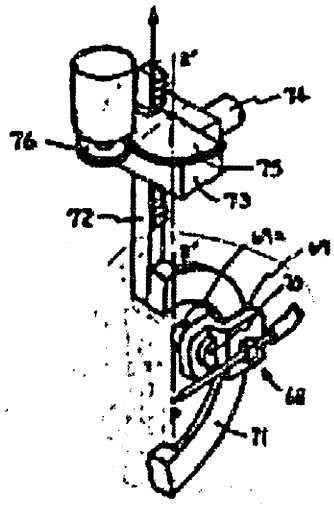

Figure 4.39 - Reverse side of the compound beveling device used in the first DLP machine embodiment.

4.3.2.2 Second Embodiment of DLP Machine

As shown in a numbered patent drawing - figure 4.40 - the second embodiment of the DLP machine fabricates a PEL die in the following manner. The DLP machine 80 contains a single loading container 82 and an inclined receiving container 84. The side walls 86 and 88 of the loading and receiving containers respectively are adjustable to correspond to the length of the die lamination blanks 90 and newly-cut die laminations 92. In operation, an array of unprocessed die laminations 90 is placed between the loading container pusher 94 and the two vertical arms 96 and 98 of the lamination descending mechanism 100. One arm (far arm in fig. 4.40) of the lamination descending mechanism 100 is adjustable to accommodate different length laminations that will be processed. The die lamination 90 in contact with the descending mechanism 100 extends beyond the

bottom edge of the loading container floor (not shown) and therefore is completely supported by the retracting pins 102 of the mechanism.

For a die lamination 90 to be loaded into the processing carriage 104, the lamination descending mechanism 100, as best seen in figures 4.41a and 4.41b, lowers the unprocessed die lamination 90 until it's bottom edge 56 comes in contact with the two sets of gripping rollers 106 of the carriage 104. When this occurs, the retracting pins 102 retract to release the loaded lamination 90 as shown in fig. 4.41b. The descending mechanism 100 then raises back to it's original position, the retracting pins 102 are extended, and the loading container pusher 94 indexes the lamination blanks forward by one lamination thickness to ready the next die for processing.

After a die lamination 90 is loaded into the processing carriage 104, the lamination gripping rollers 106 serve as a friction drive which moves (translates) the lamination in the radial direction of the processing carriage circular tracks 108. The side edges 58a and 58b of the lamination blank 90 are also guided by radially-oriented slots 110 in the processing carriage 104 which constrains the lamination's movement to the radial direction. Before any cutting takes place, four gripping rollers 106 (two on each side of the lamination blank 90) translate the lamination blank 90 to it's initial cutting position. A pair of the gripping rollers 106 on one side of the lamination blank 90 are connected with a shaft 112 and this shaft is actuated by a servo-driven DC motor 113.

The cutting head 114 for the cutting means is initially focused on one side edge of the lamination blank 90. The cutting head 114 translates on a linear track 116 along the y-axis (constraining the head in the x-z plane) with it's linear motion coming from any suitable means, e.g. servo-driven lead screw (not shown). The linear track 116 must be raised well above the level of the cutting head 114 so that it doesn't interfere with the DLP's circular tracks (discussed below). The cutting head 114 is connected to the linear track carriage 118 by a vertical offset post 120. If a laser with hard-optic beam delivery is used as the cutting means, the arrangement shown in figure 4.42a can be used in which a collimated laser beam 134 is redirected by a 45° mirror 136 and focused by the cutting head optics 138 which are attached to a y-axis linear track carriage 118 by an offset post 120. The combination of the lamination's radial translation from the servo-driven gripping rollers 106 and the y-axis motion of the cutting head 114 allows a profile to be cut into the top edge 58c of the lamination blank 90. When the cutting head 114 has finished cutting

the lamination, the head preferably remains in it's finished position and begins cutting the next lamination blank from this side. An air nozzle (not shown) located on the cutting side of the lamination 90 may be used to blow the cut lamination material to be discarded to the side opposite the lamination receiving bin 84 and into a recycling bin 124.

While the profile is being cut into the lamination 90, the ability to make bevel cuts is afforded by the lamination processing carriage 104 riding on the circular tracks 108. The axis of rotation of this track y'-y' coincides with the immediate focal or center point P of the cutting means 114. This feature eliminates the need for moving the cutting means 114 in and out (along the x-axis) as the lamination 90 is rotated about the y-axis. The processing carriage 104 is moved along the circular tracks 108 by any suitable means, but a motor-driven spur gear/track arrangement (not shown) is preferred. A simple planar bevel corresponding to the desired 3-D die surface slice is cut into the lamination blank 90 as it translates radially and rotates about the y'-y' axis and as the cutting means 114 translates along the x-axis.

Once the appropriate beveled profile cut is made in the lamination and the waste material is blown into the recycling bin 122, the sets of gripping rollers 106 lower the newly-cut lamination 92 until it drops in the inclined receiving container 84. The newly-cut lamination 92 then rotates about it's bottom edge which is in contact with the receiving container 84, and settles to the rear of the stack of previously-cut laminations, thus maintaining the correct order for a specific die. After the newly-cut die lamination 92 settles in the receiving container 84, the receiving container retracting wall 126, actuated by a motor-driven leadscrew (not shown), retracts downward by one lamination thickness in preparation for the next newly-cut lamination to be lowered into the receiving container.

The second embodiment for the DLP machine can also be fitted with a mechanism to allow compound bevels by adding a z-axis rotary actuator to the cutting means. The machine will then have 4 degrees of freedom: y-axis translation, z-axis translation, y-axis rotation, and z-axis rotation. Instead of a cutting head 114 being directly mounted to the linear track carriage 118 with an offset post 120 as shown in figure 4.42b, the cutting head is mounted with an offset post 120 to a carriage 121 mounted on a circular track 122. The cutting head carriage 121 is moved along the circular track 122 by means of a spur gear/track arrangement. The circular track 122 is rigidly connected to the y-axis linear track carriage 118 by an offset bracket 123.

Since each lamination is handled in a similar fashion, the ordering of the die laminations is automatically preserved by use of this apparatus. Either blank or previously-cut die laminati , can be machined by the apparatus. The entire operation of the second embodiment 80 including the loading container 94, the lamination descending mechanism 100, the lamination retracting pins 102, the lamination gripping roller sets 106, the lamination processing carriage 104, the y-axis linear track carriage 116, the cutting head circular track carriage 122 (if used), the receiving container retracting wall 126, and the cutting means control settings (e.g. speed, power) will be controlled by a single high-speed computer.

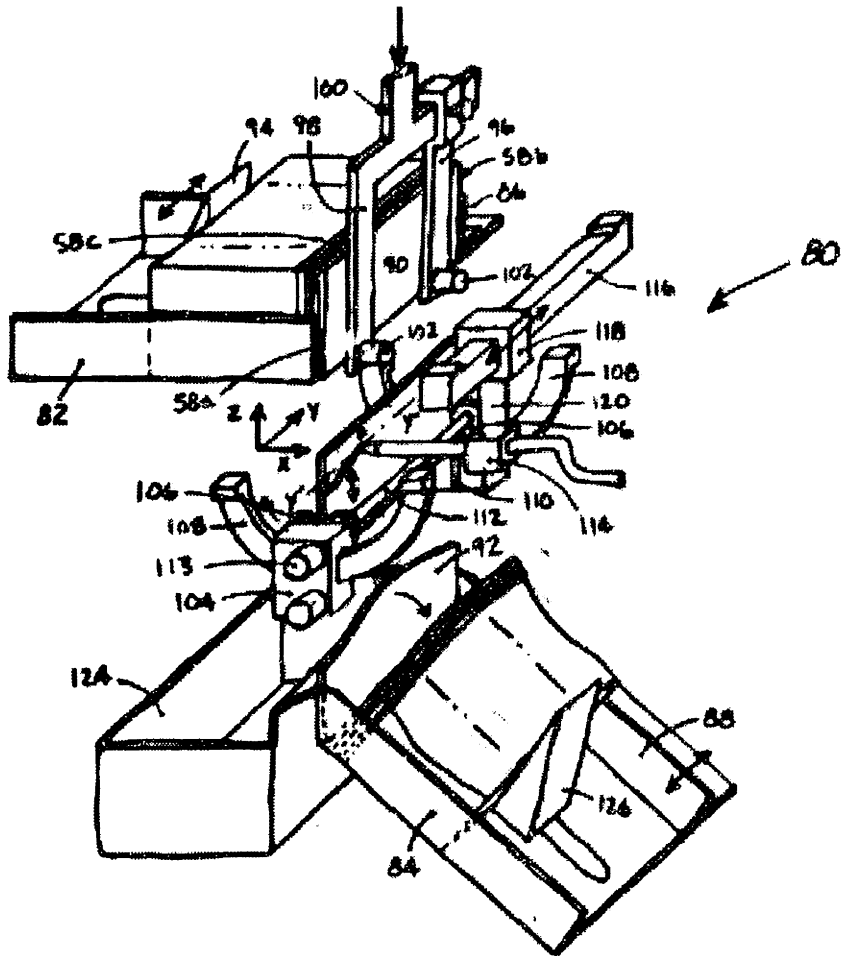

Figure 4.40 - Isometric view of the DLP machine's second design embodiment.

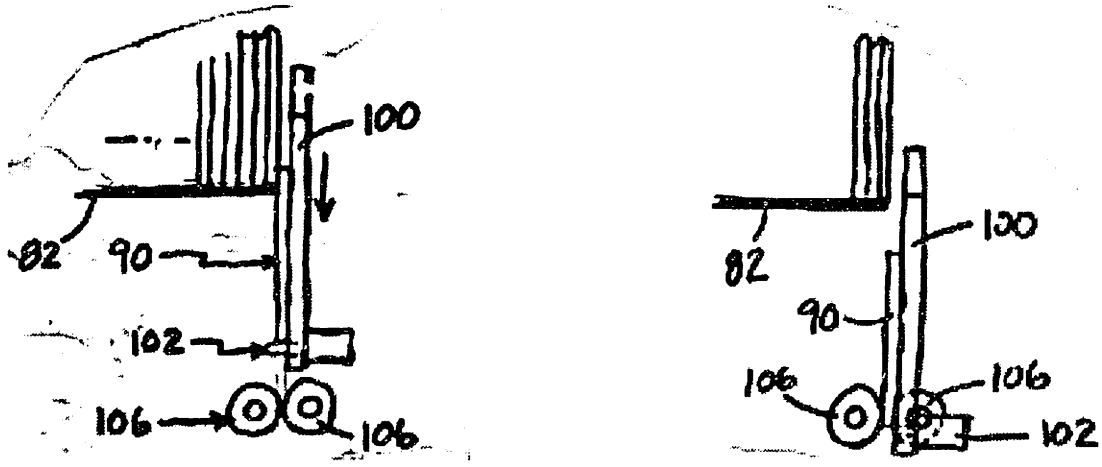

Figure 4.41 - Side views of the a) descending mechanism lowering the lamination blank and b) the roller sets gripping the lamination blank.

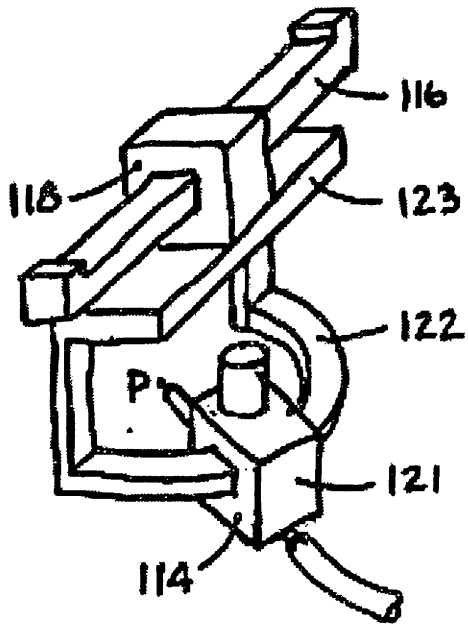

Figure 4.42 - Reverse side of the cutting device of the second DLP machine embodiment with compound beveling capabilities

4.3.3 Specifications for PEL Die Fabrication Machinery

Since the PEL die method is new, no dedicated machinery currently exists for fabricating such dies. How quickly the sheet metal forming sector of industry embraces this fabrication method will depend primarily upon the availability of this machinery. New

industrial machinery of this sort usually becomes available when a commercial machine builder (e.g. Cincinnati-Milacron, Versing) sees an economic potential from trials with prototype machinery. For a PEL die fabricating machine to have it's best chance at commercial success, the prototype machine should be able to make as wide a range of forming dies as possible. Accordingly, a list of nominal machine specifications as shown in Table 4.24 has been developed to guide the construction of the first prototype DLP machine. These specifications evolved through discussions with a group of sheet metal forming experts from twelve U.S. manufacturers during the 1994 calendar year.

Table 4.24 - DLP machine specifications

Description	Specification
Maximum Die Size	0.6 x 0.6 meters
Maximum Die Draw Height	0.25 meters
Machine Speed	2 hour fabrication time for maximum die size
Die Lamination Materials	Steel, Stainless Steel, & Aluminum
Power	220 to 440 VAC, 50 to 60 Hz.
Machining Accuracy	±0.02 mm
Machining Repeatability	±0.02 mm
Lamination Thickness Range	1.0 to 3.0 mm
Machine's Capital Cost	Competitive with currently-available CNC-Machining Centers

4.4 FABRICATING A MATCHED-SET OF STEEL PEL DIES

For use in the comparative study, a matched-set of PEL forming dies were fabricated using a 3-axis CNC machining center. The die shapes were based on the CAD surface model of the same benchmark part used to fabricate the CNC-machined dies. Un-profiled die laminations were blanked from 1.47 mm thick SAE 1010 cold drawn steel

sheet. As shown in figure 4.41a, each lamination blank was a 10.16 cm. long by 7.2 cm. high rectangular shape with a 6.5 mm diameter centrally-located hole. This hole allows a tension rod to run through the entire lamination array for clamping purposes.

4.4.1 Creation of the Machining Database

Using the same CAD model of the benchmark part (discussed in a later section) that was used for the CNC-machined dies, the machining instructions for the PEL die lamination blanks were created. The die surfaces for the PEL dies were created by offsetting the CAD surface model (zero thickness) by half the material thickness in both normal directions. [Although it's usually part of the die development procedure to account for springback in the metal, the die shapes were not changed or altered from the original part shape in this case study.] A custom-written software program was used extract the set of 2-D intersections which define the edges of the die laminations. In general, this procedure is accomplished by incrementing a Y-Z cutting plane along the X-axis and then determining the resultant 2-D intersection with the CAD model. The increment in this case is exactly $\Delta x=1.4719$ mm, as shown in figure 4.4a, which is the average lamination thickness. The average thickness was found by accurately measuring the clamped width of 69 laminations and then dividing by that number. Each intersection curve is defined by a series of 400 coordinates taken at an increment along the y-axis of $\Delta y=0.254$ mm (refer to figure 4.7). A total of 70 intersection files were used to machine the 69 laminations that make up each PEL die.

Unlike a CAM program used for CNC-machining a die surface, the custom-written software for machining data extraction did not need checks for gouging of the endmill or surface fouling (i.e. machine spindle crashing into workpiece). The reason for this is that problems of tool gouging and fouling are non-existent when bevel cutting PEL laminations. The total time required to create all 138 PEL machining files was 30 minutes. This time would certainly decrease if the data extraction program was optimized.

4.4.2 Machining and Assembling the Die Laminations

Both PEL dies required a total of 138 lamination blanks. The blanks were sheared off of a 7.2 cm wide by 1.47 mm thick strip of steel. Using a fixture, the centrally-located hole for the tension rod was drilled in 10 lamination blanks at a time. After the tension rod holes were drilled, all of the lamination blanks were clamped into a large array after which the bottom edge and one side edge were both machined flat and perpendicular to each other. The lamination blanks were then ready for processing. Total time for this preparatory operation to be performed on all of the laminations was 40 minutes.

Since the benchmark part die shape did not require compound beveling, rotation of the cutting means was limited to y-axis rotation (as is described in section 4.1.1.1) facilitating only simple planar beveling. Accordingly, a machining instruction is defined by a point (y,z) from one of the intersection files and the orientation vector (V_2,V_3). Ideally, a 4-axis machine with either a rotating endmill, an abrasive water jet nozzle, or an Nd:YAG laser cutting head would be used to machine the profiled edges into the lamination blanks. None of these types of machines were readily available but a 3-axis CNC machining center was. Due to economic and time constraints, this machine was used to machine the bevels. As shown in figure 4.12b, the lamination blanks were machined with a weaving motion of a ball endmill mounted in the spindle of the machining center. Another custom-written computer program was used to create the offset surface for the center point of the endmill's ball-end and then write the necessary machine code for the weaving cut.

After all the NC files needed to machine the PEL die laminations were created, each lamination blank was sandwiched between two sacrificial aluminum plates. This assembly was then fixed in a vise mounted to the working bed of the machining center. The stiffer aluminum plates prevented the thin lamination blank from excessive deflection during the machining operation. The weaving motion of a 6.4 mm diameter, 2-fluted, carbide ball endmill was used to machine the plates. Each plate took 2 minutes to fix in the vise and an average of 5 minutes to machine so that the total time to machine all 138 die laminations was around 16 hours. Deburring all the die laminations took another 4 hours.

The die laminations as seen in figure 4.43a were finally mounted and clamped into a rigid frame to form the complete PEL die. As shown in figure 4.43b, the frame consists of an L-shaped steel base, a lamination edge guide secured to the base, and a steel movable clamping wall which is rigidly bolted to the base after the laminations are clamped. The forming surface of the die was purposely left unground for a number of stamping trials to

see how it would perform as is. The die surface was later ground and polished for the remaining stamping trials. These dies, as shown in figure 4.1a, can be mounted and used in any type of stamping press.

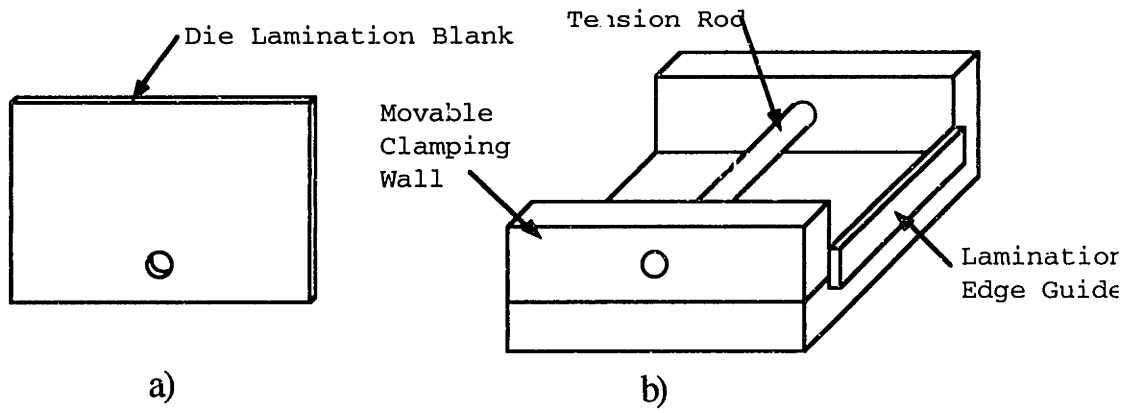

Figure 4.43 - a) A die lamination blank and b) PEL clamping frame.

Machining die laminations with the weaving motion of a ball endmill mounted in 3-axis machining center is too time-consuming and labor intensive to be considered a viable option. This machining method was used for this study only as a matter of convenience. The die laminations should be profiled by flute-edge endmilling, AWJ cutting, or laser cutting instead. The particular choice of cutting method will depend on the specifications of the die and the availability of equipment. Let us assume that the DLP machine described in section 4.3.2.1 is used to machine the die laminations. For the purpose of estimating the fabrication time for both dies, we will assume a nominal distance of 10 cm between laminations as they are moved past the laser cutting head at 7.5 meters/min. The transfer speed is adjusted according to the bevel angle being cut. Using the cutting systems listed in sections 4.2.1 (flute-edge endmilling), 4.2.2 (AWJ), and 4.2.4.5 (Nd:YAG laser cutting with hard-optic beam delivery) then the estimated total machining times for two dies are as listed in table 4.25.

Table 4.25 - Estimated machining times for matched-set of PEL dies

Bevel Cutting Method	Machining Time (min.)
Machining with the Flute-Edge of an Endmill	38
Abrasive Water Jet Cutting	51
Nd:YAG Laser Cutting with Hard-Optic Beam Delivery	31

4.4.3 Grinding and Polishing the PEL Dies

Similar to the grinding operation performed on the CNC-machined dies, the die grinder with a unitized grinding cylinder (3 were used) was used to grind out the machining mismatches of the PEL dies forming surfaces. All the machining mismatches were not completely ground out, however, because of their depth (0.25 mm in some cases). Completely grinding out these surface deformities would have altered the shape of the dies too much. Extensive lamination edge mismatching can be prevented, i.e. tighter machining tolerances can be achieved, if a non-contact beveling method is used (e.g. AWJ or laser cutting) since there's negligible tool or workpiece deflection to deal with. After the PEL die forming surface was ground as smooth as possible, the surface was polished with polishing compound. Total finishing time was 45 minutes per die (1 hour 30 minutes total).

4.5 GENERAL PROCEDURE FOR DESIGNING AND FABRICATING PEL DIES

We shall conclude this chapter by outlining the general procedure for designing and fabricating a PEL forming die.

1) Considering the sheet metal part being formed and it's expected production quantity, choose an appropriate die material. [Semiatin,1988] is an excellent reference for die material selection.

2) Design a clamping frame that incorporates the binder configuration prescribed by the FEA simulations of the forming process. The frame must also allow the entire clamped die to mounted to the forming press platen(s).

3) Based on the geometry of the die's forming surface, specify the size and shape of the lamination blanks, and the size and location(s) of the clamping rod(s).

4) Choose lamination thicknesses (preferably all the same), orientation, and interface positions that yield geometrical errors that are less than the maximum permissible error. Refer to section 4.1.1.2 for details on how to calculate this maximum error **e**. Lamination interface positions that take advantage of certain geometrical features of the die should be chosen. One example is a vertical wall which coincides with a lamination interface as shown in figure 4.44.

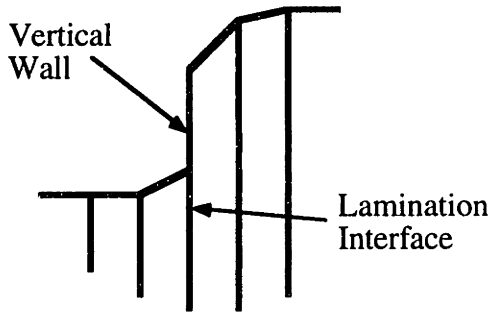

Figure 4.44 - Basing the location of a lamination interface on a die's geometrical feature.

5) Based on the estimated forming loads from an FEA simulation of the forming process, check the bending and buckling propensity of the die laminations (see section 4.1.2). Modify the lamination thicknesses as needed.

6) Depending on the accuracy of the die shape that's required, the lamination thicknesses and material considerations, choose the optimal bevel cutting method for forming die being fabricated. Refer to section 4.2 if the material is steel.

7) Using a suitable CAD software package, intersect the CAD surface model of the die with a cutting plane positioned at the various interface positions. From this resulting database, create the NC machining files for each of the laminations. The CAD software used would ideally do this operation automatically (see section 4.1.1).

8) Machine the laminations at the maximum possible feedrate f_m.

9) After each of the die lamination edges are machined and deburred, assemble the laminations in a suitable clamping frame.

10) Grind and polish the die as needed.

Chapter 5 - Discrete Forming Dies

The third and last rapid fabrication method to be investigated is a discrete die comprised of a close-packed element matrix, i.e. bed of pins, set to the desired shape and then clamped into a rigid tool. A discrete die can serve as either a permanent or reconfigurable tool. In it's permanent configuration, die elements are automatically cut to a specified length and then assembled in the correct order into a matrix. The back ends of the elements can be supported by a backing plate or the entire matrix can be brazed together into a solid tool. However, the appeal of a discrete forming die is not in a permanent tool, but rather in a rapidly reconfigurable die which can act as a universal tool and take the place of many continuous tools. This is a tempting idea to manufacturers who must deal with the high cost and lead times associated with developing the tooling used for sheet metal forming. The number of attempts to use discrete dies for forming sheet metal parts is fairly extensive [Hess,1931; Wakefield,1943; Nakajima,1969; Whiteacre,1971; Wolak,1973; Hardt,1981; Ousterhout,1991; Finckenstein,1991] but the depth of knowledge about how to design such dies is still very limited. In other words, the interest in discrete dies is high but the know-how needed to successfully design, build, and implement such dies in an industrial application is not. Many fundamental design issues involving extraction of the necessary element positioning data from a CAD part file; design details of the elements; methods of setting the shape of the die; methods for clamping the close-packed element matrix into a rigid tool; and design details of the die frame still need to be addressed. This chapter surveys the current state-of-the-art in discrete die design, discusses research that furthers the state of knowledge, describes the detailed design and construction of two high-resolution discrete dies, and then outlines the general procedure for designing, fabricating and setting a discrete die.

The pair of high-resolution dies, shown in figure 5.1a, have been constructed for both matrix clamping and sheet metal stamping experiments that are part of the comparative study. Each die consists of a 64 by 64 matrix of 1.59 mm square elements

clamped from the side with a 30 ton ram. The dies can be configured in two ways: as a simple close-packed element matrix (discussed in section 5.2.1) and as a close-packed matrix with row dividers (discussed in section 5.2.6.1.2). A benchmark part successfully stamped with these dies is shown in figure 5.1b. The detailed construction of these discrete dies will be discussed in section 5.7.

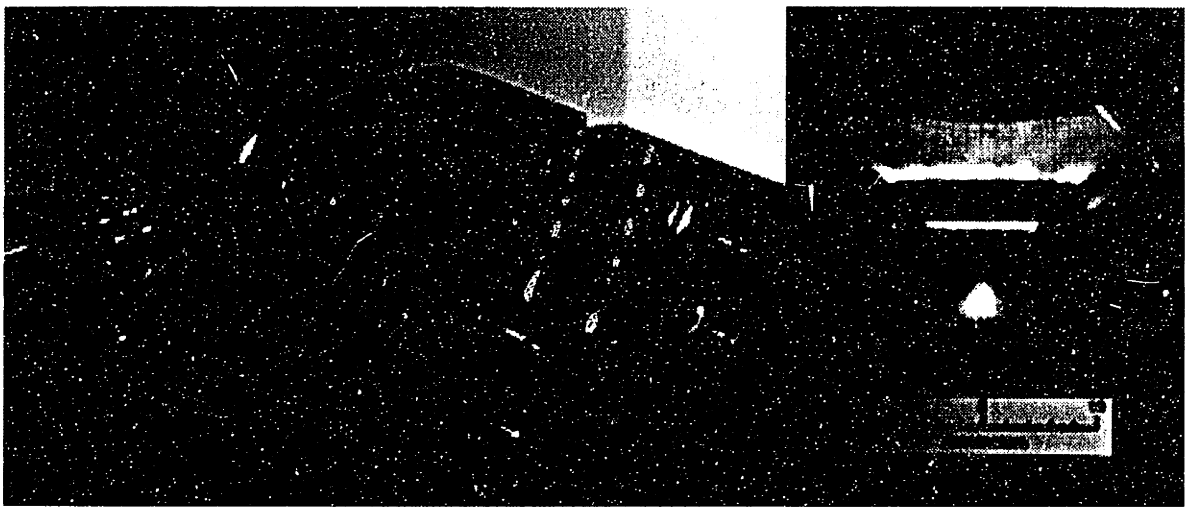

Figure 5.1 - a) High-resolution discrete die used for clamping and stamping experiments and b) benchmark part formed with a matched set of these dies.

5.1 DISCRETE ELEMENTS USED FOR RECONFIGURABLE DIES

The most important components of a discrete die are the discrete elements that comprise the reconfigurable matrix. Elements of uniform cross-sectional shape, size and length are prescribed since they are easily fabricated and assembled into a close-packed matrix and then set to the desired shape. Ideally, an element will also be strong enough to withstand the buckling and bending loads incurred while forming sheet metal parts, easily clamped with a matrix of identical elements into a rigid tool, and small enough in cross-section to allow for adequate die shape fidelity. Discussion in this section concentrates on the characteristics of a die element which impact these die design issues.

5.1.1 Die Element Details

As previously mentioned, all of the die elements that comprise the discrete die should be of uniform cross-sectional shape, size and length. Element uniformity allows simplified fabrication because identical manufacturing set-ups and steps can be used to make each element. This leads to minimized cost and lead-time in their manufacture. Uniformity also simplifies how elements are assembled into a matrix as compared to a non-uniform matrix like that shown in figure 5.2a. The uniformity in length is a necessary requirement if the element positions are to be set from the non-forming side of the discrete die. Otherwise, a matrix of non-uniform length elements (e.g. from rough) will not correctly transfer the intended die shape.

The importance of close-packing elements in a die matrix is to allow adjacent elements to support each other during high forming loads. Accordingly, the surface-to-surface contact between elements should be maximized or conversely, gaps between elements should be minimized. The only element cross-sectional shapes that can be close-packed into a consistent matrix without gaps between adjacents are a triangle, square and hexagon as shown in figure 5.2b, 5.2c and 5.2d, respectively. Round elements, shown in Figure 5.2e, are arguably the most common and least expensive cross-sectional shape available in industry for die elements. Unfortunately, they represent an extreme case in which there are no surface-to-surface contacts between elements at all, only line contacts.

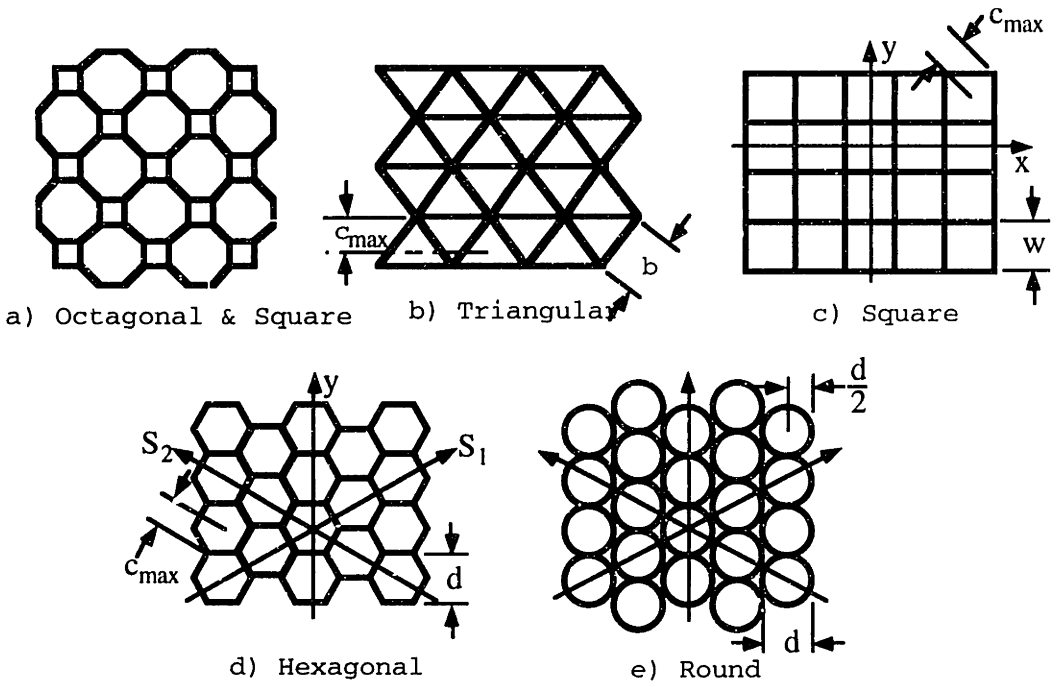

Figure 5.2 - Possible die element cross-sectional shapes

One of the most critical issues about the chosen element shape is the ability to clamp a matrix of these type of elements into a rigid tool. Consequently, the distribution of clamping load within the matrix must be known. For a reconfigurable tool, the easiest way to clamp the matrix is from one side as shown in Figure 5.3. When clamping in this manner, the number of isolated loading path directions for the clamping force is important. An isolated load path within an element matrix allows the clamping load to be transmitted from element to element in a straight line without the possibility of branching off in another direction. Without isolated load paths, certain elements in a matrix may be insufficiently clamped or not clamped at all. Nakajima had to deal with the problem of non-isolated load paths when trying to clamp a square matrix of round elements [Nakajima,1969]. Very non-uniform clamping load distribution in the matrix was the result. Clamping in an isolated loading path direction insures that each discrete die element behaves in a predictable manner, i.e. no slipping, when subjected to high forming loads. The number of isolated load path directions for various die element shapes are listed in Table 5.1.

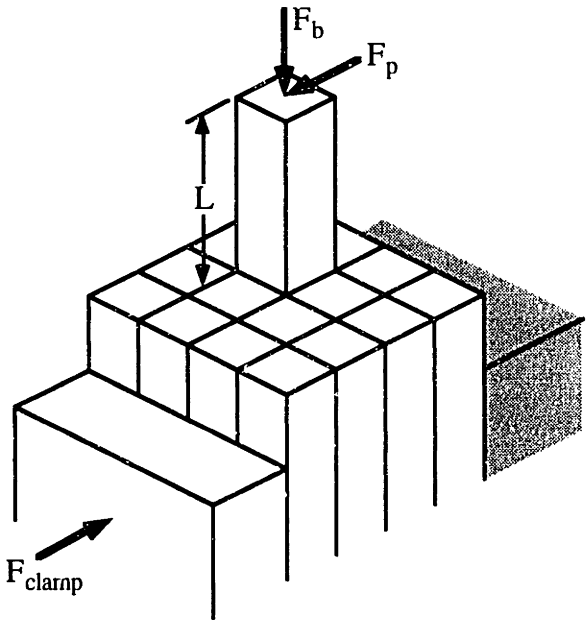

Figure 5.3 - Single element protruding from a clamped discrete element matrix.

The worse-case loading scenario for a single close-packed element is when it protrudes above adjacent elements. This means that it will not be supported by adjacent elements when subjected to high forming loads. It will be useful then to compare the structural rigidity and resistance to buckling and bending failure of various element shapes.

In this comparison, the single protruding die element will be modeled as a cantilever beam as shown in figure 5.3. Furthermore, the element is assumed to have a cross-sectional area of 1.00. Since the cost of the die element stock is primarily based on it's weight, a uniform cross-sectional area implies a uniformity in weight and cost among all of the different element shapes compared. The cantilever beam model represents a single protruding element that can be subjected to a bending load $\mathbf{F_p}$ and/or a buckling load $\mathbf{F_b}$. The bending strength of the element is found by examining the maximum bending stress at it's base. The maximum stress σ_{max} at the base of the element is calculated using the equation

$$\sigma_{max} = \frac{M \cdot c_{max}}{I} \qquad (5.1)$$

where: c_{max} = distance between the neutral axis of the element and the part of it's cross-sectional geometry farthest from this axis
I = second moment of area of the element's cross-section, and
M = the applied bending moment ($F_p \cdot L$ in this case).

The stress σ_{max} must not exceed the yield stress of the element material or else the element will plastically deform. From formula 5.1, the critical ratio for a particular element cross-sectional shape is the ratio of c_{max} /I. Specifically, the lower this ratio is, the less prone a particular shape is to bending failure. The c_{max} /I ratios corresponding to each element shape are listed in table 5.1. The elastic bending stiffness $\mathbf{K_b}$ of the element to the load F_p is calculated using the relation

$$K_b = \frac{3 \cdot E \cdot I}{L^3}. \qquad (5.2)$$

where: E = elastic modulus of the material and
L = element's protruded length.

Furthermore, the critical buckling load of the element subjected to load F_b is calculated using the relation

$$F_{b,critical} = \frac{\pi^2 \cdot E \cdot I}{4 \cdot L^2}. \qquad (5.3)$$

From equations 5.2 and 5.3, it is evident that the bending stiffness and critical buckling load of an element are proportional to the moment of inertia which is also listed in table 5.1 for all of the element shapes.

From a practical point of view, the end of the die element (used to form the stamping surface) must not have sharp edges which can dig into the sheet metal surface during forming. One of the easiest ways to resolve this problem is to make the element

ends spherical in shape. As seen in a side view shown in Figure 5.4a, the element's spherical tip will always be contacting the sheet metal at a tangency point and not at a sharp point. The diameter of the spherical end should be equal to the maximum distance across the elements cross-section as shown in Figure 5.4b. Otherwise, a sharp-edged shoulder will result as shown in Figure 5.4c. The diameter of the spherical end is also important in terms of the forming resolution of the die. Smaller element diameters mean that element spacing is decreased. This allows for a finer discretization of the die surface. The spherical end diameter for each element cross-sectional shape is listed in Table 5.1.

Table 5.1 - Comparison of element cross-sectional shapes for use in a discrete die

Element Cross-Sectional Shape	Equilateral Triangle	Square	Hexagonal	Round (limiting case)
Number of Sides	3 (minimum case)	4	6	∞ (maximum case)
# of Isolated Straight Loadpath Directions	0	2	3*	3*
Characteristic Dimension if A_{cs}=1.0	b=1.52	w=1.00	d=1.07	d=1.13
Second Moment of Area **I**	0.0962	0.0833	0.0801	0.0796
C_{max}/I	9.12	8.48	7.75	7.09
Diameter of Spherical End	1.76	1.41	1.24	1.13

* - Isolated load paths are not truly isolated from each other.

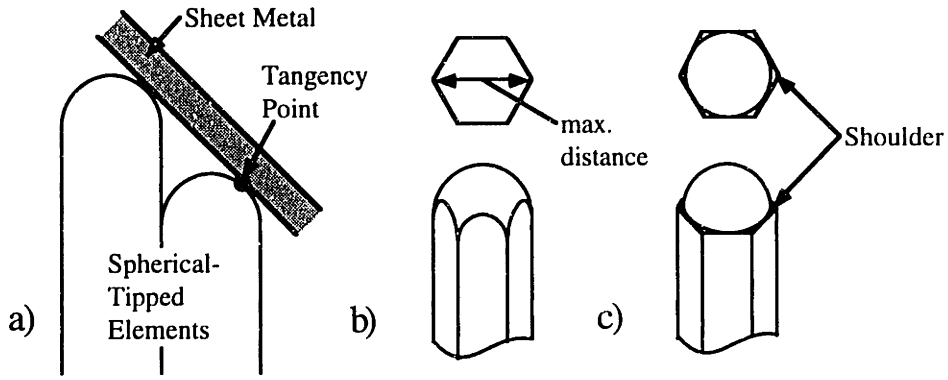

Figure 5.4 - a) Side view of a spherical-tipped die element contacting the sheet metal at a tangency point. Hexagonal die element tip b) without and c) with a shoulder.

From table 5.1, a triangular element has the highest bending strength, bending stiffness, and buckling stiffness for a given cross-sectional area. A hexagonal shape allows the smallest spherical end diameter. Considering only these characteristics would suggest that a triangular element is the optimal shape for use in a discrete die. However, the most important issue for the choice of element cross-sectional shape is the ability of an element matrix to be rigidly clamped. Triangular elements have no isolated load path directions. Adjacent elements will affect the clamping load on a specific element which means that it may or may not be sufficiently clamped. [Olsen,1980] found that a hexagonal element shape has the same problem because load path directions are not truly isolated. The only cross-sectional shape that insures load path isolation is a square. For these same reasons, square elements have been used by both Hardt et al. [Hardt,1985] and Finckenstein & Kleiner [Finkenstein,1991] in their experimental dies. Therefore, the author recommends that a square element shape be used in discrete dies with closed-packed elements.

Generally when smaller elements are used in discrete dies then finer details can be formed into sheet metal parts. However, the size of the die elements should not be smaller (accounting for the interpolator thickness) than the smallest radius of curvature in the sheet metal part to be formed. The reason for this suggestion is that the size of an element matrix which can be successfully clamped into a rigid tool is limited by the element's size. This element versus maximum die size relationship has been observed by the author, although not quantified in this thesis. One probable explanation for this relationship is that the effect of bent and warped die elements on the non-uniformity of the clamping load distribution are magnified as die size increases.

5.1.2 Element Construction

How an individual element is constructed should ideally maximize it's stiffness and minimize it's weight. The element's stiffness is maximized to decrease an it's risk of failure due to plastic bending or buckling. From equations 5.2 and 5.3, it is evident that the element's bending and buckling stiffness is directly proportional to the cross-sectional second moment of area **I**. Element weight needs to minimized so that setting the die shape

and handling the clamped die will be made easier. The weight of the element is proportional to it's cross-sectional area $\mathbf{A_{cs}}$.

As seen in figure 5.5a, an individual element of width **w** can simply be a length of bar stock with one spherical end. This type of element construction is very easy to fabricate. However, if the weight of the die needs to minimized, then the elements can also be made from hollow tubes of width **w** and wall thickness **t** with capped ends as shown in figure 5.5b. The effect that this change in the element's cross-sectional shape has on the weight and stiffness is best shown by comparing $\mathbf{A_{cs}}$ and **I** as the wall thickness varies between w/2 (solid) and 0.0 (infinitely thin wall). These values are calculated using the formulas

$$A_{cs} = w^2 - (w - 2t)^2 \quad \text{and} \quad I = \frac{1}{12} \cdot [w^4 - (w - 2t)^4]. \qquad (5.4)$$

The effect of switching from a solid to a tubular cross-section is best shown by the graph denoted by figure 5.6. In this case, the element width is 1.00 and the wall thickness varies between 0.5 to 0.0. The graph shows that for wall thicknesses above 15% of the width, the element's weight decreases more rapidly than the stiffness does. In other words, a sharp decrease in weight does not have the same effect on the elements stiffness. Therefore, tubular elements should be considered considered if the weight of the discrete die has to be minimized.

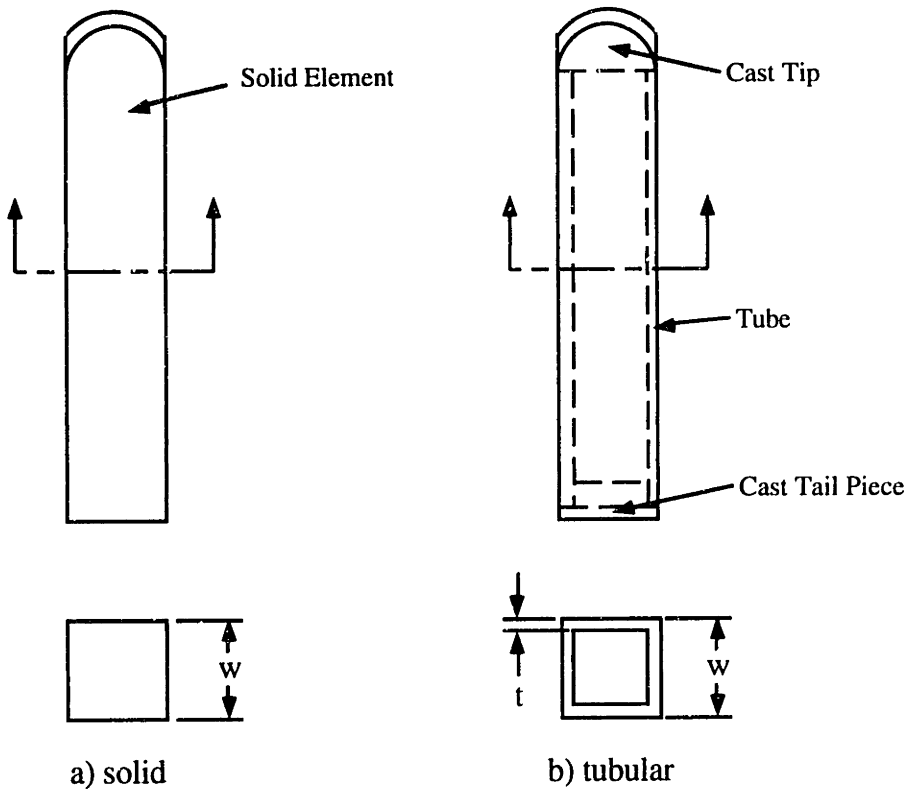

Figure 5.5 - Discrete die elements with a) solid and b) tubular cross-sections.

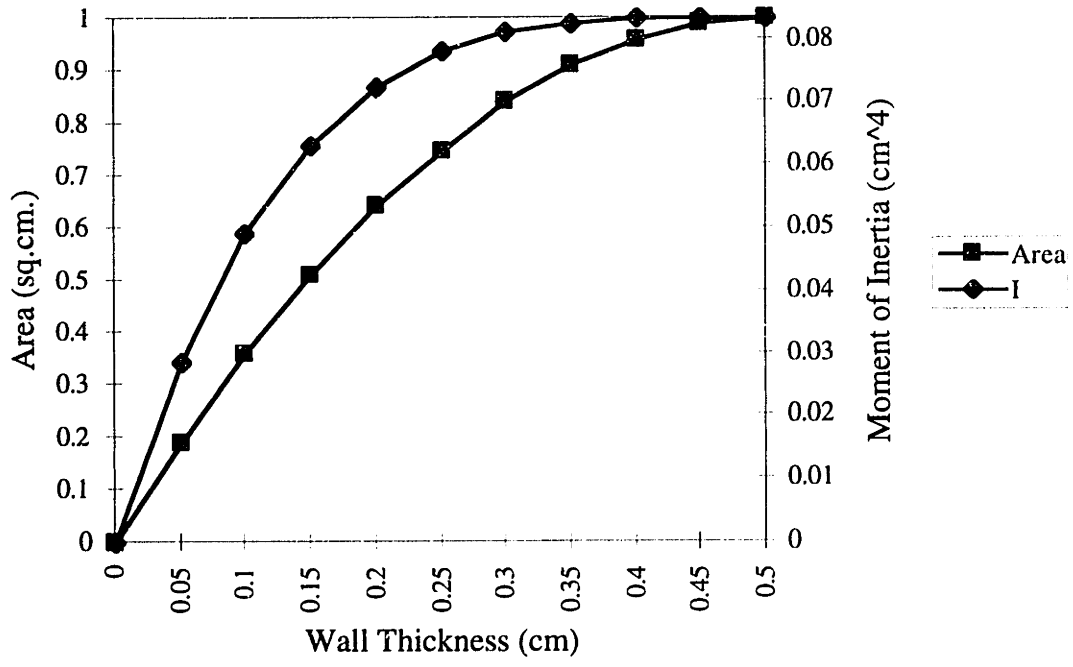

Figure 5.6 - Graph of a die element's A_{cs} and **I** versus wall thickness **t** with **w**=1.00

5.2 METHODS FOR LOCKING DISCRETE ELEMENTS

If a reconfigurable discrete die is to form sheet metal parts, the elements comprising the die must be locked into position and capable of withstanding the high forming loads encountered. Die elements that slip during forming due to insufficient locking force result in a loss of the intended die shape. Three methods of temporarily locking element positions of a discrete die are to:

(1) individually lock each element

(2) backfill the non-forming side of the matrix with some moldable backing material
like fusible metal alloy or plaster of paris and

(3) clamp the entire element matrix from one side with a high force to provide the elements with frictional resistance to the high forming loads.

The first method usually requires that the elements be individually actuated. This will be discussed later in section 5.5.3. Of the last two methods, side clamping the element matrix is considerably easier and quicker to implement than using a backing material. Since increasing the speed of die development is one of the main focuses of this thesis, only side clamping configurations will be discussed in this section.

The net total of all z-direction, i.e. into-the-die, forming loads on a side-clamped die element matrix must not exceed the maximum frictional load that the element/element interfaces can withstand. The best element cross-sectional shape in this case is square as discussed in Section 5.1.1. The easiest matrix shape to clamp when square elements are used is rectangular. Matrices can be other shapes (e.g. circle) but this makes design of the clamping means and the containment frame more difficult. Although there are many clamping configurations that can be used for a rectangular matrix, two particular ones will be discussed here because of there inherent simplicity. As shown in figure 5.7, the candidate clamping configurations are a single compression wall and dual compression wall types. For analysis purposes, the element matrix size will be **m** by **n**.

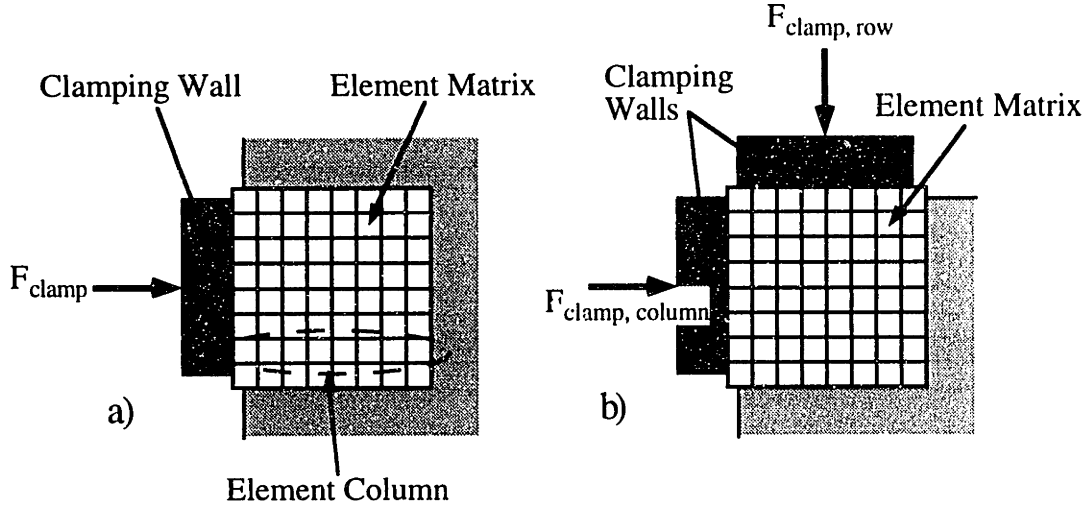

Figure 5.7 - Clamping a simple-packed element matrix with a) single compression wall and b) double compression wall.

5.2.1 Single Compression Wall Clamping Configuration

For a discrete die with a single compression wall clamping configuration and a simple close-packed matrix of square elements, the clamping load within the matrix is assumed to be transfered through the element columns in the direction of the applied load. This also assumes that the element matrix is sufficiently constrained in the lateral direction. If there is too much clearance in the lateral (row) direction, loaded columns can buckle as shown in figure 5.8. If we accept the assumption of non-interacting columns with sufficient lateral constraint, an individual element column, like that denoted in figure 5.7a, can be statically modeled as is shown in figure 5.9a. A series of arbitrary forming loads $\mathbf{F_1}$ to $\mathbf{F_m}$ are applied to the **m** constituent elements. The free-body diagram of an arbitrary element **z** within the column is shown in figure 5.9b. There is a normal force **N** applied to this element which is

$$N = \frac{F_{clamp}}{n} \qquad (5.5)$$

where: F_{clamp} = side clamping force
n = number of element columns in the matrix.

The clamping load is assumed to be evenly distributed over all the element columns. With an individual element, the summation of all the shearing loads transmitted through the frictional interfaces with neighboring elements is equal to the applied forming load $\mathbf{F_z}$ in the static case. When an element slips, the forming load F_z exceeds a certain limiting value $\mathbf{F_s}$, called the static frictional force, which is calculated with the equation

$$F_s = 2 \cdot \mu_s \cdot N \qquad (5.6)$$

where μ_s is the static frictional coefficient between elements. The factor of 2 is needed in equation 5.6 because there are two frictional interfaces for each element in a matrix. If a group of elements in the column slip, say elements x to z, then the summation of forming loads $\sum_{k=x}^{z} F_k$ has exceeded F_s. The important point to remember is that the summation of forming loads along a column cannot exceed F_s or else one or more of the elements in that column will eventually slip.

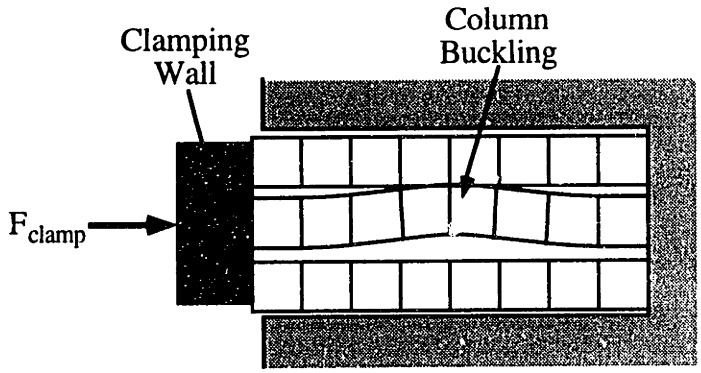

Figure 5.8 - Buckling behavior of a clamped column of discrete die elements

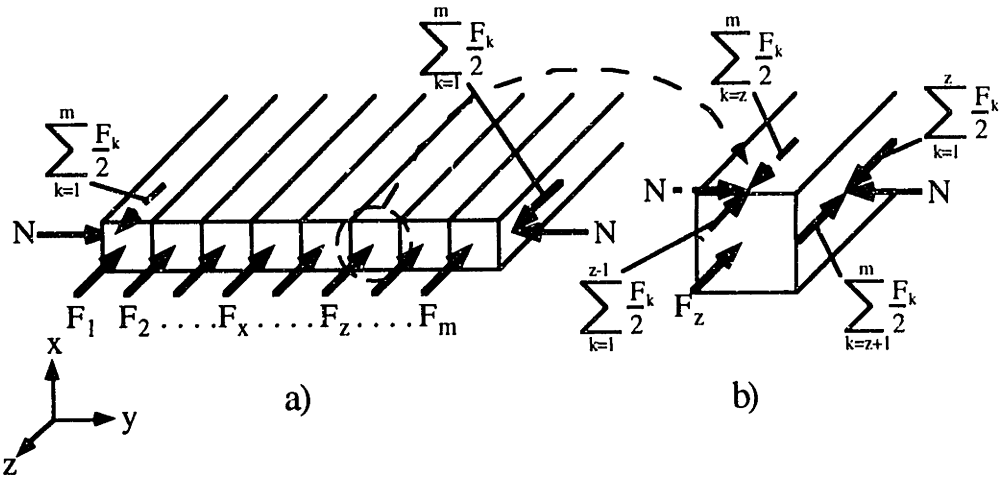

Figure 5.9 - Static structural model of a) a clamped element column and b) a single element.

If this static model of a clamped element is valid for the columnar loading associated with a single compression wall configuration, it can be used to estimate the minimum matrix clamping force required while forming a particular sheet metal part. First, the maximum forming pressure $\mathbf{P_f}$ in the z-direction which is encountered during forming must be determined. Forming pressure plots can be accurately estimated from FEA simulations of a sheet metal stamping. A conservative estimate of the minimum clamping force needed is found by assuming that P_f is applied to the entire column of elements (worst case scenario). The total forming force load on that column will be

$$\sum_{k=1}^{m} F_k = P_f \cdot w \cdot (w \cdot m) = P_f \cdot w^2 \cdot m. \qquad (5.7)$$

To insure that none of the elements in the column will slip, the frictional force F_s must be greater than this total forming load, i.e. $F_s > P_f \cdot w^2 \cdot m$. Substituting in equations 5.5 and 5.6 into this inequality yields the magnitude condition for the discrete die clamping force:

$$F_{clamp} > \frac{P_f \cdot w^2 \cdot m \cdot n}{2 \cdot \mu_s}. \qquad (5.8)$$

The accuracy of the clamped element static model shown in figure 5.9 is dependent upon the validity of the assumptions made in deriving equations 5.5 & 5.6 and knowledge of the static frictional coefficients. These assumptions include:

- no interactions, i.e. no transfer of clamping load, between adjacent columns due to column buckling and edge interactions
- clamping load transferred through the element columns only
- an equal distribution of clamping force to each element column and
- negligible lateral expansion of the clamped element matrix.

In addition, the static frictional coefficient μ_s between adjacent elements, and between an element and die containment frame must be known. The experimental verification of these assumptions and the measurement of the frictional coefficients are discussed in the following sections.

5.2.1.1 Interactions Between Adjacent Element Columns

A series of tests were performed to evaluate the degree of column/column interaction that exists in a clamped matrix of closed-packed elements. The element matrix of one discrete die (see fig. 5.1a) was sufficiently constrained in the lateral (row) direction to avoid possible column buckling and then clamped with several arbitrary loads. Whenever a protruding element was pushed with enough force, as shown in figure 5.10, to overcome the static frictional force, either the element or a group of elements (including the protruding element) in the same column slipped and began moving. Elements in adjacent columns were never dragged along with the moving elements. This experimental observation indicates that:

1) the clamping load is being transferred primarily through the columns and column/column interaction is minimal and

2) there are particular element/element frictional interfaces in a clamped column that are weakest.

However, when the lateral constraint was relaxed (i.e. one column of elements was removed), element columns buckled under the clamping load (see fig. 5.8) and interfered with neighboring columns.

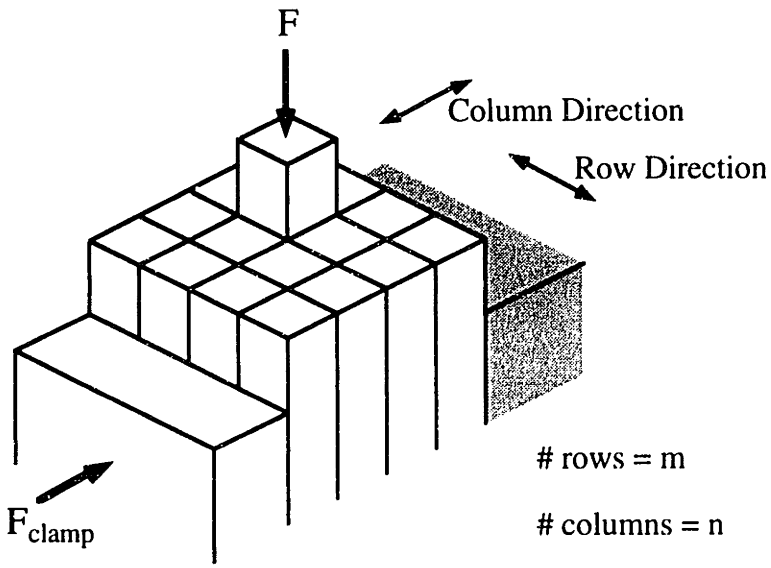

Figure 5.10 - Experimental set-up for determining column static frictional forces.

5.2.1.2 Uniformity of Die Matrix Clamping Load

Since each element column takes a portion of the clamping load without interference from adjacent elements, it is sufficient to measure the static frictional force F_s

of each column by just pushing on an individual element in that column and recording the maximum force just before the element begins to slip. By using this technique, the distribution of static frictional forces across all 64 columns of one of the high-resolution discrete dies (see figure 5.1) was measured to determine the uniformity of the clamping load within the matrix. When the static frictional forces were measured for each element column with a 140 kN clamping force applied, F_s varied dramatically as shown in the test #1 data listed in table 5.2. The standard deviation of the individual column static frictional loads is 70% of the average. In this clamping configuration, there was little uniformity in the die matrix clamping load.

The reason for the lack of a uniform load distribution is because of different tolerance stack-ups in the element columns, i.e. the columns vary in height. Consequently, the taller columns are compressed more than the shorter columns, as shown in figure 5.11a, which accounts for the variability in the load distribution. A simple remedy for this problem is to place an easily deformable material (i.e. clamping interpolator) between the compression wall and the top row of elements. As seen in figure 5.11b, the clamping interpolator flows into the gaps between the compression wall and the shorter columns to even out the load distribution. The variability of the column F_s decreases significantly when a 0.25 mm layer of ethylene vinyl acetate (Elvax) is used as a clamping interpolator. From test #2 listed in table 5.2, the standard deviation is shown to decrease to only 35% of the average F_s value by using this thin clamping interpolator.

Table 5.2 - Static frictional force distribution in columns of a clamped discrete die.

Test #	F_{clamp} (kN)	Clamping Interpolator	Column F_s (kN)				$\sum_{n=1}^{64} F_{s,n}$ (kN)	$\frac{\sum F_{s,n}}{F_{clamp}}$
			Min.	Max.	Average	Standard Deviation		
1	140	None	0.15	3.33	0.73	0.51	46.9	0.34
2	140	0.25 mm Elvax	0.24	1.30	0.65	0.23	41.4	0.30
3	140	0.80 mm Elvax	0.26	1.07	0.66	0.18	42.5	0.31

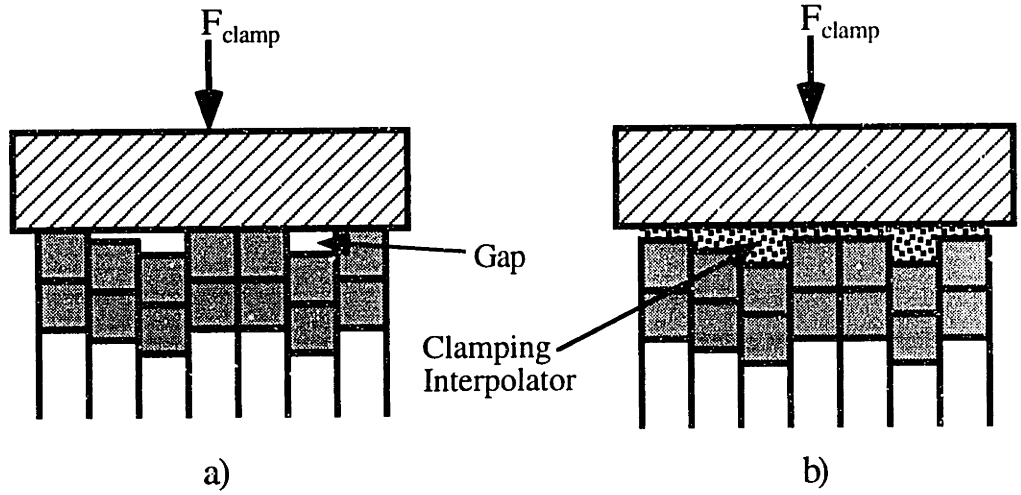

Figure 5.11 - a) Uneven clamping of element columns and b) use of a clamping interpolator.

The variability of the column F_s can be decreased even further by using a thicker clamping interpolator. If we only consider the interpolating material between the die compression wall and the first element of the column, it can be modeled as a linear elastic spring. In actuality, it will behave like a non-linear spring but this model is useful for showing the effect of different amounts of interpolator compression above each column. As shown in fig. 5.12, the entire clamping interpolator can be thought of as a set of springs connected to each column. From solid mechanics theory, the stiffness of a compressed elastic material has been shown to be proportional to the inverse of the thickness, i.e. $K_{spring} \propto \frac{1}{\text{thickness}}$. As the thickness of the interpolator increases, which is the case for shorter columns, the spring becomes softer. From the standpoint of load uniformity across all the element columns, an even softer spring (i.e. thicker interpolating layer) is better because the variation in column heights will not cause such great variations in clamping load. In fact, the standard deviation decreased to 27% of the average column F_s when a 0.80 mm thick Elvax clamping interpolator was used (see table 5.2 - test #3).

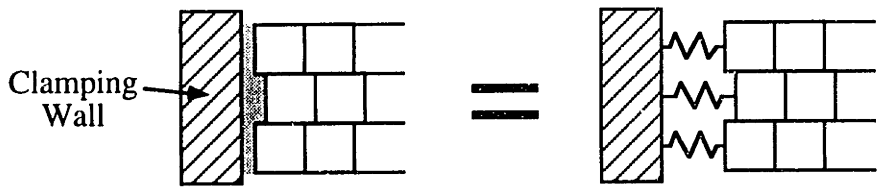

Figure 5.12 - Clamping interpolator modeled as a set of parallel springs.

5.2.1.3 Lateral Expansion of a Compressed Element Matrix

When a clamping load is applied through a single compression wall, the matrix of elements will expand laterally (i.e. row direction) due to the Poisson's effect. The amount of element matrix expansion determines the amount of lateral freeplay that the die frame can have. It is important for the die designer to know this so that he/she doesn't over-constrain the element matrix in the lateral direction. To estimate the lateral expansion (x-direction) of the matrix, a compressed element in the matrix can be modeled as shown in figure 5.13. The clamping pressure applied to a single element over the area $\mathbf{C}_{\mathbf{lamp}}$ is equal to the uniaxial normal stress σ_y. The normal stress is calculated with the equation

$$\sigma_y = -\frac{F_{clamp}}{n \cdot A_{clamp}} = -\frac{F_{clamp}}{n \cdot L \cdot w} \qquad (5.9)$$

where: L = length of the element's clamped area.

The right side of the equation is negative since we are dealing with a compressive stress. If the element is made of a linear elastic material, the relationship between σ_y and the lateral strain ε_x is

$$\varepsilon_x = -\frac{\nu \cdot \sigma_y}{E_e} \qquad (5.10)$$

where: ν = Poisson's ratio and
E_e = elastic modulus for the element material.

By substituting equation 5.9 into equation 5.10 and rearranging variables, the total lateral expansion δ_x of a compressed matrix can be estimated with the following expression

$$\delta_x = \varepsilon_x \cdot n \cdot w = \frac{\nu \cdot F_{clamp}}{L \cdot E_e}. \qquad (5.11)$$

As an example, the lateral expansion of the high-resolution dies used for the clamping experiments will be calculated. Since the 1.58 mm square elements are made of SAE 1095 steel, then ν=0.295 and E_e=200 GPa. With L=0.102 meters, the lateral expansion for a 270 kN clamping load—the maximum achievable load for the discrete die hydraulic rams—is 4 μm. This lateral expansion is negligible.

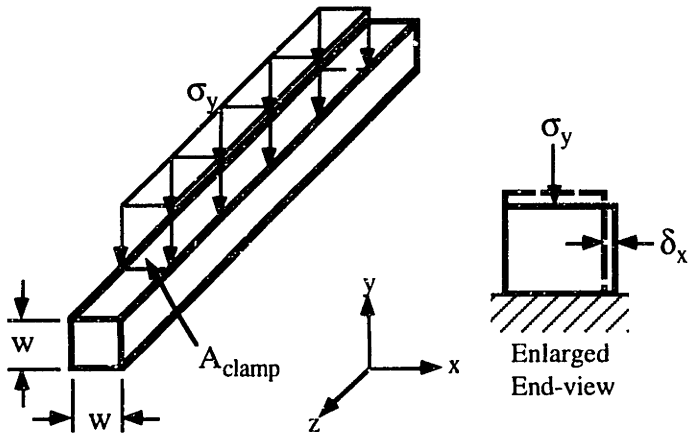

Figure 5.13 - Lateral (x-direction) expansion of a die element.

5.2.1.4 Static Frictional Coefficients Between Die Elements

As previously discussed, the static frictional coefficient μ_s between adjacent elements, and between an element and the compression or back wall of the frame need to be determined. A simple way to measure this coefficient is to use an inclining table as shown in figure 5.14. Specifically, the experimental set-up used to determine μ_s consisted of a row of elements bonded to the top of the inclining table and a weighted element set on top of this element row. The table was slowly inclined until the weighted element started to slide. The static frictional coefficient is calculated by dividing the normal load of the weighted element by it's tangential force. The frictional coefficient is related to the table inclination angle θ by the relationship

$$\mu_s = \frac{\text{tangential force}}{\text{normal force}} = \frac{W \cdot \sin\theta}{W \cdot \cos\theta} = \tan\theta \qquad (5.12)$$

where: W = weight of the sliding element.

[Bowden,1950] has shown that for a wide range of normal loads (up to a factor of 10^6 in some cases), μ_s effectively remains constant for most metals (including steel) and many polymers.

From a series of 20 sliding experiments, the average static frictional coefficient between elements is 0.19 with a sample standard deviation of 0.02. The average static frictional coefficient between and element and the frame wall was slightly higher, specifically 0.22 with a sample standard deviation of 0.02. Since the μ_s at the element/element interface is lower than that for the element/frame interface, slippage will

always occur between elements. This effect was observed in the experiments described in section 5.2.1.2, i.e. uniformity of die matrix clamping load.

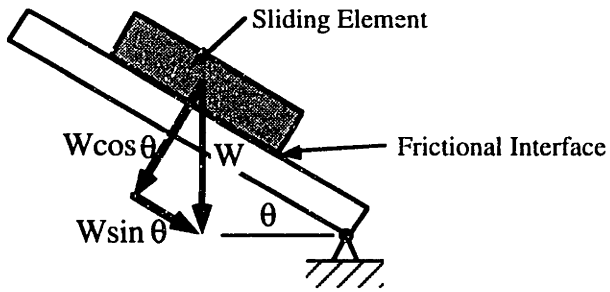

Figure 5.14 - Schematic of an inclining friction table used for μ_s measurements.

5.2.1.5 Validity of the Clamped Matrix Static Frictional Model

The validity and accuracy of the clamped matrix static frictional model described by equations 5.5 and 5.6 is based on several assumptions made in its derivation. The assumption that there are negligible interactions between adjacent columns, clamping load transfer primarily through the columns, and negligible lateral expansion of the clamped matrix are shown to be valid. The uniformity of the clamping load distribution is found to be essentially valid if a clamping interpolator is used. The real test of the frictional model is to see how well equation 5.6 predicts the results of experimental tests. From the last column of table 5.2 - test #3, the ratio of the total static frictional force to the applied clamping load was 0.31. {As a comparison, Nakajima found that the ratio of the total static frictional force of the elements and the applied side clamping load was approximately 0.25 [Nakajima,1969]. Round elements were used in this case.} If we rearrange equation 5.6 to include all the element columns in the discrete die and then use the measured element/element μ_s of 0.19, then the same ratio is

$$\frac{\sum_{n=1}^{64} F_{s,n}}{N \cdot n} = \frac{\sum_{n=1}^{64} F_{s,n}}{F_{clamp}} = 2 \cdot \mu_s = 0.38$$

which is 23% higher than the experimentally determined value. Given the uncertainty in accurately measuring static frictional coefficients [Crandall,1978], this modest experimental error is expected. The main conclusion that can be drawn from this experimental verification is that the static frictional model described in equations 5.5 and 5.6 gives

reasonably accurate estimates of the clamping load required for a specified maximum forming load.

5.2.1.6 Techniques for Enhancing a Discrete Die's Forming Load Capacity

The main limitation on forming with a simple matrix of close-packed elements, clamped from one side with a compression wall, is that the total forming load on each column cannot exceed the static frictional force described in equation 5.6. As will be shown in chapter 6, this limitation proves to be very troublesome when using a discrete die to form parts with highly localized forming pressures. However, two methods can be used to enhance the forming load capability of a discrete die. These two methods are to supply a backing pressure with a fluid-filled bladder (see figure 5.14) or to include element matrix row dividers that are rigidly attached to the die frame (see figure 5.15).

5.2.6.1.1 Backing Pressure from a Fluid-Filled Bladder

As seen in figure 5.15a, a bladder filled with pressurized fluid located on the non-forming side of a discrete die can enhance the die's capability to withstand high forming loads. For an arbitrary group of elements (x to z) in a column as shown in figure 5.15b, the bladder fluid of pressure $\mathbf{P_o}$ supplies a backing force of $P_o \cdot w^2 \cdot (z - x + 1)$. Therefore, the magnitude condition to insure that the element group does not slip is

$$\sum_{k=x}^{z} F_k - P_0 \cdot w^2 \cdot (z - x + 1) < 2 \cdot \mu_s \cdot N. \qquad (5.13)$$

To determine the maximum fluid back pressure that the can be applied, we must assume a worst case scenario, namely that an entire column of **m** elements could slip in the opposite direction from the fluid back pressure. The magnitude condition for the fluid pressure is then

$$P_o < \frac{2 \cdot \mu_s \cdot F_{clamp}}{m \cdot w^2 \cdot n}. \qquad (5.14)$$

Although backing the elements of a discrete die with fluid pressure will allow higher forming loads, the pressure that can be applied is limited by equation 5.14.

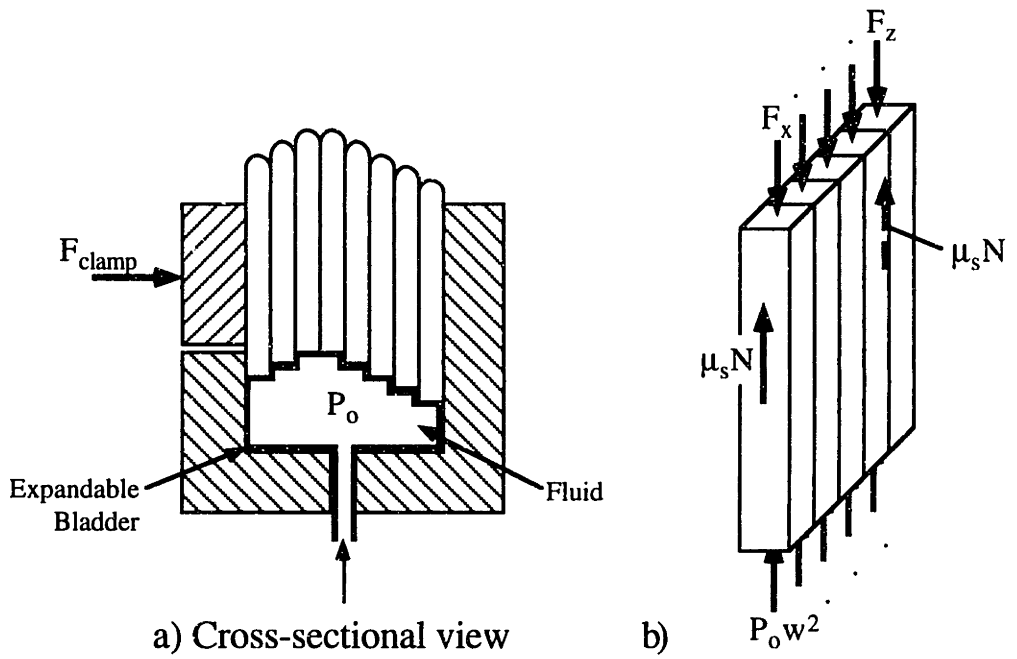

Figure 5.15 - a) Fluid backing pressure used to enhance forming load capability of a discrete die and b) free-body diagram of an element column.

5.2.6.1.2 Incorporating Rigidly-Attached Row Dividers

As shown in figure 5.16a, a more effective way of allowing a discrete die to handle higher forming loads is by incorporating sheet metal dividers that are oriented perpendicular to the direction of clamping and rigidly attached to the die frame [Hardt,1985]. In this section we analyze the static loads and stresses in a discrete die's sheet metal divider so that it may be designed correctly. With sheet metal dividers included, the forming loads on the elements are transferred (by friction) to the outer die frame through the dividers and not only through the frictional interfaces as with the close-packed configuration. As shown in figure 5.16b, each element in the matrix will not slip until the forming load F_k exceeds the frictional force F_s calculated with equation 5.6. The key feature of this configuration is that if the row dividers are correctly sized to handle the accumulation of loads, then "each" element in the matrix and not just the column of elements can withstand a forming load of F_s.

If the maximum forming pressure that the die will experience during forming is P_f, then the magnitude condition for the clamping force, i.e. clamping force required to prevent elements from slipping, is

$$F_{clamp} > \frac{P_f \cdot w^2 \cdot n}{2 \cdot \mu_s}. \qquad (5.15)$$

By comparing equation 5.15 with equation 5.8, the necessary clamping force for the element matrix with row dividers to have the same forming load capacity as an element matrix without is a factor of **m**, i.e. number of element rows, less.

Assuming that there is sufficient clamping load to prevent element slippage, the limiting force for a discrete die with row dividers is dependent on the tensile shear strength of the row divider material. Considering only a single row divider as shown in figure 5.16c, the mode of failure for the divider will be yielding. The loads tranferred to a single row divider are half the total forming loads from the two element rows in frictional contact with the divider. The total forming load $\mathbf{F_{RD}}$ applied to the divider shown in the figure is calculated using the relation

$$F_{RD} = \frac{\sum_{k=1}^{n} F_{k,\text{row A}} + \sum_{k=1}^{n} F_{k,\text{row B}}}{2}. \qquad (5.16)$$

Referring to figure 5.17a, the shear stress τ_{xz} where the row divider connects to the die frame is

$$\tau_{xz} = \frac{F_{RD}}{2 \cdot t_{RD} \cdot L_{RD}}. \qquad (5.17)$$

where: t_{RD} = row divider's thickness
L_{RD} = row divider's length.

Referring to figure 5.16c, the compressive unaxial stress σ_y within the entire row divider in a clamped element matrix is simply the clamping pressure, i.e.

$$\sigma_y = -\frac{F_{clamp}}{n \cdot w \cdot L_{RD}}. \qquad (5.18)$$

The point of maximum tensile stress in the row divider due to pure beam bending is at pt. S in figure 5.17a. If the loaded row divider is modeled as a beam with fixed end supports and a uniformly-distributed forming load, i.e. $\frac{F_{RD}}{\text{divider length}} = \frac{F_{RD}}{n \cdot w}$, then the maximum bending moment $\mathbf{M_{max}}$ occurs at the ends, i.e. x=0 and x=n·w, and the magnitude is

$$M_{max} = \left(\frac{F_{RD}}{n \cdot w}\right) \cdot \frac{(n \cdot w)^2}{12} = \frac{F_{RD} \cdot n \cdot w}{12}$$

The maximum tensile stress σ_x at pt. S is determined with the beam flexure formula

$$\sigma_x = \frac{M_{max} \cdot c}{I_{yy}}$$

where: c = distance of beam fiber farthest out from the neutral axis and
I_{yy} = second moment of area of row divider cross-section about it's neutral axis.

Since $c = \frac{L_{RD}}{2}$ and $I_{yy} = \frac{t_{RD} \cdot L_{RD}^3}{12}$ for the row divider's rectangular cross-section then

$$\sigma_x = \frac{F_{RD} \cdot n \cdot w}{2 \cdot t_{RD} \cdot L_{RD}^2}. \qquad (5.19)$$

By considering an infinitesimally small cube of material (see figure 5.17b) from the row divider at it's connection point to the die frame, i.e. pt. S, the effective combined state of stress in the material can be evaluated. Since the state of stress of this cube is known in terms stress components with respect to non-principal axes, we can use the following transformation of the effective stress used in Distortion Energy yield criterion:

$$\sigma' = \left[\frac{1}{2} \cdot \left\{(\sigma_x - \sigma_y)^2 + (\sigma_y - \sigma_z)^2 + (\sigma_z - \sigma_x)^2\right\} + 3\tau_{xy}^2 + 3\tau_{yz}^2 + 3\tau_{xz}^2\right]^{\frac{1}{2}}$$

With $\sigma_z = \tau_{xy} = \tau_{yz} = 0$ then this equation reduces to

$$\sigma' = \left(\sigma_x^2 - \sigma_x \cdot \sigma_y + \sigma_y^2 + 3 \cdot \tau_{xz}^2\right)^{\frac{1}{2}}. \qquad (5.20)$$

According to the Distortion-Energy failure theory, the row divider will fail in yielding when σ', calculated with equation 5.20, equals or exceeds the tensile yield strength (σ_{yield}) of the material, i.e. $\sigma' \geq \sigma_{yield}$. The limitation on forming loads imposed by possible row divider failure is shown by example in section 5.7.1.

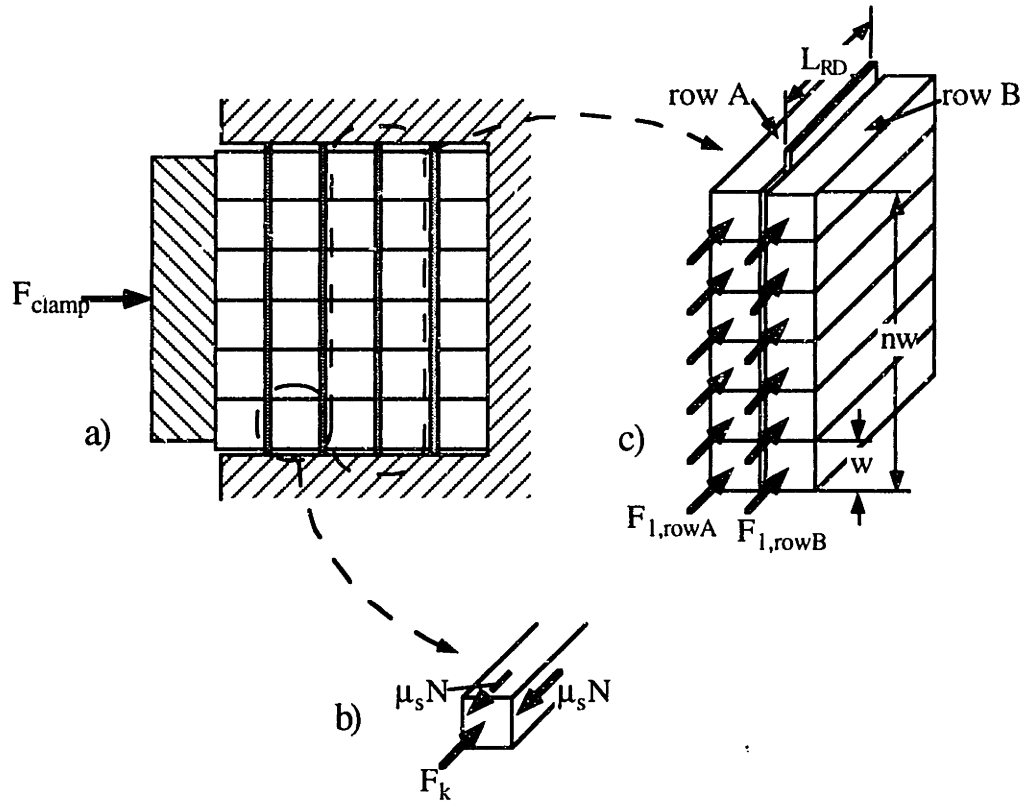

Figure 5.16 - a) Single compression wall clamping of an element matrix with row dividers, b) free-body diagram of a single element , and c) isolated view of a single row divider and adjacent element rows.

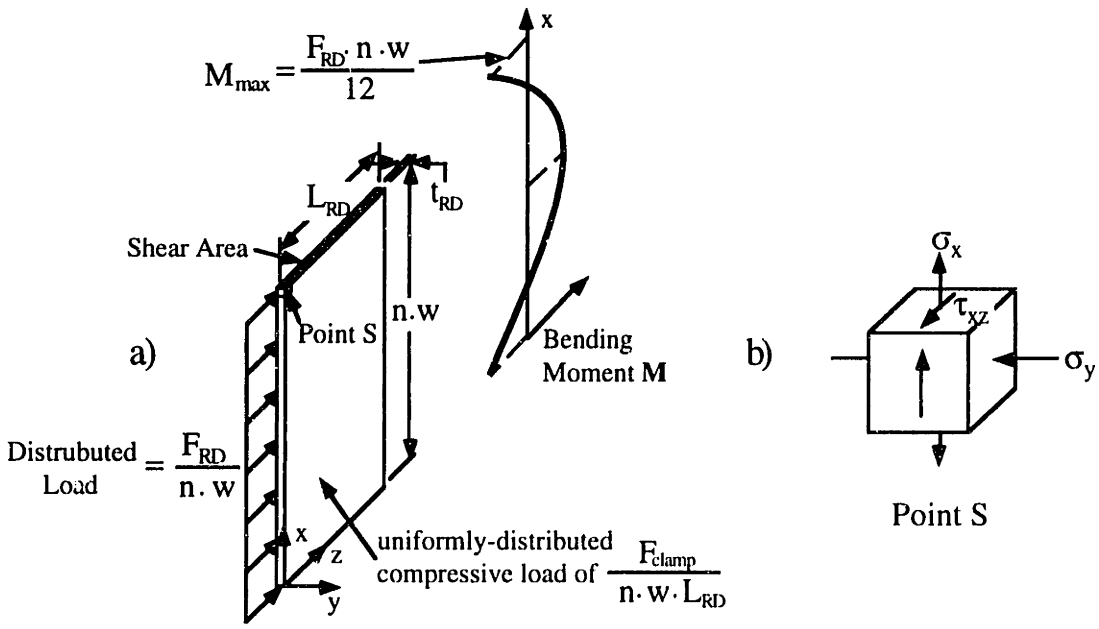

Figure 5.17 - (a) Isolated view of an element row divider modeled as a beam subjected to a uniformly-distributed shear load and (b) an infinitesimal cube of material at point S with normal and shear stresses indicated.

One disadvantage of adding row dividers to a discrete die is that each element row is spaced out from adjacent rows by the thickness of the divider t_{RD}. If not compensated for, this spacing allows elements to bend slightly under high forming loads in the column direction because adjacent elements are no longer in intimate contact. This tendency to bend decreases the accuracy of the forming surface especially on steep angle walls and fine die features. Spacing between element rows also makes for a courser discretization of the die surface.

Two remedies to this problem are to wedge the elements together during forming or to notch the elements to account for the thickness of the row divider. The concept of purposely wedging the elements together during forming with a converging frame was proposed by Knapke for the design of the MIT discrete die press discussed in section 2.2.3.2 [Knapke,1988]. As shown in figure 5.18a, this technique requires that the elements are extra long to insure that only elastic bending occurs as they are wedged together. Another method, proposed by the author, involves notching the elements on one side to account for the row divider thickness. As seen in figure 5.18b, the elements are in intimate contact with each other without using a converging frame and long-length elements. Notching of the elements must be done very carefully to make sure that there is still good contact with the row divider and the forming load is simply not transferred to the ends of the elements.

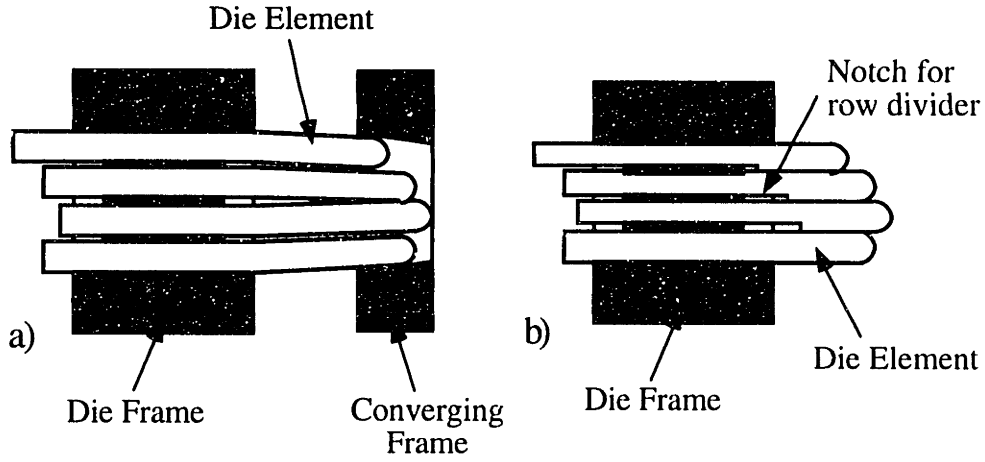

Figure 5.18 - a) Converging a die elements that are separated by row dividers and b) notching elements to account for row divider thickness.

5.2.2 Dual Compression Wall Clamping Configuration

For a simple close-packed discrete die with a dual compression wall clamping configuration as shown in figure 5.7b, the element matrix is simultaneously clamped in both the row and column directions. Finckenstein and Kleiner have used this method to clamp a discrete die matrix used for hydroforming and stretch-forming [Finckenstein,1991]. A maximum forming load to clamping load ratio of 0.13 is claimed in this case. However, because of the inherent complexity of the static structural analysis of the clamped matrix and the lack of advantages that this configuration has over a single compression wall with row dividers, only a brief analytical treatment of a dual wall configuration will be presented.

If a single element in a dual clamped matrix has an applied forming load $\mathbf{F_L}$, the free-body diagram of this element is shown in figure 5.19a. With perpendicular normal forces of $\mathbf{N_{row}}$ and $\mathbf{N_{column}}$ applied to the element, the maximum static frictional force of this element is $F_s = 2 \cdot \mu_s \cdot N_{row} + 2 \cdot \mu_s \cdot N_{column}$ where the normal forces are calculated using equation 5.5. This maximum F_s load only applies to the element if no other elements in the same row or column have applied forming loads which is highly unlikely. The perpendicular clamping loads are assumed to be decoupled so that no unwanted shearing loads are applied to the elements in the x and y directions. However, depending upon how the dual clamping loads are applied, there will be shear loads in the X and Y-directions applied to each element as shown in figure 5.19b. If a high-frequency displacement (dithering) signal is applied to the element matrix as the clamping loads are applied, these shear loads can probably be avoided because the inherent frictional shear forces are dissipated.

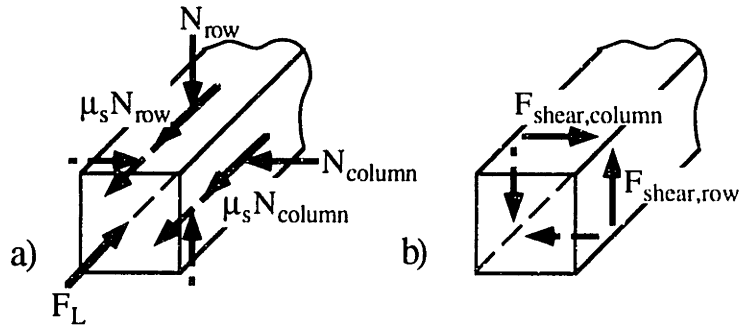

Figure 5.19 - a) Free-body diagram of an element clamped with dual compression walls and b) unwanted shear loads on the same element.

5.3 FRAME FOR CONTAINING AND CLAMPING AN ELEMENT MATRIX

The design details of the discrete elements and configurations for clamping a matrix of elements into a rigid tool are discussed in sections 5.1 and 5.2. Other discrete die design issues that require examination are the methods for clamping the element matrix with a high force and the associated structural requirements for the containment frame. Therefore, various methods for applying a high clamping force on the element matrix are presented in the first part of this section. Each clamping force method is then compared with the other methods in a case study. Finally, the structural requirements of a discrete die containment frame that must withstand these high clamping forces are discussed.

5.3.1 Methods for Creating a High Clamping Force

There are many methods that can be used to create high forces for clamping the discrete die element matrix. Purely mechanical methods include using a simple hydraulic actuator, a knuckle mechanism, and a screw or wedge. Two unconventional methods proposed by the author are to use a stack of piezoelectric laminations and thermally-inducing contraction of the containment frame around the element matrix. All of these clamping methods are finally compared to each other with a numerical example.

5.3.1.1 Simple Hydraulic Actuator

A simple high-pressure hydraulic cylinder can be used to create very high clamping forces. As seen in figure 5.19, only one hydraulic line must be connected to the cylinder if a spring return is used. The clamping force from the cylinder is calculated using the relation

$$F_{clamp} = P_o \cdot A_{cs} \cdot (1 - K_f) \qquad (5.21)$$

where:

P_o =hydraulic pressure
A_{cs} = cross-sectional area of the cylinder and
K_f = force loss coefficient of the cylinder.

The force loss coefficient must be used since there is significant friction at the piston/cylinder wall interface.

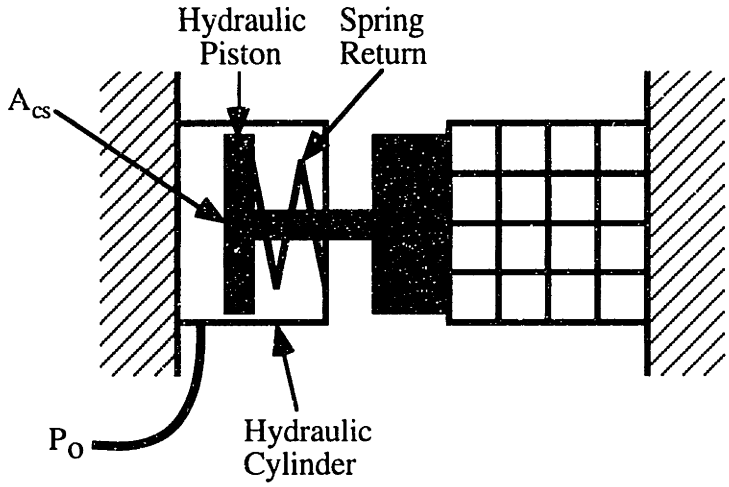

Figure 5.20 - Hydraulic actuator used for clamping an element matrix.

5.3.1.2 Toggle Mechanism

The high force required for clamping the element matrix can be generated by a toggle mechanism with equal length links. As shown in figure 5.21a, a force $\mathbf{F}_{tm}$ is applied perpendicular to the wall travel at joint C of the mechanism. The mechanical amplification of F_{tm} is determined by considering the free-body diagrams of the two links of the mechanism, A-C and C-B, as shown in figure 5.21b. By summing the moments acting on link C-B around point B, then

$$\sum M_A = \frac{F_{tm}}{2} \cdot L \cdot \cos\theta - C_y \cdot L \cdot \sin\theta = 0$$

where: θ = angle that the links make with the x-axis.

Solving for the reaction force $\mathbf{C}_y$ yields $C_y = \frac{F_{tm}}{2 \cdot \tan\theta}$. Summing the forces on link C-B in the Y-direction yields $\sum F_y = C_y + B_y = 0$ which means that $B_y = -C_y$. Since $-B_y$ is the reaction force from the clamped matrix of elements, the effective clamping force is then

$$F_{clamp} = \frac{F_{tm}}{2 \cdot \tan\theta}. \qquad (5.22)$$

The actual clamping force will be slightly less than that calculated with equation 5.22 since the effect of joint friction has not been included in its theoretical development. As shown

in figure 5.21c, the theoretical amplification factor $\frac{F_{clamp}}{F_{tm}}$ gets infinitely large as θ goes to 0°. In reality the clamping force is limited to a maximum value that is dependent on the degree of straining within the mechanism components and die frame, and their respective elasticities. Determining the limiting force requires a displacement/strain analysis of the die frame and toggle mechanism.

The high force generated by a toggle mechanism comes at the expense of compression wall displacement. Specifically the displacement of this wall is small when compared with that of the force actuator that generates F_{tm} . The compression wall must be retractable by a certain minimum displacement during the die setting operation or else interaction forces between adjacent elements will make setting too difficult. As the mechanism moves from the unclamped position angle θ to the clamped position (θ=90°), the positions of pivot point C, i.e. input force actuator, and point B, i.e. compression wall, are

$$\delta_c = -L \cdot \sin\theta \qquad (5.23a)$$

and

$$\delta_{wall} = 2 \cdot L \cdot (1 - \cos\theta), \qquad (5.23b)$$

respectively. Displacements δ_c and δ_{wall} for L=30 mm are plotted in figure 5.21d.

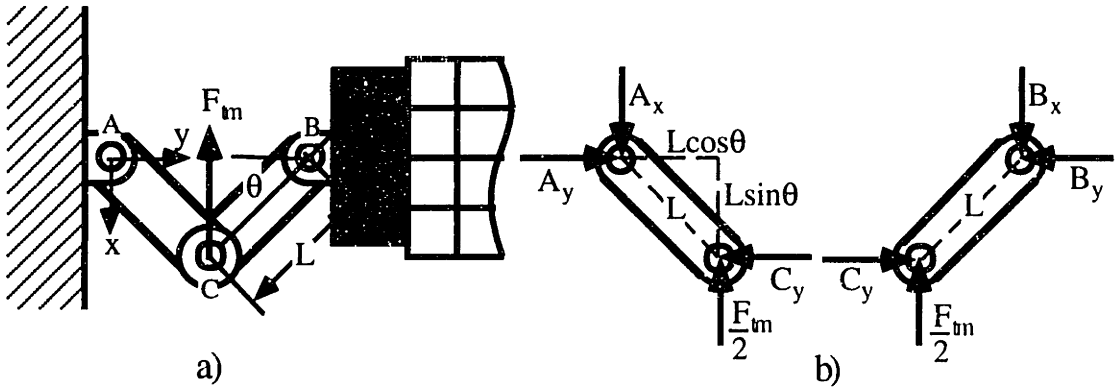

Figure 5.21 - a) Toggle mechanism used for clamping an element matrix b) free-body diagrams of mechanism links c) force amplification versus toggle angle θ and d) input force actuator and clamping wall positions versus θ.

5.3.1.3 Mechanical Wedge or Screw

A wedge mechanism can be used to create a high clamping force for clamping element matrix by amplifying an input force. As seen in figure 5.22a, the input force $\mathbf{F}_w$ applied to a wedge with an incline angle of ϕ is amplified to the clamping force F_{clamp}. The free-body diagrams of both parts of the wedge clamp are shown in figure 5.22b where $\mathbf{N}_A$

is the inclined normal force between the wedges, N_B is the normal force between part B and the horizontal support, N_R is the reaction force from the +x direction restraint on part A, μ_A is the static frictional coefficient between part A and part B, and μ_B is the static frictional coefficient between part B and the horizontal wall. Summing the Y-direction forces acting on part A yields the following equation:

$$F_{clamp} = N_A \cdot (\cos\phi - \mu_A \cdot \sin\phi). \qquad (5.24)$$

Summing the X-direction forces acting on part B yields:

$$F_W = \mu_B \cdot N_B + N_A \cdot (\mu_A \cos\phi + \sin\phi). \qquad (5.25)$$

Summing the Y-direction forces acting on part B yields:

$$N_B = N_A \cdot (\cos\phi - \mu_A \sin\phi). \qquad (5.26)$$

By substituting equation 5.26 and a rearranged equation 5.24 into equation 5.25 and then solving for F_{clamp}, the final expression is

$$F_{clamp} = \frac{F_w \cdot (\cos\phi - \mu_A \sin\phi)}{[(\mu_A + \mu_B) \cdot \cos\phi + (1 - \mu_A\mu_B) \cdot \sin\phi]}. \qquad (5.27)$$

This expression can be used to estimate the clamping load developed by a certain input force. As part B of the wedge is pushed a distance X in the +x direction, the distance δ_{wall} that part A and the compression wall moves in the +y direction is calculated with the relation

$$\delta_{wall} = X \cdot \tan\phi. \qquad (5.28)$$

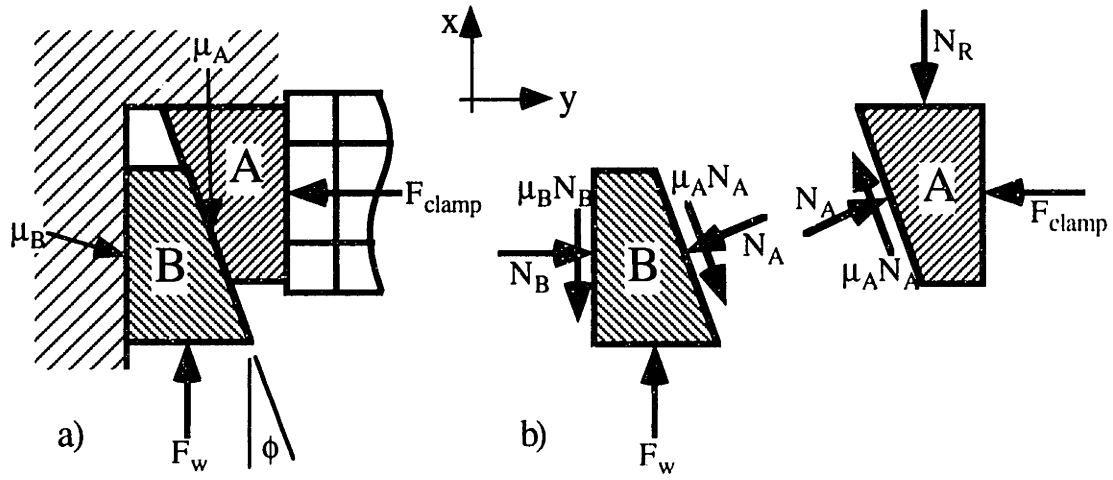

Figure 5.22 - a) Using a mechanical wedge to clamp an element matrix and b) free-body diagrams of the component parts.

A square-threaded power screw can also be used to create a high clamping force. Shigley and Mitchell present an excellent treatment of the theory on power screw operation [Shigley,1983] so the theoretical development will not be presented here. However, the formula for estimating the clamping force generated with a certain input torque **T** on the power screw is

$$F_{clamp} = \frac{2 \cdot T}{d_m} \cdot \left[\frac{\pi \cdot d_m - \mu_s \cdot p}{p + \pi \cdot \mu_s \cdot d_m} \right] \qquad (5.29)$$

where:

d_m = mean screw diameter
p = pitch of the screw and
μ_s = static frictional coefficient between the screw thread and the tapped hole.

5.3.1.4 Stack of Piezoelectric Laminations

The previous three clamping mechanisms (i.e. toggle mechanism, wedge mechanism and power screw) rely on mechanical advantage to amplify an input force into a large clamping force. However, using a stack of piezoelectric laminations only requires a large input voltage, instead of a high input force, to create a high clamping force. The idea of only having to run wire to a thin piezoelectric is very appealing to the designer of a discrete die since it greatly simplifies the mechanical design of the containment frame. For the single piezoelectric lamination shown in figure 5.23a, the clamping force $\mathbf{F_{clamp}}$ generated by a voltage **V** applied across it's thickness $\mathbf{t_p}$ is

$$F_{clamp} = \frac{V \cdot L_p \cdot W_p}{t_{pp} \cdot g_{33}} \qquad (5.30)$$

where:

g_{33} = piezoelectric voltage coefficient
L_p = length of lamination and
W_p = width of lamination.

The force generated by the piezoelectric lamination is limited by the compressive strength of the material σ_{comp}. The limiting condition for the generated force is

$$F_{clamp} < \sigma_{comp} \cdot L_p \cdot W_p. \qquad (5.31)$$

There is also a limiting voltage/thickness $\mathbf{V_{limit}}$ for a piezoelectric material above which the material properties start deteriorating. This condition is expressed as

$$\frac{V}{t_p} < V_{limit}. \qquad (5.32)$$

The force generated with a piezoelectric stack from an applied voltage is typically quite high but the expansion in the thickness direction is quite small. One method of magnifying the overall change in height is to stack a number of piezoelectric laminations in series as shown in figure 5.23b. Making an actuator out of a stack of thin piezoelectric laminations also helps to keep the voltage to thickness ratio from exceeding it's limit. The change in height Δt_p of a stack of **N** piezoelectric elements is

$$\Delta t_p = N \cdot V \cdot d_{33} \qquad (5.33)$$

where: d_{33} = piezoelectric strain coefficient.

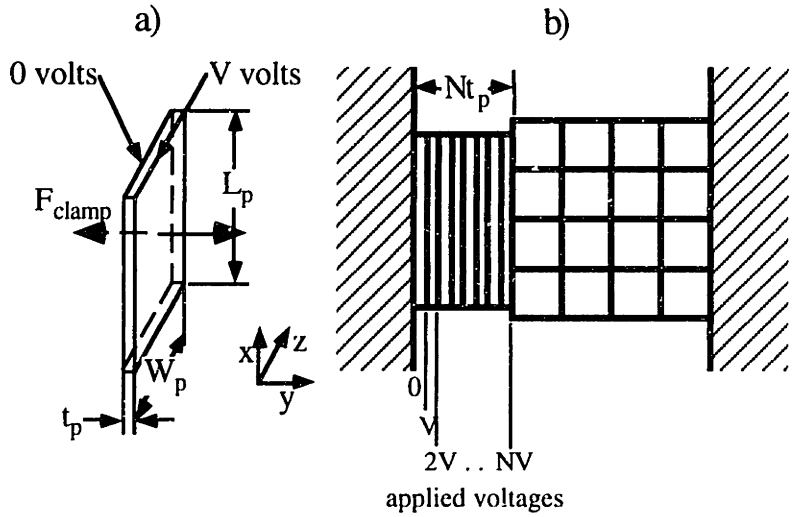

Figure 5.23 - a) Single piezoelectric lamination and b) stack of multiple laminations to increase actuator displacement.

5.3.1.5 Thermally-Induced Contraction of a Discrete Die Frame

An alternative to pushing a compression wall with some sort of actuator (e.g. hydraulic actuator, wedge) is to thermally induce contraction of the discrete die frame. Contraction of the cooled frame into the room-temperature matrix of elements creates an interference fit thereby providing a high clamping force. The frame can be contracted in both the X and Y directions thereby emulating a dual compression wall clamping wall configuration. However only the one-dimensional case, i.e. single compression wall clamping configuration, will be considered for the reasons discussed in section 5.2.2. The

following structural analysis will be used to develop an expression for estimating the clamping force of the one-dimensional case.

By considering a matrix of square elements constrained by a solid frame as shown in figure 5.24a, the frame is cooled by $\Delta T=T-T_o$ where **T** is the temperature that the frame is cooled to and $\mathbf{T_o}$ is it's initial temperature of the entire discrete die. One technique for cooling the discrete die frame is with internal cooling paths. Referring to figure 5.24a, other variables that must be defined for this structural analysis are:

A_f = the total cross-sectional area of the frame's lateral walls

$A_m = n \cdot w \cdot L$ = the cross-sectional area of the element matrix in a plane normal to the loading direction

$L_m = m \cdot w$ (for a simple close - packed matrix)

$= m \cdot w + (m-1) \cdot t_{RD}$ (for an element matrix with row dividers)

[L_m is the width of the element matrix in the column or clamping direction]

α_f = the thermal coefficient of linear expansion of the frame material

E_f = elastic modulus of the frame material and

E_m = elastic modulus of the discrete elements.

Static free-body diagrams of the frame and element matrix are shown in figure 5.24b. The variables defined in this figure are:

δ_f = total expansion of the frame
δ_{mf} = mechanical expansion of the frame due to the distributed clamping load F_{clamp}
δ_{tf} = thermal expansion of the frame
δ_m = total expansion of the element matrix.

Due to the geometric compatibility constraint, then

$$\delta_f = \delta_{mf} + \delta_{tf} = \delta_m. \qquad (5.34)$$

The stress-strain relations for each deflection are:

$$\delta_{mf} = \frac{L_m \cdot F_{clamp}}{A_f \cdot E_f}, \quad \delta_{tf} = L_m \cdot \alpha_f \cdot (T - T_o), \quad \text{and } \delta_m = \frac{L_m \cdot F_{clamp}}{A_m \cdot E_m}. \qquad (5.35)$$

By substituting equations 5.35 into equation 5.34 and the solve for F_{clamp}, the equation becomes

$$F_{clamp} = \frac{\alpha_f \cdot (T - T_o)}{\left[\frac{1}{A_m E_m} - \frac{1}{A_f \cdot E_f}\right]}. \qquad (5.36)$$

Another method for achieving a high clamping force is to have the induced contraction of the die frame as the default, i.e. room temperature, condition. In other words, the frame is contracted about the element matrix at room temperature. The die

elements are unclamped and, therefore, able to be set when the frame expands from being heated up.

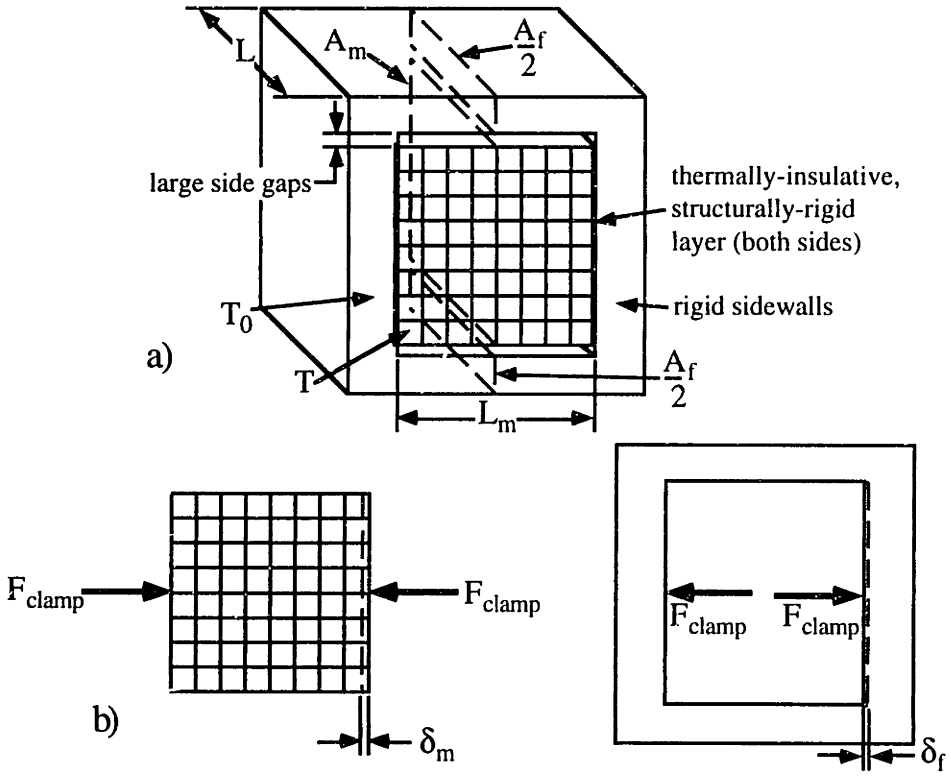

Figure 5.24 - a) Model of a solid die frame that's thermally-contracted into an element matrix and b) free-body diagrams of the matrix and frame.

5.3.1.6 Comparison of High Clamping Force Methods

As part of the process for designing a discrete die, the die engineer must consider all the different types of high clamping force actuators/methods available and then choose the one that best satisfies the design specifications. In this section, the die clamping methods presented in sections 5.3.1.1 to 5.3.1.5 will be compared to highlight the advantages and disadvantages of each. The design specifications used for the subsequent analyses are those of the high-resolution discrete dies shown in figure 5.1. The specified maximum clamping load is 267 kN and the side clamping area of the element matrix is 0.102 by 0.102 meters square so that A_p=0.0104 meters^2. Depending upon the method used to set the element matrix of a discrete die, the compression wall might have to be retracted before the setting operation begins. Since the die surface is set in a parallel

fashion (to be discussed later), the compression wall needs to be retracted by at least 1.0 mm to relieve all the unwanted internal element forces. This required retraction value was determined experimentally using the existing high-resolution discrete dies.

If a hydraulic cylinder is used, it should have a low profile, high maximum pressure, and ideally fit within the given clamping area. A cylinder which satisfies these criteria is a Simplex™ HFJ-30 low-profile hydraulic ram. It's specifications are a profile height of 6.4 cm, A_{cs}=0.00418 m^2, K_f=0.10, and maximum P_o=70 Mpa. Using equation 5.21, a hydraulic cylinder pressure P_o=71 Mpa is needed to achieve the maximum clamping load. Therefore, the Simplex hydraulic ram is adequate for this design example. Generally the advantages of using a hydraulic cylinder in this type of application are:

- the power source need not be co-located with the actuator
- control over the clamping force is simplified since the hydraulic supply pressure is known and
- retraction of the compression wall is simplified by use a spring-return piston.

However, the disadvantages with using a hydraulic cylinder in a discrete die are:

- the tendency for hydraulic fluid leakage with high-pressure cylinders into the element matrix that decreases the μ_s between the elements [Crandall,1978].
- a constant hydraulic pressure source required for clamping and
- the significant thickness of high-pressure rams compared to other types of actuators.

A toggle mechanism used for clamping the element matrix should also have as low a profile as possible. For the purpose of keeping this comparison objective, the profile height assumed for the mechanism will be same as that of the hydraulic cylinder, i.e. 6.4 cm. Link lengths L that will fit within this space are 3.0 cm. The force amplification factor and compression wall displacement for this case are shown in figure 5.21c and 5.21d, respectively. In general, the advantages of using a toggle mechanism are:

- high amplification of the input force when θ approaches 0°
- an inherent locking feature when θ goes beyond 0° (i.e. through the dead-center position) and
- the input force is applied perpendicular to the compression force which allows more room for the input force actuator compared to a parallel orientation.

Some disadvantages in using a toggle mechanism for a discrete die are:

- co-location of the input force actuator
- the compression wall displacement is small compared to that of the input force actuator.

A wedge mechanism can also be used to create a high clamping force for the discrete dies. Assuming that the components of the wedge mechanism are made out of hardened steel and that all sliding surfaces will be lubricated, the static coefficients of friction μ_A and μ_B will both be 0.11 [Crandall,1978]. Referring to equation 5.27, it is evident that a small wedge angle ϕ yields a high mechanical amplification of the input force F_w. Unfortunately, small angles also yield small compression wall displacements δ_{wall} as seen in equation 5.28. If we assume that the displacement available for the input force actuator X is 10 mm because of tight space constraints, using equation 5.28, the necessary wedge angle for the specified δ_{wall} is around 6°. The necessary input force must be 87 kN using equation 5.27. The mechanical amplification of the input force is 3.1 in this case. In general, the advantages in using a wedge for creating a high clamping force are:

- the mechanism can be very compact (i.e. low profile height)
- linear relationship between F_w and F_{clamp}
- significant compression wall displacement is possible if it's needed and
- the input force is applied perpendicular to the compression force.

Disadvantages in using a wedge mechanism for this purpose are:

- the undesirable tradeoff between the mechanical force amplification and the compression wall displacement (i.e. high force amplification requires low wedge angles which yields very little displacement) and
- co-location of the input force actuator.

The compactness of a wedge mechanism was the design characteristic that caused Finckenstein et al. to use this clamping method in their hydroforming discrete die [Finckenstein,1991]. In this case, two wedge mechanisms set in a dual compression wall clamping configuration "bottom-out" bevel springs in the opposing frame walls to achieve a specific clamping force. Furthermore, since the sliding direction of the clamping wedges are the same as the forming direction, the input force comes from the forming force actuator.

A high clamping force for the discrete die element matrix can be achieved by using a common piezoelectric ceramic such as PZT, type 5A. If a PZT actuator that's the same size as the element matrix clamping area is used, then L_p=W_p=0.102 meters. A commonly commercially-available PZT thickness t_p is 0.5 mm [Anonymous,1993b]. With $g_{33} = 0.025 \frac{\text{Volt} \cdot \text{meters}}{\text{Newton}}$ for PZT, the voltage V which yields the desired clamping force is estimated to be 3200 volts using equation 5.30. This voltage is easily achieved with commercially-available high-voltage power supplies. The voltage to thickness ratio is 640,000 volts/meter which is below the limit for the material (i.e. 1,200,000 volts/meter). According to the force limiting condition in equation 5.31, the limiting compressive force that the PZT actuator can take is 5400 kN for a compressive strength of 0.52 Gpa. The 267 kN clamping force is well below this value. Finally, the change in thickness of the actuator (i.e. displacement of the compression wall) is calculated using equation 5.33 with $d_{33} = 450 \times 10^{-12} \frac{\text{meters}}{\text{volt}}$ as 0.0015 mm. This displacement is essentially negligible. Even with N=20 (i.e. t=10 mm), the displacement of the piezoelectric stack is still only 0.03 mm. *The main conclusion that can be drawn from this last calculation is that the displacement of a piezoelectric stack is just too small to be considered a practical actuator.* In other words, it is very doubtful that the clamping force calculated with equation 5.31 is achievable.

A high clamping force can also be achieved by thermally-inducing contraction of the die frame into the element matrix thereby creating an interference fit. Let us assume that the ambient temperature T_0 of a typical stamping plant will be around 20°C. If steel is used for all of the discrete die components (i.e. frame and elements), then $\alpha_t = 11.0 \times 10^{-6} \frac{1}{°C}$ and $E_m = E_f = 210$ GPa. The frame will be the same width as the element matrix, i.e. 0.102 meters. If a frame of rectangular cross section and a thickness of 2.0 cm is used, this gives an area A_f=0.00408 meters^2. Using equation 5.36, the frame temperature must be cooled by 17°C to T=3°C in order to achieve the specified clamping force. Ice water could be used to cool the die frame down to 3°C. Alternatively, the discrete die elements can be set while the frame is heated up by 17°C and then allowed to

cool and contract into the matrix. In general, the advantages of using thermally-induced contraction of the frame are:

- no need of separate force actuators allows for a more compact frame design
- a simplified frame design and
- the need for only a chiller unit to cooling the liquid circulating in the die frame.

However, the disadvantages of using such a clamping method are:

- that the clamping load will diminish over time if the insulation layer between the element matrix and the die frame is poor causing the matrix to cool down
- the clamping force may not be very controllable because of the large time constants with a thermal system.
- the time required to cool or heat the die frame (depending on the room-temperature condition) may take too long.

The choice of a particular method/actuator for achieving a high clamping force in a discrete die will depend on the type (e.g. distributed with hydroforming, concentrated with matched-die forming) and magnitude of the forming forces encountered, the size of the die, space constraints and the manufacturing environment in general.

5.3.2 Structural Stiffness of the Discrete Die

The main design requirement for the discrete die's containment frame and compression wall is that they're stiff enough to withstand the maximum clamping load without deflecting excessively. When the frame and compression wall deflect too much, the clamping load distribution within the element matrix becomes non-uniform. This effect was noticed in the original design of the high-resolution discrete dies shown in figure 5.1. The original thickness of the back support wall (i.e. wall opposite the compression wall) was 1.6 cm. With a clamping load of only 55 kN, the static frictional force of every other element column in the simply-packed element matrix was measured. An Elvax clamping interpolator was used between the die elements and the compression wall. In figure 5.25, the maximum static frictional force is plotted against the columns position in the row direction. The general concave shape of the force distribution curve shows the decrease in clamping force for the middle columns (i.e. it's non-uniformity). The deflection of both the containment frame back wall and the compression wall were measured to see what correlation, if any, exists between the static frictional load distribution and the wall deflections. As seen in figure 5.26, the back wall deflected into a shape that's similar to that of the frictional load distribution. The compression wall also deflected in this shape but with only a 0.055 mm maximum deflection. The shape similarities between the deflected back wall and the frictional load distribution curve (figure 5.25) indicates that there is a strong correlation between deflection of the frame and the clamping load distribution of the element matrix. What is learned from this experimentally-measured effect is that the load-bearing members of the discrete die must have sufficient stiffness to keep the clamping load distribution within the element matrix uniform. The discrete die frame redesign that eliminates this problem is discussed in section 5.8.

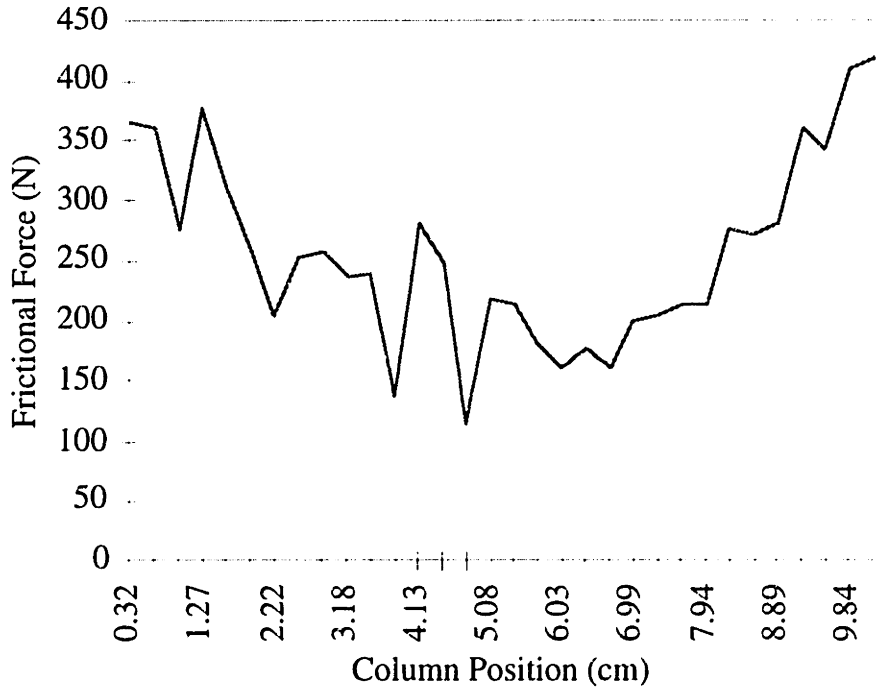

Figure 5.25 - Static frictional force of an element column versus column positions.

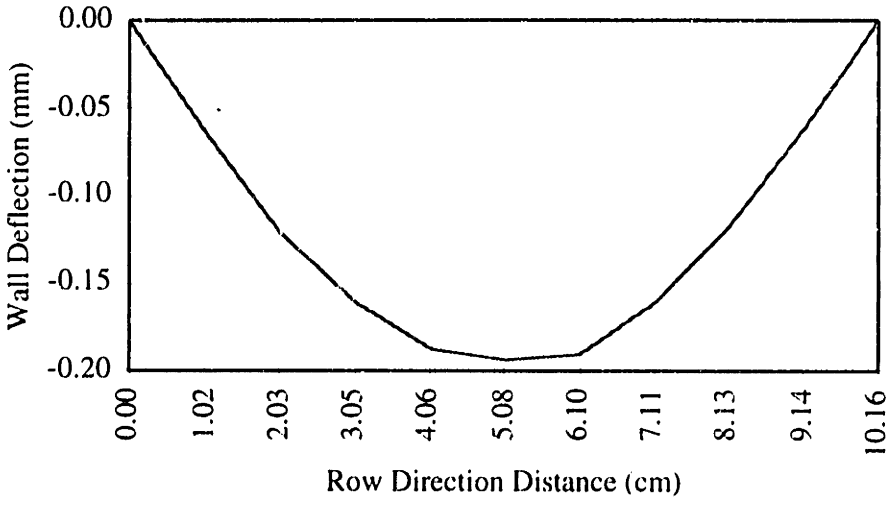

Figure 5.26 - Back wall deflection of the high resolution discrete die.

5.4 SMOOTHING THE DISCRETE DIE'S FORMING SURFACE

Regardless of which type of die forming is used (e.g. matched-die, hydroforming), there will be concentrated forming loads on the sheet metal from each of the discrete die's spherical-shaped elements. The concentrated forming loads lead to an unacceptable dimpling of the sheet metal during forming. As seen in figure 5.27, a simple remedy for this problem is to use a deformable interpolating material (e.g. neoprene) which fills in the gaps between elements and helps to distribute the concentrated forming loads [Hardt,1981]. This deformable material has been called an 'Interpolator' since it acts like a mechanical interpolator between the fixed discrete elements. [Ousterhout,1991] used neoprene and urethane forming interpolators and found that their physical and material properties changed over successive forming trials. [Eigen,1992] later pointed out that the ideal interpolating material first allowed the material to easily flow into the gaps between elements and then it hardens as it is compressively stressed during the later stages of forming. The stress-strain curve material for such a material is shown in figure 5.28. However, Eigen also identified a material, Ethylene Vinyl Acetate (Elvax), that could be premolded to the die surface—in a softened state and then allowed to cool back to room temperature—thereby filling in the gaps between adjacent elements. As is shown in figure 5.28, the ideal premolded interpolator material should simply be as hard as possible. Elvax was chosen because of it's low moldability temperature, ability to retain a molded shape after cooling, and higher hardness than neoprene or urethane. Eigen also showed that the range of part shapes that could be formed expands when an Elvax interpolator is used instead of a non-premoldable material like neoprene or urethane.

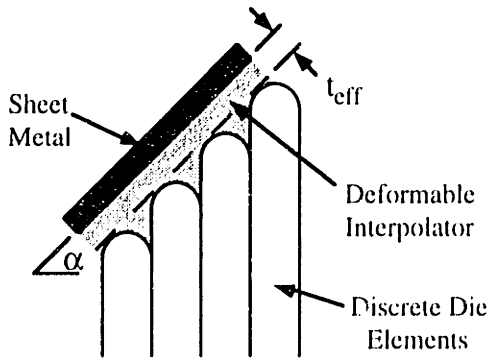

Figure 5.27 - Interpolator used to smooth out the a discrete die's forming surface.

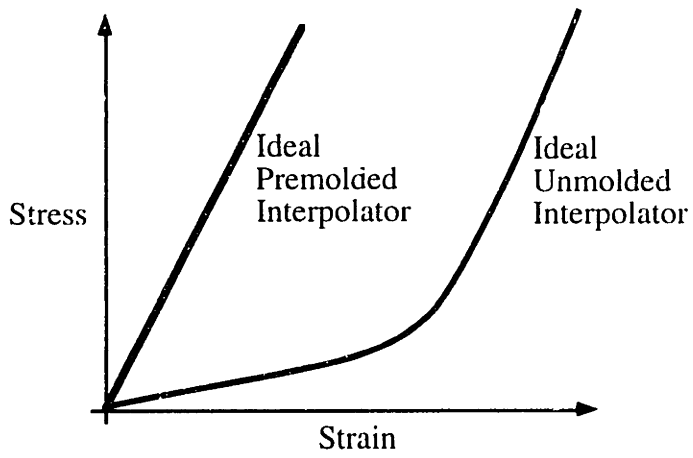

Figure 5.28 - Curves of stress vs. strain for idealized interpolator materials.

When a pre-moldable material like Elvax is used as the interpolator, determining the effective thickness is important for estimating the shape of the interpolator-covered element matrix. Since the interpolating material typically begins as a uniform thickness sheet of thickness **t** that is pressed into the dimpled surface of the die, the effective thickness $\mathbf{t}_{\mathbf{eff}}$ of the interpolator molded to a discrete die surface, inclined to an angle α, can be estimated by considering the 2-dimensional incline as shown in figure 5.27 and the single spherical end of a single element as shown in figure 5.29. The enclosed volume $\mathbf{V}_{\mathbf{enclosed}}$ shown in figure 5.29 is calculated with the expression:

$$V_{enclosed} = V_{box} - \left[\frac{V_{sphere}}{2} - 4 \cdot \left(\frac{V_{sec\,tor}}{2}\right)\right] \qquad (5.37)$$

where: V_{box} = volume of the box that encloses the element's tip

V_{sphere} = volume of a sphere of radius R

R = radius of the circle that circumscribes the elements square cross-section and

V_{sector} = sector of the sphere which is truncated by any of the elements sides.

Since $R = \frac{\sqrt{2}}{2} \cdot w$, $V_{box} = w^2 \cdot R$, $V_{sphere} = \frac{4}{3} \cdot \pi \cdot R^3$ and

$V_{sec\,tor} = \pi \cdot \left(R - \frac{w}{2}\right)^2 \cdot \left(\frac{2 \cdot R}{3} + \frac{w}{6}\right)$, then equation 5.37 simplifies to

$$V_{enclosed} = 0.1386 \cdot w^3. \qquad (5.38)$$

Referring to figure 5.30 which is valid for inclinations angles α less than 45°, the area of the shaded triangle $\mathbf{A_1}$ is

$$A_1 = \frac{P^2}{2 \cdot \tan\alpha}. \qquad (5.39)$$

In this case, the volume of material $\mathbf{V_{fill}}$ that fills into the gaps between elements underneath the tangency line is $(V_{enclosed} - A_1 \cdot w)$. Substituting equations 5.38, 5.39, and the expression for variable P defined in figure 5.30 into this preceding expression, yields

$$V_{fill} = w^3 \cdot \left\{ 0.1386 - \frac{w^2}{4} \cdot \left[\frac{1}{\tan\alpha} \cdot \left(1 - \frac{1}{\cos\alpha} \right)^2 + \sqrt{2} \cdot \left(1 - \frac{1}{\cos\alpha} \right) + \frac{\tan\alpha}{2} \right] \right\}. \qquad (5.40)$$

Referring to figure 5.31 which is valid for inclination angles α greater than 45°, the area of the shaded triangle $\mathbf{A_2}$ is

$$A_2 = \frac{\left(R - \frac{w}{2} \right)^2}{2 \cdot \tan\alpha} \qquad (5.41)$$

since the tangency line is always in contact with point O. In this second case, V_{fill} is $(V_{enclosed} - A_2 \cdot w)$. Substituting equations 5.38 and 5.41 into this preceding expression yields

$$V_{fill} = 0.1386 \cdot w^3 - \frac{w \cdot \left(R - \frac{w}{2} \right)^2}{2 \cdot \tan\alpha}. \qquad (5.42)$$

Referring to figure 5.30, the volume of interpolator material $\mathbf{V_{before}}$ in one element width between the two tangency of adjacent elements before molding is

$$V_{before} = \frac{t \cdot w^2}{\cos\alpha}. \qquad (5.43)$$

The volume of material $\mathbf{V_{after}}$ above the tangency line after molding the interpolator material (i.e. gaps are filled in) is

$$V_{after} = \frac{t_{eff} \cdot w^2}{\cos\alpha}. \qquad (5.44)$$

Assuming a constant volume situation as the element gaps are filled in during molding, then we know that $V_{after} = V_{before} - V_{fill}$. Substituting in equations 5.43 and 5.44, and solving for t_{eff} yields

$$t_{eff} = t - \frac{V_{fill} \cdot \cos\alpha}{w^2}. \qquad (5.45)$$

In summary, estimating the effective interpolator thickness with equation 5.45 requires that equation 5.40 be used if $\alpha<45°$ and equation 5.42 be used if $\alpha>45°$.

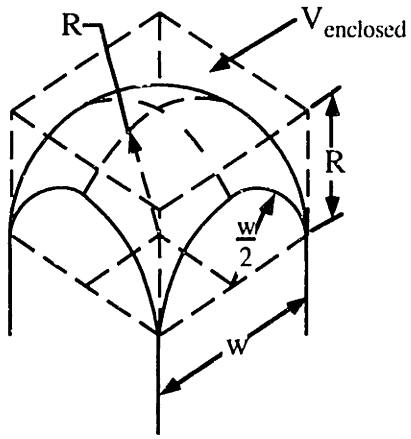

Figure 5.29 - Spherical tip of a single die element.

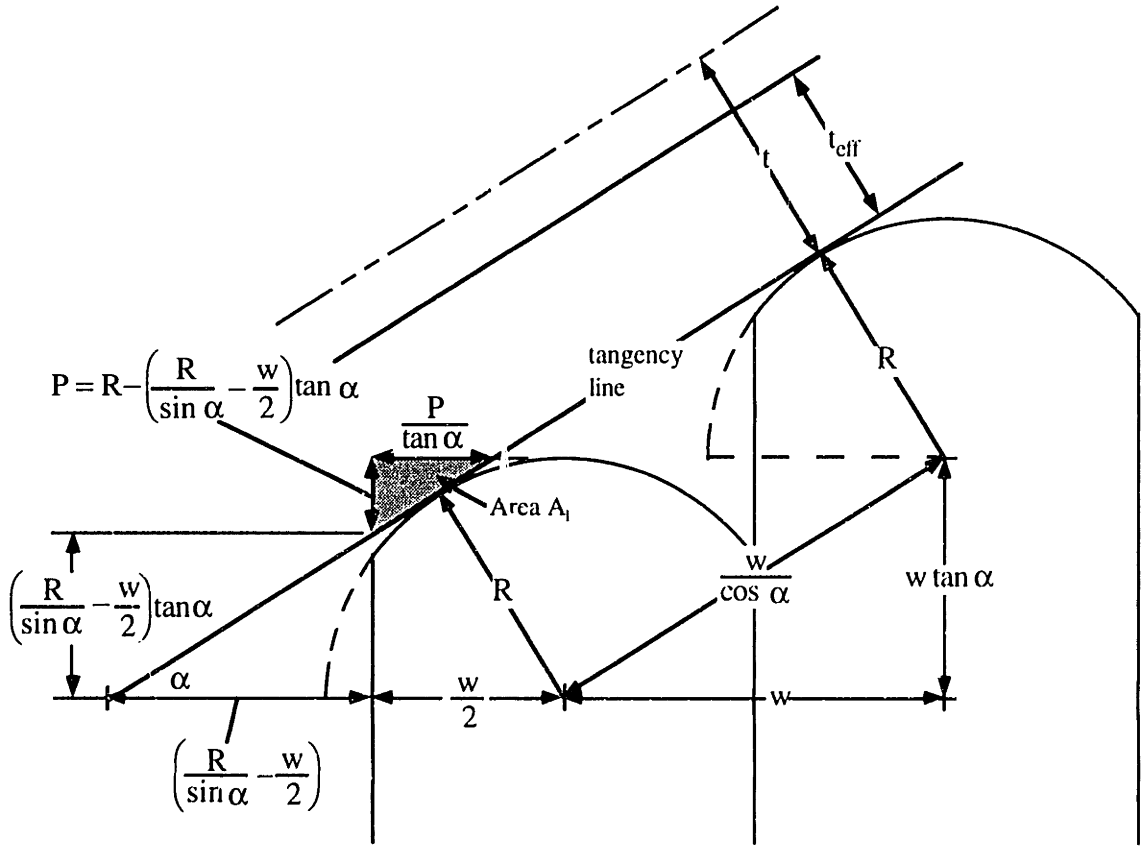

Figure 5.30 - Side view geometry of a surface interpolator preformed over spherical-tipped die elements for wall angles less than α=45°.

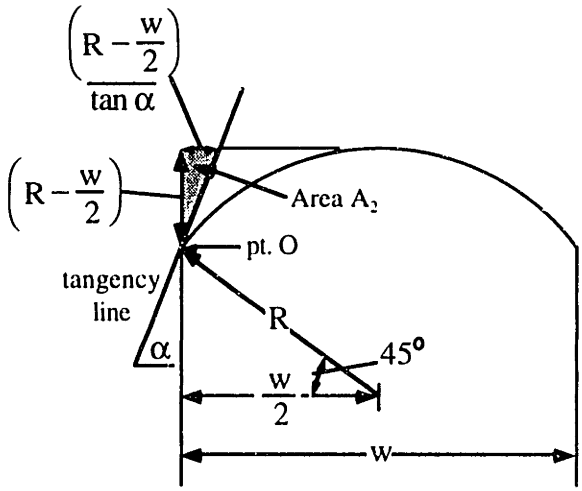

Figure 5.31 - Side-view geometry of a surface interpolator preformed over spherical-tipped die elements for wall angles greater than or equal to α=45°.

5.5 SETTING THE SHAPE OF A DISCRETE DIE

In sections 5.1 to 5.4, the construction details and mathematical relationships needed to design the various components of a reconfigurable discrete die are presented. This includes the die elements, element matrix clamping configuration, die frame details, and methods for smoothing the die surface. Once a discrete die is designed and constructed, there must be some technique for automatically setting the shape of the element matrix for this fabrication method to be considered rapid. In this section, both existing and newly-developed methods and mechanisms used for setting the desired shape of the discrete die are discussed. For the remainder of this chapter, the element matrix setting operation will simply be referred to as "setting". The two main goals for the setting method and mechanism chosen are to maximize speed and accuracy.

5.5.1 Serial Setting Methods

The simplest but unfortunately slowest method for setting an element matrix is to do it in a serial fashion, i.e. one element at a time. As seen in figure 5.32a, this can be done with an element pusher which is mounted to a 3-axis (x,y,z) CNC-controlled machine. Hardt and Webb used this method for setting a small 13x13 element experimental die used for rubberforming sheet metal parts [Hardt,1982]. During the setting operation, unwanted

interactions between adjacent elements were avoided by placing thin aluminum strips between all the elements in both the row and column directions.

[Finckenstein,1991] has developed a vertically-oriented machine which automatically sets a discrete die consisting of a 33 by 33 matrix of 6 mm square elements. Using a 4-axis servomechanism with a rotating engagement tip, the machine positions a 33 by 33 matrix of equal-length threaded rods (threaded into a common base plate) in a serial fashion. This matrix of threaded rods, similar to the infinitely variable surface generator built by [Wolak,1973], is then used to impart the desired die shape onto the discrete die. Specifically, the elements of the discrete die, which are placed above the matrix of threaded rods, are allowed to fall vertically onto the positioned rod ends thereby acquiring the desired shape. Since the die elements are all falling onto a master model, the element/element interactions do not matter. The element matrix is then clamped from the side to retain the element positions.

Another serial setting method which is faster than individually pushing each element is to sweep a knife-blade stylus back and forth across the element matrix. As shown in figure 5.32b, [Nakajima,1969] used a sweeping stylus mounted to a 3-axis numerically controlled machine tool to set a discrete die made up of round elements. The wall angle of the die shape being set was limited by the angle γ of the sweeping stylus. Furthermore, several sweeps had to be made over each element row to get the desired shape. Unwanted interactions between elements during setting were minimized (but not avoided) by mounting the sweeping stylus to an ultrasonic vibrator. Nakajima found that ultrasonic vibration tends to break up the friction between adjacent elements.

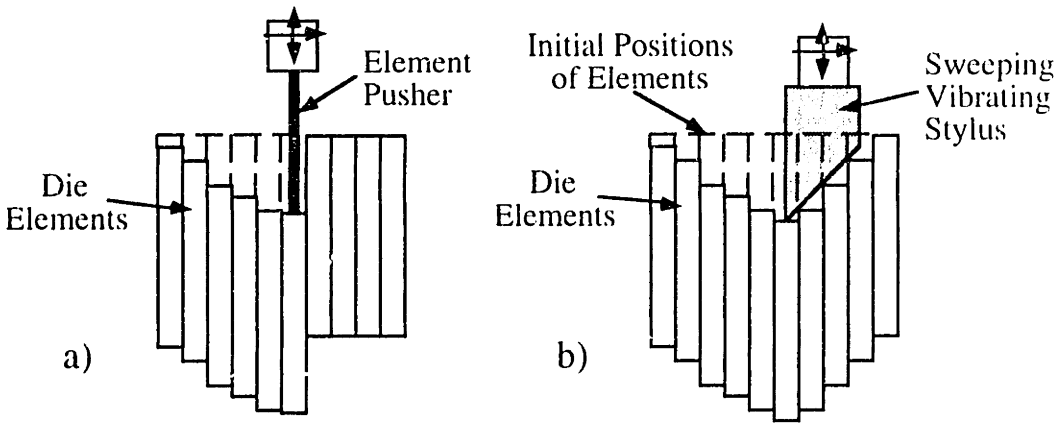

Figure 5.32 - Serial setting methods for a discrete die using a) an individual element pusher and b) a sweeping stylus.

5.5.2 Element Row Setting Methods

Naturally, the element matrix setting operation will not be as time-intensive if it's performed in a more parallel fashion. For example, setting the matrix row by row will significantly reduce this time. Robinson [see Hardt,1985] devised a clever method for setting the shape of discrete die element rows by isolating them from one another with sheet metal dividers that are rigidly attached to the die frame. This configuration, shown in figure 5.16 and also discussed in section 5.2.6.1.2, greatly enhances the forming load capacity of a clamped discrete element matrix. In terms of setting the die's shape, the advantage of this configuration is demonstrated in figure 5.33 which shows an isolated view of a single element row. When the element matrix is put under a "low" clamping force, the frictional forces at the element/row divider (denoted by triangles) exceed those of the element/element interfaces (denoted by circles). Moreover, since the element/row divider frictional forces are transferred from the dividers to the die containment frame, the individual element can be moved without disturbing any adjacent elements.

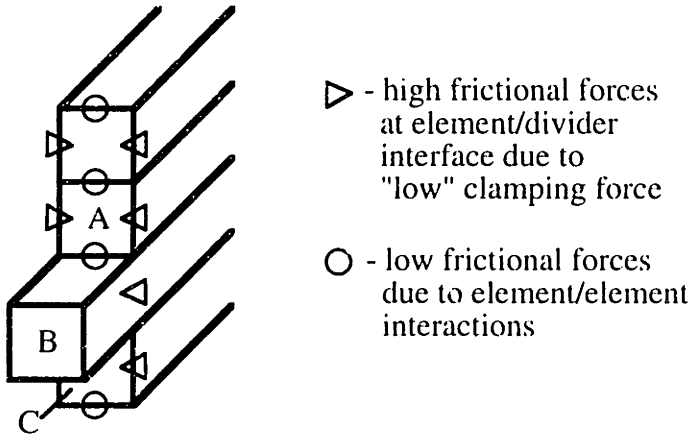

Figure 5.33 - Isolated view of an element row being set with element B not interfering with elements A and C.

By using the element row divider configuration shown in figure 5.33, all that is needed to set a particular element row is a profiling mechanism (profiler) which transfers a specific profile shape to that row. A profiler consists of a series of pushing elements

which are equal in number and spacing to a element rows of the discrete die being set. The shape transfer occurs when the profiler is pushed into the row from the non-forming side of the die. The entire discrete die element matrix is set by moving the profiler behind each element row and repeating this procedure. Several profiler designs which utilize numerous motion and force actuators have been developed for setting discrete dies. One profiler design requires 1 force actuator for clamping all the pushing elements into position, 2 translational actuators (Y and Z axis), and an individual force actuator for each of the pushing elements [see Hardt,1985 for details]. Another profiler design requires 1 force actuator for clamping the pushing elements into position, 2 translational actuators (Y and Z axis), and an individual translational actuator for setting the position of each pushing element [see Ousterhout,1991 for details].

As shown in figure 5.33, an alternative profiler design has been developed by the author which has significantly fewer actuators than the two previously-mentioned designs. Fewer actuators simplify both the mechanical design of the profiler, and the motion and force control effort needed. As illustrated in the figure, a stack of profiling plates (pushing elements) are initially pushed up against a rear wall (home position). An engagement bar engages the profiling plates by the their aligned V-notches, thereby allowing the profiling carriage to move the stack of plates horizontally (Z-direction). A specific profile is created by simultaneously moving the entire profiling carriage (i.e. translate the engaged plates in the z or element length direction), translating the engagement bar upwards (as shown in figure 5.34) to release the lower plates into their required position, and clamping the last disengaged plate with the side clamp as shown in figure 5.35. The upward motion of the plate side clamp and the engagement bar are synchronized (i.e. connected to same vertical actuator). Once that all of the plates are set to their correct positions to give the desired profile, the engagement bar stops translating vertically and then the top clamp rigidly clamps the entire stack of plates. The profiler then moves into the back side of the discrete die (pos. Z direction) which pushes the clamped stack of profiled plates into the particular row of elements being set. The Z-direction translational actuator for the profiler is not shown. After the row has been set, the profiler then moves back to it's original position. After the profiler retracts back to it's original position, the top clamp releases the plate stack and the profiling carriage moves to it's forward-most position (+ Z direction). A retracting wall extends to engage the tabs on the back end of the profiling plates as shown in figure

5.36. The profiling carriage returns to it's home position thereby dragging all of the extended profiling plates along with it (i.e. extended retracting wall engages plates as it moves in the negative Z-direction) until they are again pushed up against the rear wall. Once all of the profiling plates are returned to their starting position, the side clamp and engagement bar descend (neg. X-direction) completely to start the cycle all over again. The engagement bar engages all of the profiling plates as it descends. After each profiling cycle, the entire profiler moves transversely (Y-direction) by one element width. This alternative profiler design only requires 4 translational actuators and 1 force actuator.

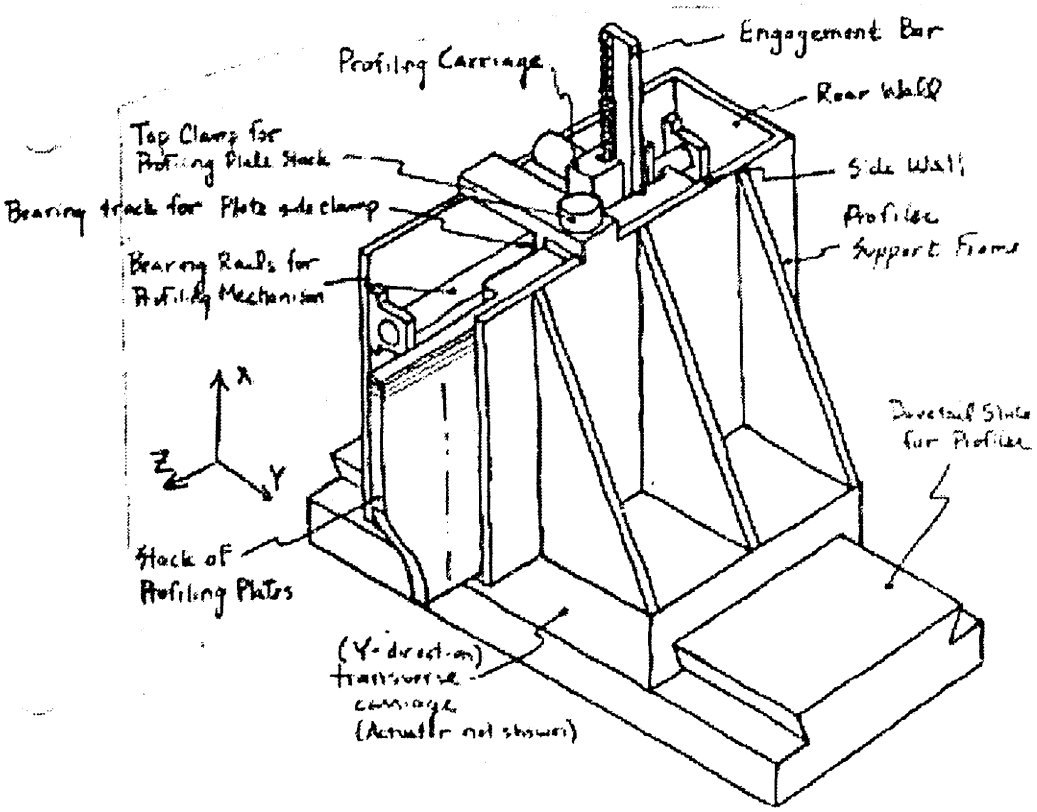

Figure 5.34 - Isometric view of the discrete die profiling mechanism

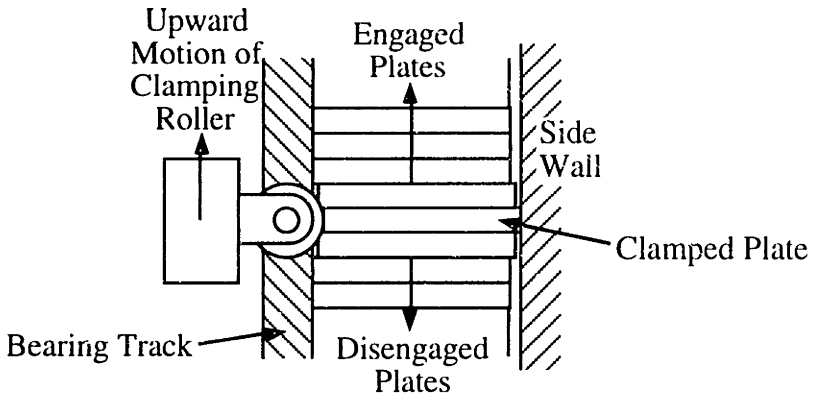

Figure 5.35 - Front view of the profiling plate side clamping mechanism.

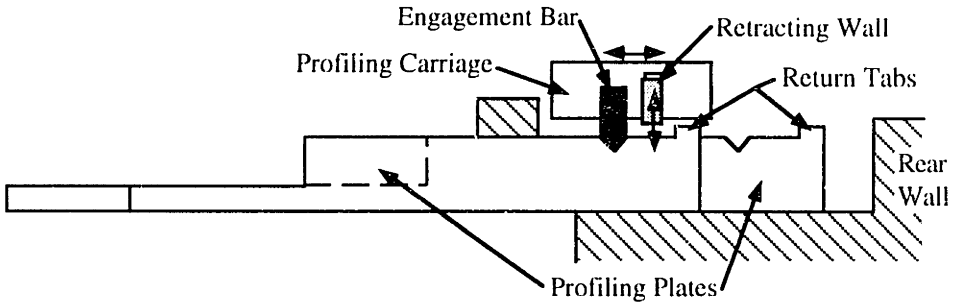

Figure 5.36 - Top view of the profiling plate stack and carriage.

5.5.3 Parallel Setting Methods

If setting the elements of a discrete die in a parallel fashion, i.e. all at once, is at all possible, this will take the least amount of time of any method. The two basic parallel setting methods are to drop the elements onto a master shape or actuate each die element individually if it's practical.

As shown in figure 5.37, the elements in a discrete die can be oriented vertically, unclamped, and then allowed to fall via gravity onto a master model of the intended die surface. It is best to let the forming side of the element matrix (i.e. spherical ends) fall into a negative image of the intended die shape. As a result the uniformity of the element lengths is not an important issue, i.e. elements can remain be rough cut on the non-forming end. If die elements tend to stick together during setting, ultrasonic vibrations applied to element matrix will help to break up the frictional forces between elements that are interfering with the setting process. This type of parallel setting method was used by [Hess,1931] for setting a pair of matched dies used for forming individual sheet metal

supports for shoes. The master models in this case were the feet of the customers. For an arbitrary die surface shape, the master model can be made out of a inexpensive material (e.g. plastic, hard wax) that doesn't have to have the high compressive strength required for sheet metal forming. Many layer manufacturing methods can be used for making these type of master models such as SLA, SLS, 3DP, and LOM (discussed in section 2.2.1.2).

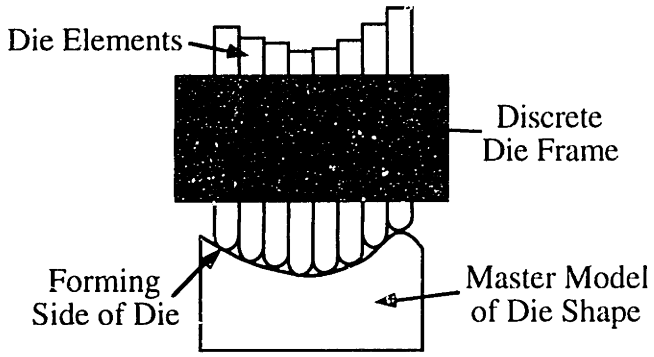

Figure 5.37 - Setting a discrete die with a master model.

Unfortunately using a master model to set the discrete die's shape does not meet the criteria set forth in section 2.3 regarding rapid fabrication methods. The criteria states that the link between the computer model and fabrication of the die shape must be direct. However, the other method involving individually-actuated elements does meet this criteria. For small elements (i.e. widths up about 20 mm), this is a very improbable method because of insufficient space for individual actuators and position sensors. Row setting methods are best used for smaller elements. When the die elements get larger, individual actuation of an element in a packed die matrix becomes more plausible. Furthermore, individually actuating each element makes individual locking also possible thereby obviating the need for side clamping of the die matrix.

For large elements, i.e. widths of 20 mm and larger, the author suggests that individual actuation and control of each element be considered. Two methods for actuating an element are by purely mechanical means and with hydraulics.

5.5.3.1 Mechanical Actuation of Individual Elements

Using a tubular element construction as proposed in section 5.1.2 and assuming there is no element rotation in a constrained matrix, one method of mechanically actuating an element is to incorporate an integral driven leadscrew and threaded base that acts as the nut (see Figure 5.38). The die element moves vertically when the leadscrew is rotated by some kind of actuator (e.g. individual DC motor). Position sensing of the element heights during the setting operation can either be performed in some parallel fashion or individually by equipping each spur gear with an optical encoder.

Assuming that the leadscrew is of sufficient axial buckling strength, mechanical actuation of the die elements has the advantage of obviating any need for side clamping. This entire vertical component of the forming load on the element tip is taken by the leadscrew in this case.

However, there are several disadvantages to this purely mechanical approach. There is a high degree of mechanical complexity associated with the high number of moving parts (e.g. solenoid cores, gears, leadscrews). This increases the chances of some mechanical failure occurring. Furthermore, if forming pressures get too high, the mode of failure of the leadsrew will be to buckle which may cause damage to the discrete die.

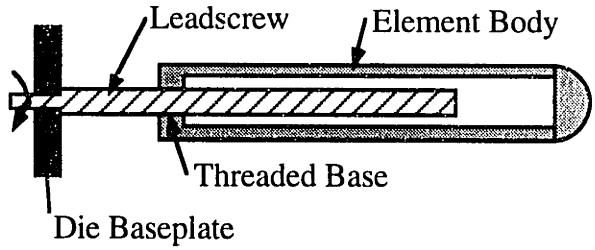

Figure 5.38 - Die element actuated with an integral motor-driven leadscrew.

5.5.3.2 Hydraulic Actuation of Individual Elements

To allow individual actuation of die elements, each element can be made into a hydraulic cylinder if a tubular element construction is used. As shown in figure 5.39, such an element will have a centrally-located hole running through it's entire length. This hole must have a smooth surface finish to insure that a good hydraulic seal is maintained and to minimize the variability in sliding friction as the element body moves upward. The upper

end of the element is capped with a cast or machined spherical tip. The joint between the element head and the element body must provide a good hydraulic seal.

Actuation becomes possible when the hollowed-out element body is slipped over a stationary hydraulic supply tube. The outer diameter of the tube's head and inner diameter of the element body produces a slight slip fit. Then an O-ring seal, that fits into a radial groove near the top of the tube, creates the hydraulic seal. The hydraulic supply tube is connected to the top side of a base plate. It allows hydraulic fluid to enter the cylinder volume and push the element body upwards. Hydraulic fluid enters from the back side of the base plate. If the dead weight of the element and/or contact friction of the compressed O-ring provides insufficient preload for maintaining the hydraulic seal, a retaining/friction plate attached to the bottom of the element body can provide extra static friction.

Volumetric flow into the die element's die cavity, and hence the element's vertical position, are controlled by a simple normally-closed hydraulic servovalve. The velocity $\mathbf{V}_e$ that an element will travel at in the upwards direction is determined from the relationship:

$$V_e = \frac{\dot{Q}_e \cdot \pi \cdot D_e^2}{4} \tag{5.46}$$

where: $\dot{Q}_e$ = volumetric flow rate of the hydraulic fluid into the element.
D_e = diameter of the hole bored into the element body.

Assuming that an incompressible hydraulic fluid and a constant volumetric flow rate supply are used, the time **t** for the element to reach an elevation $\mathbf{Z}_e$ above it's datum (starting position) is

$$t = \frac{Z_e}{V_e} = \frac{4 \cdot Z_e}{\dot{Q}_e \cdot \pi \cdot D_e^2}. \tag{5.47}$$

Using a suitable control system to control the heights of each die element, a 2-dimensional matrix of these hydraulically-actuated elements constitutes the forming die as shown in figure 5.40 (side view shown). In this configuration, all of the supply tubes are rigidly connected to a common base plate on a grid spacing equal to the width of the die elements.

Setting of the die shape is done using closed-loop control with a minimum of sensors and other control devices. Simple on/off-type hydraulic servovalves for each element are located as close as possible to the element's hydraulic inlet. This minimizes the dynamic reaction time of the actuation system. Furthermore, a grid of hydraulic supply lines coming from a single hydraulic pump will supply fluid to each element as shown in figure 5.40. During the setting operation that's shown in the same figure, all of the

elements are supplied with low-pressure fluid to force them up against a slow, upwardly-moving, position-servoed rigid platen. The platen must be stiff enough to resist any excessive deflection or out-of-plane (X-Y) rotation that diminishes the accuracy of the setting operation. The position of the platen is sensed by a single linear encoder. When a particular element has reached it's specified position, the hydraulic servovalve controlling fluid flow into that element is deactivated. This stops the fluid flow into the element and also it's upward movement. Assuming that there is sufficient frictional resistance within this particular element, neighboring elements will not be able to drag it upward any further since the hydraulic loop is closed. The platen stops moving, i.e. the die is set, when the highest element position has been reached. If needed, the position of each individual element can be verified by some parallel-type sensor as described by [Karlin,1995].

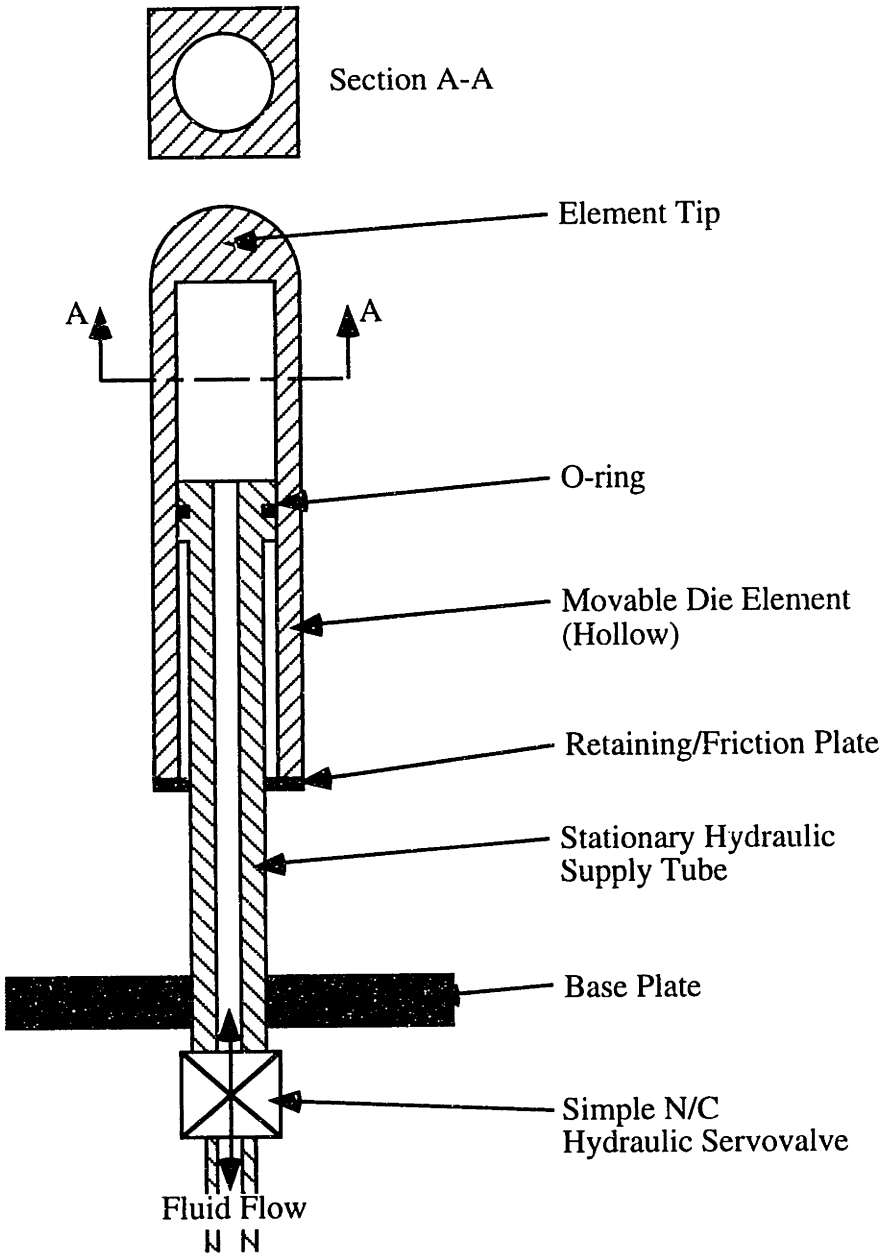

Figure 5.39 - A Hydraulically-actuated die element

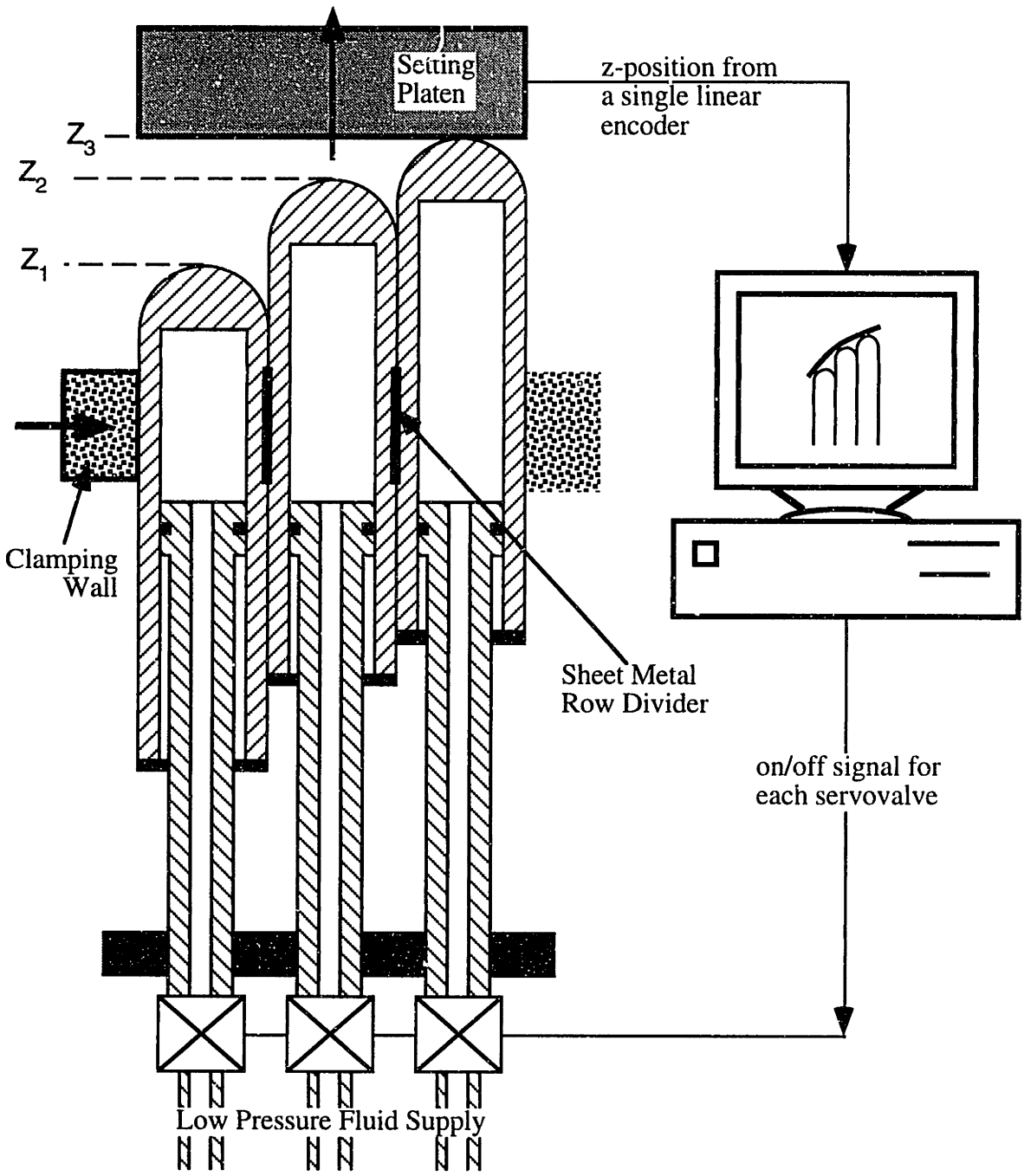

Figure 5.40 - Upwardly moving, servoed platen used to set the discrete die element positions.

Under high forming loads, i.e. high fluid pressures, a hydraulically-actuated die element will experience significant vertical deflection $\Delta \mathbf{h}$ because of the fluid's compressibility. As an example, let us assume that an axial forming force of 2 kN is applied to a 25 mm square die element of bore diameter 15 mm thereby creating an internal cylinder pressure of 11.3 MPa. Furthermore, the element will be extended so that the

resultant column height **h** of the hydraulic oil is 0.5 meters. The coefficient of compressibility (fractional volume change/pressure change) for standard hydraulic oil is 7.0×10^{-10}/Pascal. The change in height is determined from the relation:

$$\Delta h = -h \cdot (\Delta \text{ pressure}) \cdot (\text{coefficient of compressibility})$$

In this example, Δh = -4 mm. Vertical deflection of this magnitude would necessitate that the entire element matrix be side-clamped into a rigid tool, as shown in figure 5.40, during forming.

When compared to the purely mechanical actuation described in section 5.5.3.1, hydraulically-actuated elements have two advantages. The most important one is the reduced mechanical complexity of the die because of fewer moving parts, i.e. no electrically-actuated clutches, turning lead screws, or spur gears. Another advantage is that only a single power supply (hydraulic pump) is needed to actuate the elements as opposed to individual drive motors for each column.

The one disadvantage of hydraulically-actuated elements involves the compressibility of the hydraulic fluid and the associated vertical deflections from high forming loads. As a result, side clamping of the element matrix will be required in most forming situations.

As discussed in section 5.1.2, the difference in bending stiffnesses, i.e. second moments of cross-sectional area, between solid and tubular elements is not that significant. The same is also true between a solid die element and the tubular cross-section of the hydraulically-actuated die elements. For example,Referring to figure 5.41, if we let w=25 mm and D_e=15 mm (as before), the second moments of area are 32600 mm^4 and 30100 mm^4 for the solid and tubular cross-sections shown in figure 5.41, respectively. This means that bending stiffness has only decreased by 8% in this case.

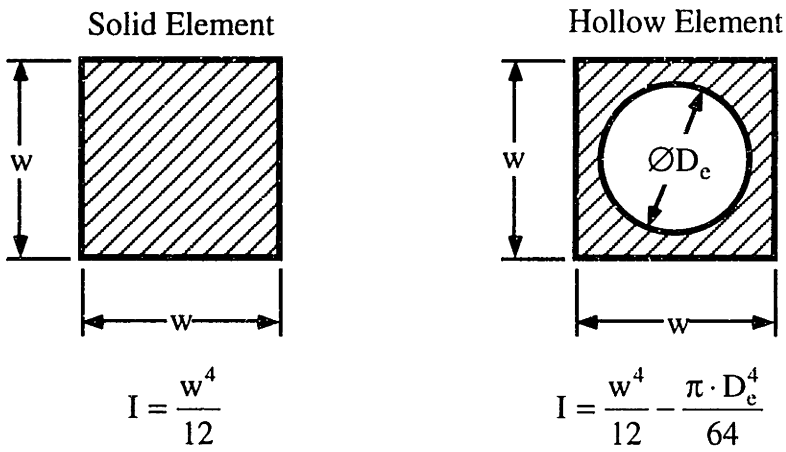

Figure 5.41 - Differences in bending stiffness between elements of solid and hollow cross-section.

5.6 DETERMINING ELEMENT POSITIONS FROM A CAD MODEL

[Ousterhout,1991] has shown experimentally that a closed-loop control algorithm can be used to automatically determine the surface shape of a discrete die, i.e. prescribe the element positions, that will stamp a particular sheet metal part shape. The local interpolator thickness, sheet metal thickness, and all physical and mechanical complexities of the forming situation are automatically accounted by the algorithm. [Karafillis,1994] has shown that this closed-loop development process can also be done using FEA simulations. Since the output from a simulation will only be the mid-plane surface of the sheet metal part while it's sandwiched between the two dies, we discuss in this section the details of determining element positions based on the geometry of the mid-plane surface.

To determine the z-positions of the die elements, let us assume that the mid-plane surface of the forming die(s) is prescribed (i.e. CAD model or locus of points output from a FEA analysis). Typically the whole die surface will be an assembly of connected parametric surface patches each defined by two parameters **u** and **v**. As shown in figure 5.42a, the x, y, and z coordinates of points on a particular patch **S(u,v)** are functions of these two parameters: $0 \leq u \leq 1$ and $0 \leq v \leq 1$. Defining complex 3-D surfaces like that of the die's midplane with parametric representations (e.g. Bezier or B-Spline surface) is very common in industry [Faux,1979]. For a point $\mathbf{P}(\mathbf{u}_1,\mathbf{v}_1)$ on the surface S(u,v), the unit normal vector $\mathbf{n}(\mathbf{u}_1,\mathbf{v}_1)$ to the surface is defined by

$$n(u_1, v_1) = \frac{P_{u1} \times P_{v1}}{|P_{u1} \times P_{v1}|} \tag{5.48}$$

where: ($\times$) is the vector cross product

P_{u1} = partial derivative $\frac{\partial S(u_1, v_1)}{\partial u}$ and

P_{v1} = partial derivative $\frac{\partial S(u_1, v_1)}{\partial v}$.

As seen in figure 5.42b, the center of an arbitrary die element's spherical tip, $\mathbf{C(x_c,y_c,z_c)}$, will be the tail of a vector **T** which contacts the mid-plane surface S(u,v) at a specific point $P(u_1,v_1)$. The length of vector T is defined by

$$\left|\bar{T}\right| = \frac{\sqrt{2} \cdot w}{2} + t_{eff} + \frac{t_{sm}}{2} \tag{5.49}$$

where: t_{eff} is estimated by equation 5.45

t_{sm} = thickness of the sheet metal blank.

Point **P** is the correct tangency point for determining the die element's z-axis position if the orientation of vector T is the same as that of unit normal vector $n(u_1,v_1)$.

The algorithm for determining the point P and hence, the correct z-height, will be described in general terms. The tail of vector T is constrained to lie somewhere along a line that is parallel to the z-axis and goes through point (x_e,y_e). The head of vector T will contact the surface S at some arbitrary point P. Several iterations will be required to find the local tangency point $P(u_1,v_1)$ since the Cartesian coordinates (x,y,z) of points on the surface are functions of u and v. [Choi,1988] developed an algorithm for finding a z-position of a parametric surface for a given point (x_e,y_e). This can serve as the initial guess of the tangency point. If two tangency points are found (e.g. near a sharp bend in the surface), then the point which yields the smaller z-position is the correct one (i.e. lowest point method). [Faux,1979] discusses the details of spatial searching algorithms that can be used to find a tangency point on a parametric surface representations.

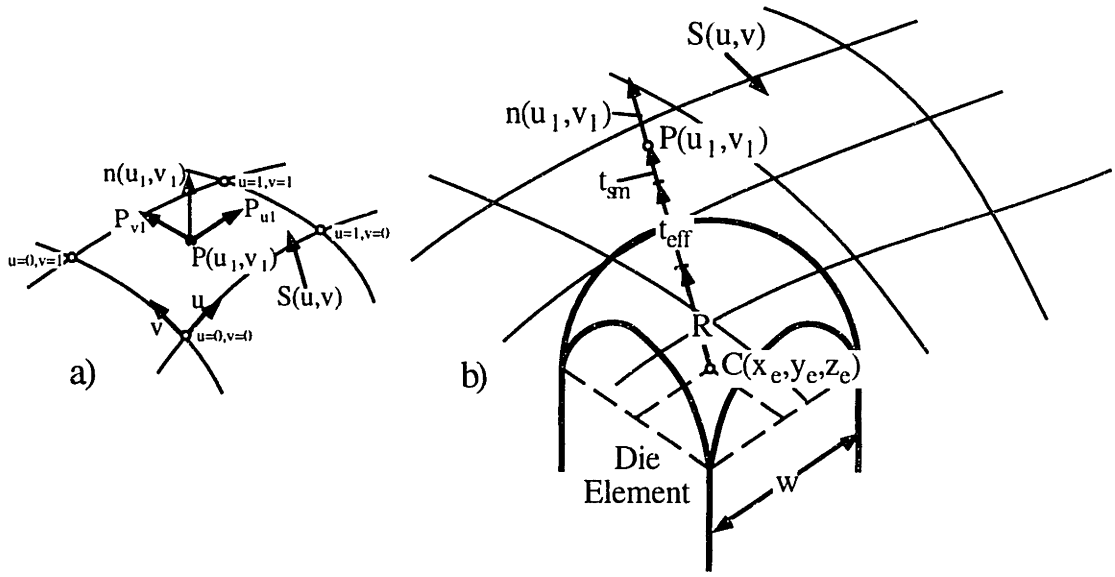

Figure 5.42 - a) Normal vector at a point P on a forming surface model and b) method for determining the tangency point of a discrete die element.

5.7 FABRICATING AND SETTING A MATCHED SET OF RECONFIGURABLE STEEL DISCRETE DIES

For the comparative study and other experimental investigations, a pair of high-resolution discrete dies, shown in figure 5.1a, were designed and. An isometric CAD drawing of one discrete die with various important features denoted is shown in figure 5.43.

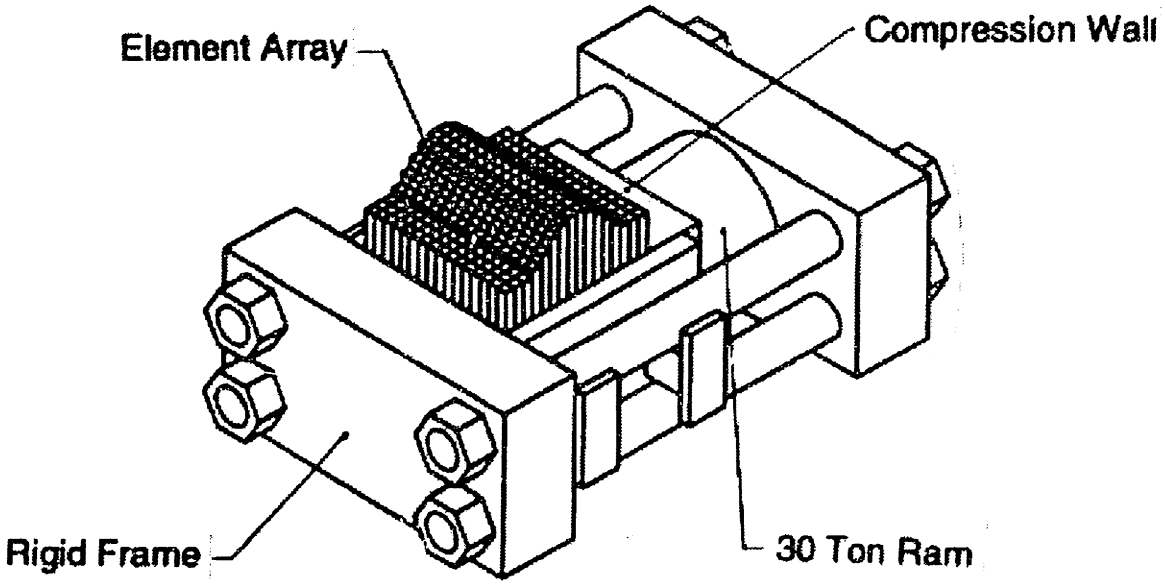

Figure 5.43 - Isometric view of a high-resolution discrete die.

5.7.1 Design and Fabrication of the Discrete Dies

Each discrete die consists of a simple close-packed matrix of 4096 square elements (64 by 64 matrix). Each element is 1.59 mm wide by 0.13 meters long and made of SAE 1095 steel. One goal in the design of these dies was to achieve as high a concentration of elements as possible within the specified 0.102 by 0.102 meter forming area. This is the reason why die elements were made out of 1.59 mm size stock because it was the smallest commercially-available steel square stock available in the U.S. at the time of construction. Since precision machining the required spherical tip shape is impractical for such a large number of small elements (8192 total), an approximately spherical shape was hand ground into the forming ends of each die element.

A single compression wall configuration (see section 5.2.1) was chosen for clamping the element matrix because of it's simplicity for design. For the type of experiments planned for these discrete dies, the side clamping force on the element matrix had to be both variable and repeatable. As discussed in section 5.3.1.6, the best type of actuator in this case is a hydraulic ram. Specifically a hydraulic ram with a low profile, ability to fit within the element matrix clamping area (i.e. 0.102 by 0.102 meters square), and as high a maximum force as possible was desired. The cylinder that best satisfied these design specifications is a Simplex™ HFJ-30 ram which is capable of creating a 267

kN (30 ton) force. Using equation 5.5 with element/element friction coefficient (μ_s) of 0.19 as discussed in section 5.2.1.4, the maximum forming load that can be applied to each element column using a simply-packed matrix is 1.6 kN. Because of success with 0.80 mm Elvax in helping to evenly distribute the clamping force over all the element columns (see section 5.3.2), this material was also used as the clamping interpolator for all the stamping experiments.

The discrete die's backwall and compression wall needed to be very stiff in order to maintain a uniform clamping load distribution in the element matrix. Based on the experimental investigation described in section 5.3.2, a maximum overall deflection of 0.05 mm was allowed for the backwall and compression wall under the maximum clamping load. By modeling the statically-loaded backwall as shown in figure 5.44, the required thickness $\mathbf{t_{bw}}$ of the steel backwall is 5.5 cm. Deflection in the compression wall for the same loading was negligible. As seen if figure 5.43, four rods were used as the tension members in the clamping load direction. The 2.5 cm diameter tension rods used are made out of SAE 4140 steel which has a yield strength of 655 MPa. The safety factor based on the material tensile yield strength is 5.0 in this case.

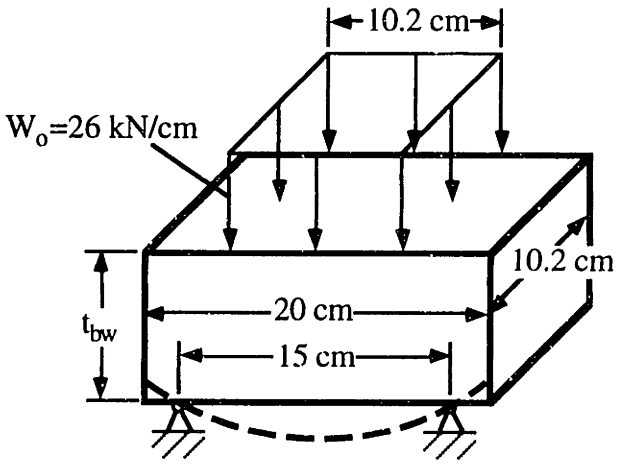

Figure 5.44 - Static structural model of the discrete die's back wall.

The discrete dies were also designed to allow the element matrix to be retrofitted with row dividers (described in section 5.2.6.1.2) for handling much higher forming loads. Based on frictional considerations alone, each row in the matrix would be capable of withstanding a maximum distributed forming load F_{RD} of 101.5 kN according to equation 5.15 ($2\mu_s$=0.38 and F_{clamp}=267 kN). However, the maximum forming load is limited by

the yield strength σ_{yield} of the sheet material used and the cross-sectional geometry of the actual row divider. The row dividers used for these discrete dies are made of SAE 1095 spring steel (σ_{yield}=1.1 GPa) and have a cross-sectional length L_{RD}=9.0 cm. To allow for F_{RD}=101.5 kN, row dividers of thickness t_{RD}=1.0 mm would have had to been used. This was considered an unacceptable row divider thickness since the column-direction resolution of the die would have been decreased by 38%, i.e. 64 element rows decreased to 40. A much thinner row divider of t_{RD}=0.102 mm was used instead. As a result the total forming load F_{RD} that a single row divider can withstand is only 9.7 kN based on equations 5.17, 5.18. 5.19 and 5.20. This is still significantly higher than the 1.6 kN limit in maximum forming load (row or column) when no row dividers are used.

Due to the accumulated thickness of the 0.102 mm row dividers, either the elements in each row would have to be notched 0.102 mm or 4 element rows would have to be removed to fit the element matrix within the same forming area. Since the same die elements are used for both the simple close-packed and row divider retrofit configurations, notching the elements was not an option. The result is a 64 column wide by 60 row long element matrix when row dividers are used.

5.7.2 Setting the Discrete Die's Forming Surface

The shape of both high-resolution discrete dies were set in a parallel fashion by dropping the die elements onto a master model of the benchmark part. During the setting operation, both the compression wall and one of the side wall have to be retracted by at least 1 mm to minimize the frictional interactions between the elements. As a result, one of the die frame side walls was designed to retract by this amount. The total time to configure both dies using master models was 1 hour since many elements had to be individually pushed against the model's surface. [In retrospect, applying ultrasonic vibrations to the dies during this setting operation may have helped to break up the element frictional interactions and also decrease the setting time.] The time required to CNC-machine both master models was roughly 2 hours. In this case, the CNC-machined dies described in section 3.5 were used in their post-ground state (but not yet polished) as the two master models. As mentioned in section 5.5.3, a master model could also have been made by rapid prototyping. The only system of this type that can create a model in a similar amount

of time to CNC-machining is LOM. For two 2.5 cm thick models, the approximate time for a commercially-available LOM machine to create these is 3 hours. Following this setting procedure, a 1.3 mm thick layer of 460 Elvax was preformed over each of the configured dies (as prescribed by Eigen,1992) to act as the effective forming surface. Applying the surface interpolators took a total of 10 minutes for both dies.

For this experimental investigation, designing and building an automatic row setting mechanism could not be justified given the cost and time constraints of the study. If these high-resolution discrete dies were used in an industrial application, a row profiling mechanism would be used to set the die shape instead of a master model. Using the profile mechanism shown in figure 5.33, the mechanical motion and associated times required to set just one of the 60 element rows (die with row dividers) are listed in table 5.3. The estimated linear actuator speeds and distances for the mechanism listed in this table are based on the geometry of the high-resolution dies and typical speeds of linear actuators (e.g. hydraulic cylinders, motor-driven leadscrews). Therefore, the total time for setting one die is $60 \text{ rows} \times 20.5 \frac{\text{sec.}}{\text{row}} \approx 20$ minutes. For two dies it would be 40 minutes.

Table 5.3 - Time analysis for row-by-row setting the high-resolution discrete dies.

Actuator Motion	Total Distance Moved (cm)	Speed (cm/sec.)	$\text{Time} = \frac{\text{Distance}}{\text{Speed}}$ (sec.)
Upward movement of the plate engagement bar (i.e. setting the profile shape).	10	1.5	6.7
Impressing profile shape into the element row.	10	2.5	4
Forward movement of the profiling carriage to catch all the profiling plates.	4	2.5	1.6
Retraction of all the profiling plates for subsequent reprofiling	4	2.5	1.6
Lowering the plate engagement bar.	10	1.5	6.6
		Total	20.5

Setting the discrete die to a particular forming surface requires that the correct element positions are determined. Using a computer program for extracting element

positions from an AutoCAD model file, the total time required to extract the positions for both high resolution dies was 20 minutes even though this information was not used for setting. This program was created by the author to use with the larger MIT discrete die press that did have an automatic profiling mechanism [see Hardt,1993].

5.7.3 Bending and Buckling of the Discrete Die Elements

The critical buckling and bending loads for a cantilevered die element (shown in figure 5.3) during forming can be estimated using equations 5.3 and 5.1, respectively. Using equation 5.1 requires that the bending moment term M is substituted with $F_{p,max} \cdot \frac{w}{2}$ where $\mathbf{F_{p,max}}$ is the critical bending load. The element chosen for analysis is from the male die configured for the benchmark part. Specifically, it is located 2.8 cm. in along the x-axis from the edge of the die. The data for this loaded element is as follows: w=1.59 mm, a=1.9 cm, E=200 GPa, and σ_{yield}=570 MPa (1095 cold-drawn steel). The critical buckling and bending loads are calculated to be 0.72 kN and 0.02 kN, respectively, showing that bending is more critical of an issue than buckling for a die element subjected to both axial and transverse forming loads.

5.8 GENERAL PROCEDURE FOR DESIGNING, FABRICATING AND SETTING RECONFIGURABLE DISCRETE DIES

We shall conclude this chapter by outlining the general procedure for designing and fabricating a reconfigurable discrete die.

1) All elements of a close-packed die matrix should be square in cross-section, equal in length to allow for reconfigurability, and have a spherical tip on their forming end. The minimum length of an element is determined by adding the height of maximum element extension beyond the forming side of the frame to the width of the discrete die frame. The choice of the element width **w** and the maximum element extension beyond the frame must be based on the maximum expected forming load determined from an FEA analysis of the most extreme sheet metal part that would be formed, and

the smallest geometrical detail that would be formed in a sheet metal with these dies. Equations 5.1 and 5.3 should be used to determine the minimum bending and buckling loads, respectively. As shown in section 5.7.3, bending failure is more of a critical issue than buckling. If a reduction of the element width is considered, the designer needs to remember that the bending stiffness $\mathbf{E \cdot I}$ of a solid square element is proportional to the fourth power of the width, i.e. $\mathbf{w^4}$. Furthermore, if an element is large enough then a tubular construction should be considered to minimize the weight of the die (see section 5.1.2).

2) Determine the dimensions of the discrete die matrix by considering the size of the largest part that will be formed. Because of warping and tolerance build-up that occurs within the element columns, the dimensions of the element matrix affects the size of the element that can be used.

3) Determine the method that will be used to set the shape of the discrete die(s). For small elements, i.e. below 20 mm wide, the row-by-row setting methods described in section 5.5.2 should be used. For larger elements, i.e. above 20 mm wide, a parallel setting method should be considered to minimize the setting time. If parallel setting is chosen then the hydraulically-actuated element design described in section 5.5.3.2 is suggested because of it's simple construction.

4) Based on the forming loads from an FEA analysis of the most extreme sheet metal part that would be formed, choose the best method for locking the configured die element matrix into a rigid tool. The recommended configuration is a single compression wall clamping a matrix of elements with row dividers. The maximum forming load per element is likely to be limited by the failure load of the row divider material (estimated with equations 5.17 through 5.20). Otherwise the forming load is based on the static frictional load described by equation 5.15. For larger elements that are individually actuated, techniques for individually locking each element can be used.

5) Determine whether or not the elements have to be notched, as described in section 5.2.6.1.2, to account for the accumulation of row divider thickness. Notching is not

needed if the elements can extend far enough beyond the frame so that no plastic bending occurs when the elements are wedged together during forming. If the elements are too short (e.g. due to limited space), notching should be used but done so carefully to make sure that the clamping load is transferred to the row dividers and not at the element ends.

6) Based on the comparisons described in section 5.3.1.6, choose the best method for achieving the high clamping force required to clamp the die element matrix. Four viable clamping methods and their respective governing physics are discussed in section 5.3.1.

7) To insure that the clamping load distribution is uniform within the element matrix, the discrete die frame must be stiff enough structurally. One design method to obtain a certain structural rigidity is to specify a maximum allowable deflection (e.g. 0.025 mm) for any die frame member. By modeling the frame member with FEA or simple elastic theory, the structural rigidity can be accurately predicted. This was the case with the high-resolution discrete dies (see section 5.7.1). Aside from requiring a rigid frame, the uniformity of the clamping load distribution will improve significantly if a thin interpolating material layer is used between the compression wall and the first row of elements (see section 5.2.1.2).

8) Use a premoldable Elvax interpolator to cover the forming surface of the discrete die prior to forming sheet metal. A interpolator thickness equal to the width of the die elements has been found to work well [Eigen,1992].

9) The procedure for extracting element positions from a CAD or computer model of the die geometry is outline in section 5.6.

Chapter 6 - Comparitive Study

As described in chapters 3, 4 and 5, three sets of matched-dies were designed and fabricated to stamp the benchmark part shape out of sheet metal. By fabricating each die set and then using it to stamp benchmark parts, objective comparisons can be made between the three candidate fabrication methods. Results and conclusions drawn from this comparative study gives manufacturers that must deal with tooling development the means to realistically evaluate which rapid fabrication methods fits best into their flexible manufacturing system. This chapter describes an experimentally-based comparison of the three candidate die fabrication methods, results of sheet metal forming experiments with each of the die sets, and then makes observations about each die method with regards to a particular set of comparison criteria.

6.1 Comparitive Study Details

Standard processes and practices of commercial sheet metal forming were used for all the experimental work. As shown in table 2.1, matched-die forming with restrained blank edges is one of the most common processes used to stamp sheet metal parts; consequently, it was used in the study. This required that a matched die set be fabricated using each of the candidate methods and also a universal blank holder. The benchmark part shape was designed with CAD and verified with FEA paralleling the current tooling development process outlined in section 1.3. Commercially-available or custom-written CAM software was used to generate the machining instructions needed for fabricating each of the required forming dies. The actual forming was done in a hydraulic press which is a common piece of machinery in the sheet metal forming sector of industry . Finally, the formed parts were measured using a commercially-available Coordinate Measuring Machine (CMM).

Comparisons made between each of the three candidate rapid fabrication methods are primarily based on lead-time and cost. Specifically, the ten criterion used for the study are:

1) Time required to fabricate or configure the dies into the shape of the benchmark part
2) Time required to reshape or reconfigure the dies into a new die shape
3) Capital cost of the machinery required for die fabrication
4) Cost of raw materials used to fabricate the dies
5) Cost of process consumables (e.g. cutting tools, power) used during die fabrication
6) Shape fidelity of parts formed with the dies
7) Limitations to die geometry imposed by the fabrication method
8) Limitations on forming load
9) Limitations on die size
10) Limitations on incorporating a blankholder.

Criterion 6 through 10 do not deal with the cost and/or lead-time of tooling development directly but rather have an indirect effect which is discussed later in this chapter.

6.2 SHEET METAL FORMING EXPERIMENTS

A series of steel benchmark parts were stamped out of the 0.64 mm thick sheet stock (same as material prescribed in the FEA simulations discussed in section 2.4) using each of the matched-die sets. As shown in figure 6.1a, the apparatus used for stamping was hydraulically-powered universal testing machine which allows recording of the force/displacement data during the stamping experiments. The edges of the sheet metal blanks were clamped in a free-floating 2-piece blankholder which was held together with 16 high-strength (i.e. grade 8) bolts. The blankholder, shown separately in figure 6.1a, is designed to accommodate a square blank size between 10.5 and 15.3 cm on a side. A particular binder force $\mathbf{F_b}$ in newtons is achieved by tightening the blankholder bolts to a specific torque [Shigley,1983] according to the formula

$$F_b = \frac{T \cdot N_b}{0.4 \cdot d_b} \cdot 4.45 \qquad (6.1)$$

where:
$\mathbf{T}$ = bolt torque in inch-lbs
$\mathbf{N_b}$ = number of bolts (16 in this case) and
$\mathbf{d_b}$ = bolt diameter in inches (0.3125).

Equation 6.1 estimates the combined tensile load of all the clamping bolts.

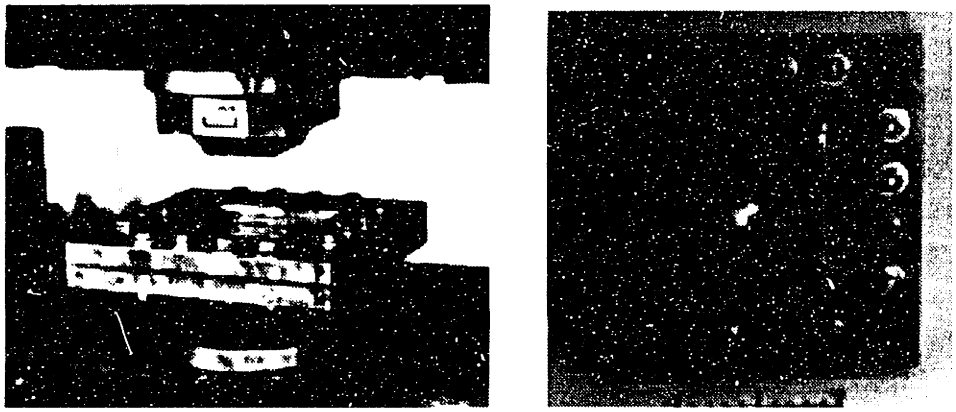

Figure 6.1 - a) Forming dies (CNC-machined) and blankholder mounted in a hydraulic forming press and b) blankholder shown alone.

6.2.1 CNC-Machined Dies

Several sheet metal parts were formed with the CNC-machined dies using various combinations of binder force, blank shape, and lubricant. This was done to find the combination of forming conditions that yielded the best looking part and also to verify the FEA simulations described in the section 2.4. The best combination was a high binder force (100 kN), low forming friction (.025 mm thick Teflon layer, $\mu<.10$ for Teflon on steel), and a 15 cm by 15 cm square blankshape with 2.5 cm chamfers at each corner to minimize the corner draw-in resistance. As shown in figure 3.1b, the formed part has sharp geometric details and no perceivable failure in the sheet metal, i.e. no tearing in the upper corners or buckling within the pan section. The part also showed mild springback (around 5.7% in height) and some buckling in all four flange corners as predicted by the FEA analysis. The buckling is a result of unsupported regions in the sheet metal that are subjected to in-plane compressive loading. There is a noticeable dimple, roughly 2x2 cm, located in the center of the reverse curvature section of the part. Presumably, this dimple is made at the very end of the stamping operation when the dies are very close together and a machining mismatch in the die surfaces causes an unwanted coining-type operation. As seen in the force/displacement history of this part (figure 6.2), the maximum recorded forming load is 55 kN.

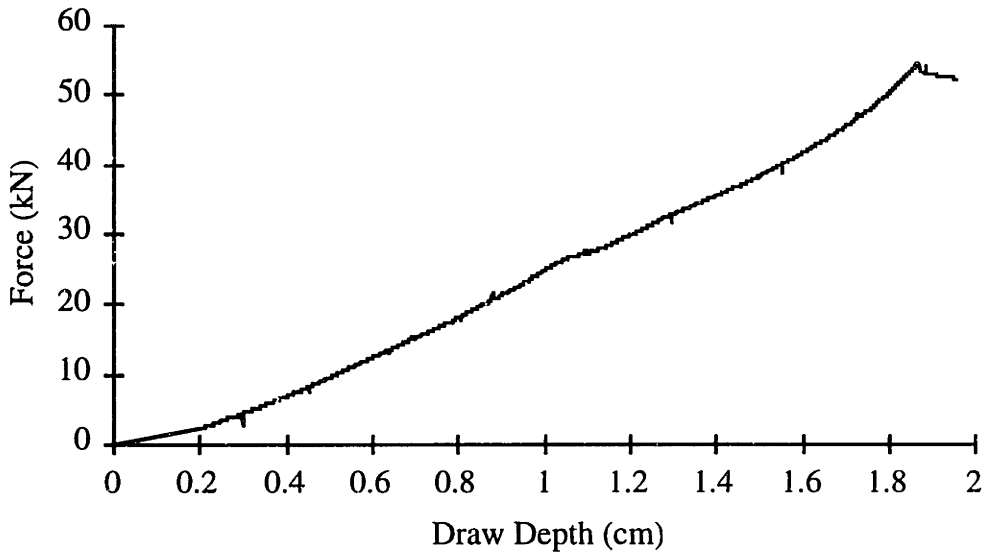

Figure 6.2 - Force/displacement history of a part stamped with CNC-machined dies.

Since the use of Teflon sheets for forming parts in an industrial setting is a rather expensive and unrealistic option, a sheet metal part was stamped using the previously mentioned forming conditions except that an inexpensive viscous oil (μ=.1 to .2 for steel on steel) was used as a lubricant. This part exhibits the same details as the previous part except that the height springback was reduced (around 2.9% in height). there is slightly more wrinkling in the four flange corners. The maximum forming load for this stamping run was 54 kN.

A vertical profile of this part's top surface, as shown in the dark line in figure 3.1b, was measured with a CMM at 0.2 mm increments in the x-direction. This profile corresponds to the top surface of section view B-B (CAD model) seen in figure 2.12. The average absolute height deviation and maximum height deviation of the measured part profile from the CAD profile is 0.43 mm and 2.26 mm, respectively. Since the dies are same shape as the CAD model, most of this error is attributable to the springback in the sheet metal. As part of an actual die development scheme, the shape of the dies and the forming conditions would be modified over several iterations until the desired part shape can be formed consistently.

6.2.2 Profiled-Edge Lamination Dies

UNGROUND DIES - For work involving product prototyping, an engineer who designs a sheet metal part will typically want to fabricate it as quickly as possible. If functionality of the prototype part is more important than surface finish, stamping with the unground (i.e. rough beveled surface) PEL dies is shown to yield acceptable results. Prior to grinding and polishing the die forming surfaces (see section 4.4.3), which takes the majority of the fabrication time, the surface of the PEL die was very rough with machining marks and minor mismatches between adjacent laminations. A part was formed only using the viscous oil lubricant between the unfinished PEL die forming surface and the sheet metal blank. Furthermore, the same binder force (100 kN) and blank size (15 cm. square with corner chamfers) as the CNC-machined die experiments were used. During the forming trial, the part started tearing at the upper corners of the pan in the direction of the laminations even before the final draw height was reached. There was also extensive indentation in the sheet metal from the lamination machining mismatches. The failure of this part came as no surprise when the condition of the forming surface and the high plane-stretching that occurs in the sheet metal are considered. This failed forming experiment suggests that forming with only the unground die may not be a viable method unless a better surface finish and matching of adjacent laminations (before grinding) can be achieved.

Another approach to forming with the rough die surface is to place a very thin interpolating layer in between the die and the sheet metal blank. This same approach is used when forming with discrete dies (see section 5.4). A series of stamping experiments were performed using various interpolating materials including Teflon, 460 Elvax (ethylene vinyl acetate), low-density polyethylene (LDPE), pure aluminum, copper, and lead. Interpolator thickness ranged from 0.20 to 0.38 mm. The binder force, blank configuration, and lubrication were kept constant for each part.

In general, the thicker (0.025 to 0.038 mm) elastomeric layers which have a high tensile strength (i.e. Elvax and LDPE) worked best as interpolators to smooth out the rough forming surfaces of the PEL dies. In fact, the best looking part was stamped with a 0.38 mm thick 460 Elvax interpolator. The height springback in the part and the maximum forming load are 4.6% and 54 kN, respectively. No wrinkling was observed in

any of the four flange corners. Inspection of the interpolating material after stamping showed that the Elvax easily flowed into the machining mismatches. There were still some slight lamination edge marks left in the stamped part, especially in the steep 68° wall. Furthermore, the shape fidelity of these stamped parts is not as good (i.e. large bend radii) as that of parts stamped with the CNC-machined die set (visual inspection only). This is undoubtedly due to the filtering effect that an interpolating layer has on the shape's spatial frequency content. [Quantifying the shape fidelity of parts formed with each die set is discussed in section 6.3.]

GROUND and POLISHED DIES - Several sheet metal parts were then formed with the ground and polished PEL dies. The same viscous oil lubricant and blank shape used in all previous forming experiments were again used for these trials. However, a lower binder force of 50 kN had to be used during stamping to avoid tearing in the upper corners of the benchmark part. The interfaces between adjacent elements of the PEL die forming surfaces probably account for the higher static friction and high localized stresses and, thus, the tearing problem. The height springback in this part and the maximum forming load are 2.9% and 55 kN, respectively.

Although there were significant lamination edge marks left in the sheet metal (refer to figure 4.1b), the shape fidelity of the part is as good as that of the part stamped with the CNC-machined dies (by visual inspection only). By comparing the CMM-measured profile of the PEL part with the desired CAD profile, the average absolute height deviation and the maximum height deviation are 0.88 mm and 3.98 mm, respectively. The height springback of the PEL part is greater than the part stamped with the CNC part probably because less stretching occurred in the sheet metal as a result of the lower binder force.

6.2.3 Discrete Dies

SIMPLE CLOSE-PACKED MATRIX - The first series of benchmark parts were stamped with the high-resolution discrete dies with a simple closely-packed element matrices, i.e. no row dividers, to see how this die configuration would perform. The element matrices were then clamped with a 220 kN clamping force. According to equation 5.5, each matrix was expected to withstand an evenly-distributed stamping load of 67 kN

before element columns began slipping. As before, the same forming conditions used for the CNC and PEL stamping experiments were used for forming these parts.

During the first forming trial, the dies were brought together until the forming load reached a maximum of only 22 kN. When the dies were separated, it was evident that many of the elements of the upper male die (5 x 5 cm square area) began to slip at this maximum load. As this area only loads about half of the element columns, the male die was expected to withstand a load of $67 \times 0.5 = 33$ kN. However, none of the elements in the female die slipped. Some of the protruding elements, especially in the upper four corners - male die side, pierced through the forming interpolator and dimpled the sheet metal part. Due to the elements that slipped, the part only had the general shape of the benchmark part and not the fine detail of the CNC-machined or PEL die parts. Other parts stamped with these discrete dies suffered the same fate.

Just to see what part shape this die configuration could handle, a "filtered" benchmark part was used as shown in the figure 6.3. The "filtered" part contains less higher spatial frequency content, i.e. no small radii, than the original benchmark part shape resulting in a more evenly-distributed forming load applied to the clamped element matrix. A sheet metal part with this shape was stamped successfully with a maximum forming load of 46 kN, no die elements that slipped and no elements that pierced through the interpolator.

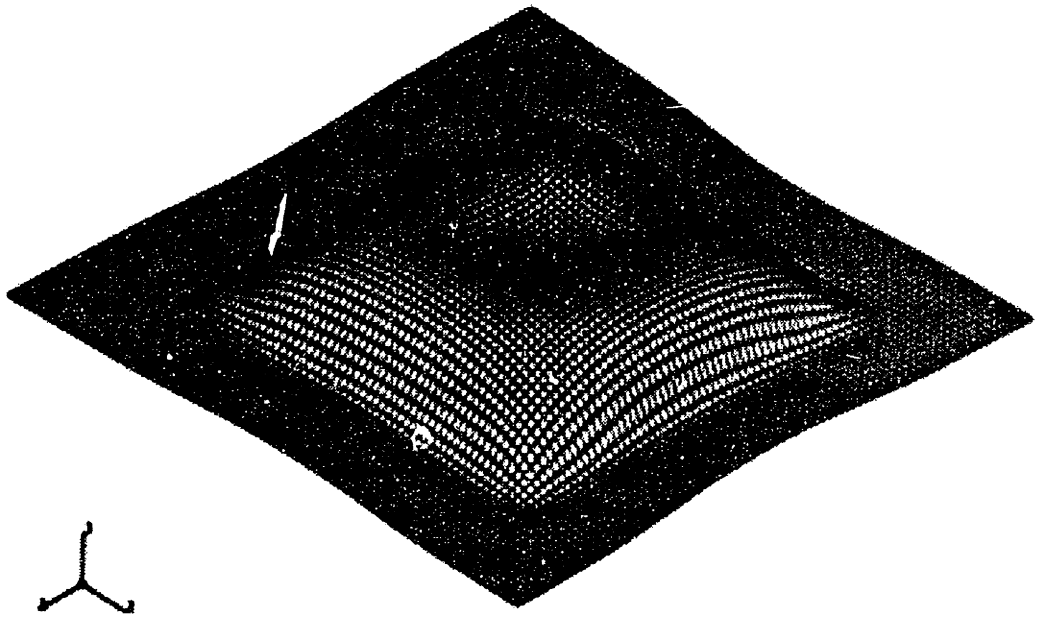

Figure 6.3 - CAD model of the "filtered" benchmark part shape stamped with the simple close-packed discrete dies

CLOSE-PACKED MATRIX WITH ROW DIVIDERS - The initial parts stamped with the discrete dies pointed out the inherent weaknesses of a simple close-packed matrix regarding the effects of high forming loads (refer to section 5.2.1.6). Because of the very high forming pressures required to make this part, especially at the upper corners of the male die, the high-resolution discrete dies had to be retrofitted with row dividers to help transfer the forming loads to the outer frame more efficiently.

Both discrete dies were configured to stamp the benchmark part. The element matrices were then clamped into rigid tools with a 245 kN clamping force. The same forming conditions used for all the previous stamping experiments were used for these runs. Without any of the elements slipping, several benchmark parts were stamped with these dies using the same two Elvax surface interpolators.

A part stamped with these dies is shown in figure 5.1b. The maximum forming load for this run was 60 kN. The discrete die part generally has less shape fidelity than the CNC and PEL parts especially at the upper and lower bends in the pan. At each of the upper four corners (male die side), a single element pierced through the interpolator and dimpled the sheet metal but no where else. Very little compressive buckling occurred in the flange corners but a very slight waviness can be detected in the flange around the entire draw section of the part. Presumably, the waviness is caused by a combination of the interpolator's compliance in these areas and the high in-plane compressive straining that the sheet metal experiences. By comparing the CMM-measured profile of the Discrete Die part with the desired CAD profile, the average absolute height deviation and the maximum height deviation are 0.98 mm and 2.45 mm, respectively.

6.3 SPATIAL FREQUENCY DESCRIPTION OF THE PART PROFILE

The average absolute and maximum height deviation values are of little use when comparing the shape fidelity of sheet metal parts stamped with different dies. A better way to compare each part's shape fidelity to the CAD shape is to map the CMM-measured 3-D coordinates into the frequency domain. As used by [Webb and Hardt,1991] in their 2-D

and 3-D closed-loop shape control algorithm, the interpolating function that describes a part shape in the spatial frequency domain is the Discrete Fourier Transform (DTF). Hence, we use it here to compare the shape fidelity of the sheet metal parts. For the sake of computational ease, only a single 2-D cross section of each stamped part was mapped into the spatial-frequency domain for comparison of shape fidelity. The DTF for a measured 2-D profile **z(n)** is given by

$$Z(m) = \sum_{n=0}^{N-1} z(n) \cdot e^{-j2\pi n(m/N)};\ m = 0,1,2,\cdots N-1 \qquad (6.2)$$

where:
m = frequency integer
n = sample integer and
N = number of samples.

Z(m) is a complex array of DFT spectral coefficients for the N equally spaced frequencies. For an arbitrary spectral coefficient, say **Z(1)=a+b·j**, the magnitude and phase can be calculated using the relations

$$|Z(1)| = \sqrt{a^2 + b^2} \text{ and } \angle Z(1) = \tan^{-1}\left(\frac{b}{a}\right), \qquad (6.3)$$

respectively. Samples of z(n), i.e. z-axis elevations, are taken in the x-direction at a sampling interval of Δx. If the spatial representation of z(n) is to be reconstructed from the frequency domain representation Z(m), then the Inverse Discrete Fourier Transform (IDFT) must be used. This is given by

$$z(n) = \sum_{m=0}^{N-1} Z(m) \cdot e^{j2\pi n(m/N)};\ n = 0,1,2,\cdots N-1. \qquad (6.4)$$

In the 2-D case, the frequency f_m associated with a specific frequency integer m is equal to $\frac{m}{N \cdot \Delta x}$ and is expressed in cycles per unit distance. As seen in figure 6.4, when the magnitude $|Z(m)|$ and the phase $\angle Z(m)$ of the spectral coefficients are plotted against the frequency integer, they are symmetrical and inversely symmetrical about m=0 (D.C. component of spectral representation), respectively. For this reason, the spectral coefficients up to $\frac{N-1}{2}$ are all that is needed to completely describe the shape the 2-D profile in the spatial frequency domain.

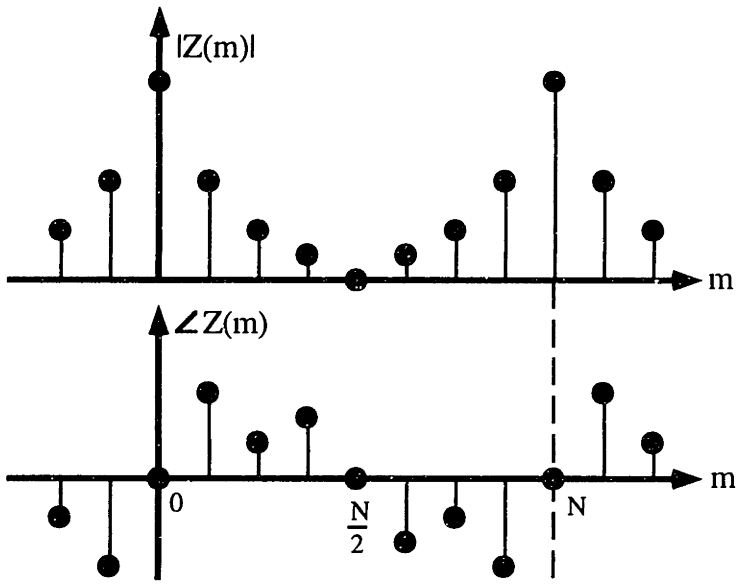

Figure 6.4 - Symmetrical nature about the DFT spectral coefficient's magnitude and phase.

As previously mentioned, each of the stamped benchmark parts shown in figures 3.1b, 4.1b, and 5.1b were measured along the sectional view line B-B shown in figure 2.12 using a Coordinate Measuring Machine (CMM). For the PEL dies, section line B-B runs across the individual laminations so that the effect of the straight bevel approximation is captured. A sampling interval of Δx=0.2 mm was used for the 417 samples taken. Accordingly, spectral coefficients up to frequency integer m=208 are all that is needed to represent the spatial frequency content of the each part profile. In this case, the spectral coefficient magnitudes above m=15 are negligible. The frequency magnitude spectrum (up to m=15) of the CAD profile and that of the measured profiles of each stamped part are listed in Table 6.1.

Table 6.1 - Spectral coefficient magnitudes for the CAD shape and stamped parts.

m	f_m (cycles/mm)	CAD Shape	CNC-Machined Die	PEL Die	Discrete Die
0	0.00	5619	5636	5645	5483
1	0.01	845	807	752	851
2	0.02	1246	1136	1145	953
3	0.04	475	442	459	335
4	0.05	170	185	196	142
5	0.06	82	68	99	42

6	0.07	58	37	47	19
7	0.08	32	13	30	21
8	0.10	41	40	42	24
9	0.11	35	40	38	20
10	0.12	9	20	21	12
11	0.13	14	10	17	10
12	0.14	8	9	13	8
13	0.16	8	6	12	6
14	0.17	6	5	9	6
15	0.18	12	9	3	5

For any 2-D cross section of the measured part, the general shape of the cross-section is characterized by low frequency components. Accordingly, fine part details (e.g. small radii of curvature) are characterized by high frequency components. In the case of section line B-B of the benchmark part, the frequency components up to 0.048 cycles/mm for each stamped part are close in magnitude to the CAD shape. This simply means that the general shape of each part is similar to that of the desired part shape. However, by comparing the higher frequency components (0.060 cycles/mm or m=5 and above) of each part with the CAD shape in figure 6.5 shows how those of the discrete die part profile are consistently lower in magnitude than the others. This simply shows us how some of the part shape fidelity is lost when stamping with the discrete dies. For higher frequency components, $|Z(m)|$ for the PEL die part are generally higher than the CNC die part. This may be attributable to the sharp lamination interfaces that are transferred to the stamped part.

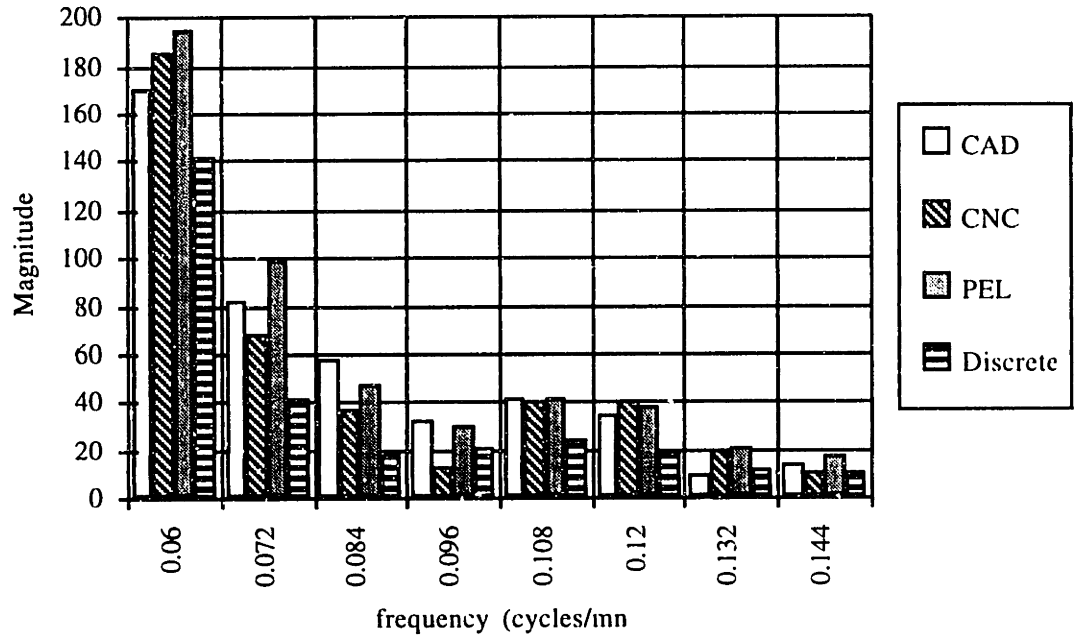

Figure 6.5 - DFT spectral coefficient magnitudes for high spatial frequencies of each part profile.

6.4 COMPARISON OF THE FABRICATION METHODS

Enough background material has been presented in chapters 3, 4, 5, and sections 6.1 through 6.3 to finally allow us to make useful comparisons between the three candidate fabrication methods. In this section, comparisons are made based on the criterion listed in section 6.1. Even though the quantitative results of this section only pertain to a particular part shape and size, and set of forming conditions, the relative comparisons made between all three methods will be valid in most other situations. The reason for this is that this comparative study is based on the most common processes and practices used for sheet metal forming in industry. In many cases, it will simply be a case of linear scaling.

6.4.1 Time Required to Fabricate or Configure the Die

The time it takes to fabricate (CNC & PEL) or configure (discrete) a set of sheet metal forming dies directly impacts both the lead time and cost of tooling development. The actual times required to fabricate the forming dies using each of the candidate methods

are summarized in table 6.1. The downward trend in time needed for machining data extraction from the CAD model reflects the number of data points that each fabrication method uses to create the forming surface shape (i.e. CNC-machining, the most and discrete dies, the least) and also the degree of shape approximation. However, the actual times in an industrial setting will depend upon how optimized the data extraction computer software is and what additional software help modules are included (e.g. gouging check in CAM). Since PEL laminations are cut in 2-dimensions only, there is no problem with tool gouging because there is no cutting tool. The preparation time before the actual die shape can be machined or set is similar for CNC-machined and PEL dies but is negligible for discrete dies when automatic profiling is used. The time needed to machine or configure the die shape is greatest for CNC-machining and it will increase significantly for harder material (e.g. tool steel) as feedrates and spindle speeds have to be reduced. In addition, as the die size increases, time scaling of the rough cutting and finish cutting operations is roughly proportional to the volume of material removed and the area of the die's forming surface, respectively. In contrast, laser cutting PEL dies is essentially unaffected by material hardness. In fact, faster cutting rates can be achieved by increasing the power of the laser as shown in figure 4.30. The machining time is roughly proportional to the surface area of the die only. The only material removed is the narrow cut made by the cutting method (e.g. laser) in the die lamination. Finally, the time required to grind and polish the rough die surface is similar for both the CNC-machining and PEL methods. The grinding time for CNC-machining will decrease significantly if 5-axis milling is used to make the finish cuts on the die surface. This is only true for die surfaces consisting of gentle curvatures. The equivalent operation for the discrete die method, i.e. applying an interpolator mask, takes only a fraction of the time that polishing and grinding of the PEL and CNC-machined die surfaces does.

Table 6.2 - Comparison of die fabrication/configuration times (hours).

	CNC Die	PEL Die	Discrete Die
Extraction of Machining or Configuration Data	1.0	0.5	0.3
Preparation before Die Shape is Machined or Configured	1.0	0.7	2.0 (master model) 0.0 (row by row)
Machining or Configuration of Die Shape	1.1	20.0 (weaving ball endmill) 0.6 (Flute-edge milling) 0.9 (AWJ) 0.5 (Nd:YAG Laser)	1.0 (master model) 0.7 (row by row)
Grinding and Polishing Die Surface	2.0	1.5	0.2 (interpolator applied only)

6.4.2 Time Required to Reshape the Die's Forming Surface

Assuming that many iterations are required to develop the correct die shape, the time required for reshaping a die's forming surface will have an even greater impact, as compared with the initial fabrication time, on the cost and lead-time of a tooling development program. The results are also summarized in table 6.2 but with a few differences noted. The main difference is that no preparation of the die(s) will be required before remachining or reconfiguring the forming surface. In addition, the machining time for the CNC die will only be 1.0 hour since no roughing operation (0.1 hours) will be needed. For dies with deep draws that require more extensive rough cutting, the change in machining time would be greater. All conclusions drawn in the previous section also apply in this case.

6.4.3 Capital Cost of Machinery Used for Die Fabrication

Although the capital investment in fabrication machinery is not directly added to the cost of tooling development in this study, it is an amortized expense that greatly influences the manufacturing company's choice of a die fabrication method. The two most important capabilities of any piece of fabrication machinery is the die size it can handle and how fast it can fabricate or configure a die.

As discussed in section 3.5, a 3-axis CNC machining center was used to fabricate the CNC-machined dies. The maximum rate at which a solid die can be machined is dependent upon the material composition and it's hardness, as seen in equation 3.5, regardless of whether there is surplus spindle power available. However, the maximum

die size that can be handled is solely dependent upon the work area of the machining center. The cost of a 3-axis machine can be estimated, as a function of the work bed area, with a linear equation based on data collected from a major U.S. machine tool builder [Horner,1995]. The data listed in table 6.3 is summarized with the equation:

$$\text{Cost}(\$) = 80000 \cdot (\text{bed work area in } m^2) + 40000. \quad (6.5)$$

Similar equations can be developed for 4 and 5-axis CNC machining centers.

Table 6.3 - Bed work area versus base price for 3-axis machining centers.

Bed Work Area (m^2)	Machine Base Price ($)
0.260	65K
0.383	75K
0.520	85K
0.838	113K

Assuming that a DLP machine fitted with a pulsed Nd:YAG laser cutter (fastest method identified) is used to fabricate the PEL dies, then the major capital cost item will be the laser. The maximum rate at which a PEL die can be fabricated is dependent upon the cutting speed of the laser. Since the dependency of a laser's maximum cutting speed on laser power has already established, then the laser power is the limiting factor in fabrication rate. According to a major international laser manufacturer, the cost of various Nd:YAG lasers (including beam delivery system) with different output powers is listed in table 6.4 [from Rofin-Sinar, Inc.]. Fitting a linear equation to this data yields the following estimation formula for the laser price versus average maximum output power:

$$\text{Cost}(\$) = 150 \cdot (\text{Laser Power in Watts}) + 45000 \quad (6.6)$$

An estimated $50,000 needs to be added to the laser cost for a DLP machine based on the embodiment #1 design (see section 4.3.2.1). Since the cutting means are stationary with DLP machine and only the laminations are moved, larger die sizes only require an enlargement of the machine's loading and receiving bins. This is a relatively inexpensive task compared to that of a CNC machining center. With CNC machining centers, expansion of the work bed area requires large stiff frames be used which quickly raises the machine's cost (as reflected in equation 6.5).

Table 6.4 - Average output power versus base price for an Nd:YAG laser cutter.

Laser Power (Watts)	Laser Peak Power (Watts)	Cost ($)
300	5000	78K
500	10000	105K
1000	15000	184K

When using discrete dies, there are two major capital cost items: the profiling mechanism and the reconfigurable discrete die(s) itself. The cost for both of the high resolution dies used for the comparative study was $20K. This is a conservative cost figure since not all of the manual labor costs are added in. A good heuristic rule for estimating the cost of a discrete die is that it will roughly scale with the volume (or weight) of material (steel in this case) used in it's construction. Although a automatic profiling mechanism for setting the high-resolution discrete dies was not built, the cost for such a machine is estimated to be $50K.

6.4.4 Cost of Raw Materials Used to Fabricate the Dies

The term 'raw materials' refers to those materials directly used in the construction of the dies. The expense of these raw materials figures directly into the total cost of die development. The CNC-machined dies were made out of two metal billets each being 670 cm^3 of C11L17 steel. The price for this type of steel at the time of purchase was $\$0.0227/cm^3$ so the total price for the billets was $30. For both of the PEL dies, 138 laminations made out of relatively inexpensive cold-drawn SAE 1010 steel sheet were used. With a lamination size of 1.5 mm thick $\times$ 7.0 cm $\times$ 10.2 cm and 1010 steel at $\$0.0132/cm^3$, the total cost for the material was $19. The most inexpensive of all the methods were the discrete dies since the only raw materials required were two 0.8 mm thick $\times$ 10.2 cm $\times$ 10.2 cm pieces of 460 Elvax. Total cost for the Elvax was about $0.20. The low Elvax cost may be misleading for large batches of parts formed with the discrete dies because an interpolator mask will only last for a few stampings. In this case, it would be better to consider the interpolator as a consumable during forming.

6.4.5 Cost of Process Consumables Used During Die Fabrication

The cost of consumables used during the fabrication of the forming dies (e.g. cutting tools) also figures directly into the cost of the tooling development. While fabricating the CNC-machined dies, the following costs were incurred: one Ø12.7 mm carbide ball endmill @ $38, one Ø6.4 mm carbide ball endmill @ $16, three unitized grinding cylinders (grinding operation) @ $3, and approximately 2.5 kW continuous power for 1.1 hours ($0.11/kW-hr) @ $0.30. The total cost was $57. For laser-cut PEL dies, the following costs have been extrapolated from the laser cutting tests described in section 4.2.4: 462 liters of pure-grade oxygen @ $22, approximately 20 kW (1 kW laser with a 5% energy conversion factor) for 0.17 hours @ $0.36, and three unitized grinding cylinders (grinding operation) @ $3. The total cost would be $25. Aside from the electrical power used for setting the dies, there were no consumables used for the discrete dies. CNC-machining a forming die clearly has the highest cost for consumables mainly due to the cutting tools which are used on that die and no other. This is a typical practice in industry.

6.4.6 Shape Fidelity of Parts Formed with the Die Sets

The shape fidelity of a die-formed sheet metal part will be defined as how well the part faithfully reproduces the intended CAD part shape. As discussed in section 6.2, the spatial frequency content of a sheet metal part is a good measure of its shape fidelity with respect to the CAD shape. According to shape measurement in the spatial frequency domain, the shape of the parts formed with the CNC-machined dies and the PEL dies are faithful to the CAD shape but not exact. With CNC-machining, the scalloped die surface left by the surface machining operation (see section 3.1) must be smoothed which introduces some approximation to the shape. As is discussed in section 4.1.1.2, there is also geometric error introduced by the straight bevel approximation of the PEL die laminations.

Of the three fabrication methods, stamping with discrete dies introduces the greatest loss in shape fidelity as is discussed in section 6.2. Both the finite size of the die elements and the deformability of the interpolating layer contribute to this problem. The smallest details (e.g. corner radius) that can be formed into a part are directly affected by the size of

the discrete die's elements. As seen in figure 6.6, the shape fidelity is also limited in terms of the maximum wall slope or the minimum in-plane (x-y plane) that can be formed [Ousterhout,1991].

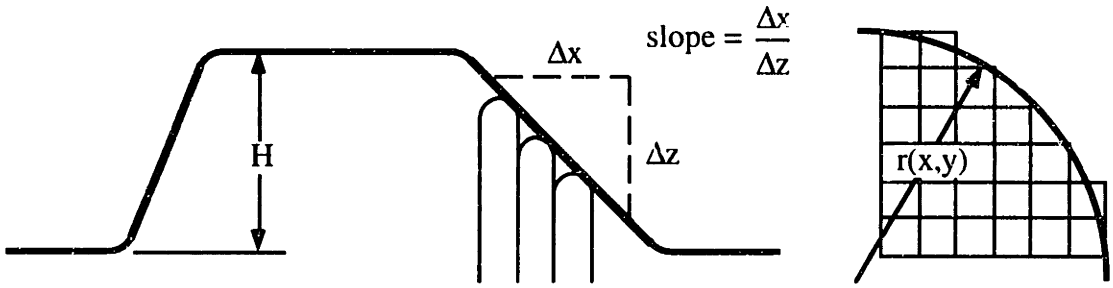

Figure 6.6 - a) Wall slope and b) in-plane radius limits on the forming fidelity of a discrete die

6.4.7 Limitations to Die Geometry Imposed by Fabrication Method

Each fabrication method imposes certain limitations on the geometrical features of the die's forming surface. The more geometrical limitations imposed, the longer it will take to fabricate the die, i.e. longer lead time. Although CNC-machining is capable of creating very complex surfaces, the machinable die geometries are limited by the accessibility and size of the cutting tool (∅6.4 mm in this case). Concave features in the die with steep walls and internal radii are limited by the tool spindle geometry and the ball endmill size, respectively. Long endmills must be used for machining deep cavities. Unfortunately, excessive deflection of a long endmill from cutting forces decreases the accuracy of the machining and increases the probability of the tool breaking. The endmill can be shortened but this decreases the depth of a cavity that can be machined into the die surface. The endmill diameter can be increased (i.e. stiffening the tool) but this limits the smallest radius of curvature (e.g. grooves and bend radii) of the die surface that can be machined. Undercuts in the die are not possible unless portions of the die are machined separately and then reassembled or if the complete die is reoriented and then reregistered. Both options will significantly increase the machining time.

The limitations on the die geometry imposed by the CNC-machining method are lessened with a PEL die fabricated by laser or AWJ cutting. Specifically, the PEL method avoids the tool accessibility problem and the geometry limitations imposed by a cutting tool. Since machining occurs in two dimensions only, i.e. profiling a lamination's top

edge, there is essentially no limitation on what profile that can be machined. Even undercuts and backdrafts in the die are possible, although maybe not practical. Furthermore, unlike CNC-machining, the threat of gouging a lamination doesn't exist when machining PEL laminations since there are no cutting tools or check surfaces to deal with. There are, however, limitations to the maximum bevel angle that can be cut into the lamination (see table 4.23). Since there is no cutting tool used in the fabrication of a PEL die, the only geometry limitation imposed by the cutting means is the width of the kerf that is cut by the laser or the AWJ. The kerf width range is 0.1 and 0.7 mm. Another limitation on the die geometry is the radius of curvatures in the X-Z plane (across lamination widths) should not be any smaller than the lamination thickness (1.5 mm in this case).

There are also limitations on the die geometry with discrete dies. These type of dies most crudely approximate the intended die surface because of the element size and the interpolator thickness (≈2.4 mm in this case). Undercuts with discrete dies are not at all possible because a die element can only have one z-position. These limitations are less of an issue to fabrication time, as compared with CNC-machining and PEL methods, since the time to set the discrete die remains essentially constant regardless of the die shape.

6.4.8 Limitations on Forming Load

If the loads encountered during forming of a sheet metal part are too high for a particular die construction, i.e. solid CNC-machined, PEL, or discrete, to handle then the part must be redesigned to form with lower loads. A part redesign translates into a longer development time. For a solid CNC-machined die, the only limitation on forming loads is that contact stresses between the sheet metal part and the die during forming cannot exceed the compressive strength of the die material (234 MPa in for C11L17 steel). When this happens then permanent damage to the die surface will occur.

PEL and discrete dies have more limitations due to their non-continuous construction. For a PEL die, high contact stresses are also a problem (σ_{yield}=379 MPa for SAE 1010 steel). More important is the fact that high transverse loads can cause excessive deflection in the laminations and inaccuracies in the die shape. Discrete dies are even more vulnerable to some sort of failure or loss of shape from forming loads. Furthermore, the

interpolator can fail (σ_{yield}=18 MPa for 460 Elvax) resulting in dimpling of the part. Discrete die elements also have the potential to bend elastically which results in a loss of die shape.

6.4.9 Limitations on Die Size

As part of a flexible manufacturing system, the die fabrication method used for tooling development should ideally impose no limitations on a die's size. The only size limits on CNC-machining a die is the work volume of the machining center used. Currently, there are very large gantry-style multi-axis machining centers available which are used for milling automotive body panel dies [Horner,1995]. A similar situation exists for PEL dies in that the only size restriction is the capacity of the DLP machine. Because of the stationary cutting means of the DLP machine design (see section 4.3.2), expanding the loading and receiving containers for larger die laminations is a relatively simple matter.

For discrete dies, the maximum size that a die can be is a function of the element size because of potential manufacturing tolerance build-up. For example, the dimensional tolerances of 3.0 mm square steel stock available in the U.S. is typically $^{+.00}_{-.05}$ mm. Although it's a statistically improbable situation, a 60 element high, i.e. 18 cm, column has the potential to be 1 element width, i.e. 3.0 mm, shorter than neighboring element columns if all the elements in the column are only 2.95 mm. This would be an unacceptable situation.

6.4.10 Limitations on Incorporating a Blankholder

The shape and configuration (e.g. flat holder, edge beads) of the blankholder is usually designed simultaneously with the shape of the forming die. How easily the blankholder is incorporated into the finished tooling is very important to reducing the time and cost of tooling development. The techniques for incorporating a blankholder in CNC-machined dies are well known with few limitations. It is slightly more difficult with PEL dies because of the restrictions that the clamping/registration frame imposes. The most limitations on incorporating a blankholder are with discrete dies because of the massive die

frame required, and the inability of the die elements to be used as an effective binding surface.

6.5 Summary

In this chapter, the details of a comparative study involving CNC-machined, PEL and discrete dies are described. Besides simply fabricating the dies, the study entailed forming a benchmark part using each die set and then measuring the shape of the stamped parts. Specific observations regarding each of the ten comparison criteria have been discussed. We leave the comprehensive summary of this study to the last chapter (7) of this thesis.

Chapter 7 - Summary and Recommendations for Future Work

In the study described in chapter 6, all three of the candidate fabrication methods are compared to each other with regards to their performance in a flexible manufacturing system, particularly one utilizes closed-loop process control principles in tooling development. The study first entailed designing and building a set of matched dies by CNC-machining solid billets, individually profiling laminations in an array and setting a reconfigurable matrix of discrete elements. The dies were used for stamping experiments of a benchmark sheet metal part. The first series of parts were stamped with the polished CNC-machined dies using various forming conditions, i.e. lubrication, blankholder force, blank shape and size. From these initial stamping trials the FEA analysis was verified and the forming conditions for all subsequent stamping experiments were optimized. A series of parts were then stamped with the unground PEL dies to determine if such rapidly made dies would give acceptable results. These dies were shown to work well if the rough forming surface is covered with a thin (0.1 mm) interpolating layer. When the PEL die surfaces were finally polished, the parts stamped with these dies had the same shape fidelity as those stamped with the CNC-machined dies. Finally, a series of parts were stamped with the discrete dies using a simple closed-packed configuration and a thick (0.8 mm) surface interpolator. For part shapes (e.g. gently-curving panels) and forming processes (e.g. stretch-forming, hydroforming) involving evenly-distributed forming loads, a simple close-packed configuration can work. However, for part shapes or processes with highly concentrated forming loads (e.g. deep drawing), a close-packed matrix with row dividers must be used.

The following discussion generalizes about the three fabrication methods based on cost and lead-time comparisons. Fabricating a PEL die and setting a discrete die is generally faster than CNC-machining a die of similar size, especially if harder die materials (e.g. tool steel) are involved. The current capital cost of CNC fabrication equipment (i.e.

machining centers) is less than that of a laser-based DLP machine due to the cost of the laser. However, expanding the size of a DLP machine will be less expensive. From an estimated cost analysis, costs of discrete die machinery, i.e. reconfigurable dies and setting equipment, are comparable to that of CNC machinery. Of the three fabrication methods, the costs of raw materials and process consumables are lowest for discrete dies because of their reconfigurable and universal nature.

Comparisons based on the shape resolution and flexibility can also be used to generalize about the three fabrication methods. Compared to CNC-machined and PEL dies, discrete dies, with their discretized forming surfaces, yield parts with the worst shape fidelity. Die geometry is limited with CNC-machining because of tooling accessibility problems and the size of the cutting tool. This is not the case with PEL dies since the laser-cut kerf is very thin and individual laminations are machined in 2-dimensions only. Regarding limitations to the forming force, discrete dies are vulnerable to interpolator failure, element slippage from high forming loads, and element bending. These types of die failure can be minimized or eliminated by the proper choice of clamping method, element size and interpolator material. The only major limitation with CNC-machined and PEL dies is the compressive strength of the die material. The discrete die method is the only one of the three with limitations on die size. The size of a discrete is a function of constituent elements in that when the element size increases, so to does the maximum achievable die size. Unfortunately the discretization of the forming surface also becomes coarser. Finally, the only method that imposes significant limitations on the blankholder configuration are discrete dies.

From these comparative study results, some general conclusions about all three fabrication methods involved can be formulated. Generally, the PEL die method is very similar to CNC-machining a billet with regards to most of the comparison criteria. However, a PEL die construction improves tooling accessibility, reduces limitations on the die geometry and allows for faster fabrication because laser cutting (and AWJ to some degree) is not dependent upon material hardness. CNC-machining a billet is better than a PEL die construction in a situation where a completely solid die is not needed (e.g. rapid temperature rise of die preferred for hot forming). In this situation, it is easier to decrease the die's thermal mass by CNC machining. Compared with both of these fabrication methods, there are limits on part shape fidelity, maximum forming loads, die geometry,

and blankholder incorporation with a discrete die construction. However, discrete dies excel in terms of cost and fabrication time. This particular combination of process characteristics is ideal when many different types of gently-curving parts need to be formed in small lot sizes. This is the case for the aerospace industry (e.g. stretch-formed body panels) and the defense industry (e.g. military vehicle body panels that don't have the same level of shape detail as their commercial vehicles).

By comparing them with the current rapid, low-cost fabrication method used in industry, i.e. CNC-machining a solid billet, both the PEL die and discrete die methods are also shown to be rapid, low-cost and, most importantly, worthy of further development. Rapid tooling methods, including the three candidate fabrication methods, are seeing increased usage in industry by professionals who need better ways to develop and bring their products to market in ways that are quicker and more economical than ever before. Layer manufacturing, i.e. rapid prototyping, methods are what is driving this increased popularity. Unfortunately these methods are not well suited for sheet metal forming dies where high strength, toughness, and smooth surface finishes are required. Refer to section section 2.3 and [Aubin,1994]. This makes a strong case to the sheet metal forming sector of industry to significantly advance the state-of-the-art for both PEL and discrete sheet metal forming dies.

The following summaries focus on how the state-of-the-art for each die fabrication method, particularly PEL and discrete dies, has been advanced as a result of this thesis work. In addition, recommendations for future work are presented to further develop each fabrication method for their eventual implementation in industry. Finally, a new hybrid method, which was conceived following the completion of the study, is briefly discussed.

7.1 CNC-MACHINED DIES

CNC-machining a solid billet is the current standard in industry for fabricating sheet metal forming dies. It continues to be a viable rapid fabrication method for implementation in a flexible manufacturing system. The goal of CNC-machining is to directly create the required forming surface as fast as possible without any intermediate manufacturing operations (e.g. casting). Three-axis machining (x, y, and z translation) machining with a ball endmill is currently the most prevalent method for accomplishing

this task. It is ideal for corners, grooves, and small radiuses of curvature in the die surface. Inclining the ball endmill with respect to the surface improves both the machined surface finish and life of the cutting tool. However, inclining the endmill requires the addition of a fourth machine axis (rotational). To dramatically decrease the time required to grind and polish large, gently-sloping die surfaces, five-axis machining (i.e. two additional rotational axes) with a radiused endmill can be used. High speed machining can also be used to decrease the machining time. For a CNC-machined die, the time required for rough cutting the die shape is inversely proportional to volume of material to be removed For a given feedrate and step-over distance, the finish cutting operation on the die surface is proportional to the forming surface area. The controller used by CNC machining center also effects the machining time. Ideally, a controller should have as small a BPT as possible to avoid bottlenecking of the machining instructions, and a large processing-block look-ahead capability in order to anticipate sudden changes in machining direction or feedrate.

Grinding and polishing of the CNC-machined (i.e. scalloped) die surface can be performed manually or with automatic grinding end effectors mounted to a robotic arm. The time required for the grinding operation is roughly proportional to the volume of the scallops left by finish cutting. To show the usefulness of estimating scallop height, material volume to be ground off, and machining time, the formulas presented in chapter 3 are used the design of the steel CNC-machined dies.

Since CNC-machining is the "standard" method for making dies, there is a vast body of knowledge about CNC-machinery, cutting tools, cutting methods, computer simulation of CNC-machining and generation of tooling paths. The general procedure for designing and fabricating CNC-machined dies is discussed in section 3.6. With regards to the CNC-machining of sheet metal forming dies, the following future work is recommended:

- The volume of material left by the finish cutting operation V_r that needs to be ground away from the die surface should be able to be estimated. The assumption that the time required to grind away the machining scallops is proportional to this value is proposed in equations 3.4 and 3.10. This assumption should be

experimentally verified, if not done so already, to determine how well equations 3.4 and 3.10 can estimate the time required to grind a die's surface smooth.

7.2 PROFILED-EDGE LAMINATION DIES

A new laminated construction referred to as an array of Profiled-Edge Laminations has been developed as a rapid fabrication method for sheet metal forming dies. This method improves upon the current method of stacking and bonding contoured laminations in terms of handling laminations during processing, registering and clamping the laminations into a rigid die, and reshaping the die during the tooling development process. The general procedure for extracting the machining instructions for each die lamination is outlined in detail for a die shape that requires only 3-D or planar beveling. A method for easily estimating the geometrical error introduced by the straight bevel approximation is introduced. The propensity for PEL die delamination is shown to be more sensitive to bending failure than buckling failure. Three cutting methods - machining with the flute-edge of an endmill, abrasive water jet cutting, and Nd:YAG laser cutting - are shown to be viable techniques for machining bevels into die laminations. The optimal process parameters for cutting steel laminations are identified for each cutting method through DOE experimental techniques. Although commercially-available CNC cutting machinery can be used to process the die laminations, two different designs for a dedicated PEL die fabrication machine are proposed. The apparatus, which will be called a Die Lamination Profiling (DLP) machine, efficiently automates the cutting and handling of the PEL die laminations.

Many of the new analytical tools and design ideas for PEL dies are used in the design and fabrication of a matched set of PEL sheet metal forming dies. In addition, the general procedure for designing and fabricating PEL dies is outlined. To further the work of this thesis, the following recommendations for future work on PEL dies are presented.

- The various algorithms for determining the 2-D intersection curve between the CAD model of the die surface and a y-z cutting plane (i.e. interface between adjacent PEL laminations) should be compared to each other with regards to shape accuracy and computational speed. An commercially-available CAD or CAM

software program should be retrofitted with this capability using the best available algorithm. This will allow the PEL die machining database for any arbitrary forming surface to be easily created.

• A technique or algorithm should be developed that determines the best orientation of the PEL laminations to minimize the overall approximation error. The approximation error is the deviation of the lamination's machined bevel from the actual CAD surface.

• PEL die delamination is an issue of great concern to die designers and engineers who have investigated laminated die constructions. To help resolve this issue, experiments should be performed to determine how well equations 4.11 and 4.12 predict the bending and buckling behavior of PEL laminations.

• The flexibility of the PEL die construction should be investigated further. For example, can a PEL die construction handle die inserts?

• For lamination bevels machined with the flute-edge of an endmill, a full factorial set of experiments including other control factors like number of cutting edges on the endmill and lamination thickness, i.e. workpiece stiffness, should be performed.

• When the lamination profiled-edges are machined with AWJ, the kerf width and taper should be quantified for various process parameters, bevel angles, materials, and material thickness since only a superficial treatment was given in this thesis. This type of experimental data is required so that these effects can be compensated for during PEL lamination processing.

• For AWJ cutting, the effect that the upstream water pressure and lamination thickness have on the kerf taper angle should be investigated. The taper angle presumably decreases with higher water pressures and thicker materials.

• Since a plasma-arc is very good at cutting thick metal plate, this cutting method might be ideally suited for creating PEL dies made of thick laminations where the accuracy of laser or AWJ cutting is not needed.

• The investigation of laser-cut lamination bevels only dealt with one material: carbon steel, which is a common material for sheet metal forming dies. Laser cutting other die materials like tool steel, Invar, aluminum, and certain plastics were not investigated as part of the thesis research. Because of the differences in energy absorbtivity vs. laser light wavelength, reactivity with oxygen, and melting temperature of these other die materials, laser types (e.g. CO_2) and configurations (e.g. fiber-optic beam delivery) other than pulsed Nd:YAG with hard-optic delivery may work better for these other materials.

• If the problems with cutting bevels into steel using an Nd:YAG laser beam delivered with fiber-optics can be overcome, this cutting technique should be reinvestigated. It offers many advantages over hard-optic delivery in terms of a more simplified DLP machine design.

• Since one of the main goals of this thesis is to commercialize the PEL fabrication method and the DLP machine concept, a small-scale prototype machine must be designed and built with input from a willing industrial partner. Table 4.22 can be used to help establish the design specifications of the machine.

• Since a solid die may be needed after the correct die shape is developed, methods for permanently bonding PEL laminations together into a solid tool (e.g. brazing, diffusion-bonding) should be investigated.

7.3 DISCRETE ELEMENT DIES

After reviewing the current state-of-the-art for reconfigurable discrete dies, many new analytical techniques for predicting performance and design concepts for improving performance of these type dies have been developed. The theoretical basis for using

elements of square cross-section in a clamped element matrix instead of other geometric shapes (e.g. hexagonal) is explained. The main reason is that square elements provide an essential predictability of the clamping load distribution within an element matrix. Furthermore, square elements of tubular construction are shown to have advantages over solid elements. The primary advantage is that the element's weight decreases faster than it's stiffness does as the wall thickness decreases.

When die elements are close-packed into a matrix and clamped into a rigid tool, the behavior of a single compression wall clamping configuration is shown to be very predictable and also effective at withstanding low forming loads. A basic static frictional model proposed for an element clamped within such a die matrix is shown to be within 23% of the experimental results. The uniformity of the clamping load (single compression wall) within the element matrix is shown to improve when a deformable interpolating material is used between the compression wall and the first row of elements. Transfer of the clamping load is shown to be almost entirely through element columns (i.e. in the direction of clamping). This means that the forming load accumulation in an element column is transferred to the outer die frame by friction at the outer elements which proves to be troublesome (i.e. element slippage) when high forming loads are encountered. However, thin sheet metal dividers between element rows that are rigidly attached to the frame greatly enhance the forming load capacity of the clamped element matrix. Since the row dividers slightly space out the element rows, notching the elements is suggested to account for the accumulated thickness instead of wedging the elements together during forming. A dual compression wall configuration can also be used to clamp the element matrix but a single compression wall configuration with row dividers is shown to be more easily implementable and able to handle higher forming loads for the same clamping load.

Various methods for achieving the high force necessary to clamp the element matrix into a rigid tool are investigated in a theoretical study and then compared with each other. A simple hydraulic actuator allows for a very high variable clamping force but can take up considerable space compared to the other methods. A toggle mechanism has high input force amplification and an inherent locking feature but gives poor control over the force. Using a wedge mechanism, there is a tradeoff between the displacement of the clamping wall and the force amplification. When significant compression wall retraction is required (e.g. for setting), the steep wedge inclines yield much lower force amplification

than the knuckle mechanism. However, using a wedge configuration is the most compact of all the designs. Negligible displacement of a piezoelectric ceramic actuator may preclude its use as a clamping method. An interference fit created by thermal contraction of the die frame around the element matrix is a new idea that appears to be very promising. A simplified frame design and large forces achievable (although possibly not very controllable) makes thermal contraction an appealing method. Non-uniformity in clamping load was noticed with an element matrix contained in a relatively elastic frame. When high clamping forces are used to secure an element matrix, a stiff frame is essential to assure that the clamping load distribution remains uniform.

The best method for setting a discrete die made of large elements (e.g. stretchforming die) is to do it in a parallel fashion (i.e. setting all elements at the same time). A new idea for accomplishing this task is to make each element into a small hydraulic actuator which allows for individual control over each element. In this way, unwanted frictional interactions between elements becomes a non-issue. However, control over each element becomes virtually impossible when the elements get too small. The best method for setting small elements is in a row by row fashion. An automatic profiling mechanism requiring fewer force and displacement actuators than previous designs is proposed for accomplishing this task. The general procedure for determining the die's element positions for a given CAD model of a die surface is presented. If a premolded interpolator is used to cover the forming surface of the newly-set element matrix, it's effective thickness can be estimated by considering the change in volume as the gaps between elements are filled in.

In light of these new developments in discrete die design, the design and construction details of a pair of high-resolution discrete dies are presented. The general procedure for designing, fabricating and setting a reconfigurable discrete die is also presented. Furthermore, the following recommendations for future work on discrete dies are discussed below:

- A tubular element construction offers a decrease in weight with a correspondingly less reduction in element stiffness as the wall thickness decreases. However, the clamping behavior (e.g. transverse buckling propensity) of tubular elements should be investigated.

• In terms of forming load capacity enhancement, how effective is applying a fluid backing pressure to the back of the element matrix? This question needs to be addressed.

• Although the effectiveness of incorporating sheet metal dividers for enhancing forming load capacity has been experimentally qualified, the effect should also be quantified and compared with the theoretical model proposed in this thesis.

• The issues of notching elements (see section 5.2.6.1.2) to account for the accumulated thickness of the incorporated sheet metal dividers should be investigated. In addition, the economics of this approach compared to just using a converging frame should be investigated.

• The effectiveness of a dual compression wall configuration should be investigated and compared with the single compression wall configurations.

• An experimental study is needed that investigates the effectiveness of various clamping actuators or methods at achieving and maintaining a high clamping force. The actuators or methods used in the study will include a hydraulic ram, toggle mechanism, wedge mechanism, and the interference fit clamping induced by the thermal-contraction of the die frame.

• The formulas for estimating the effective thickness of an interpolator which is premolded to the discrete die surface should be experimentally verified. Are these relationships useful for estimating the shape of the discrete die forming surface? What are useful relationships for the case where the incline is not in the X-Z or Y-Z plane?

• As a logical extension to the work of [Eigen,1992], a comprehensive study of premoldable interpolator materials, besides Elvax, for use on discrete dies is

needed. Furthermore, rapid and effective methods for premolding such materials onto a discrete die surface need to be developed.

• The alternative profiling mechanism design shown in figure 5.34 should be theoretically investigated. If the design appears to be an improvement on previous profiling mechanism designs then an actual prototype should be designed and built.

• The hydraulically-actuated element design concept offered in section 5.5.3 must be developed further. For large element dies, this design offers a relatively simple method for setting the forming shape of the die in a rapid parallel fashion.

• What is the relationship between the a discrete die element size and the maximum size that a die made of these element can be? This topic should be experimentally investigated to see if there is any useful heuristic or theoretical relationship that can be developed for designers.

• A software program capable of extracting the required element positions from a parametrical representation (e.g. Bezier composite surface) should be developed using the general algorithm outlined in section 5.6.

7.4 CNC-MACHINED LAMINATION (CML) FORMING DIES

As pointed out in section 6.5.7, the range of die shapes that can be CNC-machined from a solid billet is limited by the accessibility of the cutting tool. This limitation on the forming surface geometry is avoided in a PEL die construction because machining is only in two dimensions. However, the straight bevels cut into the PEL laminations can only approximate the die shape whereas the CNC-machined die introduces much less of a surface approximation if closely-spaced finish cuts are used. By combining CNC-machining with a PEL construction, the advantages of both methods (i.e. unlimited shape range of PEL dies and close adherence to desired die shape with CNC-machining) can be realized. The details of this new hybrid fabrication technique, which will be called the CNC-Machined Lamination (CML) method, are discussed in this section.

As seen in figure 7.1, a CML die generally comprises an array of vertically-oriented laminations just like a PEL die. Unlike the PEL die, the top edge of each CML die lamination better captures the essence of a forming surface because it's CNC-machinined and not beveled. The laminations will be typically be thicker than those used for a PEL die in order to withstand the higher cutting forces associated with CNC-machining (Refer to sections 4.2.1 and 4.4 as an example). The die lamination members may be held together in a stacked array by a simple tension bolt as shown in figure 7.1 or with a clamping frame similar to that shown in figure 4.2 for the PEL die. A common registration edge on each lamination allows for easy and uniform registration of the die before clamping. One or more holes uniformly positioned in the sides of each lamination allows the whole array to be clamped so that no adhesive or other means of holding the array of die lamination members together is required. If the shape of the forming surface has to be changed during the die development process, the die laminations can easily be separated for remachining. Like the PEL die, a CML die can be made into a solid die apart from this process by suitable means (e.g. diffusion-bonding). The top edge of each die lamination has a portion of the intended die surface. When placed together in a vertical stacked array, the top edges of the die lamination members, in the aggregate, form the top surface of the die.

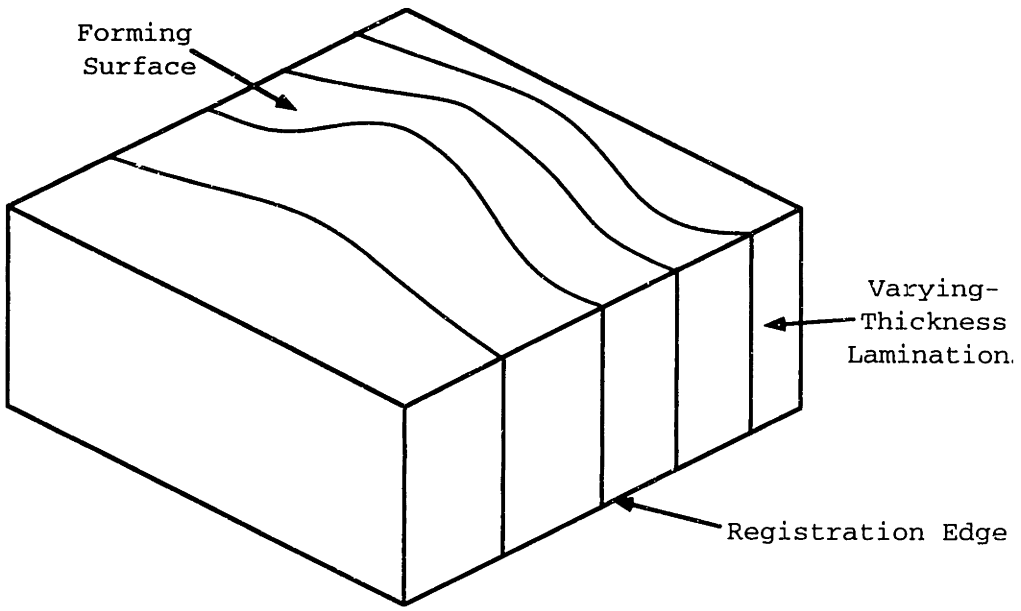

Figure 7.1 - Isometric view of a CML die

7.4.1 CNC Machinery and Machining Methods for CML Dies

As shown in figure 7.2, a die surface feature like a deep cavity is easily machined into a series of individual die laminations by surface contouring. This type of surface feature would be very difficult, if not impossible, to do if the die were solid. The same methods and machinery used for CNC-machining a solid billet (see section 3.1) can be used to machine a CML die lamination. This includes three-axis machining with an endmill (Sect. 3.1.1), four-axis machining with a ball endmill (Sect. 3.1.2), and five-axis machining with a radiused endmill (Sect. 3.1.3).

With virtually no constraints on the access of the tool, machining the top surface of the thick lamination at almost any orientation will be possible. To take advantage of the increased accessibility for tooling afforded by laminated construction, the recently developed 6-axis CNC machining centers can also be used to machine the die laminations. For example, the Octahedral Hexapod developed by Ingersoll Milling Machine Tool Co. provides 6-axis machining capability and a structure that is extremely rigid and self-contained which is ideal for surface contour machining [Anonymous,1993]. With contour machining of the die laminations, minimal grinding of the die will be required.

Compared to a PEL die, the burden of handling individual CML die laminations during machining is much less since thicker laminations used necessitating a smaller number of laminations to make up the die. If the number of laminations to be processed is relatively small, manual handling of the laminations between the top surface machining operations is an option. However, if the number of laminations to processed is relatively large, an automatic handling mechanism like the one described for the first embodiment of the DLP machine (section 4.3.2.1) should be used.

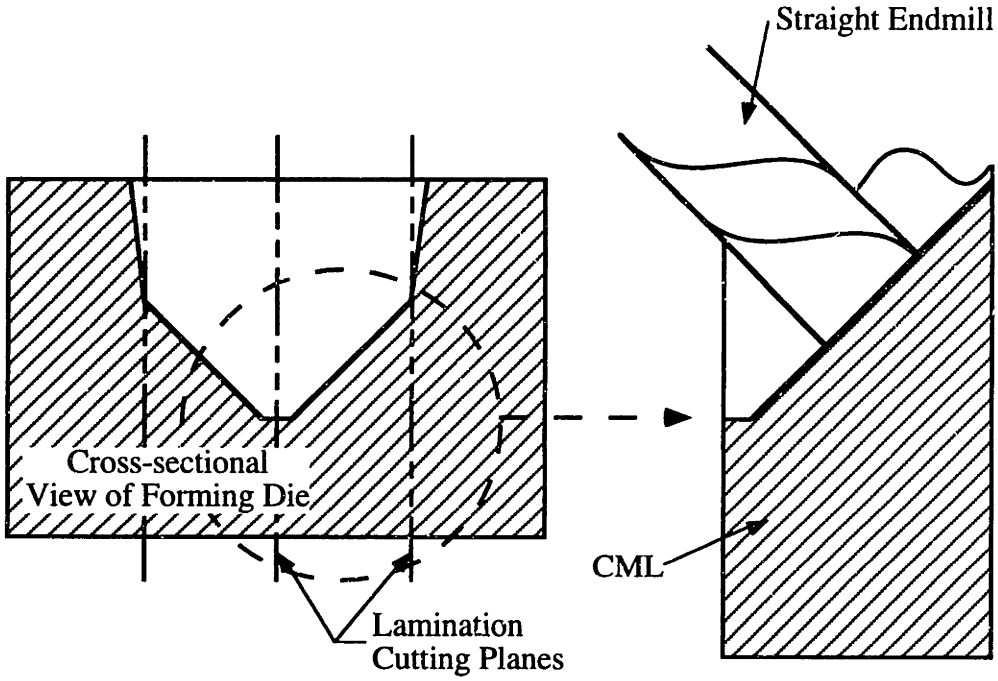

Figure 7.2 - Surface contouring of an individual CML.

7.4.2 Determination of Lamination Thickness

A gently-curving convex surface is ideally milled (5-axis CNC machining center) with a regular or radiused endmill because little or no scalloping of the surface will occur. For CML die laminations, the segment of the die surface to be machined into it's top edge should ideally be convex or nearly convex for this reason. Therefore, the goal in determining lamination thickness and the positions of the contact planes is to strategically break up the complex 3-D forming surface of the die into segments with little or no concavity. One economical constraint on the thickness of a lamination is that it should not be a custom thickness which requires extra machining but rather a standard stock thickness. Once the width and positions of the laminations in the array are determined, the actual laminations should be clamped together so that the overall width of the die can be accurately measured in the thickness direction. This measurement will help to minimize the tolerance build-up error of the stock thickness.

Laminations have to be stiff enough to avoid excessive deflection from machining forces and more importantly, minimize self-excited vibration during machining. There are many causes of self-excited vibration, called chatter, in milling operations including tool

geometry, the number of teeth on the endmill n_t, the machine tool stiffness, and the cutting tool/lamination interaction. Methods for reducing chatter including reducing n_t (reduces machining frequency); changing the tool geometry (stiffer tool raises it's natural frequency); changing the spindle speed to break the tool, workpiece, and machine harmonics; increase the stiffness of the machine tool; and improve the fixturing of the lamination in the direction of the cutting forces [Smith,1989]. In the case of CML dies, this means that die laminations will have a lower bound to the thickness in order to prevent or minimize the effect of chatter.

7.4.3 Example: Bottom Die for the Benchmark Part

To investigate how lamination thickness and contact positions are chosen, the bottom die of the benchmark part was made out of aluminum using a CML construction. Standard lamination thickness of 6.4 mm and 9.5 mm were chosen. The cross-sectional view B-B of the benchmark part shown in figure 6.1 was used to manually choose the order, thickness, and position of each die lamination. When the array of laminations was clamped together to have it's overall width measured, it was 10.3 cm wide which was 0.1 mm oversized. Therefore, 0.1 mm was machined off one of the last 9.5 mm thick laminations. Finish cuts to the entire die surface were done with a Ø6.4 mm ball endmill mounted in a 3-axis machining center. The CML bottom die is shown in figure 7.3. For illustrative purposes, some of the machined laminations are separated from the rest of the die.

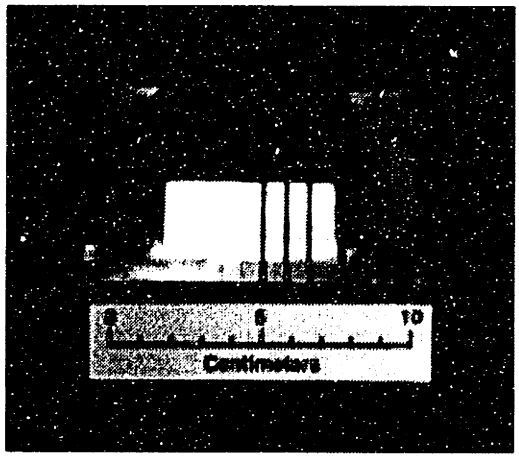

Figure 7.3 - CML bottom die for the benchmark part.

7.4.4 Future Work on CML Dies

The following recommendations for future work on CML dies are suggested:

- An algorithm needs to be developed that will determine the optimal orientation and interface locations using standard lamination thickness for an arbitrary 3-D die forming surface. The algorithm should optimally break up the surface into convex or nearly convex segments and also deal with issues of tooling access.

- If one doesn't exist already, an algorithm needs to be developed that will determine the optimal tool trajectory needed to rapidly machine each CML die lamination.

- A time/cost study that compares CNC-machining of a solid billet with a die fabrication with a CML construction should be performed. The results of this study will prove or disprove the claims put forth at the beginning of section 7.4. A die shape that takes advantage of the CML constructions tooling accessibility should be chosen (e.g. deep draw die). The surface fidelity of each die should be measured with a CMM to determine how well a CML die captures the intended die shape.

- Whether a CML array needs to be clamped in a frame or simply by some tension bolts needs to be investigated.

- Diffusion bonding of a CML should be experimentally investigated to see how much time and cost it adds to the fabrication process.

- If the CML methods seems to be commercially viable, an automatic handling system for variable thickness CML laminations should be designed and built. A five-axis or six-axis machining center would be retrofitted with this automatic handling mechanism.

Bibliography

Anonymous, "NC Speeds The Pace," *Steel*, Vol. 162, No. 16, April 15, (1968), pp. 55-58.

Anonymous, "Fusible Alloy Tooling," *Materials and Design*, Vol. 10, No. 5, Sept./Oct. (1989), pp. 265-267.

Anonymous, *Facts About: Laser Cutting*, Publication by AGA AB, Lindigö, Sweden, (1991).

Anonymous, "The Cutting Edge of Machine Tools," *Manufacturing Engineering*, Vol. 111, No. 5, Nov. (1993), pg. 24.

Anonymous, *Product Catalog #2*, Piezo Systems, Inc. Cambridge, MA, (1993b).

Appleton, E. and Mason, B., "Sheetmetal Forming for Small Batches Using Sacrificial Tooling," *The Production Engineer*, Vol. 64, No. 9, Oct. (1984), pp. 58-61.

Aubin, R.F., "A World Wide Assessment of Rapid Prototyping Technologies," *UTRC Report No. 94-13*, United Technologies Research Center , East Hartford, CT, Jan. (1994).

Berger, Ulrich, "Rapid Prototyping Technologies for Advanced Sheet Metal Forming," *Proceedings of the Rapid Prototyping and Manufacturing '93 Conference*, Dearborn, Michigan, May 11-13, (1993).

Berry, H.D., "Intricate Shapes Built Up From Stacked Stampings," *Iron Age*, Vol. 128, No. 26, Dec. 29, (1966), pp. 44-45.

Bezier, P., "Style, Mathematics, and NC," *Computer-Aided Design*, Vol. 22, No. 9, Nov. (1990), pp. 524-26.

Bowden, F.P. and Tabor, M., *The Friction and Lubrication of Solids*, Clarendon Press, Oxford, England, (1950).

Bobrow, J.E., "NC Machine Tool Path Generation from CSG Part Representations," *Computer-Aided Design*, Vol. 17, No. 2, March (1985), pp. 69-76.

Bransch, H.N., "Cutting and Drilling Using Nd:YAG Lasers with Fiber-optic Beam Delivery," *Proceedings of the International Conference on Lasers '91*, (1991), pp. 465-471.

Chan, Y.K. and Knight, W.A., "A System for the Computer-Aided Manufacture of EDM Electrodes for Dies and Molds," *1980 Manufacturing Engineering Transactions: Proceedings of the Eighth North American Manufacturing Conference*, Rolla, Missouri, May 18-21, (1980), pp. 336-343.

Chryssolouris, G., *Laser Machining: Theory and Practice*, Springer-Verlag, Inc., New York, (1991).

Chiangi, B. "The Use of Virtual Reality in Prototyping and Manufacturing," *Proceedings of IBEC '94: Advanced Technologies and Processes*, Vol. 10, Detroit, Michigan, Sept. 26-29, (1994), pp. 32-33.

Choi, B.K., Lee, C.S., Hwang, J.S., and Jun, C.S., "Compound Surface Modelling and Machining," *Computer-Aided Design*, Vol. 20, No. 3, April (1988), pp. 127-136.

Choi, B.K., Park, J.W., and Jun, C.S.,"Cutter-Location Data Optimization in 5-Axis Surface Machining," *Computer-Aided Design*, Vol. 25, No. 6, June (1993), pp. 377-386.

Colt, J., *Hypertherm® Technology: How HyDefinition Plasma Cutting Technology Works Compared with Conventional Plasma; Its Benefits and Capabilities*, Publication by Hypertherm Inc., Hanover, N.H., (1995).

Connolly, G.,"Multiaxis Laser Cuts Manufacturing Time of Aerospace Parts," *Mechanical Engineering*, Vol. 116, No. 2, February (1994), pp. 64-65.

Crandall, S.H., Dahl, N.C., and Lardner, T.J., *An Introduction to the Mechanics of Solids, 2nd Edition*, McGraw-Hill, Inc., New York, (1978).

DaRe, M., DeBernardi, R., Hatt, F., and Guida, M., "Fiat Uses CAE to Stamp Metal for New Oil Pan," *Mechanical Engineering*, Vol. 116, No. 4, April (1994), pp. 60-61.

Discussion with **Dastidar, P.**, Senior Engineer, Advanced Manufacturing, Carrier Corporation, Syracuse, N.Y., May 16, (1995).

Davies, R., and Austin, E.R., *Developments in High Speed Metal Formng*, Industrial Press Inc., New York, (1970).

Deckard, C.R., "Method and Apparatus for Producing Parts by Selective Sintering," *U.S. Patent no. 4863538*, Issued Sept. 5, (1989).

DeVor, R.E., Tsong, T-h, and Sutherland, J.W., *Statistical Quality Design and Control: Contemporary Concepts and Methods*, Macmillan Publishing Co., New York, (1992).

DiMatteo, P.L., "Method of Generating and Constructing Three-Dimensional Bodies," *U.S. Patent no. 3932923*, Issued January 20, (1976).

DiPietro, P. and Yao, Y.L., "An Investigation Into Characterizing and Optimizing Laser Cutting Quality—A Review," *International Journal of Machine Tools and Manufacturing*, Vol. 34, No. 2, (1994), pp. 225-243.

Eckart, D., and Kruska, J-U, "Flexibles Streckziehen von Feinblechen (Flexible Stretchforming of Thin Sheet Metal)" (In German), Bander Bleche Rohre, Vol. 34, No. 5, May (1993), pp. 38-49.

Elber, G., "Accessibility in 5-Axis Milling Environment," *Computer-Aided Design*, Vol. 26, No. 11, Nov. (1994), pp. 796-802.

Eigen, G.F., "Smoothing Methods for Discrete Die Forming," *M.S. Thesis*, Dept. of Mechanical Engineering, MIT, June (1992).

Faux, I.D., and Pratt, M.J., *Computational Geometry for Design and Manufacture*, Ellis Horwood Ltd., Chichester, England, (1979).

Feygin, M., "LOM System Goes Into Production," *Proceedings of the 2nd International Conference on Rapid Prototyping*, (1991), pp. 351-357.

Finckenstein, E.v., and Kleiner, M., "Flexible Numerically Controlled Tool System for Hydro-Mechanical Deep Drawing" (In German), Annals of the CIRP, Vol. 40, No. 1, (1991), pp. 311-314.

*1994 **FMA** Member Resource Directory*, Fabricators & Manufacturers Association, Chicago, Illinois, (1994).

Gupta, Paraq, "Rapid Prototyping in Die Manufacturing," *Proceedings of the Rapid Prototyping and Manufacturing '93 Conference*, Dearborn, Michigan, May 11-13, (1993).

Haas, Eberhard, "Method for the Manufacture of a Tool-Set for the Forming of Sheet Metal Objects," *U.S. Patent no. 3956085*, Issued May 11, (1976).

Hardt, D.E., and Gossard, D.C., "A Variable Geometry Die for Sheet Metal Forming: Design and Control," *Proceedings of the Joint Automatic Control Conference*, San Francisco, California, August (1980).

Hardt, D.E., Olsen, B.A., Allison, B.T., and Pasch, K., "Sheet Metal Forming With Discrete Die Surfaces," *Ninth North American Manufacturing Research Conference Proceedings*, May (1981), pp. 140-144.

Hardt, D.E. and Webb, R.D., "Sheet Metal Die Forming Using Closed-Loop Shape Control," *Annals of CIRP*, (1982), pp. 165-169.

Hardt, D.E., Robinson, R.E., and Webb, R.D., "Closed-Loop Control of Die Stamped Sheet Metal Parts: Algorithm Development and Flexible Forming Machine Design," *Proceedings of the Advanced Systems for Manufacturing Conference*, Madison, Wisconsin, May 14-17, (1985), pp. 21-28.

Hardt, D.E., Boyce, M.C., and Walczyk, D.F., "A Flexible Forming System for Rapid Response Production of Sheet Metal Parts," Proceedings of IBEC '93, Detroit, Michigan, Sept. 21-23, (1993), pp. 61-69.

Hasegawa, K.,"Die Design and Manufacturing," **maybe SAE or IBEC, 1993.**

Hess, F., "Process and Apparatus for Manufacturing Anatomically Accurate Individual Foot Supports for Shoes," *U.S. Patent no. 1826783*, Issued October 13, (1931).

Hicks, A.A., "Three-Dimensional Die," *U.S. Patent no. 2968838*, Issued January 24, (1961).

Hilton, P., "Making the Leap to Rapid Tool Making," *Mechanical Engineering*, Vol. 117, No. 7, July (1995), pp. 75-76.

Honecker, A., and Mattiasson, K. "Finite Element Procedures for 3-D Sheet Metal Forming Simulation," *Proceedings of NUMIFORM '89*, Rotterdam, Balkema, (1989), p. 457.

Memorandum from **Horner, A.H.**, Office Manager, Gilbert & Richards, Inc., North Haven, Connecticut, Feb. 22, (1995).

Hosford, W.F. and Caddell, R.M., *Metal Forming: Mechanics and Metallurgy*, Prentice-Hall, Englewood Cliffs, N.J., (1983).

Huang, Y. and Oliver, J.H., "Non-Constant Parameter NC Tool Path Generation on Sculpted Surfaces," *International Journal of Advanced Manufacturing Technology*, Vol. 9, (1994), pp. 281-290.

Hull, C.W., "Apparatus for Production of Three-Dimensional Objects by Stereolithography," *U.S. Patent no. 4575330*, Issued March 11, (1986).

Ip, W.L.R., and Loftus, M., "The Application of an Inclined Endmill Machining Strategy on 3-Axis Machining Centers," *International Journal of Machine Tools and Manufacturing*, Vol. 33, No. 2, (1993), pp. 115-133.

James, K.F. and Joyce, A.H., "Method of Making Sheet Metal Forming Dies," *U.S. Patent no. 3313007*, Issued April 11, (1967).

Jensen, K.L., "Making Electrodes for EDM with Rapid Prototyping," *Proceedings of the Third International Conference on Rapid Prototyping*, Dayton, Ohio, June 7-10, (1992), pp. 295-301.

Jensen, K.L., and Hovton, R., "Making Electrodes for EDM with Rapid Prototyping," *Proceedings of the 2nd European Conference on Rapid Prototyping and Manufacturing*, University of Nottingham, England, July 15-16, (1993), pp. 157-166.

Kalis, E.R., "Reinforced Plastic Die," *U.S. Patent no. 3101065*, Issued August 20, (1963).

Kalpakjian, S., *Manufacturing Processes for Engineering Materials*, Addison -Wesley Publishing, Reading, Massachusetts, (1984).

Kalpakjian, S., *Manufacturing Engineering and Technology*, 2nd Edition, Addison-Wesley Publishing, Reading, Massachusetts, (1992).

Karafillis, A.P., "Tooling Design of Sheet Metal Forming Processes by Using Finite-Element Analysis," *M.S. Thesis*, Dept. of Mechanical Engineering, MIT, (1992).

Karafillis, A.P. and Boyce, M.C., "Tooling Design in Sheet Metal Forming Using Springback Calculations," *International Journal of Mechanical Sciences*, 113, 34, (1992).

Karafillis, A.P., "Tooling Design for Three-Dimensional Sheet Metal Forming Using Finite-Element Analysis," *Ph.D. Thesis*, Dept. of Mechanical Engineering, MIT, August (1994).

Karlin, J., "Three-Dimensional Imaging Methods for Manufacturing, With Emphasis on the Laser Speckle Technique," *M.S. Thesis*, Dept. of Mechanical Engineering, MIT, June (1995).

Knapke, J.A., "Evaluation of a Variable-Configuration-Die Sheet Metal Forming Machine," *M.S. Thesis*, Dept. of Mechanical Engineering, MIT, (1988).

Krowl, W.G., "Urethane Dies," *U.S. Patent no. 4509358*, Issued April 9, (1985).

Kruth, J.P., "Material Incress Manufacturing by Rapid Prototyping Techniques," *Annals of the CIRP*, Vol. 40, No. 2, (1991), pp. 603-614.

Kunieda, M. and Nakagawa, T., "Manufacturing of Laminated Deep Drawing Dies by Laser Beam Cutting," *Proceedings of the 1st International Conference on Technology of Plasticity*, Vol. 1, Tokyo, Japan, (1984), pp. 520-525.

Kuragano, T., "FRESDAM System for Design of Aesthetically Pleasing Free-Form Objects and Generation of Collision-Free Tool Paths," *Computer-Aided Design*, Vol. 24, No. 11, Nov. (1992), pp. 573-581.

Langdon, Ray, "Low-Cost Press-Tools'" *Automotive Engineer*, Vol. 18, No. 2, April/May (1993), pp. 52-53.

Lange, K. (Editor), *Handbook of Metal Forming*, McGraw-Hill, New York, (1985).

Lilly, B.W., Bailey, R.W., and Altan, T., "Automated Finishing of Dies and Molds: A State of the Art Review," *Computer-Aided Design and Manufacturing of Dies and Molds*, The Production Engineering Division, ASME, Vol. 32, (1988).

Marciniak, K., "Influence of Surface Shape on Admissible Tool Positions in 5-Axis Face Milling," *Computer-Aided Design*, Vol. 19, No. 5, June (1987), pp. 233-236.

Matsui, S., Matsumura, H., Ikemoto, Y., and Shimizu, H, "High Precision Cutting Method for Metallic Materials by Abrasive Waterjet," *Proceedings of the 6th American Water Jet Conference*, Houston, TX, August 24-27, (1991), pp. 127-137.

Discussion with **Mayes, B.**, Die Development Foreman, Warren Stamping Plant, Chrysler Corp., Warren, MI, March 5, (1993).

Michaels, S., Sachs, E.M., and Cima, M.J., "Metal Parts Generation by Three Dimensional Printing," *Proceedings of the Solid Freeform Fabrication Symposium*, Austin, Texas, Aug. 3-5, (1992), pp. 244-250.

Miura, H., "Resin Die for Sheet Metal Pressing and Method for Producing Same," *U.S. Patent no. 5081861*, Issued January 21, (1992).

Morrison, L. "Press Alloy," Manufacturing Engineer, June (1992), pp. 20-21.

Murakawa, M., Miyazawa, H., Kobayashi, N., and Ohkawa, K., "Oblique Profile Cutting By Laser," Proceedings of Lamp '87, Osaka, Japan, May, (1987), pp.255-260.

Nakagawa, T., Kunieda, M. and Liu, S.D., "Laser Cut Sheet Laminated Forming Dies by Diffusion Bonding," *Proceedings of the 25th International Machine Tool Design and Research Conference*, U. of Birmingham, England, April 22-24, (1985), pp. 505-510.

Nakagawa, T., "Recent Manufacturing Technologies for Auto-Body Panel Forming Tools," *Journal of Materials Processing Technology*, 46 (1994), pp. 277-290.

Nakajima, N., "A Newly Developed Technique to Fabricate Complicated Dies and Electrodes with Wires," *Bulletin of Japanese Society of Manufacturing Engineers (JSME)*, Vol. 12, No. 54, (1969), pp. 1546-1554.

Nakamura, S., Sugiura, H., Onoe, H., and Ikemoto, K., "Hydromechanical Drawing of Automotive Parts," *Journal of Materials Processing Technology*, Vol. 46, (1994), pp. 491-503.

Memorandum from **Nardiello, J.A.**, Senior Engineer, Advanced Technology and Development Center, Northrup-Grumman Corp., Bethpage, N.Y., March 28, (1995).

Nilsson, S., "Prototype and Low-Volume Fabrication of Automotive Sheet Metal Parts Applying Flexforming," *Steel Stamping Technology: Applications and Impact, SAE International Congress and Exposition*, Detroit, Michigan, Feb. 27 - March 23, (1989), Report No. SP-779, pp. 97-107.

Noaker, P.M., "Milling's Speed Limits." *Manufacturing Engineering*, Vol. 114, No. 5, May (1995), pp. 57-65.

Oberg, E., Jones, F.D., and Horton, H.L., *Machinery's Handbook, 23rd Edition*, Industrial Press Inc., New York, (1988).

O'Connor, L., "Agile Manufacturing in a Responsive Factory," *Mechanical Engineering*, Vol. 116, No. 7, July (1994), pp. 54-57.

Olsen, B.A., "Die Forming of Sheet Metal Using Discrete Die Surfaces," *S.M. Thesis*, Dept. of Mechanical Engineering, Massachusetts Institute of Technology, (1980).

Ousterhout, K.B., "Design and Control of a Flexible Process for Three-Dimensional Sheet Metal Forming," *Ph.D. Thesis*, Dept. of Mechanical Engineering, Massachusetts Institute of Technology, (1991).

Phadke, M.S., *Quality Engineering Using Robust Design*, Prentice-Hall, Englewood Cliffs, N.J., (1989).

Phillips, M.B., and Odell, G.M., "An Algorithm for Locating and Displaying the Intersection of Two Arbitrary Surfaces," *IEEE Computer Graphics and Applications*, Vol. 4, No. 9, Sept. (1984).

Pinson, G.T., "Apparatus for Forming Sheet Metal," *U.S. Patent no. 4212188*, Issued July 15, (1980).

Powell, J., *CO_2 Laser Cutting* Springer-Verlag, Inc., New York, (1993).

***Pro/ENGINEER** User's Guide Version 13.0*, Parametric Technologies Corp., Waltham, Massachusetts, (1994).

Querreiro, A.M., "Laminated Stretch Form Die," *U.S. Patent no. 3558409*, Issued January 26, (1971).

Robinson, R.E., "Design of an Automated Variable Configuration Die and Press for Sheet Metal Forming," *M.S. Thesis*, Dept. of Mechanical Engineering, MIT, (1987).

Sachs, E., Cima, M., Bredt, J., Curodeau, A. Fan, T., and Brancazio, D., "CAD-Casting: Direct Fabrication of Ceramic Shells and Cores by Three Dimensional Printing," *Manuafacturing Review*, Vol. 5, No. 2, June (1992), pp. 117-126.

Sachs, E.M., Haggerty, J.S. and Williams, P.A., "Three-Dimensional Printing Techniques," *U.S. Patent no. 5204055*, Issued April 20, (1993).

Schey, J.A., *Introduction to Manufacturing Processes, Second Edition*, McGraw Hill, New York, (1987).

Schubert, P.B., editor, *Die Methods: Design, Fabrication, Maintenance, and Application*, Industrial Press Inc., New York, (1966), pp. 265-342.

Semiatin, S.L. et al., *Metals Handbook: Volume 14, Forming and Forging*, Ninth Edition, ASM International, Metals Park, Ohio, (1988).

Shigley, J.E., and Mitchell, L.D., *Mechanical Engineering Design*, 4th edition, McGraw-Hill, New York, (1983).

Siekirk, J.F., "Process Variable Effects on Sheet Metal Quality," Journal *of Applied Metalworking*, Vol. 4, No. 3, July (1986), pp. 262-269.

Smith, O., *Press-Working of Metals,* 1st Edition, John Wiley and Sons, New York, (1896).

Smith, G.T., *Advanced Machining: The Handbook of Cutting Technology*, Springer-Verlag, New York, (1989).

Tikhomirov, R.A., Babanin, V.F., Petukhov, E.N., Starikov, I.D., and Kovalev, V.A., *High-Pressure Jetcutting*, ASME Press, New York, (1992).

Timeshenko, S.P., and Gere, J.M., *Theory of Elastic Stability*, McGraw-Hill Book Co., New York, (1961).

Todoroki, M, Imazu, H., Nomura, H, Yamaguchi, N, Asano, J., Ishibashi, K., Yamamoto, K., "Apparatus and Method for Producing Variable Configuration Die," *U.S. Patent #5253176*, Issued Oct. 12, (1993).

Vaccari, J.A., "The Promise of Laser Forming," *LAI Notes*, May 20, (1994).

Discussion with **Wagner, Richard**, Die Cost Estimator, Autodie International, Inc., Grand Rapids, Michigan, May 22, (1995).

Wakefield, W.H., "Die and Method of Making Same," *U.S. Patent no. 2332360*, Issued October 19, (1943).

Walker, D.C., "Design of a Process Improvement Methodology for Die Construction," *M.S. Thesis*, Dept. of Mechanical Engineering, Massachusetts Institute of Technology, June (1993).

Walters, T., "Press," *U.S. Patent no. 2334520*, Issued November 16, (1943).

Weaver, W.R., "Process for the Manufacture of Laminated Tooling," *U.S. Patent #5031483*, Issued July 16, (1991).

Webb, R.D. and Hardt, D.E., "A Transfer Function Description of Sheet Metal Forming for Process Control," *ASME Journal of Engineering for Industry*, Vol. 133, No. 44, (1991).

Discussion with **West, D.**, Manufacturing Engineer, The Boeing Company, Seattle, WA, on June 24, (1994).

Whitacre, F.E., "Incremental Die Construction Having a Hole Piercing Capability," *U.S. Patent no. 3559450*, Issued February 2, (1971).

Discussion with **White, D.**, Ford Research Laboratory, Ford Motor Co., Dearborn, Michigan, December 16, (1993).

Wick, C., Benedict, J., and Veilleux, R. (editors), *Tooling and Manufacturing Engineers Handbook, 4th Edition, Volume 2: Forming*, Society of Manufacturing Engineers, Dearborn, Michigan, (1984).

Williams, C.J., and Skinner, T., "Spring-Forming Device," *U.S. Patent no. 1465152*, Issued August 14, (1923).

Williams, R.P., "Precision Stretch Forming Large Shapes," *Manufacturing Engineering*, Vol. 78, No. 2, Feb. (1977), pp. 44-46.

Wilson, D.V., "Shaping Things To Come - A Metallurgist's View Part 1," *Sheet Metal Industries*, Dec. (1980), pp. 1056-1062.

Wolak, J., Bodoia, J.R., Sherrer, R.E., and Worm, P., "A Preliminary Study of an Infinitely Variable Surface Generator and Its Application to Die Forming," *Manufacturing Engineering Transactions*, Vol. 2, (1973), pp. 155-160.

Womack, J.P., Jones, D.T., and Roos, D., *The Machine That Changed The World*, Harper Perennial, New York, (1991).

Zeni, M.I., "Five Axis Machining of Stamping Dies," *M.S. Thesis*, Massachusetts Institute of Technology, May (1995).

Biographical Note

The author, Daniel F. Walczyk, was born on October 9, 1963 in the Syracuse, New York. He was raised in the small hamlet of Brewerton which is situated on the shores of Oneida Lake, a large freshwater lake in central New York. After getting his A.S. in engineering science from Onondaga Community College (Syracuse) in 1983, he worked for 2 years as a machine designer/draftsman at the Schneider Packaging Equipment Co. of Brewerton, N.Y. Eventually, Mr. Walczyk finished his B.S. degree in mechanical engineering from Syracuse University in 1986 while interning at the Radar Systems Division of the General Electric Co. After graduation, he was hired as a full-time mechanical engineer by the G.E. Sonar Systems Division, also in Syracuse. After working slightly over 2 years for G.E., he enrolled as a mechanical engineering graduate student in 1989 at Rensselaer Polytechnic Institute (RPI) located in Troy, N.Y. Mr. Walczyk also began working part-time as a research engineer at the G.E. Corporate Research and Development facility in Niskayuna, N.Y. After finishing his M.S. in mechanical engineering in 1991, he was accepted into the Ph.D. program in the department of mechanical engineering at MIT. In 1994, Mr. Walczyk was registered as a professional engineer in the State of New York. Following the completion of his Ph.D. work at MIT, he spent 3 months as a DAAD fellow at the Laboratory for Machine Tools and Production Engineering at RWTH Aachen in Aachen, Germany. In January of 1996, Mr. Walczyk will be joining the faculty at RPI as an assistant professor in the department of mechanical engineering, aeronautical engineering, and mechanics.